Surrogate Technologies for Suspended Solid Dynamics Assessment in Surface Waters

Zur Erlangung des akademischen Grades einer

DOKTORIN DER INGENIEURWISSENSCHAFTEN (Dr. -Ing.)

von der KIT-Fakultät für
Bauingenieur-, Geo- und Umweltwissenschaften

des Karlsruher Instituts für Technologie (KIT)
genehmigte
DISSERTATION
von

Liege Fernanda Koston Wosiacki, Dipl.-Ing., M.Sc.
aus Curitiba (Brasilien)

Tag der mündlichen Prüfung: 20.08.2020

Referent: Prof. Dr.-Ing. Tobias Bleninger (UFPR)
Referent: Prof. Dr.-Ing. Stephan Fuchs (KIT)

Karlsruhe (Deutschland) und Curitiba (Brasilien)
2020

This document is licensed under a Creative Commons
Attribution-ShareAlike 4.0 International License (CC BY-SA 4.0):
https://creativecommons.org/licenses/by-sa/4.0/deed.en

FEDERAL UNIVERSITY OF PARANÁ

LIÉGE FERNANDA KOSTON WOSIACKI

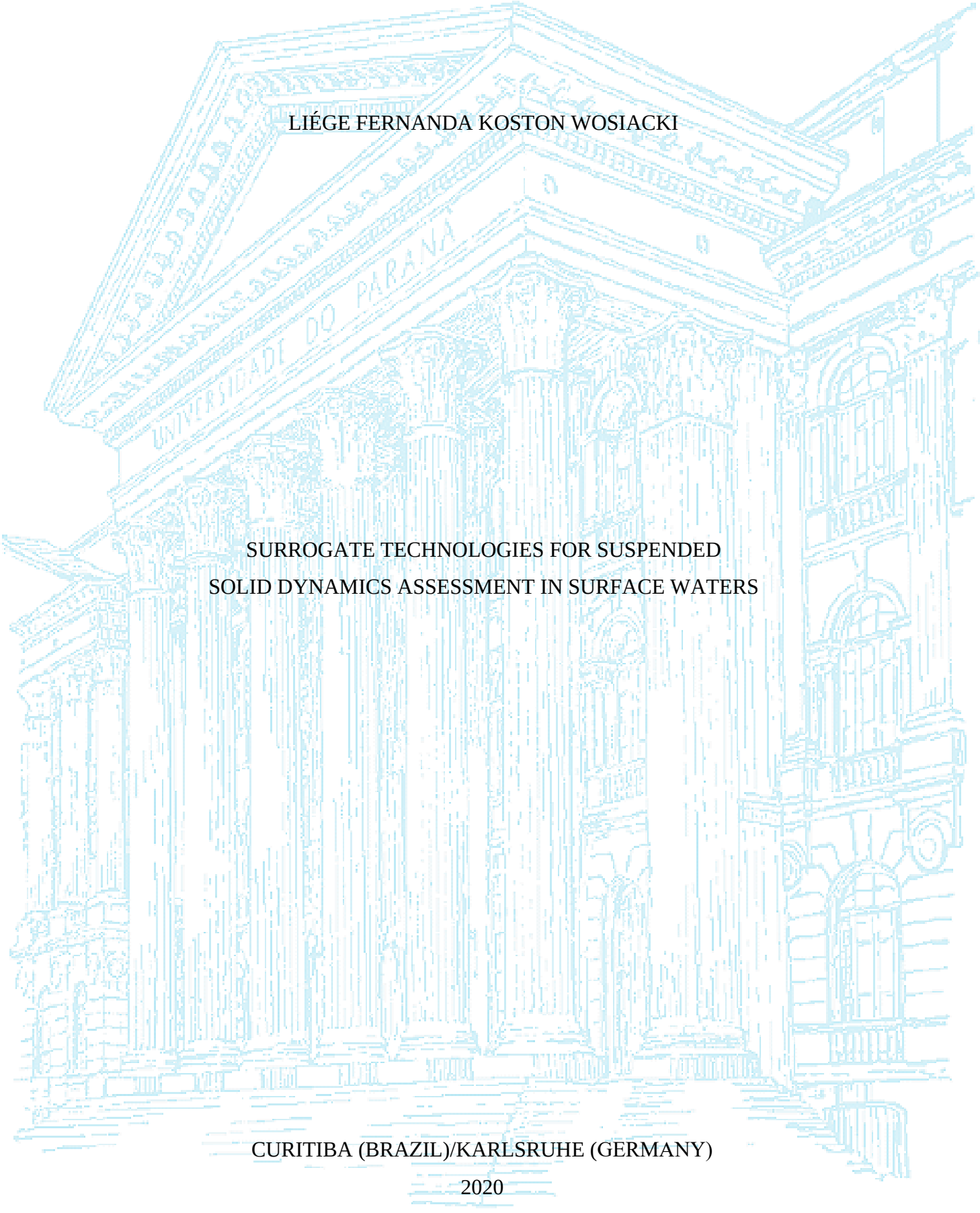

SURROGATE TECHNOLOGIES FOR SUSPENDED SOLID DYNAMICS ASSESSMENT IN SURFACE WATERS

CURITIBA (BRAZIL)/KARLSRUHE (GERMANY)

2020

LIÉGE FERNANDA KOSTON WOSIACKI

SURROGATE TECHNOLOGIES FOR SUSPENDED SOLID DYNAMICS ASSESSMENT IN SURFACE WATERS

Thesis submitted in partial fulfillment of the requirements of the Graduate Program on Water Resources and Environmental Engineering from Federal University of Paraná(UFPR), in Cotutelle Agreement between UFPR and KIT (Karlsruhe Institute of Technology, in Karlsruhe, Germany).

Supervisor: Dr-Ing. Tobias Bleninger (UFPR).

Co-Supervisor: Dr-Ing. Stephan Fuchs (KIT).

CURITIBA (BRAZIL)/KARLSRUHE (GERMANY)
2020

ACKNOWLEDGMENTS

First of all, I would like to thank my parents, Jeane and Wolney, for being always on my back, supporting me and lifting me up when things got difficult. Everything I do is to make you proud of me.

Special thanks go to Pedro, my husband, for all patience and support, even if it had costed my absence for long periods.

I also want to thank my colleagues from the "salinha", who become my friends — Felipe, Laís, Patrícia, Sabrina, Aninha and Lucas, for their support and for the funniest productivity environment, which made everything lighter.

Special thanks to Lediane and Luziadne, two gifts that this journey brought me. I have no words to thank you for being literaly at my side during the good and bad times. Thank you for your friendship and for always being there.

Thanks to my friend Lívia for all the coffee-breaks, partnership, friendship, advices, and for sharing the same passion for science with me.

Many thanks go to the entire PPGERHA family: Luciane and Prof. Heloíse and Carol Kozak for guiding me in my first steps in the lab. To Prof. Cristóvão for his kindness, his always exciting help in field campaigns and for many phylosophical questions. To Bruna Poli for your support and company when I first arrived in Germany. To all the amazing researchers that are part of this family who kindly shared their knowledge, their arms (on carrying all the equipment from the car to the lab, from the lab to the car) and their coffee (without coffee I don't know anything) during this journey.

Thanks to all my colleagues from Germany (from KIT and KLU - Koblenz-Landau University) and for the very good time I spent there with Mayra, Klajdi, Adrian, Stephan, Lisa, Jens, Wendy and Irina. Also, many thanks to Andreas Schenk, for helping me with the amazing opportunity to go to USGS/USA.

Thanks to my co-supervisor Prof. Stephan Fuchs for the brainstorming and revisions of manuscripts/thesis and for the efforts to make the double-degree possible. Thanks to my supervisor Prof. Tobias Bleninger for all patience, advices, support in difficult times and for sharing his knowledge and experience — either in the University or during the happy-hours.

This thesis and experiences wouldn't be possible without financial support from CAPES (Brazil) and GRACE (Germany).

"Todos temos dentro de nós
uma insuspeita reserva de força
que emerge quando a vida nos põe à prova."
(do livro A Ilha Sob o Mar — Isabel Allende)

ABSTRACT

In general, solids refer to the matter that is suspended or dissolved in water. It can result from the erosive processes in the watershed, such as runoff, bank erosion or from the riverbed, it can be formed by mineral, organic particles or a combination of both. Its dynamics in surface waters is bound to natural and anthropic processes within the watershed, as weathering or land use. Besides the environmental issues, the knowledge about solid dynamics is a fundamental tool in the assessment of the economic viability of several projects, such as the establishment and/or maintenance of a hydro way, a harbor, an irrigation canal or even the construction of a dam, for energy or water supply. However, despite all efforts and investments to obtain solid information through a robust sedimentometric network, conventional methods still do not always supply the needed information, either by operational, analytical or safety issues and because of it, the use of alternative technologies to obtain solid information in surface waters has been encouraged. Among them, it has been rising the use of acoustic methods, which are a non-intrusive technique that allows indirect quantification of suspended solids in high temporal and spatial resolution. Therefore, the proposed research aims to apply the existent methods based on the formulations proposed by Urick (1975), of the modified SONAR equation and validate a field-scale solid mapping technology using acoustic measurements with an ADCP (Acoustic Doppler Current Profiler) to obtain sedimentometric data in lotic and lentic systems. The main idea was to apply the solid-acoustic correlation methodology in two rivers (Taquari River in Mato Grosso do Sul State and at Passauna River, in Parana) and then apply the established settings first developed for the lotic environment, in a lentic environment: Passauna Reservoir (in the same watershed as Passauna River). Results have shown that the methods applied to lotic environments, with mostly non-cohesive content and high solid concentration, can be extended to a lentic environment, with mostly cohesive content and low solid concentration. Also, the results shown that the method applied has accomplished the objectives and it was possible to measure and identify solid variation throughout the water column, in all study sites, and longitudinal measurements at the lentic environment.

Key-words: Solids. ADCP. Surrogate-Tecnologies. Lentic-Environment.

ZUSAMMENFASSUNG

Feststofftransport im Wasser bezieht sich im Allgemeinen auf gelöste oder suspendierte Stoffe. Diese können aus erosiven Prozessen des Einzugsgebiets stammen, von Ufererosion oder auch aus dem Flussbett. Es handelt sich hierbei um mineralische, organische Partikel oder eine Kombination aus beiden. Die Feststoffdynamik in Oberflächengewässern ist an natürliche und anthropogene Prozesse innerhalb des Einzugsgebiets, wie Verwitterung oder Landnutzung gebunden. Neben den Umweltaspekten ist das Wissen über die Feststoffdynamik ein grundlegendes Instrument für die Beurteilung der Wirtschaftlichkeit mehrerer Projekte, z. B. der Errichtung und Instandhaltung einer Wasserstraße, eines Hafens, eines Bewässerungskanals oder des Baus eines Damms, zur Energie- oder Wasserversorgung. Herkömmliche Methoden zur Bestimmung der Konzentrationen und deren Verteilung entsprechen jedoch oft nicht den Erfordernissen in zeitlicher und räumlicher Auflösung. Eine vielversprechende Alternative basierend auf akustischen Methoden wurde in dieser Arbeit untersucht. Akustische Messungen können eine indirekte Quantifizierung suspendierter Feststoffe in hoher zeitlicher und räumlicher Auflösung ermöglichen. Daher zielt die vorgeschlagene Forschung darauf ab, die vorhandenen Methoden, die auf den von citeonline urick1975 vorgeschlagenen Formulierungen der modifizierten Schallausbreitungsgleichung basierend, anzuwenden. Ziel ist es Feststoffkonzentrationen flächig im Feldmaßstab zu erfassen. Hierfür wurde Messungen mit einem akustischen ADCP (Acoustic Doppler Current Profiler) durchgeführt. Zur Validierung wurden konventionelle Messungen zur Feststoffkonzentrationsbestimmung durchgeführt. Untersuchungen wurden in Fliessgewässern und einem Stausee, somit unter unterschiedlichen Strömungsbedingungen durchgeführt. Die Untersuchungsgebiete waren im Taquari-Fluss (Pantanal, Brasilien) und Passauna Fluss (Curitiba, Brasilien), sowie dem Passauna Stausee (Curitiba, Brasilien). Die Ergebnisse haben gezeigt, dass die Methoden, die auf Fließgewässer mit größtenteils nicht kohäsivem Material und hohen Feststoffkonzentrationen angewendet wurden, auch auf ein stehendes Gewässer mit größtenteils kohäsivem Material und niedrigeren Feststoffkonzentrationen ausgedehnt werden können. Die angewandte Methodik wurde dann herangezogen, um die Messergebnisse hochaufgelöst über Fließquerschnitte darzustellen, oder über Transekte im Falle der Stauhaltung. Diese gaben Aufschluss über Transportwege und Bereiche mit höherer und niedriger Konzentration.

Schlüsselworte: Feststoffe. ADCP. Ersatztechnologien. Sedimenttransport.

RESUMO

De maneira geral, o termo sólidos refere-se à matéria que encontra-se suspensa ou dissolvida na água, resultante dos processos erosivos que ocorrem na bacia hidrográfica, pela erosão do leito e das margens ou que são carreados por escoamento superficial. Os sólidos podem ser formados por partículas minerais, orgânicas ou por uma combinação desses, e sua dinâmica em águas superficiais está vinculada a processos naturais e antrópicos na bacia, tais como intemperismo ou pelas diferentes formas de uso do solo. Além de questões relativas ao meio ambiente, o conhecimento sobre sua dinâmica é uma ferramenta fundamental na avalição da viabilidade econômica de diferentes projetos, tais como implantação ou manutenção de uma hidrovia, de um porto, de um canal de irrigação, na construção de barramentos, entre outros. No entanto, apesar de todos os esforços e investimentos para que seja estabelecida uma robusta rede de monitoramento, os métodos convencionais implantados na maioria dos postos nem sempre suprem a necessidade de informações, seja por questões operacionais, analíticas ou de segurança. Dessa forma, nos últimos anos o uso de tecnologias alternativas para obter informações de sólidos em águas superficiais vem sendo estimulado. Entre elas, tem-se o uso de métodos acústicos, uma técnica não intrusiva que permite quantificar indiretamente os sólidos em suspensão em alta resolução temporal e espacial. Assim sendo, propôs-se no presente estudo o desenvolvimento de uma tecnologia do mapeamento dos sólidos em suspensão usando medidas acústicas com um ADCP (Perfilador Acústico Doppler) para obter dados hidrosedimentológicos em sistemas lóticos e lênticos, tendo como base o modelo da equação modificada do SONAR proposta por Urick (1975). A ideia principal foi aplicar a metodologia que correlaciona a concentração dos sólidos suspensos com o sinal acústico em dois rios (rio Taquari, no Mato Grosso do Sul e no rio Passauna, no Paraná) e, em seguida, aplicar as configurações previamente estabelecidas nesses ambientes ao reservatório do Rio Passauna (à jusante da seção considerada como ambiente lótico do Rio Passauna). Os resultados mostraram que os métodos aplicados a ambientes lóticos, com um teor significativo de sólidos não coesivos e alta concentração de sólidos, podem ser estendidos ao ambiente lêntico, com teor significativo de sólidos mais finos (mais coesivos, propensos aos processos de agregação e desagregação) e baixa concentração de sólidos. Além disso, os resultados mostraram que foi possível medir e identificar variações de sólidos ao longo da coluna de água dentro da seção transversal, em todos os locais de estudo e nas medições longitudinais, de montante para jusante, no ambiente lêntico.

Palavras-chave: Sólidos. ADCP. Tecnologias-Alternativas. Ambientes-Lênticos.

LIST OF FIGURES

Figure 1 – Modes and mechanisms of solid transport, where τ is the streamflow shear stress. . . . 24
Figure 2 – Suspended load transport profiles. . . . 25
Figure 3 – Solid Deposit Formation in the transitional zone between lotic and lentic environments. . . . 26
Figure 4 – Density Current Formation: a transition from non-stratified to stratified flow. . . . 28
Figure 5 – The behavior of a gravity current in a two-layered stratified environment: (a) interflows (b) underflows, and (c) split flows. . . . 29
Figure 6 – (a) Sampling by Equal Width Increment (EWI), where the sampled volume (V_{EWI}) is proportional to the discharge and the Transitional Rate (TR_{EWI}, which is the sampling velocity) is constant at each vertical and (b) Sampling by Equal Discharge Increment(EDI), where the sampled volume (V_{EDI}) is equal and the Transitional Rate (TR_{EDI}, which is the sampling velocity) is different, proportional to water velocity, at each vertical. . . . 30
Figure 7 – Solid Series. . . . 31
Figure 8 – Wave sound propagation and related parameters. . . . 32
Figure 9 – Emitted pulse and reflected backscatter. . . . 34
Figure 10 – Velocity components measurement. . . . 35
Figure 11 – Measured Area and Cross-Section component. . . . 36
Figure 12 – Operating scheme of LISST equipment series - diffraction laser. . . . 38
Figure 13 – Examples of bias in the LISST volumetric concentrations produced by the presence of out-of-range particles (for LISST-100X, version). . . . 39
Figure 14 – Water-solid system described with a cycle of erosion, transport, deposition and consolidation, involved in particle aggregation/disaggregation and sorption/adsorption of contaminants. Below the scheme, the corresponding influence factors and the respective properties are presented. 39
Figure 15 – Spatial distribution of a) flow velocity, b) SSC and c) Suspended Load. Adapted from: Baranya and Józsa (2013). . . . 43
Figure 16 – Density current formation recognized by Haun and Lizano (2016) at Peñas Blancas reservoir, in Costa Rica. . . . 44
Figure 17 – Density current formation measured by Umeda, Yokoyama and Ishikawa (2006) by echosounder and ADCP measurements at Shichikashuku reservoir, in Japan. . . . 45

Figure 18 – Summary of the proposed methodology to be presented in the following sections. 49
Figure 19 – Taquari River Location and the Monitored Cross-section. 50
Figure 20 – Mean Precipitation and Discharge at Taquari River at Coxim Station (Code:1854004). 51
Figure 21 – Passauna Basin Location. 52
Figure 22 – Mean Precipitation and Discharge at Passauna River at Colonia Dom Pedro Station (Precipitation Data) and BR-277-Campo Largo Station (Discharge Data). 53
Figure 23 – Study Area. 54
Figure 24 – Comparison of the water color in the study area among different days: (a)March 5th, 2019 and (b) January 21th, 2018 55
Figure 25 – Longitudinal Transect and Cross-section sketch at Passauna Reservoir. 56
Figure 26 – ADP-M9 features. Adapted from: Sontek (2016). 57
Figure 27 – LISST-200x with the battery attached. 59
Figure 28 – Water Sampler Devices (a) USD-49 and (b) Van Dorne. 60
Figure 29 – Filtration System and Filters after analysis at Vertical 3 at Ferraria's Bridge from the 4th campaign (04/23/2018). 61
Figure 30 – Backscatter correction flowchart. 64
Figure 31 – Operational scheme used in the algorithm point sampling method analysis. 65
Figure 32 – LISST processing flowchart. 67
Figure 33 – (a) Mean velocity profiles during all measurement campaigns, Horizontal velocities during the measurement campaigns of (b) May/17 and (d) July/17 and Mean Backscatter Signal obtained during the measurement campaigns of (c) May/17 and (e) July/17. 69
Figure 34 – Relation between the parameters obtained during the campaigns. P7 is the accumulated precipitation registered from 7 days before the measurement campaign. All parameters's values were arranged from the lowest measured discharge to the highest measured discharge. 70
Figure 35 – Granulometric Curve for Taquari River. 71
Figure 36 – Correlation curve between SSC and ADCP corrected backscatter signal (CBS) at Taquari River. 72
Figure 37 – Measured ADCP signal in the cross-section: (a) without the 1MHz measured cells and (b) with the 1MHz cells filled with the extrapolations obtained by the average of the signal measured by the 3MHz cells. . . . 73
Figure 38 – Non-Extrapolated and Extrapolated Cross-Section, data from April/17: (a) Non-Extrapolated SSC, (b) Extrapolated SSC, (c) Non-Extrapolated Qss, (d) Extrapolated Qss. 76

Figure 39 – Granulometric Curve for Passauna River. 78
Figure 40 – Relation between the parameters obtained during the campaigns. P7 is the accumulated precipitation registered from 7 days before the measurement campaign. All parameters's values were arranged from the lowest measured discharge to the highest measured discharge. 79
Figure 41 – Correlation curve between SSC and ADCP corrected signal at Passauna River. 79
Figure 42 – Mapping throughout the cross-section: (a) TSS from Aug/18 and (b) Qss from Aug/18, (c) TSS from 18Oct/18 and (d) Qss from 18Oct/18. 82
Figure 43 – Ferraria Bridge point sampling points location. 83
Figure 44 – Granulometric Curve at Ferraria Bridge. 84
Figure 45 – Relation between the parameters obtained during the campaigns. P7 is the accumulated precipitation registered from 7 days before the measurement campaign and the yellow boxes represent the upper and lower limits of the TSS laboratory analysis in each campaign, considering the sampling distribution presented at Figure 43. All parameters's values were arranged from the lowest measured precipitation data to the highest measured precipitation data. 85
Figure 46 – Correlation curve between SSC and ADCP corrected signal at Ferraria Bridge. 86
Figure 47 – Comparison between extrapolated and no-extrapolated TSS at Ferraria Bridge in Aug/17 (dry situation) and in 18Oct/18 (rainy situation). . . 88
Figure 48 – Longitudinal transects and point measurements througout the transects. 89
Figure 49 – Feb/18 monitoring campaign: (a) Temperature Profiles from Buffer, Ferraria bridge (FB) and PPA points, (b) Longitudinal Transect and (c) Ferraria Bridge Cross-Section. All values exposed in the transects are TSS in mg/L. 90
Figure 50 – 18Oct/18 monitoring campaign: Ferraria Bridge Cross-Section Mapping and Temperature Profile. 91
Figure 51 – 20Oct/18 monitoring campaign: (a) Temperature Profiles from Ferraria bridge (FB) and PPA points, (b) Longitudinal Transect and (c) Ferraria Bridge Cross-Section. All values exposed in the transects are TSS in mg/L. 92
Figure 52 – 05Feb/19 monitoring campaign: (a) Temperature Profiles from Ferraria bridge (FB) and PPA points, (b) Longitudinal Transect and (c) Ferraria Bridge Cross-Section. All values exposed in the transects are TSS in mg/L. 93

Figure 53 – Granulometry from Grab (G) and Cores (C) obtained by Sotiri, Hilgert and Fuchs (2019) at Passauna Reservoir. Adapted from: Sotiri, Hilgert and Fuchs (2019). 94
Figure 54 – Comparisons of the measurements performed on 18Oct/18 among numerical modeling for (a) Temperature and (b) Tracer Normalized Concentration (courtesy from Wendy Gonzales) and (c) the mapped cross-section made with the ADCP already discussed at Figure 50. 96
Figure 55 – Comparisons of the measurements performed on 20Oct/18 among numerical modeling for (a) Temperature and (b) Tracer Normalized Concentration (courtesy from Wendy Gonzales) the mapped longitudinal transect and (d) the mapped cross-section made with the ADCP, both already discussed at Figure 51. 97
Figure 56 – Comparisons of the measurements performed on 04Feb/19 among numerical modelling for (a) Temperature and (b) Tracer Normalized Concentration (courtesy from Wendy Gonzales), (c) the TSS in the water surface obtained by close remote sensing, after Wagner (2019), (d) a composition obtained by drone images (courtesy from Jens Kern) and (e) the ADCP mapped cross-setion obtained at the presented study. . . 98
Figure 57 – Comparisons of the measurements performed on 05Feb/19 among numerical modeling for (a) Temperature and (b) Tracer Normalized Concentration (courtesy from Wendy Gonzales), (c) the TSS in the water surface obtained by close remote sensing, after Wagner (2019), (d) the mapped longitudinal transect and (e) the mapped cross-section made with the ADCP, both already discussed at Figure 52. 99

Figure 58 – Optical Transmission. 118
Figure 59 – Scattering Data for LISST200x (a) before and (b) after the filtering application. 118

Figure 60 – Mean discharge and mean solid concentration during the field campaigns. 121

Figure 61 – Mapped cross-section in Mar/17 (a) TSS, (b)Qss and in Apr/17 (c) TSS, (d) Qss. 122
Figure 62 – Mapped cross-section in May/17 (a) TSS, (b)Qss and in June/17 (c) TSS, (d) Qss. 123
Figure 63 – Mapped cross-section in July/17 (a) TSS, (b)Qss and in August/17 (c) TSS, (d) Qss. 123
Figure 64 – Mapped cross-section in Jan/18 (a) TSS, (b)Qss. 124
Figure 65 – Mapped cross-section in May/17 (a) TSS, (b)Qss and in Apr/18 (c) TSS, (d) Qss. 125

Figure 66 – Mapped cross-section in Aug/18 (a) TSS, (b)Qss and in 18Oct/18 (c) TSS, (d) Qss. 125
Figure 67 – Mapped cross-section in 20Oct/18 (a) TSS, (b)Qss. 126
Figure 68 – Mapped cross-section in (a) Aug/17, (b) Feb/18, (c) 18Oct/18 and (d) 20Oct/18. 127
Figure 69 – Mapped cross-section in (a) 04Feb/19, (b) 05Feb/19 and (c) Apr/19. . 127

LIST OF TABLES

Table 1 – Density of Water and Solid Mixtures (kg/L) as a function of Temperature and Solid Concentration (mg/L). Adapted from Morris and Fan (1998). 27
Table 2 – Wave sound velocities at $1atm$. Adapted from Halliday and Resnick (2009). 33
Table 3 – Most recent studies regarding surrogate technologies application for SS and density currents determination. 46
Table 4 – Summary of the instrumentation and related measured parameters in each Study Area. 62
Table 5 – Backscatter correction functions descriptions. 63
Table 6 – Mean parameters evaluated during the Moving bed analysis. 68
Table 7 – Mean discharge and mean solid concentration during the field campaigns. 70
Table 8 – Comparison between the solid attenuation coefficients per campaign: α_s, total solid attenuation; α_{ss}, scattering attenuation and α_{sv}, viscous attenuation. 72
Table 9 – Comparison between the SSC obtained from the laboratory analysis and the SSC obtained from the CBS regression and 1MHz-measured areas filled in with nearby 3MHz data — SSC units in mg/L. 74
Table 10 – Difference between the measured SSC and the SSC obtained from ADCP correlation - considering the results without any extrapolations and with extrapolations — SSC units in mg/L. 74
Table 11 – Difference between the measured Qss and the Qss obtained from ADCP correlation - considering the results without any extrapolations and with extrapolations — Qss units in $10^3 Ton/day$ 75
Table 12 – Mean discharge and solid parameters during the field campaigns. 77
Table 13 – Comparison between the solid attenuation coefficients per campaign: α_s, total solid attenuation; α_{ss}, scattering attenuation and α_{sv}, viscous attenuation. 80
Table 14 – Difference between the TSS from laboratory and the TSS obtained from ADCP correlation at Passauna River. Units in mg/L. 80
Table 15 – Difference between the Qss from laboratory and the Qss obtained from ADCP correlation at Passauna River. Units in Ton/day. 81
Table 16 – Mean parameters measured in the V2 vertical. 84
Table 17 – Ferraria Bridge spatial resolution water sampling points per campaign. . 84

Table 18 – Comparison between the solid attenuation coefficients per campaign: α_s, total solid attenuation; α_{ss}, scattering attenuation and α_{sv}, viscous attenuation. 87
Table 19 – Difference between the TSS from laboratory and the TSS obtained from ADCP correlation at Passauna Reservoir. Units in mg/L. 88
Table 20 – Relative Error between the Smart Pulse and Fixed mode – comparison between 3MHz. 120

TABLE OF CONTENTS

1 Introduction . . . 19
1.1 Hypothesis and Objectives . . . 21
1.1.1 Structure of the work . . . 21

2 Theoretical Background . . . 23
2.1 Solid Dynamics . . . 23
2.1.1 Lotic Environments . . . 23
2.1.2 Lentic Environments . . . 25
2.2 Suspended Solids Monitoring Techniques . . . 29
2.2.1 Conventional Methods . . . 29
2.2.2 Surrogates Technologies . . . 31

3 Recent Publications Overview . . . 41
3.1 The use of combined surrogate technologies to determine Solid Concentration 41
3.2 Surrogate technologies applied to a lentic environment . . . 44
3.3 Summary of the combined surrogate technologies . . . 45
3.4 Summary . . . 46

4 Materials and Methods . . . 48
4.1 Site Description . . . 49
4.1.1 Lotic Environments: Taquari River and Passauna River . . . 49
4.1.1.1 Taquari River . . . 49
4.1.1.2 Passauna River . . . 52
4.1.2 Lentic Environment: Passauna Reservoir . . . 54
4.2 Instrumentation and field procedures . . . 56
4.2.1 Acoustic Doppler Current Profiler (ADCP) — ADP-M9 . . . 57
4.2.2 Laser In-Situ Scattering Transmissiometer - LISST . . . 58
4.2.3 Water Sampling Instruments and Laboratory Analysis . . . 59
4.3 Data Processing . . . 61
4.3.1 Backscatter Correction — dB2SS code . . . 62
4.3.2 LISST data processing and analysis . . . 65

5 Results and Discussions . . . 68
5.1 Taquari River . . . 68
5.1.1 Velocity, backscatter and SSC distribution . . . 68
5.1.2 Backscatter Correlation for Taquari River . . . 71
5.1.3 Mapping of Suspended Solid Concentration . . . 72

5.1.3.1 Extrapolation for non-measured regions . . . 73
5.1.4 Summary . . . 76
5.2 Passauna River . . . 77
5.2.1 Backscatter Correction . . . 79
5.2.2 Mapping of Total Suspended Solid Concentration . . . 80
5.2.3 Summary . . . 82
5.3 Passauna Reservoir . . . 83
5.3.1 Backscatter Corrections . . . 86
5.3.2 Mapping of Total Suspended Solid Concentration . . . 87
5.3.2.1 Longitudinal transects . . . 89
5.3.3 Comparison within other TSS studies conducted at Passauna Reservoir . . . 95
5.4 Discussion . . . 100
5.4.1 Summary . . . 101

6 Conclusion and Outlook . . . 103
6.1 Improvements for solid measurements in a Lotic Environment . . . 103
6.2 Development of the method for Lentic Environment . . . 104
6.3 Recommendation for future work . . . 106

Bibliography . . . 107

Appendix 113

APPENDIX A ADP-M9 Backscatter Attenuation Corrections . . . 114

APPENDIX B LISST-200X Processing Analysis . . . 117
B.1 In-situ technique and data treatment . . . 117
B.2 Sensor Corrections . . . 117

APPENDIX C ADP-M9 Verification of frequency at different operation modes 120

APPENDIX D Mapping Results . . . 122
D.1 Taquari River Mapped cross-setion . . . 122
D.2 Passauna River Mapped cross-setion . . . 125
D.3 Ferraria Bridge Mapped cross-setion . . . 127

1 Introduction

The sedimentological dynamics in surface waters is a complex phenomenon and it is bound to the ecological and anthropic processes within the watershed. The sediments present in a water body are solid particles resulting from the erosive processes in the watershed, bank erosion or from the riverbed itself which can be formed by mineral or organic particles (e.g. pieces of shells, leaves, animals, etc.). With this in mind, from now on the term sediment will be replaced by the term solid through this document.

In the social context, along with populational growth, it is also observed the rising pressure on water resources. Therefore, the knowledge about erosion, movement, and sedimentation processes within a watershed is important not only for environmental studies but also to assess the economic feasibility of numerous engineering projects (LIMA et al., 2001) which are planned especially in the BRICS (Brazil, Russia, India, China, South Africa) countries. For instance, knowledge on solid transport dynamics is important for the planning and maintenance of a waterway, harbors, irrigation channels, and especially for hydropower and drinking water reservoirs.

The construction of a dam in a river causes an interruption of the river flux, resulting in flow velocity reduction and increase in solids deposition along the reservoir, which will lose its storage capacity and increase system degradation. Hence, knowledge about solids (quantification and transport characteristics) in these environments makes possible to understand how to proceed in the soil conservation practice programs, check dams safety and the mechanisms of bypass and sluicing, practices often used to reduce solids inflow or remove settled solids from a reservoir (USBR, 2006). So, regardless of the ending purpose of such constructions, the knowledge of its lifetime and water quality is bounded to the sediment load in the water.

Measurements of solids in water bodies, however, are a challenge when requiring results for large regions (all over a reservoir or a river branch) and in addition to sufficient temporal resolutions to be able to describe dominant solid transport mechanisms. Therefore, knowledge is important for engineering measures, such as river training methods, dredging, bank protection, reservoir and dam design, etc. Current techniques are based on taking water samples, which are analyzed for solid concentrations in the laboratory. For example, Brazil has nowadays about 1685 sedimentometric monitoring stations (ANA, 2020). However, high uncertainties are usually reported and several research questions arise:

- Are the measurement frequencies and methods sufficient for describing solid dynamics?

- Are there differences between in-situ concentrations and results obtained by sampling and laboratory analysis?
- Are there reliable techniques for in-situ analysis?
- Are there methods to allow measurements over large regions and subsequent mapping of the results?
- Can those methods detect phenomena such as turbidity currents or sediment plumes in reservoirs?

A very promising approach to tackle those questions is the use of surrogate technologies (alternative in-situ methods) to measure solid transport dynamics.

Some of the current trends are related to the use of Remote Sensing Analysis on large scale by using satellite images (MONTANHER; NOVO; BARBOSA, 2013), on a medium scale, by using airborne photogrammetry (ROIG et al., 2013; OLIVETTI, 2020) or on a local scale by using, for example, a hyper-spectrometer sensor or a common camera (MOSBRUCKER et al., 2015; WAGNER, 2019). The disadvantages of those are their limitations on water surface measurements only. Other optical-based surrogate technologies overcoming this limitation are turbidimeters or optical diffraction devices (e.g. the LISST equipment — Laser In-situ Scattering Transmissiometer), which however are limited to point measurements and are not easily applicable for mapping applications. In that sense the use of acoustic profilers, e.g. ADCPs, are the most considered, offering an additional advantage in providing not only results for solid concentration, but also 3D velocity profiles and turbulence characteristics.

Acoustic profiling techniques are considered non-intrusive and allow indirect quantification of suspended solids in high temporal and spatial resolution (Guerrero et al., 2016). They also can be an important tool to obtain sediment information during extreme rain events, when it is not safe to measure with conventional techniques (SZUPIANY et al., 2019).

As described by Wood and Teasdale (2013), Landers et al. (2016), and Szupiany et al. (2019), surrogate technologies can be a cost-effective component of a long-term solid monitoring program. Once a regression model is developed between surrogate data and suspended solid obtained in the laboratory, samples can be collected in less spatial or temporal resolution, reducing long-term operation and maintenance costs.

However, so far, this methodology has become operational only for side-looking ADCPs (MOORE et al., 2013; LANDERS et al., 2016) and only in river cross-sections, where it is possible to assume that the solid concentration is uniform at the same depth within a measured cross-section. In the past few years, interest has risen in using down-looking moving ADCP measurements to capture the variation of solid concentrations in

the water column and all along the driven trajectory. First tests are reported in, first — Guerrero, Szupiany and Amsler (2011); Baranya and Józsa (2013); Guerrero et al. (2016) and Haun and Lizano (2018), however mainly related to applications in lotic environments with high flow velocities associated to high solid concentrations with mostly sand content. This thesis thus aims to fill the gaps and assess the feasibility of solid concentration mapping in lentic environments, using an ADCP.

1.1 Hypothesis and Objectives

Considering that the solid-acoustic analysis has already been developed for lotic environments (i.e. river cross-sections), this study's objective is to assess the feasibility and limitations to using acoustic measurements (by down-looking moving ADCP measurements) to map solid concentration and transport information in a lentic environment.

Expected results are mapped solid concentrations in different environments including information on solid characteristics (fine and cohesive solid particles and lower concentrations) and comparisons with rivers (coarser solid content and higher concentrations). In addition, the mapped concentration is used to describe dominant transport processes and pathways for river inflows into reservoirs (turbidity currents or density currents).

In order to achieve those objectives, a field-scale solid mapping technology using acoustic measurements to obtain hydro sedimentological data at reservoir inflows will be developed and validated.

The specifics objectives are:

- To apply and validate the ADCP backscatter processing method to obtain suspended solid concentrations (SSC) and transport characteristics in fluvial (lotic) environments.
- Extension and enhancement of the ADCP backscatter processing method to obtain total solids concentration (TSS) in a reservoir (lentic) environment including density effects (reservoir stratification and turbidity or density current).
- Development of a mapping technology applying the backscatter processing to longitudinal and transversal section measurements to identify and quantify turbidity/density current formations.

1.1.1 Structure of the work

This document, is structured in 6 chapters including:

- The present Chapter: Introduction (Chapter 1), where it is presented the problematics around solids monitoring and where it is given an overview about the current study and also presented the hypothesis and objectives.
- Chapter 2, where it is going to be presented the theoretical background about the subject, presenting some concepts of the that have been widely studied.
- Chapter 3 presents the most recent contributions in the proposed subject, presenting some studies related to lotic and lentic environments in the past feel years.
- Chapter 4 explains extensively the methodology applied in the field measurement campaigns, the laboratory procedures and the acoustic post-processing analysis to obtain the correlations and mapping of the monitored cross-sections.
- At Chapter 5 it is presented the results and discussions about the results obtained in these environments.
- And finally, Chapter 6 where is presented the closure of the work with a summary of the main findings and an outlook for future researches to improve the acoustics analysis.

2 Theoretical Background

Often, the dynamic of solids is pointed out as the cause of many engineering problems, such as shortening of reservoirs lifetime, soil losses, mud related to flood events, among others.

Although there is evidence in history that men built systems of canals for many purposes (the irrigation canals in Mesopotamia, reservoirs in Egypt, rivers regulations in China and many other hydraulics constructions in Greece, Persia, India and Roman Empire) the influence of the solid over the flow has been studied only recently. According to Graf (1984), solids influence and interaction were first scientifically noticed only during the Renaissance period, when many scientists tried to describe the flow resistance as a solid-liquid interfacial problem.

2.1 Solid Dynamics

2.1.1 Lotic Environments

Solid transport in rivers is a complex phenomenon and is bound to the ecological and anthropical processes within the watershed, such as the presence of agricultural activities, urbanization, the presence of highways, waterways, harbors, among others. All of these processes can contribute to solid yield, which can be up to 200 $ton/km^2/year$ in tropical countries (LATRUBESSE; STEVAUX; SINHA, 2005).

According to APHA (1999), which gives the guidelines for laboratory analysis, solids refer to matter suspended or dissolved in water or wastewater and can be characterized by: its concentration (massic concentration — mass per volume: mg/L, or volumetric concentration — volume of solids per water volume: mL/L, μ/L), size (radius or diameter, in μm or mm) and load (usually given in mass per time: kg/sec, Ton/day). The methods to determine each one of the aforementioned characteristics are going to be deeply discussed further.

The path of a solid particle involves processes related to the *disaggregation* of a consolidated material (eg. soil or rock), in small particles with different sizes. Therefore, these particles will be carried out from an *erosion* process influenced by the stream-flow. According to Rijn (1984), a solid particle will be carried out if the sedimentation velocity is lower than the vertical eddy velocity, caused by turbulence, responsible to maintains it in suspension.

In hydraulic systems, the transport of solid matter can be classified in different modes and mechanisms. According to Figure 1, in a streamflow, the particles can be carried on the bottom (*bedload*) or suspended in the water column (*suspended load* and

wash load[1]), depending on the size of the particle and the flow conditions.

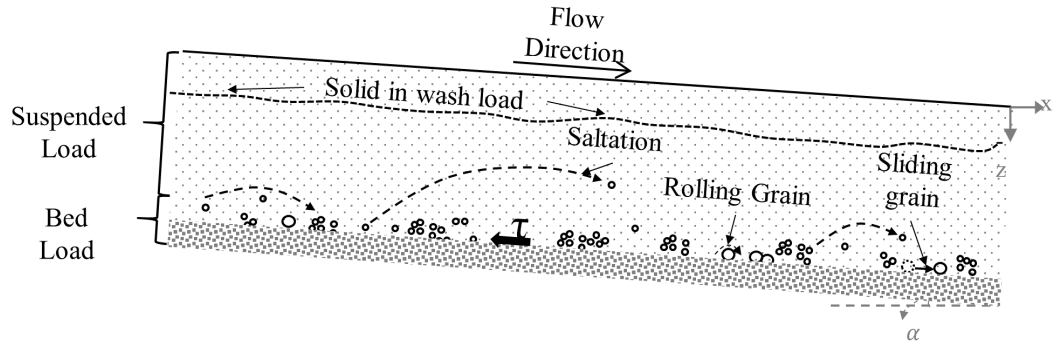

Figure 1 – Modes and mechanisms of solid transport, where τ is the streamflow shear stress.

Adapted from: Graf (1998).

Bedload is related to the larger particles and the transport mechanism can occur by a successive motion of rolling, sliding and saltating processes. The suspended load is related to the smaller particles and in this kind of transport the particles stay occasionally in contact with the bed, but most of the time the particles are suspended in the water column. As a result, in practical terms, the sum of these two kinds of mechanisms gives the Total Load.

To quantify solid transportation a great number of formulations and methods have been studied and applied throughout the years, most of them based on experimental results. Some of them are related only to the bed-load, the suspended load or the total load, which are in general the result of the sum of bed-load and suspended load.

If we are interested in the erosion/deposition process it is necessary to apply bed-load equations with different considerations. For example, a group of formulations given by Meyer-Peter and Müeller (1948) and Shields (1936), take into account the shear stress (τ) over the bed and the mean flow velocity. A second, and more complex group, considers turbulence as the main flow characteristic that leads to solid transportation in the bed. A third group, with proposed formulations by Bagnold (1966), Engelund and Hansen (1967) and Yang and Stall (1974), considers a relation between bed-load and flow potential.

At this point it is important to highlight that the equations describe the cross-sectional averaged transport, using cross-sectional averaged hydrodynamic parameters, which do not allow to map the transport characteristics, as proposed in this study.

It is important to consider that, although the use of such equations depends on a good field data collection, each formulation was developed for a specific flow range and morphological conditions, so their use must respect their hypothesis, simplifications and characteristics to be applied to the study location (SANTOS et al., 2001).

[1] This kind of load does not depend on the streamflow, it is part of an unpredictable load.

Regarding suspended load (Qss), we consider that particles are kept suspended by turbulence. As highlighted by Graf (1984) suspended load is always accompanied by bedload and the transition between the two modes of transport is gradual.

To predict the suspended load it is necessary to obtain the velocities and the solids concentration in the water column. Assuming a steady flow development, Figure 2 shows the profiles of both parameters and therefore the suspended load resulting profile.

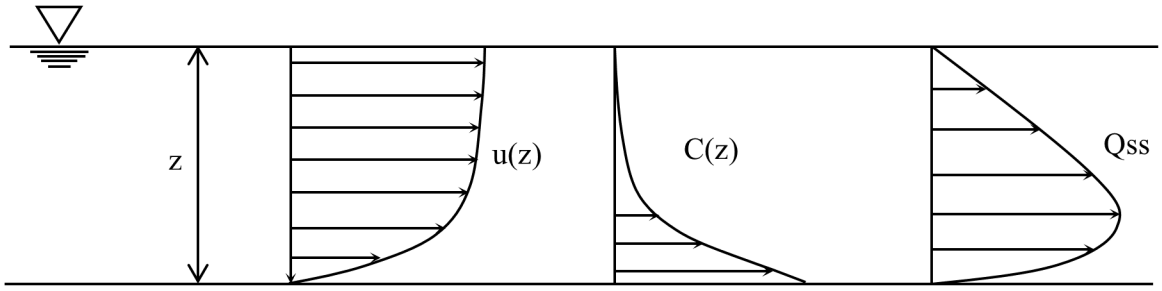

Figure 2 – Suspended load transport profiles.

Adapted from: Carvalho et al. (2000b)

As pointed out by Santos et al. (2001), the temporal solid distribution is related to the flow discharge: the larger the discharge the bigger the concentration of solids in the water column (equation 2.1). Although this relation is not always linear, it is possible to describe it as a solid rating curve, which makes possible to estimate the suspended load over time — so the bigger the amount of solid and discharge data available, the more reliable the suspended load estimative.

$$Qss = \int_{z_0}^{z} \int_{y_0}^{y} \int_{x_0}^{x} C_s(x, y, z) \cdot u(x, y, z) dx dy dz, \tag{2.1}$$

where Q_{ss} is the suspended load, $C_s(x, y, z)$ is the concentration and $u(x, y, z)$ is the velocity profile. Both vary in all dimensions: over the depth, from z_0 to z and in the both directions (x and y): from x_0 to x and from y_0 to y.

2.1.2 Lentic Environments

As the river flows into a lake or a reservoir the cross-sectional area enlarged and the flow velocity decreases. These characteristics reduce the stream solid transport capacity and lead to a sedimentation process that can happen immediately in the river mouth and throughout the reservoir length. Figure 3 sketches the transitional zone — from the lotic to the lentic environment, indicating the morphological changes of the region that are going to be briefly described in the sequence.

According to Shotbolt, Thomas and Hutchinson (2005) sedimentation processes, in a lentic environment, can be classified into primary and secondary processes, where primary processes refer to the initial deposition at the entrance of the reservoir (the topset bed and foreset bed formation from Figure 3) and the secondary processes are related to the resuspension and redistribution of previously deposited solids.

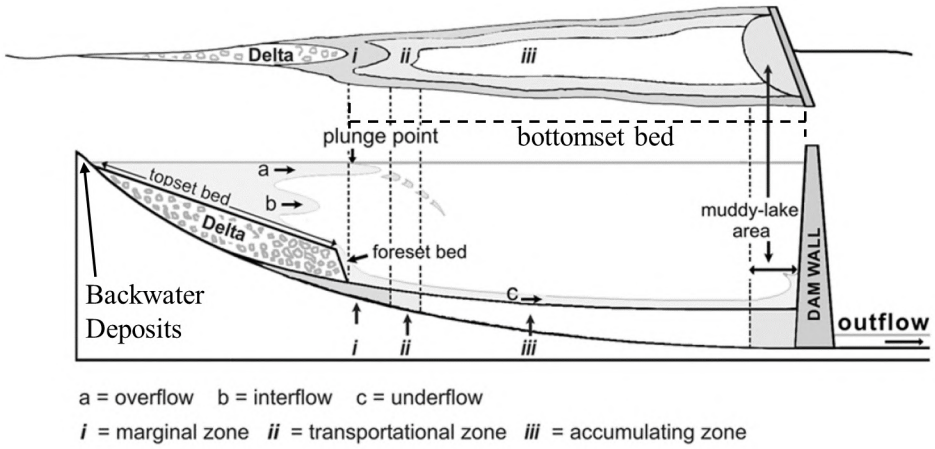

Figure 3 – Solid Deposit Formation in the transitional zone between lotic and lentic environments.

Adapted from Carvalho et al. (2000b),Morris and Fan (1998) and Shotbolt, Thomas and Hutchinson (2005).

As enumerated by Morris and Fan (1998), the topset bed corresponds to delta deposits due to the settling of the solid material that comes with the flow. The settled material can vary from coarse solids (sand) or may also contain a large fraction of finer solids (as silt and clay). Still, according to Morris and Fan (1998), the foreset bed represents the face of the delta advancing into the reservoir with a steeper slope and finest material.

Carvalho et al. (2000a) consider an additional morphodynamics formation, which is also part of the topset bed, called backwater deposit. This formation configures a deposit formation still in the fluvial system before it enters the reservoir. The authors also point out that this kind of formation can be responsible for flood events in the upstream, while those deposit formations inside the reservoir, cited by Morris and Fan (1998), are responsible to decrease the reservoir storage capability.

Another formation that happens after the delta, in the bottomset zone, is the bed deposits, which is also part of the delta formation. Depending on the length and configuration of the reservoir that formation can reach the dam and cause damages in its components (Morris and Fan (1998)).

Considering the system dynamics, these zones are not temporal or spatial stable. During flood events, for instance, the delta can accumulate large volumes of solids and

after that, during a drawdown situation, the deposits can be reworked into an equilibrium state due to a typical situation of morphodynamic-flow interaction.

As the water goes from the river towards the reservoir, besides the aforementioned changes in the morphodynamics of the water body there are some phenomena related to hydrodynamics, such as density current formations that can be responsible for the sedimentation pattern and spread over the reservoir.

Density Currents

Density currents occur due to the density difference between two fluids. According to Morris and Fan (1998), differences in both: temperature and solid concentration contribute to stratification in a reservoir, Table 1 shows the effect of the suspended solid on density and how it can vary with temperature. Still, according to the same authors, turbidity density currents occurs when the solid enters in a reservoir and plunge in clean water and travels down along the talweg in the reservoir.

Table 1 – Density of Water and Solid Mixtures (kg/L) as a function of Temperature and Solid Concentration (mg/L). Adapted from Morris and Fan (1998).

Temperature	Pure Water	Water + Solid		
		1000 mg/L	10 000 mg/L	100 000 mg/L
0	0.9998	1.0004	1.0061	1.0621
4	1.0000	1.0006	1.0062	1.0622
10	0.9997	1.0003	1.0059	1.0620
20	0.9982	0.9989	1.0044	1.0605
30	0.9957	0.9963	1.0019	1.0581

The zone where the inflowing turbid water entering a reservoir plunges beneath the clear water, thereby producing stratified flow, is called the plunge point or plunge line (MORRIS; FAN, 1998). As reviewed by Haun and Lizano (2016) density currents, can be defined as a layer of water that plunges and continues moving as stratified flow in equilibrium with the fluid.

As exposed by Graf (1984), in a lake or reservoir, the finer material will be carried for long distances, depending on the size of the particles, without settling. In this case, if the current reaches the dam it will produce a submerged muddy lake with a high concentration of fine solid (see: Figure 3).

Figure 4 shows the transition from non-stratified to stratified flow and the plunge point line. Although its location is after the delta zone, the plunge point is limited by the pool level, the discharge, the suspended solid concentration and the reservoir geometry.

The determination of the plunge point can be estimated based on the densimetric Froud number (equation 2.2).

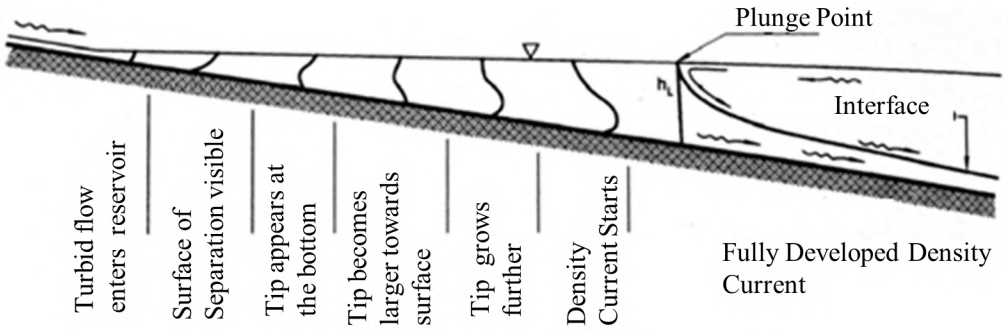

Figure 4 – Density Current Formation: a transition from non-stratified to stratified flow. Adapted from Morris and Fan (1998).

$$F_p = \frac{u}{\sqrt{\frac{\Delta\rho}{\rho'} g h}}, \tag{2.2}$$

where u is the mean velocity, h is the water depth at the plunge point, ρ is the density of the clear water, ρ' is the density of the turbid water, and $\Delta\rho = \rho' - \rho$.

According to Morris and Fan (1998), flume tests and reservoir measurements indicate that the densimetric Froude number has a value of about 0.78 at the plunge point.

As observed by Cortés (2014) and showed in Figure 5 the density current can behave in different ways:

(a) interflow, when the density current is lighter than the lower layer, then it will behave as an intrusion form on the thermocline;

(b) split flows, which occurs when the density current splits into a density step to form two intrusions;

(c) underflows, when the inlet is denser than the middle and

(d) overflows, as the situation showed in Figure 3-a, when the density current enters the reservoir before reaching the plunge point.

After it sinks, it can follow the talweg of the reservoir and as reviewed by Haun and Lizano (2016), the travel time of a density current can range between 0.03 and 0.05 m/s.

As reviewed by Shotbolt, Thomas and Hutchinson (2005), turbidity flows are important during storm events, but the non-stratified flow is dominant under normal flow

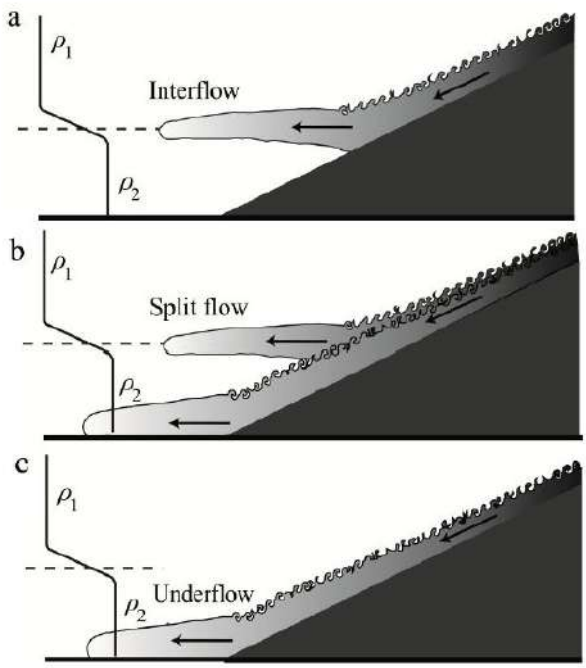

Figure 5 – The behavior of a gravity current in a two-layered stratified environment: (a) interflows (b) underflows, and (c) split flows.

Adapted from:Cortés (2014).

conditions when low-energy inputs are not capable to penetrating far into the water body and carry solids and substances.

2.2 Suspended Solids Monitoring Techniques

So far, it is clear that solids monitoring is a key to decision making. So, the choice of an appropriated method and the monitoring practice will give to the manager an indication of the temporal and spatial variation of the solids. This section will describe the conventional methods and the presentation of the most applied surrogate methods for solid determination.

2.2.1 Conventional Methods

The main purpose of sampling is to obtain solid concentration and grain size distribution in the water column. The samples obtained for suspended load determination are composed of a mix of dissolved[2] and suspended solids.

The conventional methods for sampling solids in the water column are usually classified as *point samples* or *vertical integration samples*.

The method can be performed considering different depths in each sampled vertical, for example, for stables cross-sections, the sampling can be taken as 1 single point at

[2] in this study the dissolved part is the solid fraction lower than $0.6\mu m$

0.6 from total depth; 2 points at 0.6 and 0.2 from total depth; and for 3 points at 1, 0.5 from the total depth and another one near the bottom. Carvalho et al. (2000b) suggests 5 vertical points at 0.1, 0.3, 0.5, 0.7 and 0.9 from total depth, if there is solid variation throughout the water column.

For vertical integration Carvalho (2008) presents two methodologies:

- Method of Equal Width Increment (*EWI*), where the cross-section is divided into equal width segments for sampling, in which all the samples can be mixed and then only a single analysis is performed, representing an average from the whole cross-section — Figure 6a.
- Method of Equal Discharge Increment (*EDI*), for this application it is necessary to know the discharge distribution along the cross-section. The method consists of sampling in the middle of each vertical. As in the EIW method, all the samples can be mixed and then only a single analysis is performed, representing an average from the whole cross-section — Figure 6b.

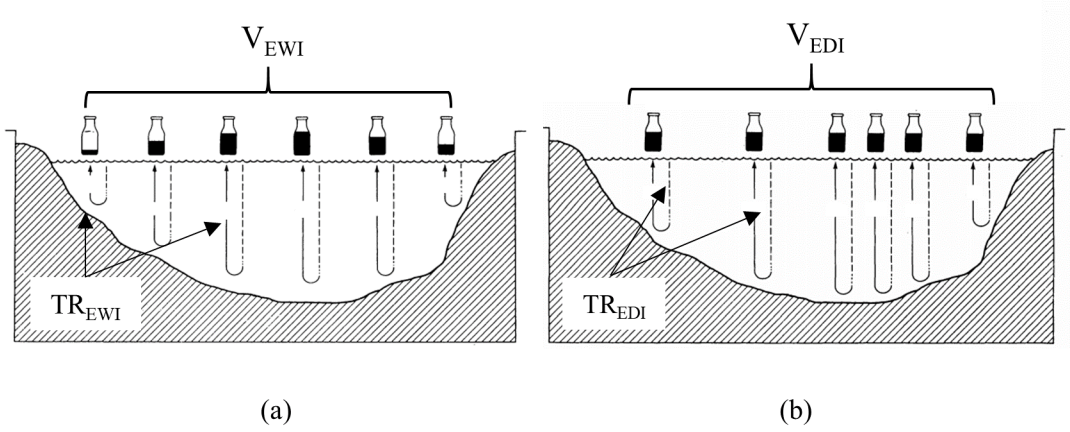

Figure 6 – (a) Sampling by Equal Width Increment (EWI), where the sampled volume (V_{EWI}) is proportional to the discharge and the Transitional Rate (TR_{EWI}, which is the sampling velocity) is constant at each vertical and (b) Sampling by Equal Discharge Increment(EDI), where the sampled volume (V_{EDI}) is equal and the Transitional Rate (TR_{EDI}, which is the sampling velocity) is different, proportional to water velocity, at each vertical.

Adapted from: Edwards and Glysson (1988).

After sampling the water for solid estimative it is necessary to proceed for laboratory analysis. However, before showing the conventional laboratory analysis, at this stage, it is important to rise and clarify the conceptual difference between suspended solids concentration (SSC) and total suspended solids (TSS).

As reviewed by Galloway, Evans and Green. (2005), SSC and TSS commonly are used to quantify concentrations of suspended solid-phase material in surface water. But

the analytical method to determine one or another can differ. The basic idea is that the SSC is obtained from the total sampled volume, which means if a bottle of 1 liter was collected, the whole bottle will be analyzed. The TSS analytical method uses a volume fraction, from the original water sample, obtained immediately after the sample has been well mixed.

According to Galloway, Evans and Green. (2005), the analytical methods differ and the two may not be equivalent when solid-phase material, especially sand, becomes more concentrated (this fact was also observed in some analysis conducted in this present study). It happens mainly due to the fast settling velocity of the coarser materials. In the presented study the analytical method regarding the finer fractions was obtained as TSS. For samples with a high amount of coarse materials (eg. sand), the solid concentration was determined as SSC.

The most common analytical process to obtain solid concentration is based on the gravimetric methods. Hence, the different forms of solid determination can be obtained by drying and wet weight difference of the remained solid, over a certain sampling volume. Figure 7 shows a flow-chart with different fractions of solids that can be determined during the analytical process in the laboratory.

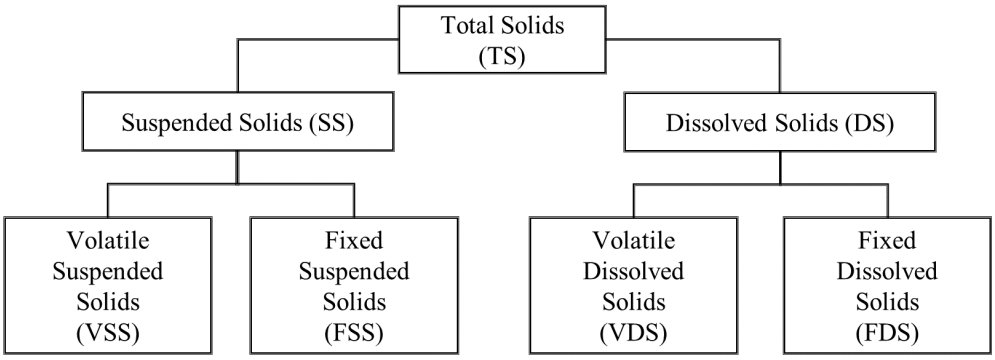

Figure 7 – Solid Series.

After APHA (1999).

In this study, for finer solids, the required fraction will be SS. This fraction, according to APHA (1999) is the remained amount of solid retained by a glass fiber filter of 2 μm or smaller. Considering the same definition, SABESP (1999) assumes a minimum filter porosity of 1.2 μm for this analysis. In this study was used a glass fiber filter of 0.6 μm.

2.2.2 Surrogates Technologies

In this Section will be presented the acoustic and the optical instruments proposed as surrogate technologies to obtain suspended solids (SS) and granulometry, respectively.

Acoustic Method

The Acoustic Doppler Current Profiler (ADCP) [3] was first developed to measure the water velocity and the discharge from a river cross-section by measuring the velocity of particles in the water. The acoustic method follows the velocity-area methodology for discharge estimation and its mechanism is based on the sound-wave propagation emitted by transducers that operate in frequencies that can vary depending on the type of the equipment. In this study, the ADP-M9, from Sontek-Xylem, will be used and more details about it will be given in Chapter 4.

The sound wave consists of a pressure wave that travels in an elastic environment, such as liquid, solids or gases. The wavelength (λ) is the consecutive distance between two regions of high or low pressure. In a bi-dimensional representation, when a source emits a pulse, the sound initiates its propagation in concentric circles around the source. These circles are known as the front wave - surfaces where the fluid oscillates. Near the source, the front waves are spherical. As they travel further, they become larger and can be approached as flat waves. In Figure 8, it is possible to observe the wave propagation from a point source and the associated wave parameters.

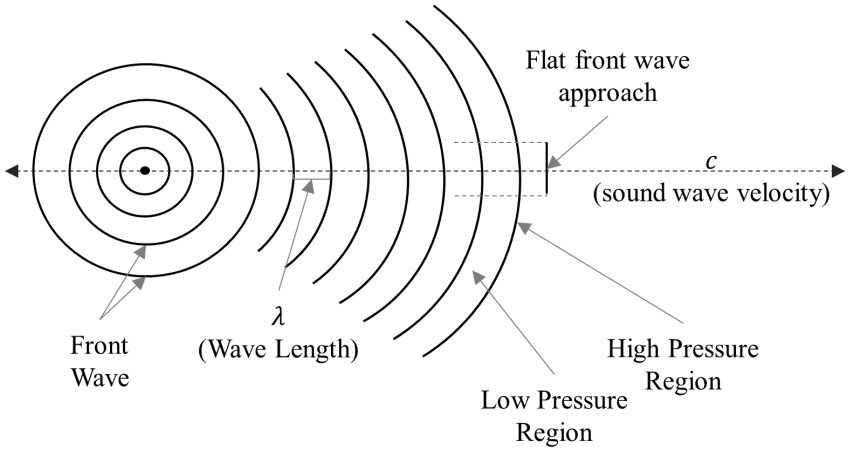

Figure 8 – Wave sound propagation and related parameters.

Adapted from Halliday and Resnick (2009).

Additionally to Figure 8, there is also the frequency, f, which is the number of waves that pass through a point in a certain time and C, which is the sound wave velocity. The relation for frequency can be written as (equation 2.3):

[3] As observed by Gamaro (2012), the device that measures the discharge by using the doppler effect is widely known by the acronym: ADCP. But, in fact, this is a specific name given by the manufacturer that makes it commercial. The name for this device will vary from one manufacture to another, for example: ADP, ADVM and Workhorse.

$$C = f\lambda. \tag{2.3}$$

Sound can travel at different speeds depending on the temperature or salinity at the medium. Table 2 shows the sound wave velocity in different mediums.

Table 2 – Wave sound velocities at $1atm$. Adapted from Halliday and Resnick (2009).

Medium	Velocity (m/s)
Air $(0\ ^{\circ}C\ )$	331
Air $(20\ ^{\circ}C)$	343
Water $(0\ ^{\circ}C)$	1402
Water $(20^{\circ}C)$	1482
Sea Water $(20^{\circ}C)$ and 35% of salinity	1522

The Doppler technology uses a sensor that is continuously transmitting ultrasonic signals at some frequency. The particles in the medium reflect this signal and depending on its position and velocity it will shift the frequency of the reflected signal. The shift in the frequency is detected by the sensor and used to estimate the flow velocity according to equation 2.4. To estimate the velocity the main assumption is that the suspended particles are moving at the same velocity as the water flow.

$$\Delta f = 2f\left(\frac{V}{C}\right), \tag{2.4}$$

where Δf is the frequency change, f is the emitted frequency and V is the relative velocity between the source and the particle.

As quoted by Wood (2017), the lower the frequency, the longer the distance that the sound can travel, however, the resolution of velocity data will decrease. On the other hand, the higher the frequency, the shorter the distance or range that the sound can travel, and in this case, the resolution of the velocity data will increase. Still, according to Wood (2017) a higher frequency is more appropriate for vertically oriented acoustic devices, particularly when flow depths are shallow and higher resolution is needed over short distances.

In Figure 9, it is possible to observe the wave behavior when it is emitted by the transducer and reflected by the suspended matter (a mixture of solids and organic particles), when it returns as a backscatter signal to the transducer.

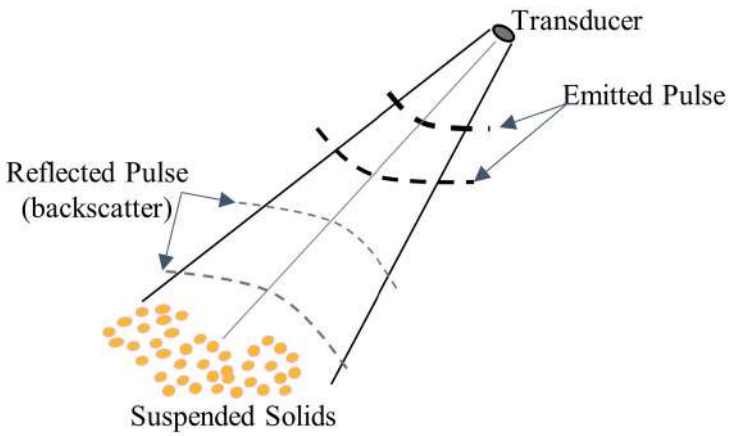

Figure 9 – Emitted pulse and reflected backscatter.

Adapted from: Gamaro (2012).

The ADCP measures the velocity straight from the emitted pulse directions, considering: (a) the duration of the acoustic return to determine the position of the particles; (b) the Doppler shift to computing the particle velocity, thus the water velocity and (c) the determination of the signal noise to ratio (SNR), which is a measure on the number of reflections, thus the quantity of the particles in the flow.

Generally, the device has at least three transducers with the same frequency, some devices have the fourth transducer in order to obtain the error estimation. The error can be obtained by the difference between the estimated vertical velocity component in each direction. Two pairs of transducers are aligned with the North-South direction and the other is aligned with the East-West direction, as it can be observed in Figure 10. where Δf is the frequency change, f is the emitted frequency and V is the relative velocity between the source and the particle.

For continuum measurements, the ADCP divides the water column into depth cells (known as bins) and for each one of these cells, the device calculates the average velocity and their directions. As pointed out by Mueller et al. (2013) on the surface, the ADCP cannot measure velocities due to the required *blanking* distance. On the bed, it also cannot be done due to *side-lobe* interference. In these layers, where it is not possible to measure the velocity, the estimation is usually done by the extrapolation of a theoretical profile.

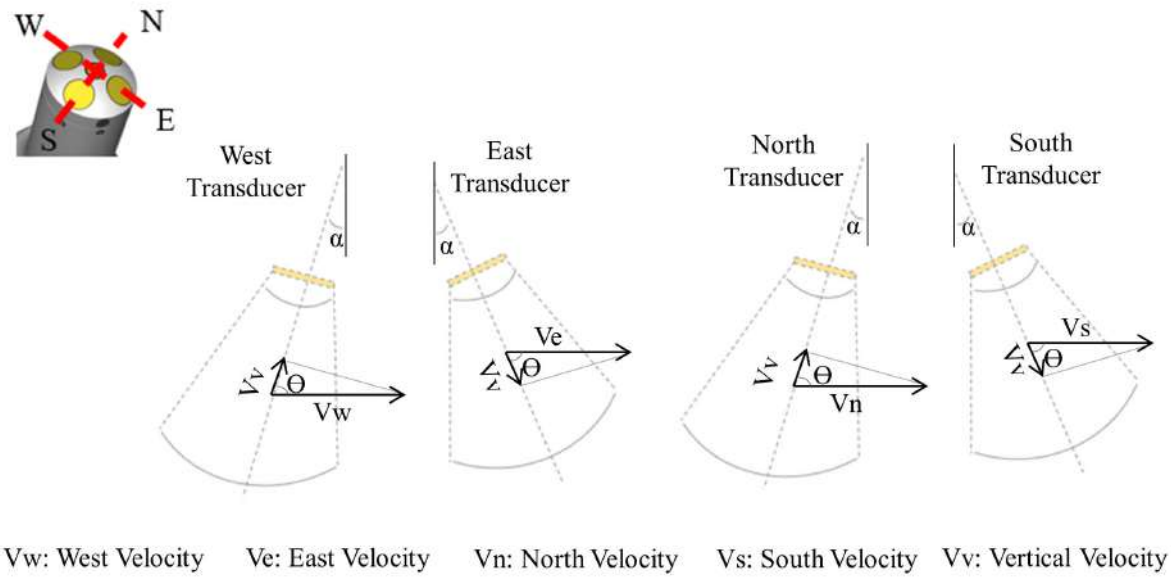

Figure 10 – Velocity components measurement.

Adapted from: Gamaro (2012).

The blank is a device's limitation produced by the transducer vibration. Where the transducer is at the same time the transmitter and the receiver, a short distance (blank) is needed after the signal transmission to allow the transducer to adjust itself to receive the shifted signal. The side-lobe is a parallel beam emitted by the device which reaches the bed before the main beam, producing a strong noise in the bed. There are also no measured areas near the banks, due to the low depth and the reflection caused by the edges. In this case, the velocity is obtained by keeping the device measuring in a fixed position at a certain distance from the edge, in order to obtain an average profile for further software extrapolation.

Finally, after all these considerations, the discharge is obtained in a similar procedure as in conventional estimation, considering the channel area, A, (obtained during the crossing) and the measured velocity, v — $Q = v.A$ (Figure 11).

For the signal attenuation and relation with suspended solids, the mechanism is based on the quantification of the backscatter by the suspended particles. This quantification allows us to estimate a correlation between the received signal and the distribution of suspended matter in the measured area. Hence, the larger the concentration, the larger the difference between the emitted and reflected signals.

According to Terabe (2004), the main advantage of its application is the possibility to make continuum measurements, without cause interference in the local condition of streamflow, because the equipment is not introduced into the water as the manual equipment.

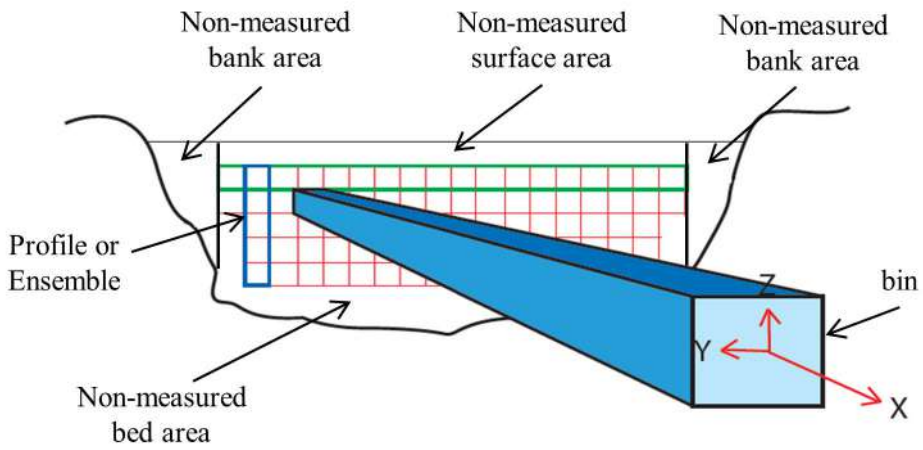

Figure 11 – Measured Area and Cross-Section component.

After Sontek (2016).

The determination of SSC by the reflected beam in the water requires some knowledge about several variables (Deines (1999)), such as:

1. The power transmitted into the water;
2. The acoustic characteristics from the equipment and its response;
3. The signal attenuation caused by propagation losses - water and solid attenuation, reflection and beam spread;

All of these factors can be mathematically translated into models that can be described by solid, hydrodynamics and device characteristics. Equation 2.5 shows the applied equation, where SNR_{mean} is the mean of the 4 beams of the ADCP throughout each vertical. $20\log(\psi R)$ is the spread attenuation, $2\alpha_w R$ is the water absorption and $2\alpha_s R$ is the solid attenuation term.

$$CBS = SNR_{mean} + 20\log(\psi R) + 2\alpha_w R + 2\alpha_s R, \tag{2.5}$$

where CBS is the corrected backscatter (in dB), the coefficient ψ is a near field correction factor related to the effect of spherical spreading, close to the transducer (adimensional), R is the slant range from the transducer head to the measured ADCP cell (in meters), α_w is the absorption energy by the water (in dB/m) and α_s is the attenuation due to the suspended matter (in dB/m).

The models applied in this study are based on the models presented by Guerrero et al. (2016) – for water absorption and for solid attenuation.

After the corrections it is possible to obtain an adjusted curve from the form presented at Equation 2.5, that correlates the corrected backscatter (CBS) in dB with the $Log10$ of SS in mg/L.

$$log(SS) = a.CBS + b, \tag{2.6}$$

$$SS = 10^{(a+b \cdot CBS)} \tag{2.7}$$

where a and b are the angular and linear coefficient of the adjusted curve.

Optical Method

The Laser In-situ Scattering Transmissometry (LISST) [4] is an optical technique that involves not only the estimative of SS, but also the granulometry, both *in-situ*. It is a submersible multi-parameter system for point measurements of the particle size distribution (PSD) and volumetric concentration (VC).

The LISSTs equipment are based on laser diffraction. Which consists of a collimated laser beam (L) (Figure 12) sent through an amount of suspended solid that is traveling with the flow. The intercepted light from the collimated beam will scatter (R) at a particular angle, based on particle diameter and will be detected by a silicon ring detector (D). Behind the ring-detector is placed a photodiode (P). A hole in the center of the ring-detector (D) allows the tightly focused laser beam to pass through. The photodiode P senses the power in this beam. A reduction in this power due to particles constitutes a measure of attenuation. This attenuation is used only to de-attenuate the light on rings. Following this de-attenuation, and after then subtracting a background (i.e. light on rings with filtered water), an inversion procedure produces the 36-element PSD (SEQUOIASC, 2017).

All this detection process on PSD will vary from 32 to 36 small forward angles, which corresponds to the particle size ranges between 2.5 to 500 μm and 1 to 500 μm, depending on the LISST version: LISST-100x and LISST-200x, respectively.

The equipment measures internally at $20Hz$, but due to data logger limitations, the individual measurements are averaged into a sample, and it is this sample average that is stored at a maximum sample rate of $1Hz$. As a default, the instrument operates in the Fixed Sample Rate mode at a $1Hz$ rate with 10 measurements per average. This average is obtained in 0.53 and 0.34 seconds, for LISST-200x and LISST-100x respectively (Sequoia (2015) and Sequoia (2018)).

[4] from Sequoiasc, Inc.

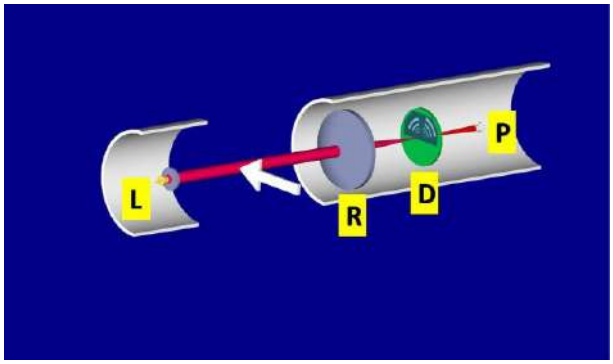

Figure 12 – Operating scheme of LISST equipment series - diffraction laser.
After SequoiaSc (2017).

According to Czuba et al. (2015) limitations on the use and application of the devices are related to the particle shape, particle composition, the range of the particle sizes, strong thermal stratifications and density fluctuations.

Depending on the application, some of the mentioned limitations can affect mainly the volume concentration determination. For example, as highlighted by Felix, Albayrak and Boes (2017), highly non-spherical particle shapes lead to overestimated LISST concentrations. Laboratory analysis (FELIX; ALBAYRAK; BOES, 2013) showed that the smallest irregular particles scatter more light than equivalent spheres (for feldspar and mica minerals) overestimating the SSC in 1.5 and 8 times the known value.

The composition of the particles is another factor that can affect the measurements. For particles $< 20\ \mu m$ the color becomes an important factor, since it will interact differently with the light. Also for small particles, the proportion between organic matter and mineral is important. Regarding the size, as cited by Czuba et al. (2015) the measurements of particles smaller or larger than those that the instrument can detect can affect the concentration.

Figure 13 sketches the situation indicated by Felix, Albayrak and Boes (2017) regarding the LISST limitations, when eventually some PSD values need to be discarded (from bin 1 to 3, in gray) because of some environmental issues or equipment limitations, such as: non-spherical particle shapes, the presence of small out-of-range particles (since is a backward relation, small particles will scatter more in the upper angles and produce a fake result regarding concentration in the small bins) and effects of the refractive index.

Despite all limitations, this technique shows a very good alternative for granulometry determination. Granulometry is always a problematic parameter to be determined, because of all the factors that can affect the aggregation and disaggregation (Figure 14).

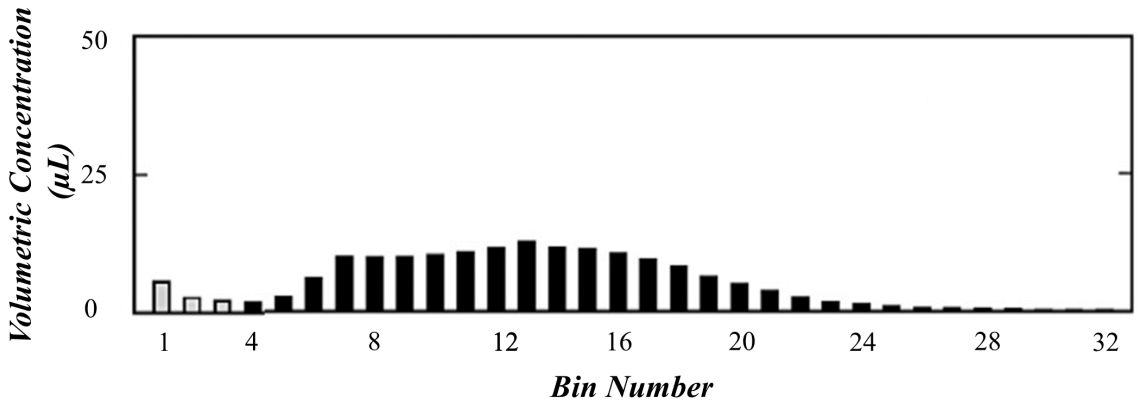

Figure 13 – Examples of bias in the LISST volumetric concentrations produced by the presence of out-of-range particles (for LISST-100X, version).

Adapted from Felix, Albayrak and Boes (2017).

As highlighted by Klassen (2017) factors as water sampling, storage, transportation (turbulence), temperature, pH variations and ultrasonic waves can change significantly the particle sizes and create a different granulometric curve in the laboratory than that one existing in the environment.

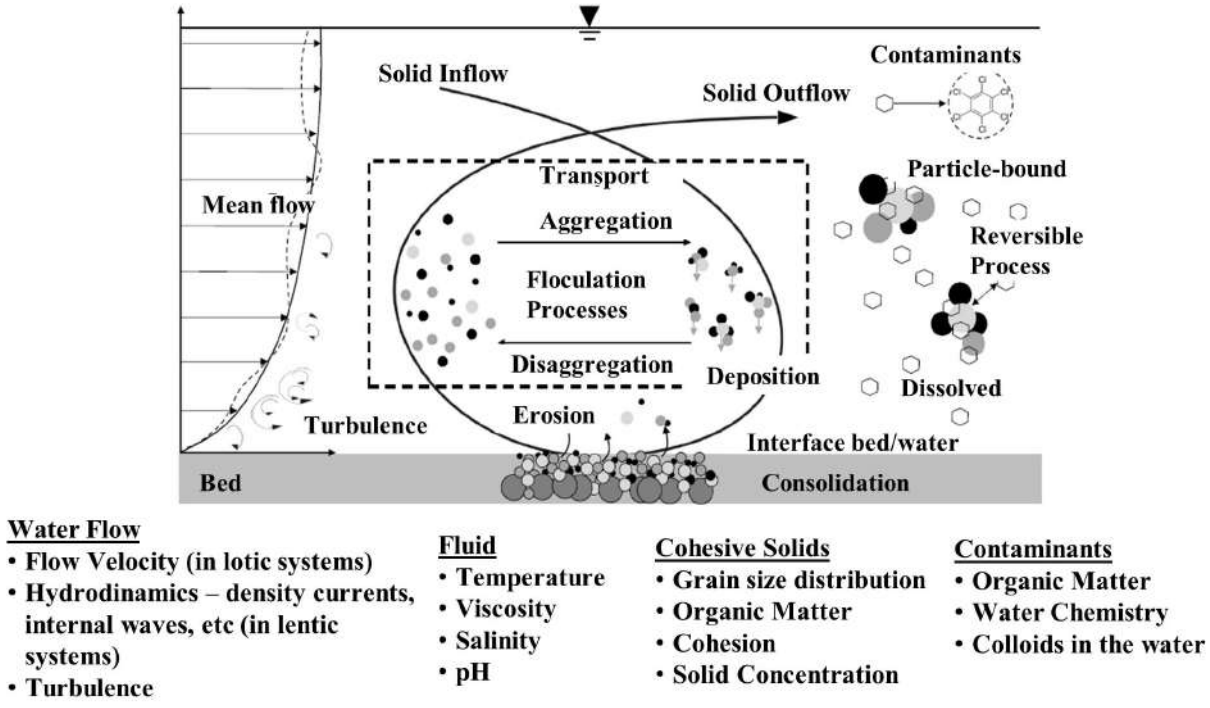

Figure 14 – Water-solid system described with a cycle of erosion, transport, deposition and consolidation, involved in particle aggregation/disaggregation and sorption/adsorption of contaminants. Below the scheme, the corresponding influence factors and the respective properties are presented.

Summary

Throughout this chapter it was briefly shown the theory to be applied in this study about solid dynamics in lotic and lentic environments and the sampling method, considering the conventional (sampling an laboratory analysis) and surrogate technologies, such as acoustic and optical measurements.

With this in mind, in the next chapter will be shown the most recent publications about the application of the cited equipment in solid studies followed by the methodology applied (Chapter 4) in this study to obtain SS information from surrogate technologies.

3 Recent Publications Overview

First developed for oceanic studies, the use of acoustic technology has been widely studied for a large number of applications. The first ADCP was produced in the $'70s$ as an adaptation of a Doppler speed log - an instrument that measures the speed of ships through the water or over the sea bottom (RD-INSTRUMENTS, 2011). In the $'80s$ the device was produced in a commercial scale and by the $'90s$ it became popular in the scientific community, with a wide range of studies related to its many options of applications, among them, the use of ADCP to estimate load (bed and suspended) and SS — Gamaro (2012).

This section will present the most recent and relevant contributions for the proposed study.

3.1 The use of combined surrogate technologies to determine Solid Concentration

Most publications related to surrogate technologies for solid dynamics studies are done in rivers, a system for which most of the models and devices were developed and which have a very good response. Related to ADCP applications, according to Deines (1999) (which gives us a very good contribution indicating a method that considers a proportional relation between the signal intensity and the solid concentration), when supported by careful calibration procedures, the acoustic signal can be used to obtain continuum measurement of discharges, loads and solid concentration, depending on the applied technique.

To reach reliable results, researches are combining different methods and comparing the results, in order to check the best approach. In this context, it has been common the combination of ADCP measurements and optical sensors (LISST, Tubidity-meters or OBS[1]) or water sampling and SSC correlations to study solid dynamics in the environment (GARTNER, 2004; GUERRERO; SZUPIANY; AMSLER, 2011; BARANYA; JÓZSA, 2013; WOOD; TEASDALE, 2013; GUERRERO et al., 2016; LANDERS et al., 2016; HAUN; LIZANO, 2018).

These combinations of techniques and devices were explored in the study proposed by Gartner (2004). He studied the solid dynamics comparing and correlating results from static ADCP, LISST and OBS measurements at different stations located in San Francisco Bay, USA. He considered the scattering for different particle sizes using the Rayleigh scattering model ($2\pi a_p/\lambda < 1$, where a_p is the particle diameter) as a criterion to define a range of suspended solid determination as a function of his ADCP frequencies. In his

[1] Optical Backscatter Sensor - a high intensity infra-red emitting diode (IRED), from Campbell Sci.

study, the author highlighted the backscatter intensity particle size dependency, stating that the method requires a steady size distribution for a good agreement.

This statement highlighted by Gartner (2004) was also mentioned by Wood and Teasdale (2013) and Guerrero et al. (2016), regarding the importance to take into account the medium characteristics, because the losses also depend on other parameters, such as temperature, salinity and SS.

Wood and Teasdale (2013) evaluated the use of acoustic surrogate technologies, such as: acoustic-backscatter, laser-diffraction and turbidity-meter to estimate real-time SSC at two rivers in the USA. At this study on the use of LISST, different from others cited studies, the authors did not assume a density value to convert volumetric concentration ($\mu L/L$) in massic concentration (mg/L), they applied a simple linear regression (SSC_v x SSC_m) to obtain real-time update about SSC variations. As a result, they obtained better correlations for the acoustic method that covers a larger part of the channel than the other evaluated surrogates technologies.

Guerrero, Szupiany and Amsler (2011) attempted for the first time, in scientific-practical terms, to characterize particle distribution and to determinate SSC in a large river, using a multi-frequency arrangement (two devices: 600 kHz and 1200 kHz).

Baranya and Józsa (2013) studied the ADCP x SSC correlation and quantified the lack of information related to the non-measured areas from ADCP. Also, they noted that the error in the SSC estimative can increase as the circumference of the particle approaches to the wavelength. In their study, they also mapped SSC at 7 cross-sections of 600 meters apart along of Danube River, the obtained results include interpolation along the water column at each cross-section, as shown in Figure 15. The authors estimated SSC based on a linear regression between the measured SSC and the relative backscatter. From sensitivity tests that analyzed how the solid flux will vary due to changes in the echo intensity, they observed that a variation of 20% in ADCP echo intensity can result in a variation of 10% in the estimation of SSC.

Based on these studies, later on, Guerrero et al. (2016) evaluated the acoustic properties of suspended solids and the consequences of the applicability of the ADCP correction methods. Take into account that Parana river represents a large sandy river and the Danube has characteristic of a sand-gravel bed and clay-silt particles being transported in the water column, comparing the results from each river they concluded that fine fractions resulted in appreciable viscous attenuation — it was greater in the Danube than in Parana, this was possible to observe due to application of a particle size distribution method.

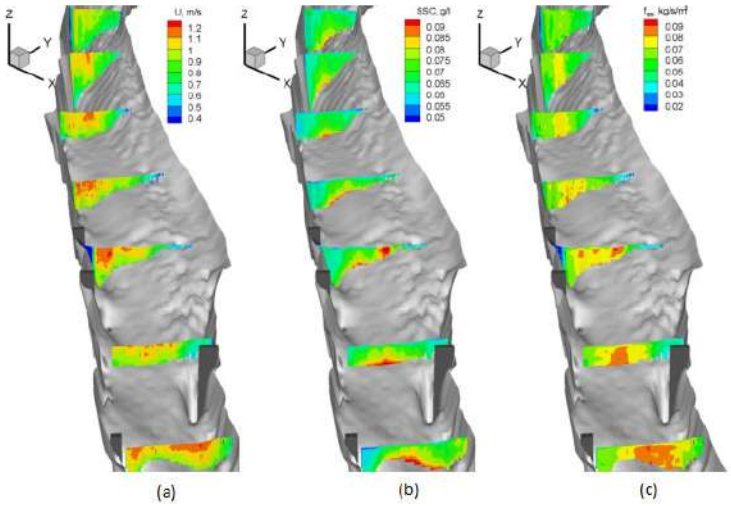

Figure 15 – Spatial distribution of a) flow velocity, b) SSC and c) Suspended Load. Adapted from: Baranya and Józsa (2013).

As a result of the operationalization efforts, for side-looking ADCPs, in 2016 USGS has published a manual of Techniques and Methods to guide the interested user through the process of establishing a station, collecting the data and developing the surrogate relation. In addition to this publication, researches from USGS are working on a proposal that aims to standardize the applied methodology and the obtained information (LANDERS et al., 2016).

Considering the aforementioned efforts on the operationalization of the use of the ADCP in the past years some specialists proposed two similar software to obtain SS information from down-looking ADCP and several point sampling within the cross-section: The STA software, proposed by Wood et al. (2019) and the ASET software proposed by Ruben et al. (2020). Both software are prepared to calibrate the RD Instrument ADCP, only.

All those already cited studies (and potential calibration software) have in common the application in river systems. There are not so many measurements and studies applied to a lentic environment (with low flow velocities) (HAUN; LIZANO, 2018). Some of the applications to these systems are related to density current formation (HAUN; LIZANO, 2016; UMEDA; YOKOYAMA; ISHIKAWA, 2006) or study of benthonic colonies (WOOD; GARTNER, 2010).

The next Section will present some of the studies that intend to apply a similar method proposed in this research to estimate solids concentration and density currents in a lentic environment.

3.2 Surrogate technologies applied to a lentic environment

The most recent application of surrogate technology to SS estimative in a reservoir was done by Haun and Lizano (2018) at Peñas Blancas reservoir in Costa Rica. They combined ADCP and LISST-SL[2] measurements in order to study the concentration of suspended solids all over the reservoir by establishing cross-sections over the lake.

With ADCP correlation and analysis they observed that the SS decreased during the campaign along the reservoir. According to the authors, the differences in the SS were not identified by conventional measurements that stated the same range of variation between the transects.

Besides the SS analysis along the reservoir, the authors aimed to evaluate the uncertainties related to the extrapolation of the ADCP signal near the bed and in the blanking zone using LISST-SL measurements for validation. They evaluated the differences on the SS when the extrapolations were not taken into account and found out that the differences increased as the depth increased, with values ranging from 0.6% up to 19.4% of difference (from the shallower to the deepest cross-section, in a reservoir).

Another application in a reservoir environment was done by Haun and Lizano (2016) when during a measurement campaign at Peñas Blancas reservoir they recognized a density current formation detected by the ADCP and decided to track it by doing longitudinal transects along the reservoir (Figure 16). The density current formation was confirmed by LISST-SL measurements that identified small differences in SS and granulometry.

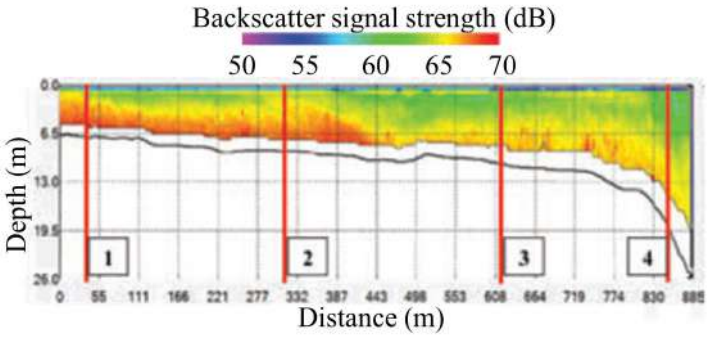

Figure 16 – Density current formation recognized by Haun and Lizano (2016) at Peñas Blancas reservoir, in Costa Rica.

Adapted from: Haun and Lizano (2016).

Umeda, Yokoyama and Ishikawa (2006) published a study that combined ADCP velocity measurement techniques to a reservoir longitudinal transect with turbidity and

[2] stream-line alined optical device from Sequoias Instrument Inc.

water quality parameters supported by echosounder measurements and numerical modeling (Figure 17). In their study, they obtained the density current field velocity in the water flow measurements at Shichikashuku reservoir, in Japan. From the field measurement validation for the numerical modeling simulation, they concluded that standard simulations models are capable of reproducing sedimentation phenomena considering only a few parameters.

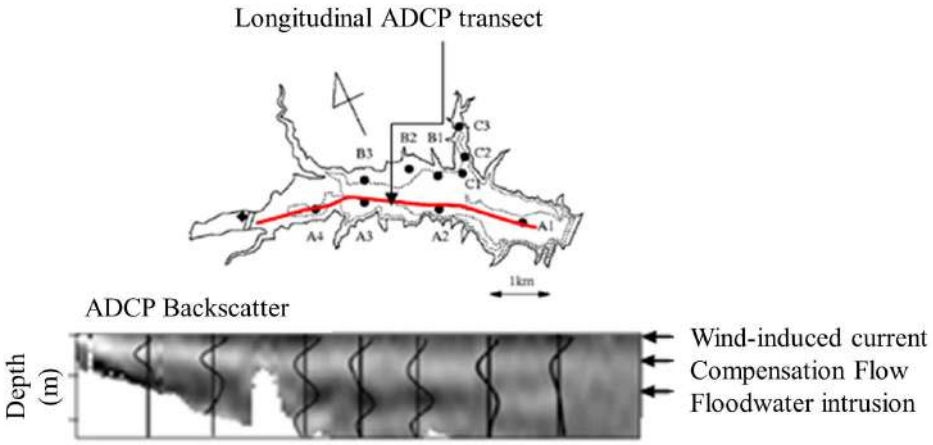

Figure 17 – Density current formation measured by Umeda, Yokoyama and Ishikawa (2006) by echosounder and ADCP measurements at Shichikashuku reservoir, in Japan.

Adapted from: Umeda, Yokoyama and Ishikawa (2006).

These three aforementioned studies were the only ones that used surrogate technologies to observe the development of a solid plume in lentic environments. Although the studies aimed to evaluate the density current velocity and visualize it through supersonic images and SS evaluations the studies did not report the ADCP correction and SS correlation applied to the density current evaluation.

3.3 Summary of the combined surrogate technologies

This section presents a summary (see Table 3) of the most recent studies to be considered in the application of the methods for rivers and lakes/reservoirs. As already mentioned, most of the studies were conducted mainly in rivers under standard conditions (significant flow velocities, SS concentration and granulometry).

Table 3 – Most recent studies regarding surrogate technologies application for SS and density currents determination.

Author(s)	Applycation Area	Main Driven Forces	Main Objective of the study
Gartner (2004)	Estuary - San Francisco Bay	Tides, Inlet rivers	ADCP x SSC correlation and comparison of estimated SSC from ADCP with OBS estimative.
Umeda, Yokoyama and Ishikawa (2006)	Reservoir - Shichikashuku	Inlet flows, Temperature, Wind, Atmospheric Pressure	The Study of washload sedimentation at Shichikashuku reservoir in Japan
Guerrero, Szupiany and Amsler (2011)	River - Parana River	River Flow	Used a two-frequency method to study SSC and grain size distribution.
Guerrero, Rüther and Szupiany (2012)	Laboratory Analysis	Laboratoy Controlled Discharge	Following the previous studies conducted by Guerrero, Szupiany and Amsler (2011), the authors carried out laboratory tests with the two frequencies method for grain size assesment using two ADCPs.
Baranya and Józsa (2013)	River - Danube River	River Flow	The authors studied the ADCP x SSC correlation and quantified the lack of information related to the non-measured areas from ADCP.
Guerrero et al. (2016)	Rivers - Parana and Danube	River flow	studied the acoustic properties of suspended solid and the consequences of the applicability of the ADCP correction methods
Haun and Lizano (2016)	Reservoir - Peñas Blancas	Inlet rivers, Temperature, Wind, Atmospheric Pressure	Track a density current formation during a flood event a Peñas Blancas Reservoir.
Haun and Lizano (2018)	Reservoir - Peñas Blancas	Inlet rivers, Temperature, Wind, Atmospheric Pressure	Study of suspended load within a tropical reservoir, by a week monitoring campaign in the rainy season stablishing cross-sections along the reservoir and observing the solid mass concentration decreasing along of it.

3.4 Summary

This Chapter has shown a summary of the most recent publications that based the presented research and its hypothesis and objectives.

Within the presented background around the surrogate technologies issues, specifically about the use of acoustics to estimate solid concentration, it has been clear that most of the researches were conducted mainly in lotic places with the presence of coarser

and non-cohesive solid content.

On the other hand, very few studies were conducted in order to study and support decisions making in lentic environments with the significative presence of finer solids and low flow velocities, such as reservoirs.

In order to accomplish the objectives presented in Chapter 1, the next chapter will present the methodology applied in this research to obtain SS information in lotic and lentic environments.

4 Materials and Methods

As presented in Chapter 3, most of the methods presented in literature are very well developed for lotic environments, with mostly non-cohesive particles. Therefore, the main idea will be first to understand and apply the methods at to these environments (to show the method domain) and then apply it to a lentic environment, with lower velocities and high cohesive particle content.

As summarized in the Figure 18, the general idea will be first to apply the methodology to a lotic environment, in a river (**step 1**) with high flow and high solid discharge — Taquari River, in order to test and understand the equipment and the correlations. Then the methodology will be applied to another lotic environment, at Passauna River considered a transitional area, with a lower discharge and different solid dynamics and characteristics, close to the lentic zone.

After that, in **step 2** the same methodology will be applied at Passauna Reservoir, a lentic environment, in order to estimate the TSS and visualize the TSS distribution over the depth and further (in the **step 3**), to analyze the density current inlet in a reservoir.

During the steps 1 and 2 will be tested the methods: *I-Field Measurements and Sampling*, *II-Data Processing and Laboratory Analysis* and *ADCP* x *SS Correlation*. Then, after the correlation establishment, at step 3: *the density current exploration* will be analyzed.

The proposed study is based on results produced within the SeWaMa Project (Innovative approaches for future solid and water management in Brazil) within the NoPa call (funded by CAPES and DAAD, 2015 - 2018) and the MUDAK project (Multidisciplinary data acquisition as the key for a globally applicable water resource management - http://www.mudak-wrm.kit.edu/) both are a consortium between Germany and Brazil, integrating Universities, municipal sanitation company and companies from the private sector. The projects involve researchers from different areas studying sedimentation in reservoirs, water quality aspects, land use and GHG production and emission in a water supply reservoir.

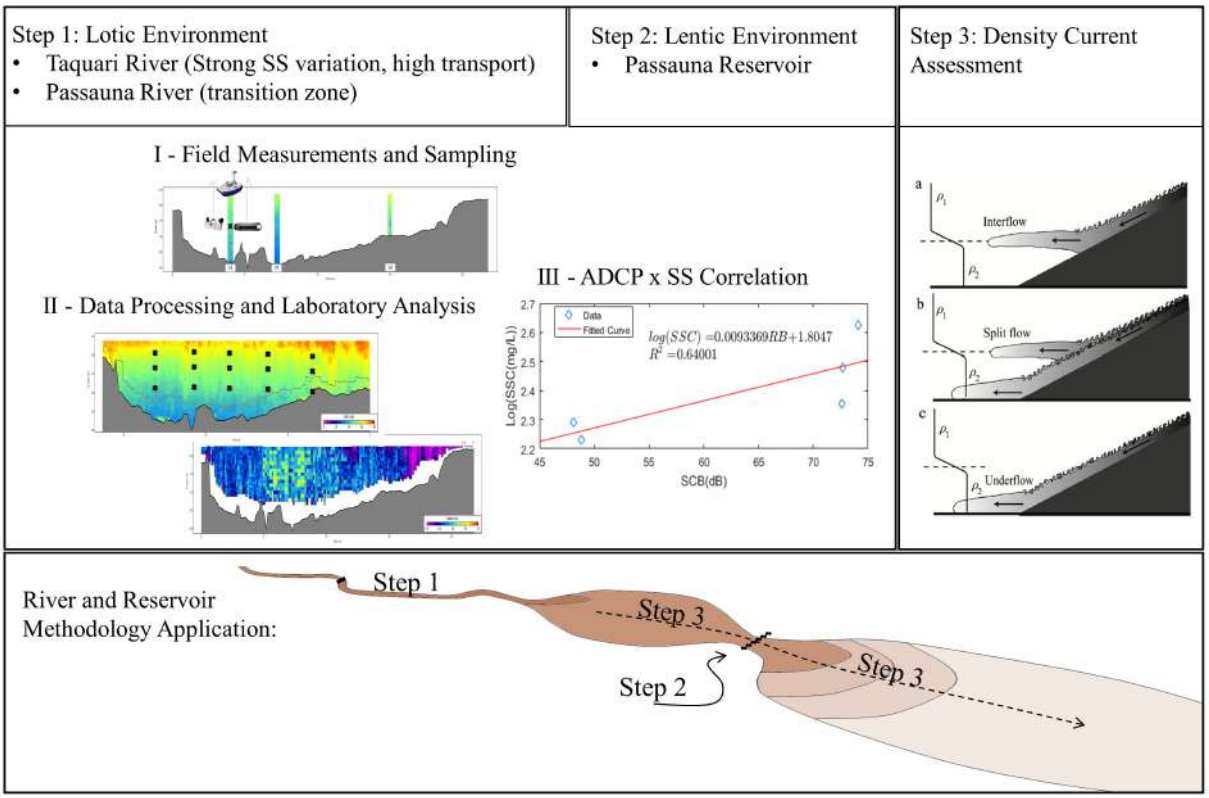

Figure 18 – Summary of the proposed methodology to be presented in the following sections.

4.1 Site Description

4.1.1 Lotic Environments: Taquari River and Passauna River

At this section will be given a short description of the lotic environments used to test the method for ADCP and suspended solid correlation. These two rivers were chosen because of their characteristics and their relation with the methods used in this research.

By its characteristics, Taquari River might be approximated as standard conditions for ADCP correlation found in the literature (discharge, granulometry, SS, etc.).

Passauna River presents different situation patterns (discharge, granulometry, SS, etc.) from those normally studied for ADCP correlation and will work as a transition environment (from lotic to lentic environment) in the application of the proposed method.

4.1.1.1 Taquari River

Taquari River is an important river from Paraguay Basin. It is located in the Pantanal Biome, the largest freshwater wetland system in the world, with a high diversity of flora and fauna. It is the main river from the Taquari Basin and one of the biggest tributaries of the Paraguay River Basin. The river is commonly known for its intense solid dynamics with high erosion and transport capacities.

Figure 19 shows the cross-section in the Taquari River before its confluence with Coxim River, at Coxim city, in a place where the streamlines can be consider aligned and the flux permanent and uniform. The cross-section has about 100 m width and between 3 m to 4 m deep, in the deepest part of the channel.

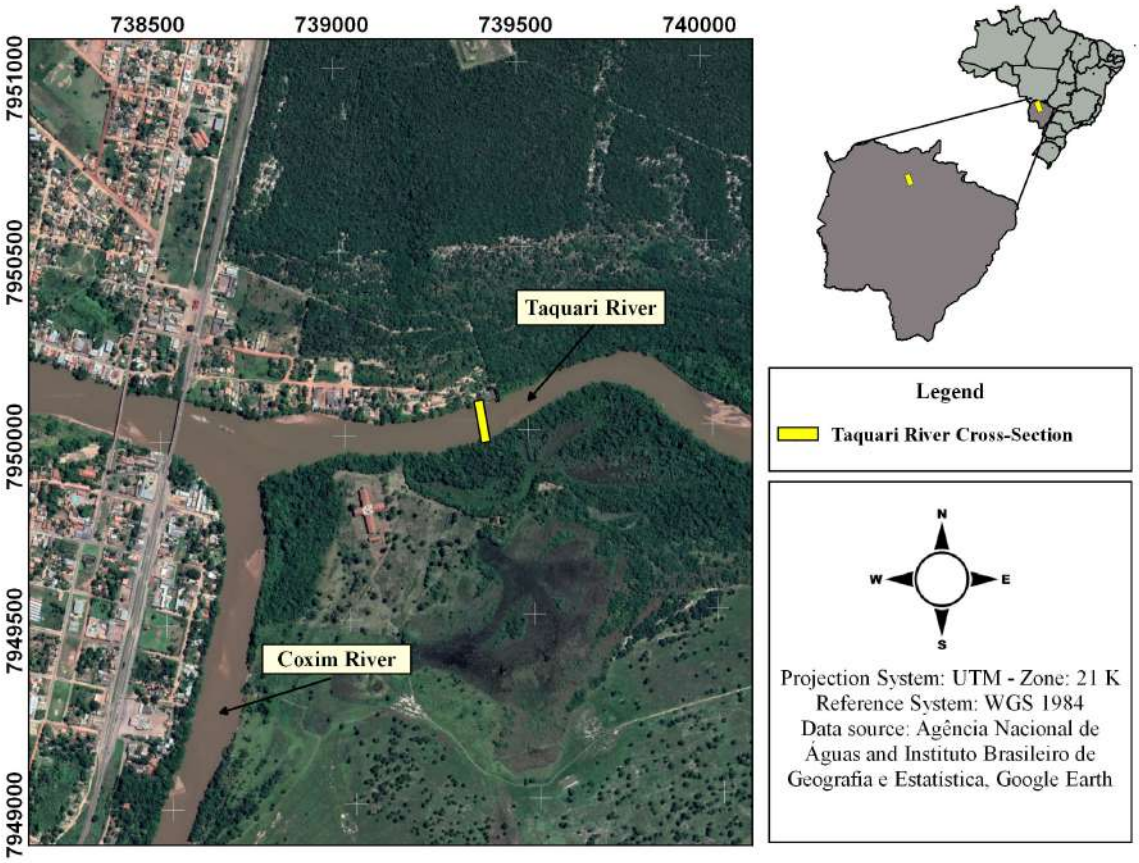

Figure 19 – Taquari River Location and the Monitored Cross-section.

After: Wosiacki et al. (2018).

According to Brazilian Water Institution (ANA - Agência Nacional de Águas - Coxim Station, Code: 1854004) data set, the discharge vary from about $300m^3/s$ up to $500m^3/s$ and the precipitation vary from about $25mm$ to up to $200mm$ in the dry and rainy season, respectively (total precipitation of $1200mm/yr$, in average) — Figure 20.

For this study it was done a total of 7 field campaigns in cooperation with UFMS[1] team. The campaigns happened between March of 2017 and January of 2018, when measurements were taken with the ADCP and water sampling to obtain SSC. The used devices and tools were: (a) ADP-M9 from Sontek-Xylem®, Figure 26, and (b) USD-49 Water Sampler, Figure 28a, which is a hand-line suspended solid sampler with about 27.5

[1] Federal University of Mato Grosso do Sul - HEroS: Hydrology, Erosion and Sedimentation Lab - https://heros.ufms.br

kg used to obtain integrated measurement from the water column — more details about the devices will be discussed thoroughly in the following sections.

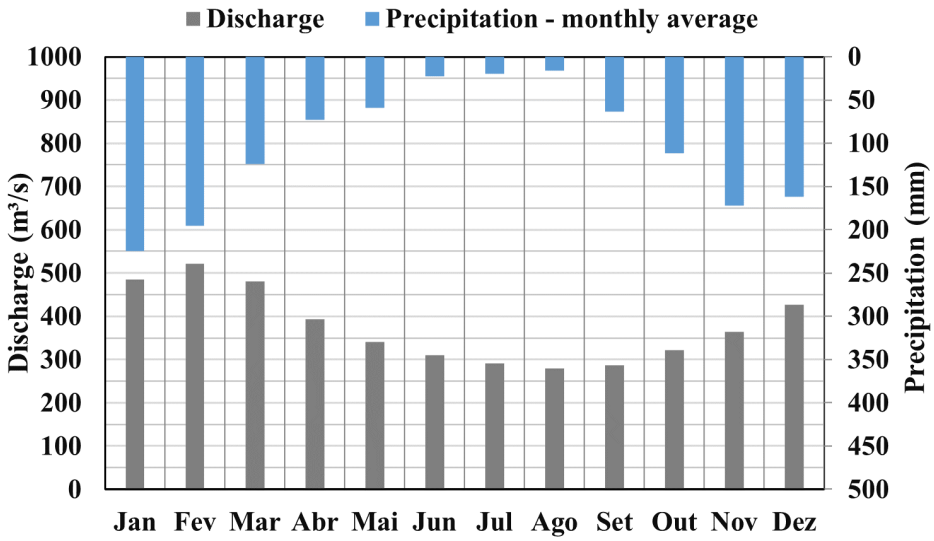

Figure 20 – Mean Precipitation and Discharge at Taquari River at Coxim Station (Code:1854004).

Source: ANA (2019).

To measure, the ADCP was setup for a Smart Pulse frequency mode, where the frequency is automatically chosen by the device based on the depth[2]. First were taken measurements along of the cross-section, to obtain the discharge. Since Taquari River has a strong bedload, was also taken a total of 6 static verticals, in every campaign, to correct the obtained velocities and avoid discharge's super-estimation when using the bottom track positioning. The 6 verticals were chosen based on the results of the Hidrossedimentos 3.1 tool, developed by Agricultural and Rural Extension Research Company from Santa Catarina State (EPAGRI -SC). Based on that the cross-section was divided according to the Equal Discharge Increment (EDI).

The water sampling was taken right after the static ADCP measurements, in the same verticals, to obtain a correlation between the received signal from ADCP and the SSC. For the 7 campaigns, all the 6 depth-integrated samples (400 mL per sample), were mixed to obtain one representative sample for the entire cross-section.

After each field campaign the samples were processed to analyze the granulometry and solid concentration. In a general way, the procedure was based on sieving of the largest grains (sand) according to the American Geophysical Union classification (LANE, 1947), considering a sieve granulometry as: 2.0, 1.0, 0.5, 0.25, 0.125 and 0.0063mm.

For the finest grains (silt and clay) the adopted procedure followed Carvalho

[2] Later on was adopted a single-frequency measurements, only applied for Passauna River and Passauna Reservoir — see next Section.

(2008), where the method is determined by solid concentration: if it is between 300 and 10000 (mg/L), the particle selection is done by a gravitational method where the fractions are divided according its sedimentation at a specific time (settling tube); if the concentration is between 3000 and 10000 (mg/L) it is used the pipetting method (CARVALHO, 2008). More details regarding laboratory analysis for the integrated samples can be obtained at Suekame (2020).

4.1.1.2 Passauna River

Passauna River is the main river of Passauna basin. It is located on the border of the cities of Araucaria, Campo Largo and Curitiba, in Parana State, Brazil (Figure 21). The monitoring cross-section is located at the bridge of BR277 highway and has about 15 m width and 1.5 m deep, in the deepst part of the channel.

At this location, were conducted a total of 5 field campaigns (from February of 2017 to Octobe of 2018), where 2 campaigns happened in October/2018 (Oct, 18th and Oct,20th)during an extreme event monitoring. At this situation was possible to obtain the highest flow velocities and TSS from the entire data set already monitored for this study.

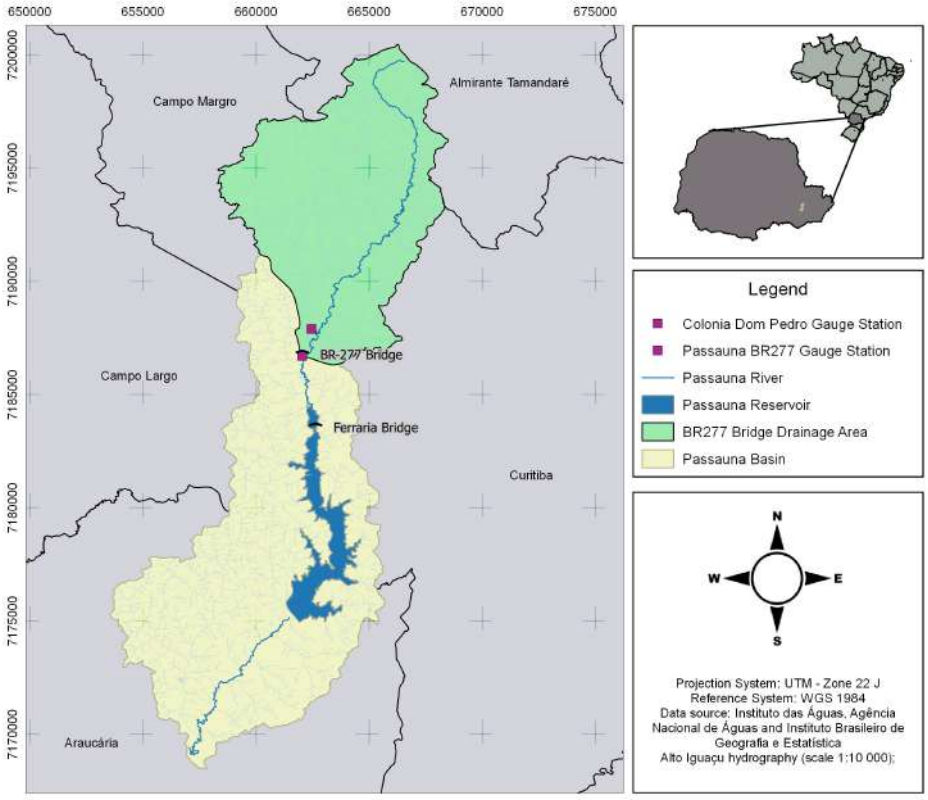

Figure 21 – Passauna Basin Location.

Also, at this cross-section is located one gauge station from ANA (BR-277 Campo

Largo Station, code: 65021800[3]). Additionaly there is another monitoring station from ANA located about 2.0 *km* of the BR277 bridge with precipitation data available (Colônia Dom Pedro Station, code: 65021770[4]).

The watershed is located in a climate region classified as *Cfb*[5] (Köppen-Geiger classification), with a few extremes of temperature and ample precipitation in all months. Figure 22 summarizes the mean precipitation and discharge throughout the year. It is possible to observe that mean precipitation varies from a minimum of about 74.63 *mm* in August to a maximum of 189.19 *mm* in January with a total annual precipitation about 1500 *mm* to 1600 *mm*.

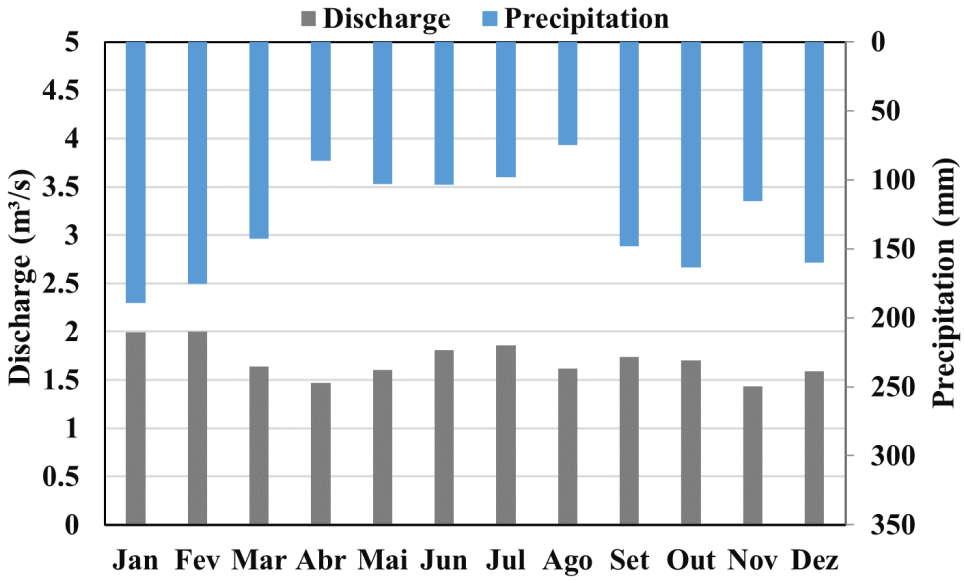

Figure 22 – Mean Precipitation and Discharge at Passauna River at Colonia Dom Pedro Station (Precipitation Data) and BR-277-Campo Largo Station (Discharge Data).

Source: SIH (2019).

The field procedures followed the same methods applied at Taquari River: first were taken measurements with ADCP (cross-section and static measurements) followed by water sampling. Different from Taquari River proceedures, here were made point sampling using the Van Dorne bottle. The granulometry data was measured *in-situ* with the LISST and to obtain temperature and sound velocity information it was used a CTD (also from Sontek-Xylem, to made the previously ADCP signal corrections).

Not all the measurements made with the LISST could be used due to technical problems related to *(a)* operational questions (the team was learning how to use the device), and then *(b)* related to the post-processing analysis (the comparison between two

[3] Sistema de Informações Hidrológicas (SIH) data base
[4] Sistema de Informações Hidrológicas (SIH) data base
[5] Marine West Coast Climate

versions of the same device presented different measurement results for TSS — LISST-100x and LISST-200x).

After each field campaign the water samples were analyzed in the laboratory in order to obtain the TSS — more details about the devices will be discussed thoroughly in the sequence.

4.1.2 Lentic Environment: Passauna Reservoir

Passauna Reservoir is located in the Passauna River basin (see Figure 21). The reservoir was full in the end of $'80s$ and according to Sanepar (2013), it produces a flow rate supply of 1800 L/s which corresponds roughly to 20% of all integrated supply system from Curitiba and its metropolitan area. It has a surface area around 11 km^2 and a volume of 71.6 hm^3.

This reservoir has a peculiarity related to its transitional area which differs from most of reservoirs. As showed in Figure 23, in the upstream – distant about 2 km from the entrance, the Passauna River loses the characteristic of a well fitted river and starts to flow in meanders. Depending on the period this meanders can be flooded (in rainy days) or not (in dry days) resulting in a *natural wetland* until reach the *forebay*.

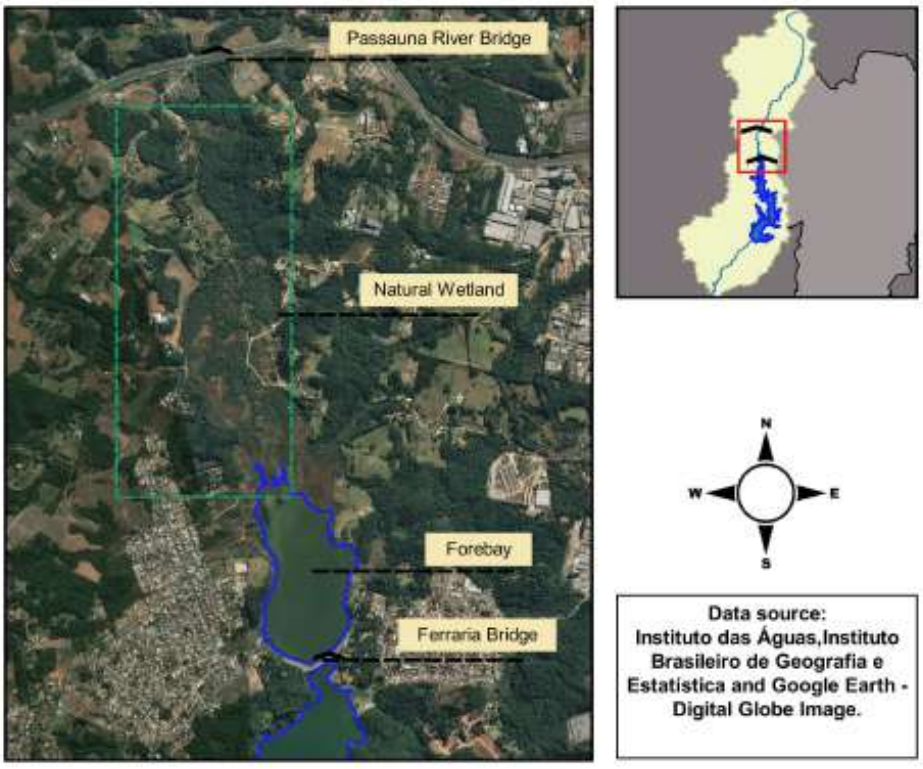

Figure 23 – Study Area.

At this location the main idea will be to apply the already tested methods (at Taquari and Passauna Rivers) at Ferraria Bridge and extrapolate it to longitudinal tran-

sects (from upstream to downstream) with ADCP, to evaluate the density current formations.

The study area will be concentrated in the upper part of the reservoir and it will include a region immediately downstream of the forebay, where some variations in the suspended plume were visually identified — Figure 24.

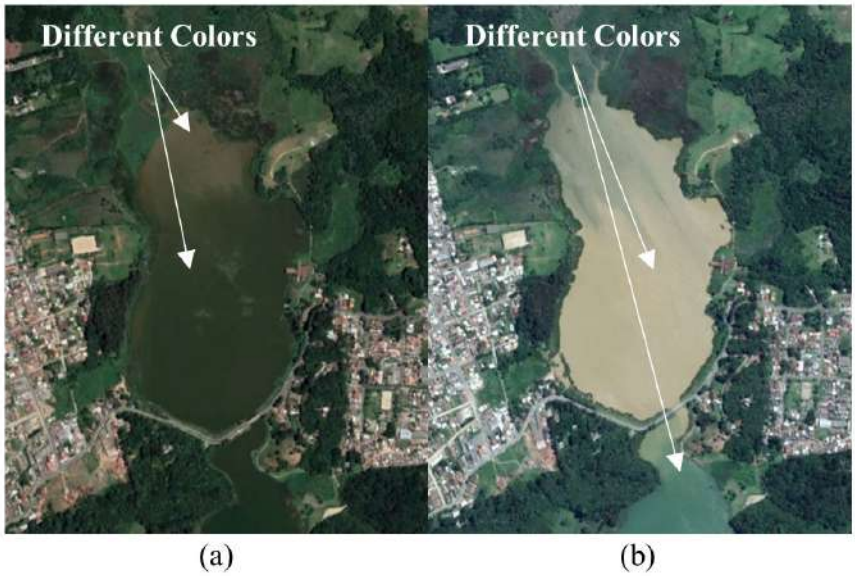

Figure 24 – Comparison of the water color in the study area among different days: (a)March 5th, 2019 and (b) January 21th, 2018

In terms of solid content, in the Passauna Reservoir Bocalon (2007) found a significative content of silt and clay fraction ($< 75\mu m$), around 63% during the raining season and around 53%, during the dry season for Ferraria Bridge. Pitrat (2010) found values around 80% to 90% for silt and clay during the dry and rainy seasons at Ferraria Bridge.

Sotiri, Hilgert and Fuchs (2019), analyzing bottom solids, has found that in more than 95% of the solid material the granulometry is lower than $63\mu m$ and assotiated bulk-wet density values ranging from $1.2g/cm^3$ up to $1.6g/cm^3$ in the bottom solid at Ferraria Bridge. They also find that the bottom solid content is mostly sand fraction, followed by silt-clay fraction, while the forebay is overwhelmingly composed by clay-silt fraction. The analysis done by these authors consisted in the laboratory sieving analysis for granulometry content estimative.

For this research, a total of 7 campaigns was conducted at Ferraria Bridge, from August of 2017 to February of 2019. As for Passauna River, two campaigns happened during an extreme rainy event, which were the campaigns that happened in October, 18th and 20th of 2018.

In all presented field campaigns were made point measurements at Ferraria's Bridge with ADCP, CTD and Water Sampling. The LISST measurements started from

August of 2018, with the aquisition of the LISST-200x by Federal University of Parana.

The measurement proceedures follow the measurements done in Taquari and Passauna River, with ADCP static measurements conducted in 3 verticals in the Ferraria Bridge cross-section, followed by point water sampling (with the Van Dorne bottle) and LISST measurements (Figure 25).

At 3 campaigns were made longitudinal transects, from upstream to downstream, in the reservoir using the ADCP, as shown Figure 25.

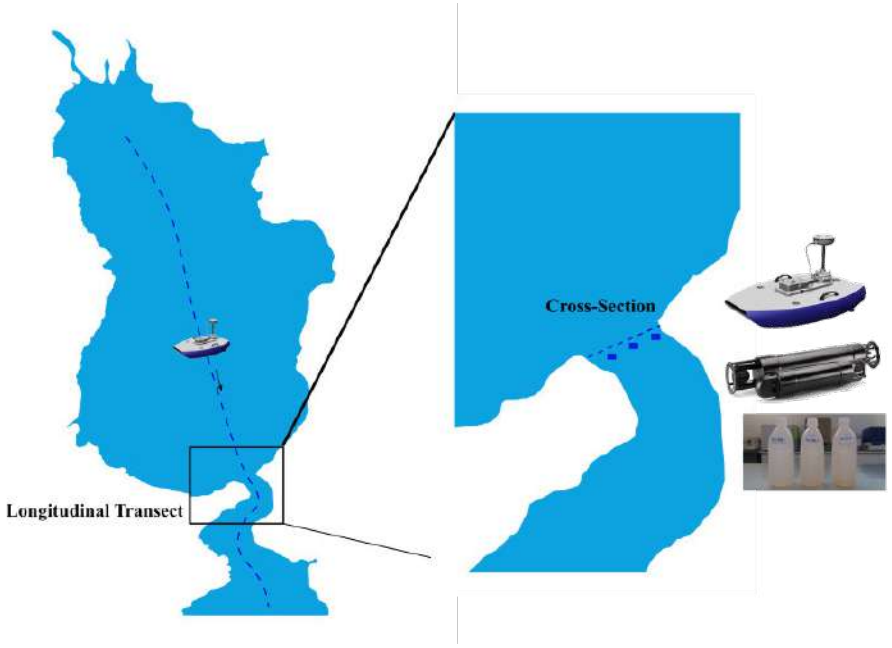

Figure 25 – Longitudinal Transect and Cross-section sketch at Passauna Reservoir.

The field procedures presented at this section were done to accomplish the **steps 2** and **3** from Figure 4.

4.2 Instrumentation and field procedures

As already mentioned, to obtain the data needed were used the ADP-M9 and the CTD instruments (from *Sontek/Xylem,Inc*) and the LISST-200x (from *Sequoia Scientific, Inc.*). For water sampling in the reservoir was used the Van Dorne bottle and a USD-49 sampler, from USGS[6] for water sampling at Taquari River. After the field measurements and water sampling, all the samples were taken to laboratory analysis for SS determination.

The ADP-M9 application is the one used to developed the whole technique presented in this study. On the other hand the LISST and the CTD devices, as well the sampling bottles, were used just as a tool to obtain the parameters for the application of the correlation methodology.

[6] United States Geological Survey

In the following will be described all cited equipments.

4.2.1 Acoustic Doppler Current Profiler (ADCP) — ADP-M9

The ADP-M9 is a multibeam acoustic probe composed of 9 beams: 2 sets with 4 transducer, operating at 1 MHz and 3 MHz, and 1 vertical transducer used to obtain the depth, operating at 0.5 MHz. The ADP-M9 has a profiling range distance from 0.06 m of up to 40 m and a profiling range velocity about ± 20 m/s, $\pm 25\%$ and a vertical resolution of 128 cells, from 0.02 m to 4 m size — Sontek (2016).

Usually, the user can choose the operating frequency mode, if Fixed Frequency Mode (FFM): 1 MHz or 3 MHz or SmartPulse Mode (SPM). The SPM is the most indicated to obtain discharge measurements because the device will automatically change to the appropriate frequency for the local depth. The FFM is only indicated if the user already knows the local conditions to set the device properly, for discharge measurements[7].

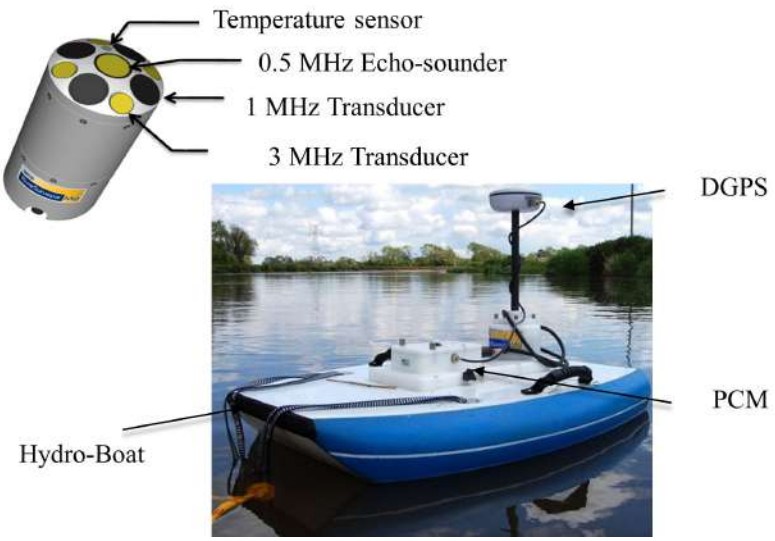

Figure 26 – ADP-M9 features. Adapted from: Sontek (2016).

As presented in Figure 26, it is also composed of an internal compass and a differential GPS (DGPS) used to rise the GPS precision and a PCM (Power and Communication Module), which provides power to the ADCP using a rechargeable battery pack.

The ADCP device was used in two different ways: *(a)* continuum measurement along the cross-section to obtain the discharge estimation and *(b)* static measurements along the cross-section.

At this study most of the measurements were taken considering a FFM of 3 MHz, the only exception was at Taquari River were all of the measurements (the static ones and the cross-sections) were done with the SPM – in this case, the post-processing methods

[7] Although to build the correlation CBSxSS is necessary a single frequency mode.

involved the application of a *filter*[8] to make possible the backscatter correction. This *filter* is responsible to select only the cells measured with 3 MHz frequency.

At Passauna River if the purpose was to obtain the ADCP signal for SSC correlation the measurements were done with FFM, if the purpose were to obtain the flow discharge the measurements were done with the SPM.

In the reservoir, it was identified that the crossing method with the ADCP along a cross-section would not be possible for discharge estimation, because even in a narrower section as at Ferraria Bridge, the flow velocity is too low.

4.2.2 Laser In-Situ Scattering Transmissiometer - LISST

In this study, the first intention was to use two LISSTs devices to do the SS and granulometry analysis: one called LISST-100x[9] in cooperation with Koblenz-Landau University and another one called LISST-200x recently acquired by Federal University of Parana.

However, different from what was expected, both equipment presented differences in measurements made at the same place. The manufacturer was sought to provide clarification and during its analysis, it was found a misalignment in the LISST-100x bin the LISST-200x had all components working fine. Because of it, specifically for this study, the LISST-100x measurements were discarded and only the LISST-200x were considered.

Furthermore, it was also noticed that these equipment weren't appropriated to obtain SS measurements. So, it was decided in this study to use it as a tool only to obtain granulometry information — specifically the D50 which is required to apply the proposed methodology.

The determining factor for this decision was that the LISST measures the SSC in volumetric units. Most of the applied formulation need it on massic units. In one way or another, a conversion factor (solid density) must be determined. Although there is an effort to create a calibration curve to obtain this conversion factor, which due the solid characteristics is not the common used in the literature (2.65 g/L), this is not part of this study. So far, the TSS will be determined only by laboratory analysis which is a well known and consolidated technique.

To make the measurements, the LISST was released in the same depth where the water was sampled for laboratory analysis, at Ferraria's Bridge and Passauna River Bridge. The measurements were done by leaving the equipment stand for some minutes (between 2 - 4 minutes) at each depth, in order to stabilize the sensors and the temperature.

[8] the filtering process consists basically on the replacement of the 1MHz cells by the average of the 3 MHz cells — this step will be deeply discussed later on.

[9] LISST-100x Type C

Figure 27 – LISST-200x with the battery attached.

During operation, the output from the diffracted laser beam, optical transmission, pressure sensor and water temperature are recorded as raw data and can be downloaded and processed later on for granulometry and total volume concentration (SEQUOIA, 2018).

After the field measurements, the data must be post-processed in Matlab script in order to obtain all the data provided to build the granulometric curve.

4.2.3 Water Sampling Instruments and Laboratory Analysis

The water sampling was done considering two methods depending on the site: at Taquari River the samples were taken with USD-49 sampler (Figure 28a), which is a medium-weight hand-line suspended-solid sampler used to collected integrated water samples. The sampler can be lowered and raised, hand over hand, with a flexible suspension line. As previously cited, the sampler cannot touch the bottom and it must be at least at 15 *cm* from the bottom, to guarantee that the sampling will be only of suspended solids.

At Passauna River and Reservoir, the sampling were taken with a Van Dorne Water Sampler (Figure 28b), which is a device used to collect instantaneous and discrete (point) samples. The device must be submerged until it reaches the desired depth and then the closure mechanism is activated by the user.

Figure 28 – Water Sampler Devices (a) USD-49 and (b) Van Dorne.

After each field campaign, the samples were taken to the laboratory to be analyzed. All the laboratory procedures related to the SSC were based on the gravimetric method, which is based on the weight difference. During the process, it is measured the difference between wet and dry weight related to a certain sampling volume considered for each analysis.

For the Taquari River, due to the high amount of suspended solids the concentration was obtained by the visual accumulation tube method which is first used for granulometry information and then through the weight and previous volume determination it is possible to obtain the SSC. All the laboratory procedures and analysis for the Taquari River were done in cooperation with the Federal University of Mato Grosso do Sul (UFMS) and is described in more details by Suekame (2020) that followed the methods described at Carvalho et al. (2000b). In a general way, the determination of SSC and granulometry at Taquari River is a simple task, since all the laboratory procedures are carefully taken, the number of solids generally provides good results.

The laboratory analysis and procedures for Passauna River and Reservoir were closely followed by the author and due to some particularities it demanded more careful and adaptation methods application in the lab.

The analysis followed the majority of the procedures indicated by APHA (1999) — see Chapter 2. Although the whole solid series was determined, for the proposed analysis only the Total Suspended Solid (TSS) fraction was considered.

For each sampling point, the samples were analyzed at least 3 times, where were considered a minimum of 1 liter per analysis. Considering the low concentrations presented in the reservoir and even in the Passauna River, usually, the samples were collected in 5 liters bottles and the triplicated were well homogenized and partitioned in 1 liter beaker each and then filtered, dried and weighed.

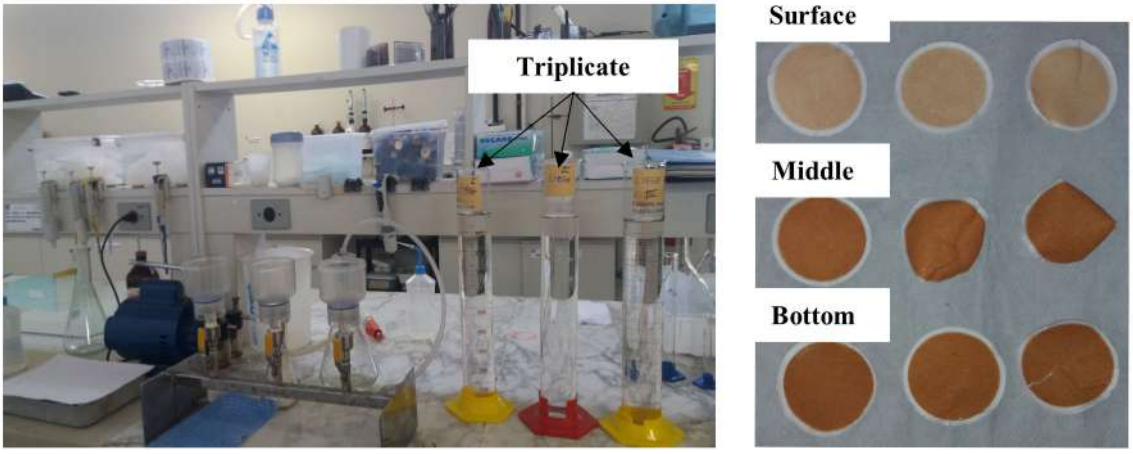

Figure 29 – Filtration System and Filters after analysis at Vertical 3 at Ferraria's Bridge from the 4th campaign (04/23/2018).

4.3 Data Processing

Most of data processing and analysis was done considering MATLAB and Excel algorithms. In a general way, the sensors already have an option to export their measured data as a MATLAB or ASCII format:

- The ADP-M9 provides the Sontek RyverSurveyor, a software designed to measure river discharge and depth from a moving or stationary vessel. The software can be used to observe the real-time measurement and also to post-processing analysis of discharge and flow velocities. However, it is not able to make the solid-ADCP corrections, so it is necessary to export the data in "ASCII format" or "*mat" extension to post-processing the variables.
- The LISST comes with the SOP software (Standard Operating Procedure functionality of the program) used to visualize and export the data in ***.RBN** extension that can be easy read by the Matlab routines supplied by the manufacturer: *getscat_L200X.m* and *invert_L200X.p* functions[10].

Regarding the ADCP, the backscatter processing algorithm had to follow two different processing ways due to the adopted setup measurement procedures, for Taquari and Passauna catchment.

[10] the functions are availabe at the 'Software and Downloads' tab on the LISST-200X webpage: http://www.sequoiasci.com/product/lisst-200x/. Noticed that when the function was used for the first time there was a problem in the algorithm that was easly solved by contacting the manufacturer: The variable returned by the function which contains **cscat** is actually named **RBNdata.cscat**, so instead *invert_L200X(**Cscat**,Random,Sharpen,ShowProgressBar)* used it as *invert_L200X(**RBNdata.cscat**,Random,Sharpen,ShowProgressBar)*

At Taquari River the measurements with ADCP were done with the SPM, also the static one used for SSC correlation. As already mentioned, the sampling procedures were different for this system. So, although the model application was the same, some particularities in the data treatment and processing were different.

At Passauna Catchment, the measurements with ADCP were done considering the FFM, and the sampling and laboratory analysis were also different from those one applied at Taquari River.

Table 4 summarizes the obtained parameters for each tool.

Table 4 – Summary of the instrumentation and related measured parameters in each Study Area.

Intrument/Tool	Parameter	Study Site Application
ADP-M9	Flow discharge (Q)	Taquari and Passauna River
	SS correlation	Taquari and Passauna River and Passauna Reservoir
	Temperature at the Surface	Taquari and Passauna River and Passauna Reservoir
LISST-200X	D50	Passauna River and Passauna Reservoir
CTD	Temperature and Sound Velocity Profiles	Passauna River and Passauna Reservoir
Laboratory Analysis	APHA (1999) procedures for SS	Passauna River and Passauna Reservoir
	Carvalho (2008) procedures for SS	Taquari River
	Carvalho (2008) procedures for D50	Taquari River

4.3.1 Backscatter Correction — dB2SS code

An algorithm created by the author called **dB2SS**, was written to extract and correct the Signal to Noise Ratio (SNR) and correlate it with SS data, by using the Modified Sonar Equation (Equation 2.5) to make the corrections and reach the form of Equation 2.7 to obtain the correlation — all the models and formulations of this step are presented at Appendix A.

Below the aforementioned equations were repeated to help the reader:

$$CBS = SNR_{mean} + 20\log(\psi R) + 2\alpha_w R + 2\alpha_s R,$$
$$log(SS) = a.CBS + b,$$
$$SS = 10^{(a+b\cdot CBS)}$$

Summarized at Table 5 and Figure 30 are the algorithm steps used to obtain the *SS* x *CBS* correlation. It was applied 5 functions (written in Matlab Environment), each one with different purposes during the calculations: *Func_mergefiles*, *Func_mean_speed*, *Func_bs_correction*, *Func_rmvoutlier* and *Func_LSRFit*.

Table 5 – Backscatter correction functions descriptions.

Function name	Description/Processing	Result
$Func_mergefiles$	It is a "pre-postprocessing" function used to merge the solid information and the ADCP data file structure, in order to produce a single file to be read in the main program	Data file with ADCP and solid content
$Func_mean_speed$	It calculates the mean velocity, mean signal and the corrected depth of each correspondent ADCP cell based. This function uses the function *rmvoutlier*, applied at the ADCP 4 beams (SNR).	It returns the mean Speed, Mean SNR, Depth and the corrected position of the 1st calculated cell
$Func_rmvoutlier$	It removes the outliers considering the quantile method (Q1 and Q3 limits) from the 4 transducers	It returns a matrix without outliers
$Func_bs_correction$	It makes all backscatter correction considering the steps presented at Appendix A	It rreturns the CBS for each campaing and/or measured point in the water column
$Func_LSRFit$	It fits a regression line based on Least-Square Regression.	It returns the angular and linear coefficient from the fitted curve.

During the processing it was important to remember that for Taquari River and Passauna system the field procedures were differents (the sampling methods and ADCP setup). To analyze such differences and to adapt the algorithm correction to the Passauna case, some differences during the post-processing analysis had to be taken into account.

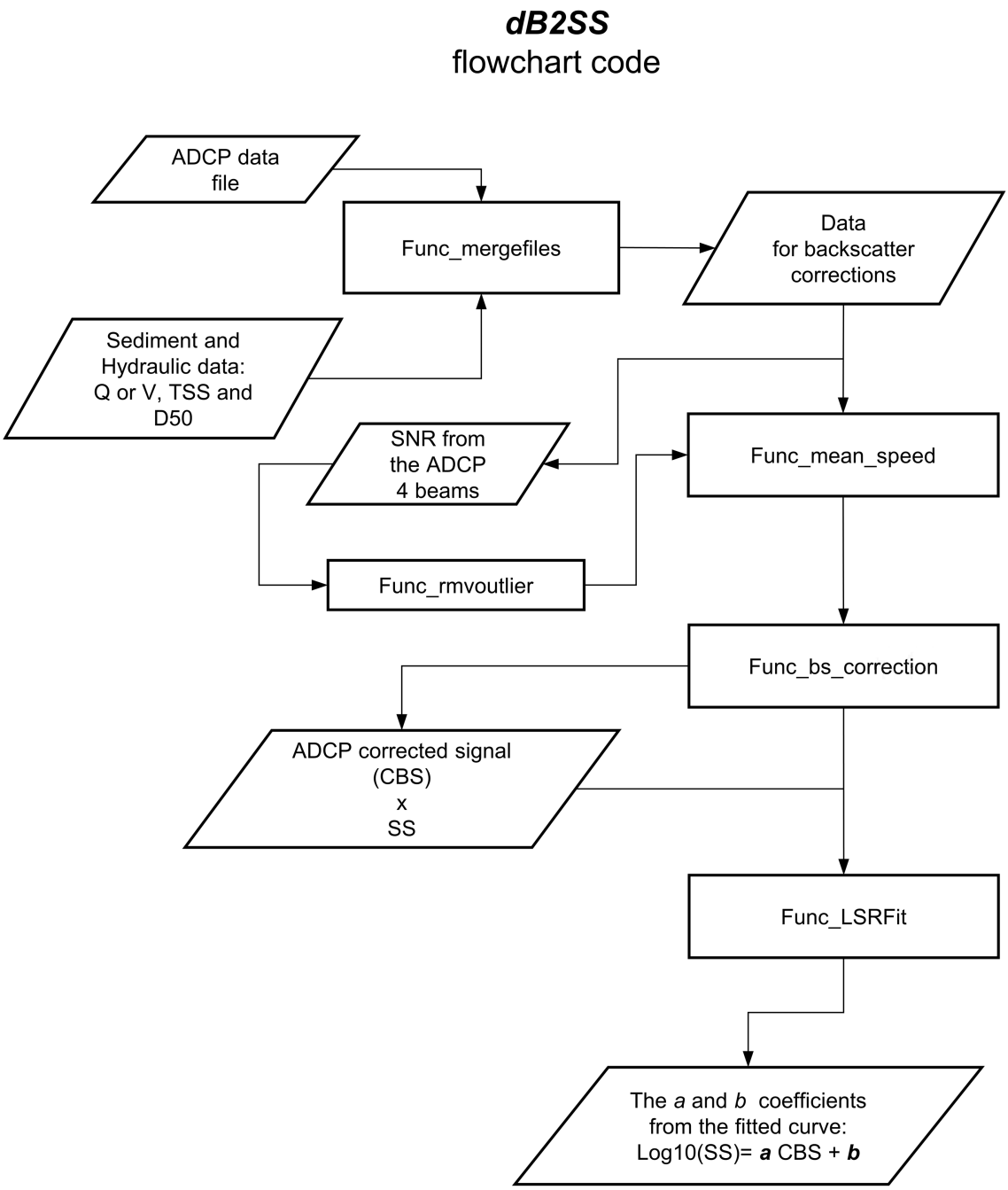

Figure 30 – Backscatter correction flowchart.

The main difference between the point and the integrated ADCP backscatter correction algorithm is that in the point analysis the backscatter correlation was done at the same depth where the water was sampled. So, the algorithm read the TSS at the corresponded depth and integrated the backscatter throughout the water until that depth.

In this way the water column is divided into the corresponding number of samples, eg. for Passauna Reservoir: the cross-section was divided into 3 verticals and were taken

3 water sampling points at each vertical. Then, in the algorithm, the water column is divided according to a given depth, and for each campaign (3 verticals, 3 measurement points at each vertical) the analysis will result in 9 pairs of TSS x CBS, as shown in Figure 31.

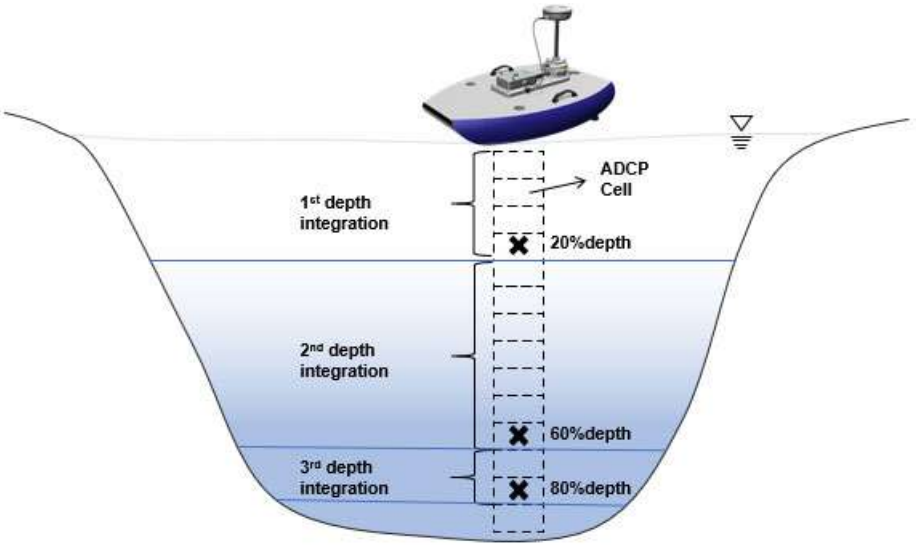

Figure 31 – Operational scheme used in the algorithm point sampling method analysis.

At the integrated analysis (Taquari River), the water sample was mixed and analyzed in a composed way and the correction was applied for the average of the SNR. Obtaining from this analysis only one pair of SSC x CBS at each campaign.

4.3.2 LISST data processing and analysis

The LISST analysis was based on the steps presented in Figure 32, which are described in detail in Appendix B.

As indicated by the manufacturer, considering a good device setup, calibration and field practice, it is possible to obtain the processed data through the application of the *getscat_L200X* and *invert_L200X* functions. However, during the post-processing analysis, it was noticed that would be necessary to apply a filter and a smooth method in order to avoid outlier influence.

Since the instrument can be affected by a range of factors intrinsic to the environment and the handling, it is necessary to consider some criteria and filtering to obtain better and reliable results. In this sense it is not uncommon to clear some data from the results if it is considered an outlier or if the measurement was done under suspicious circumstances – eg. too turbid or too clean water.

The first measurement criteria to be taken into account is the transmission power (T) data value, which is the proportion of light being transported in a turbid medium. With this mind, for a reliable data set obtaining, T should be between 0.1 and 0.995

(SEQUOIA, 2018) — the greater the T, the means that more light is passing through the medium, so the clear the water and the lower T value, the more turbid the water. In fact, the manufacturer advises being aware of the transmission data lower than 0.3 and greater than 0.98. Therefore, if the data is out of this range it should be discarded.

Additionally, the data were analyzed according to its average and all data out of the $1st$ and the $3rd$ quantile (25% and 75%, respectively) was not considered. Similar data treatment was adopted by EMMANUEL et al. (2018), considering only data between the $15th$ and $75th$ percentiles, this procedure was taken by them in order to avoid outlying data, mainly the positive spikes due to bubbles.

Another step was the addition of a move mean filter to all data, in order to smooth the data and avoid abrupt variations from one size to another, throughout the entire class analysis.

Besides the post-processing already mentioned, additionally, the *getscat_L200X* and *invert_L200X* functions are provided by the manufacturer and are used to obtain raw scattering data (scattering and transmission) from the binary device data file and to return the uncalibrated volume distribution in μL, respectively (SEQUOIASC, 2015).

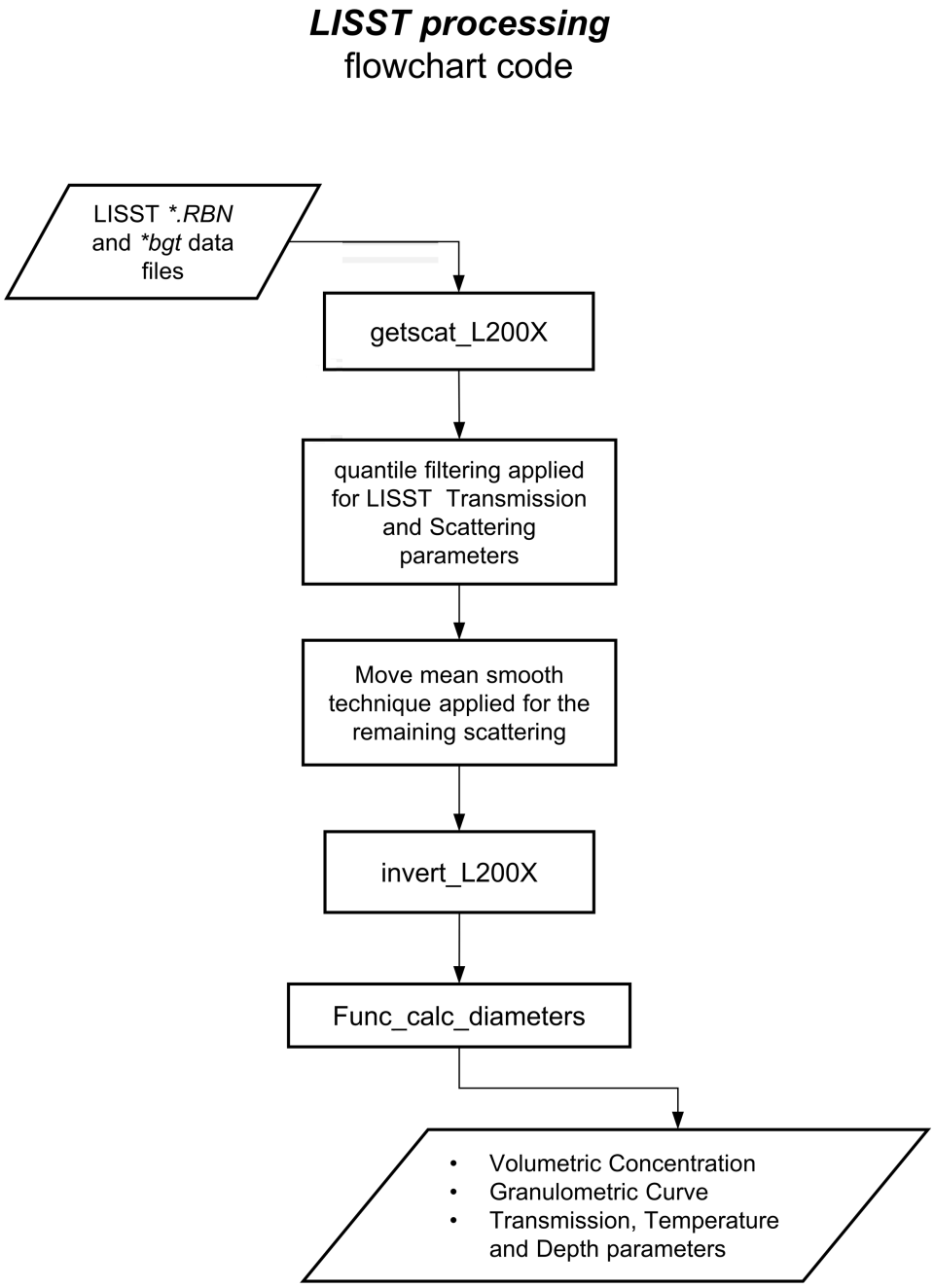

Figure 32 – LISST processing flowchart.

5 Results and Discussions

This section presents the results regarding the measurements done with the tools and steps presented in Chapter 4, for Taquari and Passauna Rivers and Passauna Reservoir. The data for Taquari River was produced by the Federal University of Mato Grosso do Sul (in Brazil) - Environmental Technologies Graduate Program and the data for Passauna system was obtained in the frame of NoPa and Mudak Project coordinated by a consortium between Federal University of Parana (in Brazil) and Karlsruhe Institute of Technology (in Germany).

The results are presented starting with the analysis of the measured parameters and the mapping of the raw data over the cross-section, as well as for some profiles. This is followed by the results for correcting the backscatter signal, and the correlation for SSC or TSS. In the end, the processed results for the profiles are mapped over the whole cross-section and longitudinal profiles (at Passauna reservoir, only).

5.1 Taquari River

5.1.1 Velocity, backscatter and SSC distribution

To obtain discharge and velocity measurements, the procedures during the field campaign and the post-processing analysis followed the guidelines indicated at Mueller (2013). Since the Taquari River has dynamic solid transport conditions, the procedures also included an evaluation of the presence of the moving bed, which indicated a possible error in the estimated velocity from 3% in July/17 up to 12% in March/17 (Table 6).

Table 6 – Mean parameters evaluated during the Moving bed analysis.

	Campaigns						
	Mar	Apr	May	Jun	Jul	Aug	Jan
Mean Moving-Bed velocity (m/s)	0.15	0.07	0.07	0.05	0.03	0.06	0.11
Mean Water Velocity (m/s)	1.27	1.00	1.00	0.95	0.91	0.96	0.99
Potential error	12%	7%	7%	5%	3%	6%	11%

The velocity profiles in all measurement campaigns are shown in Figure 33. To illustrate, it is also shown the horizontal velocities and backscatter signal (mean SNR) from May/17 and Jul/17, in a rainy and in a dry situation, respectively.

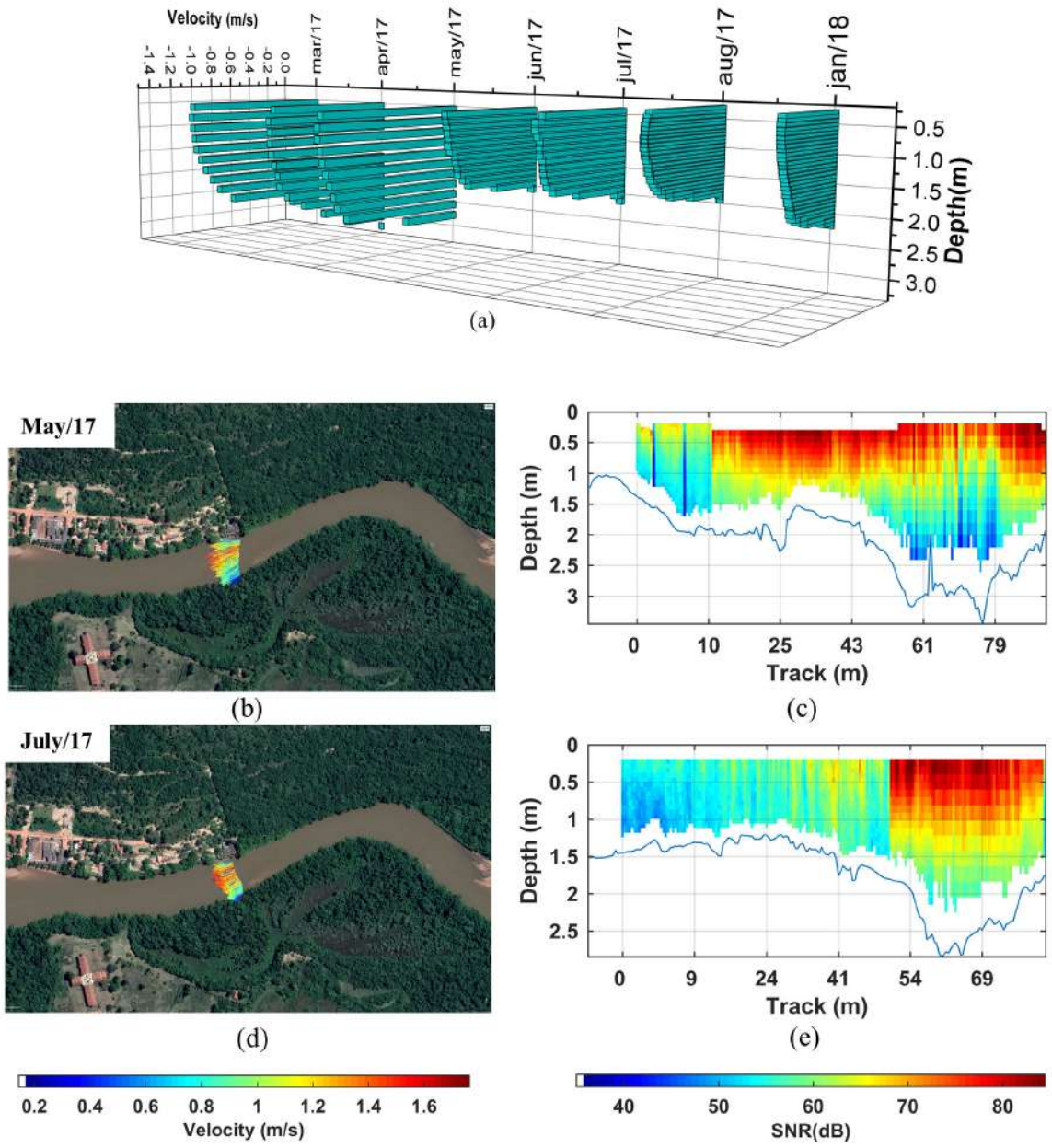

Figure 33 – (a) Mean velocity profiles during all measurement campaigns, Horizontal velocities during the measurement campaigns of (b) May/17 and (d) July/17 and Mean Backscatter Signal obtained during the measurement campaigns of (c) May/17 and (e) July/17.

The velocities varied from $0.64m/s$ in Jan/18 to up to $1.28m/s$ in May/17. Although in May the measurements didn't have the largest discharge value, the SSC was highest when compared to all other sample dates due to the amount of precipitation in the previous day before the measurement campaign (as presented in Table 7 and Figure 34).

Table 7 – Mean discharge and mean solid concentration during the field campaigns.

	Campaigns						
	Mar	Apr	May	Jun	Jul	Aug	Jan
$Q(m^3/s)$	252.25	162.96	221.66	129.82	117.16	131.28	227.57
$D50(mm)$	120	134	104	107	134	135	136
SSC Laboratory (mg/L)	300.3	169.9	422.5	195.4	113.6	124.1	207.8

Figure 34 shows the relation among the parameters measured during the campaigns and the accumulated precipitation registered from 7 days before the measurement campaign. As we can see the variation of the parameters showed that the SSC increases with the discharge and the precipitation. The highest SSC was observed in May/17, suggesting a washload influence due to the high precipitation rate in the period — Figure 34 is arranged from the lowest measured discharge, in Jul/17, to the highest measured discharge, in Mar/17.

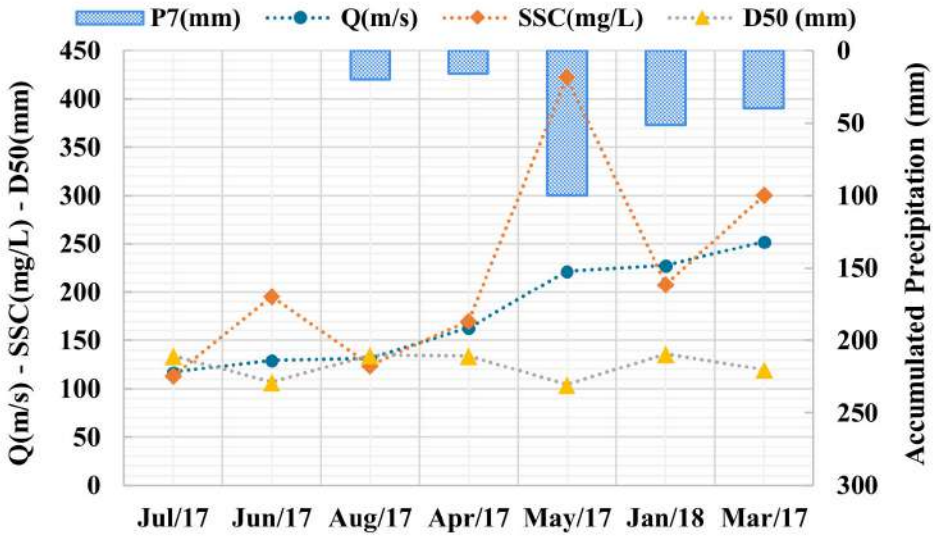

Figure 34 – Relation between the parameters obtained during the campaigns. P7 is the accumulated precipitation registered from 7 days before the measurement campaign. All parameters's values were arranged from the lowest measured discharge to the highest measured discharge.

For all the field campaigns, D50 stayed uniform so it had a poor correlation with other measured parameters. The particle size distribution curves for all sampling events are shown in Figure 35 and it is possible to confirm the presence of the fine fractions that tend to aggregate. As an average of all campaigns, the sampled suspended solid

was comprised of 83% of sand and 17% of silt and clay particles. The presence of fine particles is significant in most campaigns following precipitation events, mainly in May/17, corroborating the washload assumption previously mentioned.

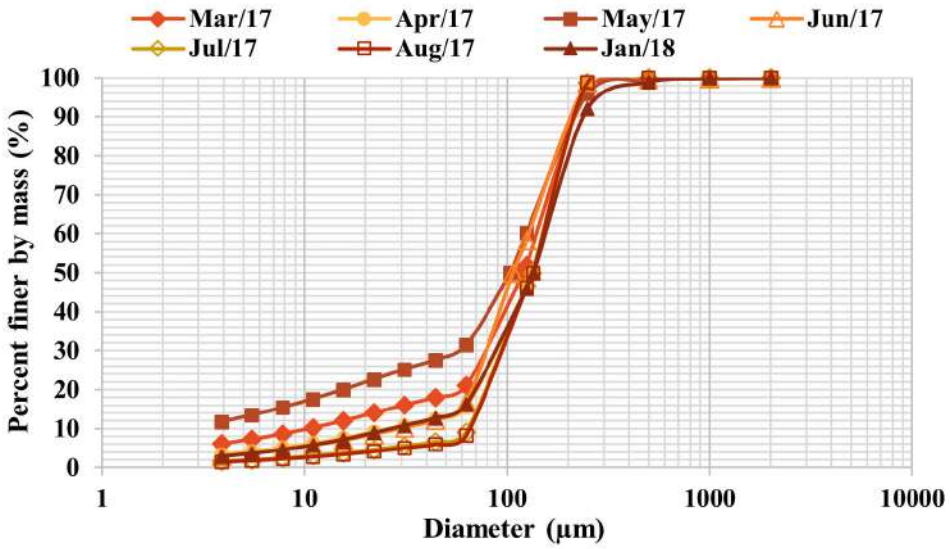

Figure 35 – Granulometric Curve for Taquari River.

5.1.2 Backscatter Correlation for Taquari River

As mentioned, the measurements at Taquari River considered the SPM and the depth-integrated water sampling to obtain SSC information. So, to be sure about the differences caused by the use of SPM instead of the FFM, it was evaluated both modes. All details about this procedure can be found in Appendix C, where it was found that it caused a difference of only 5% in the SSC, on average. Which can be considered insignificant, taking into account the amount of SSC present in Taquari River.

After all the corrections and the aforementioned analysis, Figure 36 shows the correlation between SSC and the corrected backscatter obtained for Taquari River.

Also, during the correction processing, it was evaluated the influence of the particles in the signal attenuation. It was possible by the assessment of the total solid attenuation term given by the third term from the Equation 2.5, where $\alpha_s = \alpha_{ss} + \alpha_{sv}$, a combination of scattering (α_{ss}) and viscous (α_{sv}) attenuation.

The contribution of both terms is summarized in Table 8, where it is possible to notice that, for Taquari River, sand attenuation plays an important role in the solid attenuation backscatter. In fact, considering all campaigns the sand attenuation accounted for up to 95% of the total solid attenuation. The biggest contribution of the fines in the total solid attenuation happened mainly in May and accounted only for 5% of the total solid backscatter attenuation.

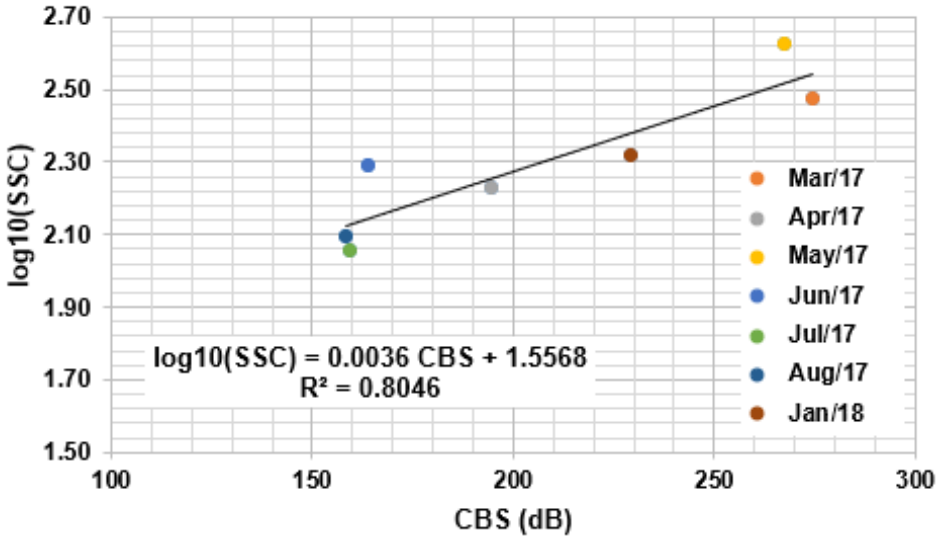

Figure 36 – Correlation curve between SSC and ADCP corrected backscatter signal (CBS) at Taquari River.

Table 8 – Comparison between the solid attenuation coefficients per campaign: α_s, total solid attenuation; α_{ss}, scattering attenuation and α_{sv}, viscous attenuation.

	Mar/17	Apr/17	May/17	jun/17	jul/17	Aug/17	jan/18	Average
α_{sv}	2.57	1.3	4.19	1.9	0.88	0.95	1.56	1.91
α_{ss}	75.06	52.88	78.85	39.84	36.46	39.52	65.61	55.46
α_s	77.63	54.19	83.04	41.73	37.34	40.47	67.17	57.37

In one analysis made by Guerrero et al. (2016), at Parana River (Argentina), they found that the attenuation coefficient for sand suspended from the riverbed was two orders of magnitude higher than the backscattering coefficient for the washload content (usually the finest particles). The goal of the solid backscatter attenuation analysis was to check how the fine solids could influence the final SSC average.

In this study, we found that the difference in these coefficients was one order of magnitude, on average the attenuation coefficient for suspended sand was 55.43 dB/m and the backscattering coefficient for the fine fraction was about 1.9 dB/m.

5.1.3 Mapping of Suspended Solid Concentration

The advantage of ADCP measurements against the manual sampling is that the ADCP measurements can rapidly provide a much higher spatial resolution of SSC in a cross-section than is possible with manual samples alone. The correlations obtained for different ADCP measured SNR intensities with the sampled and analyzed laboratory results can be used to compute SSC concentrations for each measured ADCP cell when measuring the full cross-section, thus showing and quantifying SSC variations over the cross-section.

5.1.3.1 Extrapolation for non-measured regions

As pointed out by Mueller et al. (2013), ADCPs cannot measure the whole cross-section. Non-measured regions are close to the surface (ADCP transducer draft and required blanking distance caused by the ringing of transducers), close to the banks (insufficient depths to measure with ADCP), and close to the bed (due to the acoustic side-lobe effect). The near-surface blanking distance is due to the limitation produced by the transducer vibration. As the transducer is both the transmitter and the receiver, a short distance (blank) is needed after the signal transmission to allow the transducer to adjust itself to receive the shifted signal. The side-lobe is an area of weak acoustic energy parallel to the main acoustic beams emitted by the device which reaches the bed before the main beam, producing interference when the device interprets the acoustic reflection from the main beam.

Before starting the extrapolation procedures near the bed, banks, and surface, it was necessary to fill part of the cross-section area where data collected using the 1MHz beams were removed (Figure 37). To do so, those cells were replaced by the average values of the ADCP corrected signal measured with the 3MHz frequency beams, since all signal corrections were done for this frequency, only.

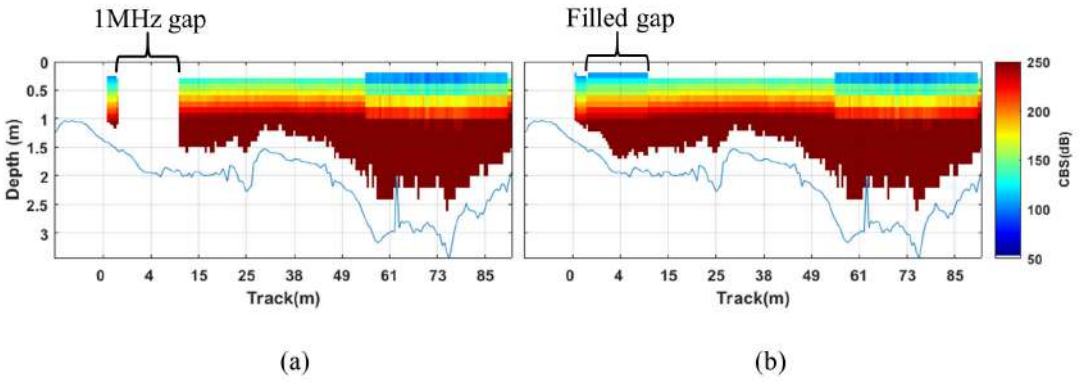

Figure 37 – Measured ADCP signal in the cross-section: (a) without the 1MHz measured cells and (b) with the 1MHz cells filled with the extrapolations obtained by the average of the signal measured by the 3MHz cells.

The comparison between the SSC obtained from laboratory ($SSC_{Laboratory}$) and the ADCP filled cross section ($SSC_{No-Extrapolated}$), as shown in Figure 37, indicate that, on average, the $SSC_{No-Extrapolated}$ was 9% lower than the $SSC_{Laboratory}$. The biggest differences were observed for May and Jun/2017 samples, where the $SSC_{No-Extrapolated}$ was 18% and 42% lower than the $SSC_{Laboratory}$ (Table 9).

Such differences were expected when we considered the representation given in the correlation curve (Figure 36), as already mentioned the correlation points from May

and June had the worst representation, with the greatest absolute difference among all correlated points.

Table 9 – Comparison between the SSC obtained from the laboratory analysis and the SSC obtained from the CBS regression and 1MHz-measured areas filled in with nearby 3MHz data — SSC units in mg/L.

	Campaigns							
	Mar/17	Apr/17	May/17	Jun/17	Jul/17	Aug/17	Jan/18	Avg
$SSC_{Laboratory}$	300.30	169.90	422.50	195.40	113.60	124.10	207.80	
$SSC_{No-Extrapolated}$	318.60	180.94	347.98	112.74	117.11	113.76	206.07	
Difference	6%	6%	−18%	−42%	3%	−8%	−1%	−9%

After filling in the measured portions of the cross-section with nearby 3MHz data, it was proceeded with extrapolating data in the unmeasured areas: near the bed, surface and banks. The near-bed extrapolation was done using an SSC x Depth exponential fitted curve. The curve was fitted to the measured ADCP data in each ensemble (in the full cross-section measurement) and extended to the bed as determined by the ADCP-measured depth. The near-banks extrapolation was done for the unmeasured areas between the last ADCP measured vertical and the edge of the water on each bank. The extrapolated area was considered triangular (with a uniform slope). A constant SSC value was assumed to be present from the first/last, valid ADCP-measured vertical to each bank. The near-surface extrapolation was simply done by extending a constant SSC value from the first measured ADCP cell in an ensemble to the water surface.

Table 10 shows the comparison between the SSC obtained from Laboratory analysis ($SSC_{Laboratory}$) and both SSC obtained by the ADCP x SSC correlation: $SSC_{No-Extrapolated}$ mapping with no extrapolation and $SSC_{Extrapolated}$ with all mentioned extrapolations (1MHz + Bed + Surface + Bank extrapolations). Also, Table 11 shows the comparison between the Suspended Load, Qss: $Qss_{Laboratory}$, $Qss_{No-Extrapolated}$ mapping with no extrapolation and $Qss_{Extrapolated}$ with all mentioned extrapolations.

In terms of suspended load (Qss) the differences between $Qss_{No-Extrapolated}$ and $Qss_{Extrapolated}$ indicated that, on average, including the extrapolated areas resulted in a 63% increase in load.

Table 10 – Difference between the measured SSC and the SSC obtained from ADCP correlation - considering the results without any extrapolations and with extrapolations — SSC units in mg/L.

	Campaigns							
	Mar/17	Apr/17	May/17	Jun/17	Jul/17	Aug/17	Jan/18	Avg
$SSC_{Laboratory}$	300.30	169.90	422.50	195.40	113.60	124.10	207.80	
$SSC_{No-Extrapolated}$	318.60	180.94	347.98	112.74	117.11	113.76	206.07	
$SSC_{Extrapolated}$	365.93	179.61	417.91	108.30	113.23	109.24	216.58	
Difference[1]	6%	6%	−18%	−42%	3%	−8%	−1%	−8%
Difference[2]	22%	6%	−1%	−45%	0%	−12%	4%	−4%

[1]Difference between $SSC_{Laboratory}$ and $SSC_{No-Extrapolated}$.

[2]Difference between $SSC_{Laboratory}$ and $SSC_{Extrapolated}$.

Table 11 – Difference between the measured Qss and the Qss obtained from ADCP correlation - considering the results without any extrapolations and with extrapolations — Qss units in $10^3 Ton/day$

	Campaigns							
	Mar/17	Apr/17	May/17	Jun/17	Jul/17	Aug/17	Jan/18	Avg
$Qss_{Laboratory}$	6.5	2.3	8.0	2.2	1.1	1.4	4.0	
$Qss_{No-Extrapolated}$	4.2	1.6	4.2	0.81	0.8	0.8	2.5	
$Qss_{Extrapolated}$	7.9	2.5	8.0	1.2	1.1	1.2	4.3	
Difference[1]	−35%	−29%	−48%	−63%	−31%	−43%	−38%	−41%
Difference[2]	22%	6%	−1%	−45%	0%	−12%	4%	−4%
Difference[3]	86%	49%	89%	50%	44%	56%	69%	63%

[1]Difference between $Qss_{Laboratory}$ and $Qss_{No-Extrapolated}$.

[2]Difference between $Qss_{Laboratory}$ and $Qss_{Extrapolated}$.

[3]Difference between $Qss_{No-Extrapolated}$ and $Qss_{Extrapolated}$.

The comparison with the $Qss_{Laboratory}$ indicates that, on average, the loads estimated using the extrapolation methods were only 4% lower than the average sampled loads ($Qss_{Laboratory}$). On the other hand, ignoring the extrapolated areas resulted in an average estimated load that was 41% lower than the $Qss_{Laboratory}$.

Differences due the extrapolation were also observed by Haun and Lizano (2018), they notice that the differences were increasing as the depth was increasing with values that range from 0.6% up to 19.4% of difference (from the shallower to the deepest cross-section, in a reservoir).

As we can observe in Figure 38, which illustrates both, the SSC and Qss extrapolated, in the whole cross-section in April/2017 (the measurement campaign with SSC values that best fit the correlation curve), most of the differences were observed for the concentrations close to the bed which (following the theoretical profile for SSC in rivers – Rouse profile), are higher than the concentrations observed throughout the water column.

Also, the corrected backscatter presented in Figure 38 matches the expected and mapped patterns SSC and therefore the Qss, presented in Figure 37, which shows that the corrected SNR and resulting estimated SSC and Qss increase with depth.

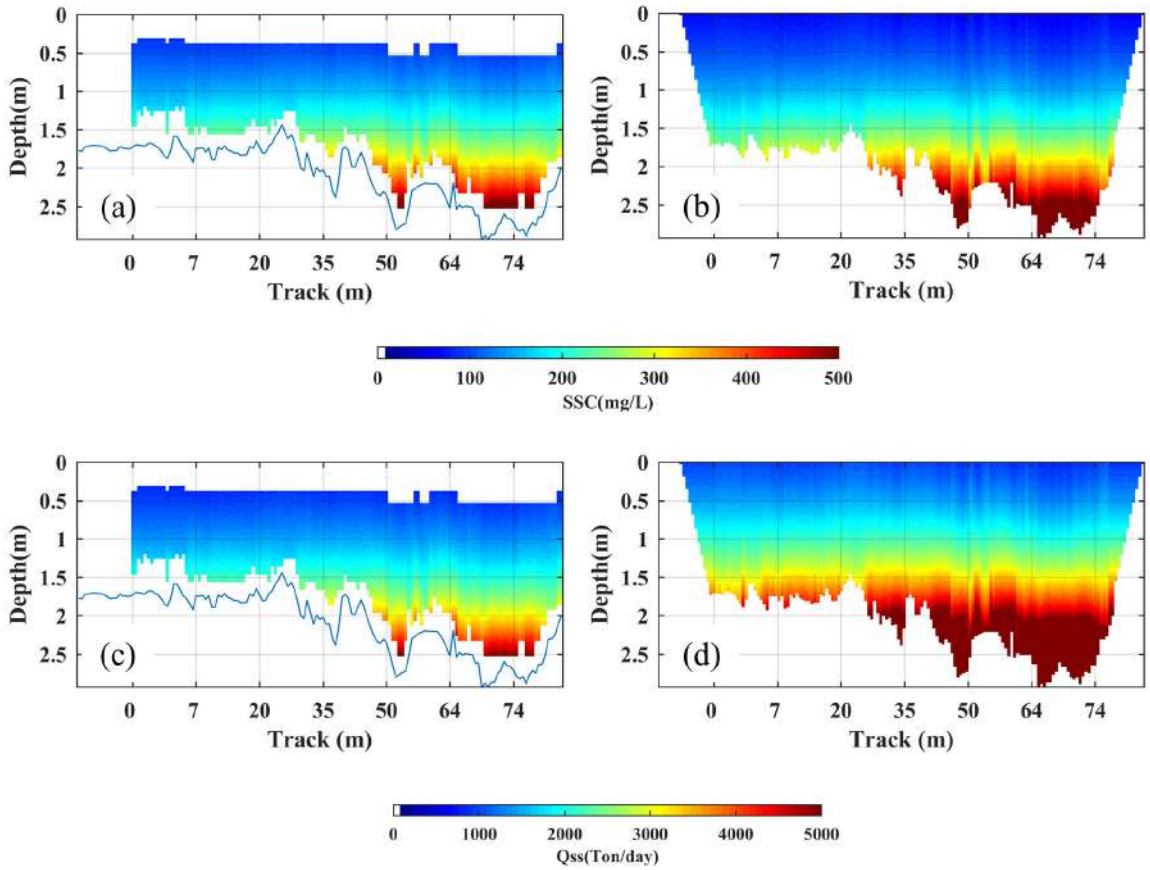

Figure 38 – Non-Extrapolated and Extrapolated Cross-Section, data from April/17: (a) Non-Extrapolated SSC, (b) Extrapolated SSC, (c) Non-Extrapolated Qss, (d) Extrapolated Qss.

5.1.4 Summary

In this section, it was performed the ADCP correction for Taquari River. Due to some particularities during the field campaigns and also due to the solid characteristics, before obtaining the CBS it was performed corrections regarding the frequency in the SPM and due to the solid attenuation coefficient. The final correlation has presented a determination coefficient (R^2) as 0.8046.

So, the final SSC and Qss mapping and average values were obtained after the extrapolation from the blanking zones: bed, bank and surface extrapolations.

The corrections techniques applied at Taquari River were used as a validation of the method in order to prove that under *ideal* conditions, such as: lotic environment, high flow velocities, high solid concentration and non-cohesive particles (silt and sand diameters), the formulations are suitable to the proposed methodology.

5.2 Passauna River

In the frame of the presented research, the Passauna River can be considered as a transitional environment for the corrections technique application. It is a lotic environment and it is the main tributary of the Passauna Reservoir, which means that the conditions to be found here will be very close to those to be found at the reservoir, but higher velocities and particle diameters.

Table 12 shows the TSS and discharge fluctuations along the field campaigns. The extreme event is evident in October, 2018 where the discharge was about 12 m^3/s and the associated TSS concentration was 209 mg/L, equivalent to 70% of the maximum concentration value $TSS_{max} = 294\ mg/L$ and 70% above the concentration average obtained during the whole time serie for this region (RAUEN; CASTRO; SILVA, 2017).

Table 12 – Mean discharge and solid parameters during the field campaigns.

	Campaigns				
	May/17	Apr/18	Aug/18	18Oct/18	20Oct/18
Q(m^3/s)	0.95	1.59	0.52	11.3	1.93
D50(μm)	93.17[1]	93.17[1]	93.17	37.22[2]	37.22
$TSS_{Laboratory}$	10.3 ± 0.4	13.31 ± 1.6	17.67 ± 6.1	209 ± 1.4	31.5 ± 2.1

[1]Filled with D50 data from Aug/18

[2]Filled with D50 data from 20Oct/18

Regarding the diameter determination, as exposed in Table 12, not all the campaigns had granulometric data. Due to some operational questions related to inappropriate use of the equipment in the field, it was decided do not to use some measurements (from April/18 and 18Oct/18) measurements due to the production of suspicious data.

Figure 39 shows the granulometric curve for 2 campaigns when the LISST was used to obtain the particle size measurements. From these two campaigns, we can observe that Passauna River presents a high content of fine and cohesive material, silt and clay, which is about 65% and about 35% of sand.

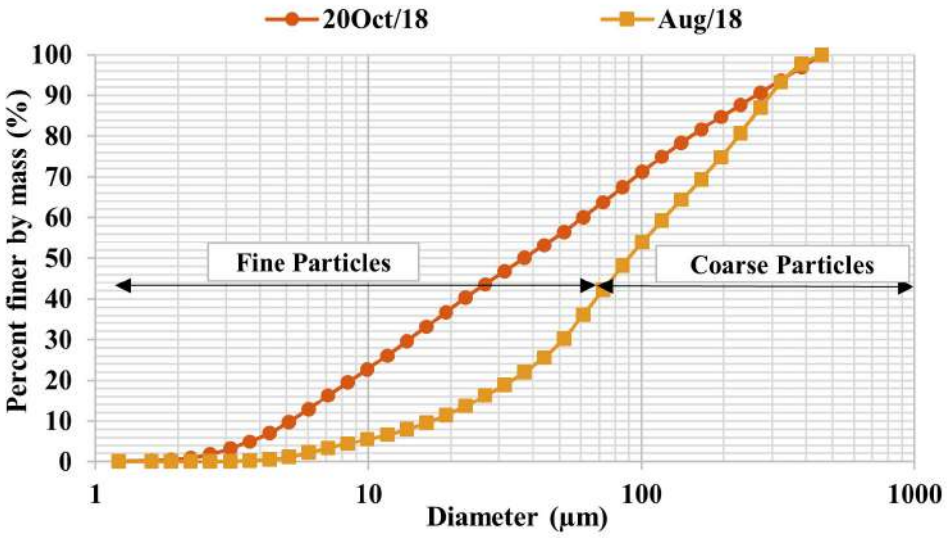

Figure 39 – Granulometric Curve for Passauna River.

To the other campaigns, it was used the available granulometric data to replace the missing values. To do so, it was considered the hydraulic and meteorological situation of the campaign day.

Figure 40 shows the relation among the parameters measured during the campaigns and the accumulated precipitation registered on the day of the measurement campaign. As we can see the variation of the parameters showed that the higher the discharge, the higher the SSC (notice that Figure 34 is arranged from the lowest measured discharge, in Aug/18, to the highest measured discharge, in 18Oct/18).

The granulometric analysis indicates that the largest diameters happened during the drought season (Aug/18) and the smallest during the rainy season (20Oct/18). As explained by Klassen (2017), cohesive particles (as the one we are leading at Passauna River), in the natural environment is subject to a great number of factors that can influence the aggregation and disaggregation of the particles. For example, one of these factors is the high velocities produced by turbulence. During the rainy events, the high turbulence may be responsible for the disaggregation of the flocs and during the drought situation may favor the formation of aggregates and therefore particles with larger diameters.

Another question related to the particle characteristics is the solid density from the suspended solids, that due their characteristics differ from the common values found in the literature (usually about $2.65 kg/L$). At Passauna River, the solids are finer presenting a medium diameter of around $D50 = 50 \mu m$, with a solid density of $1.91 \pm 0.2 kg/m^3$, according to the laboratory analysis results.

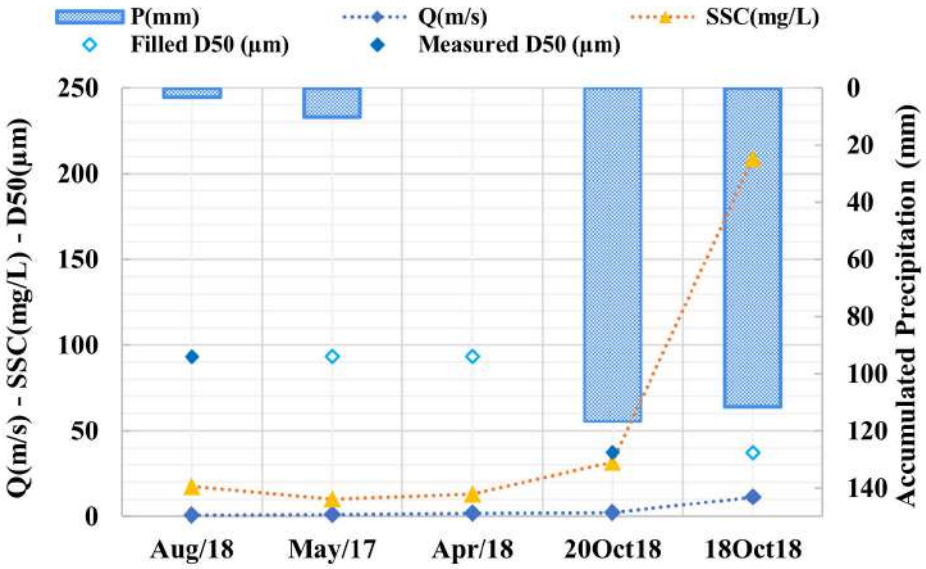

Figure 40 – Relation between the parameters obtained during the campaigns. P7 is the accumulated precipitation registered from 7 days before the measurement campaign. All parameters's values were arranged from the lowest measured discharge to the highest measured discharge.

5.2.1 Backscatter Correction

Figure 41 shows the correlation curve obtained for Passauna River, with an agreement of $R^2 = 0.9401$. Here was made point sampling and the number of samples was random in each campaign. Because of it, the corrections considered only the middle sampled point as well only the related ADCP vertical throughout the cross-section. In this context, most of the settings used for Taquari River (integrated analysis), was also applied here, but with different solids characteristics and TSS.

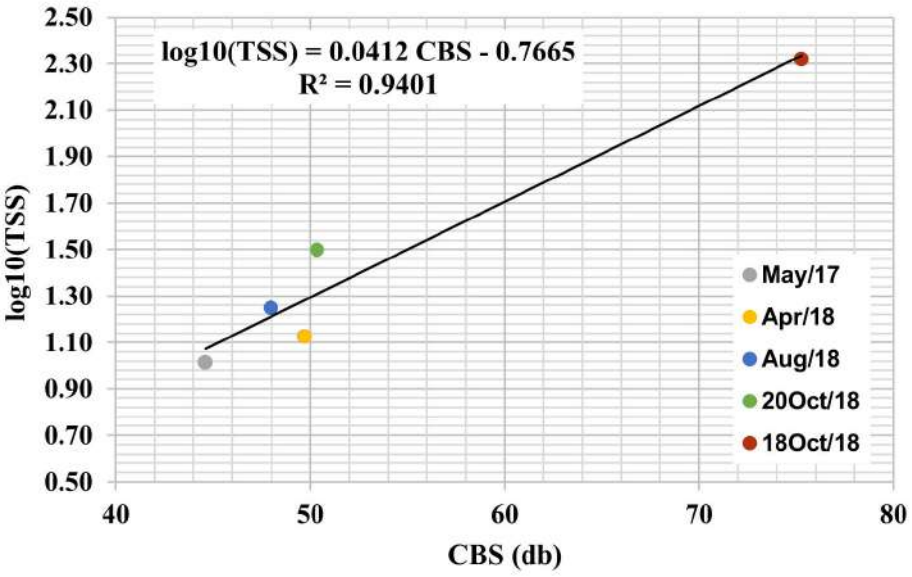

Figure 41 – Correlation curve between SSC and ADCP corrected signal at Passauna River.

Regarding the analysis of the solid attenuation term, as expected due to the granulometric content, it was noticed that the finest material plays an important role in the signal attenuation (Table 13).

Its importance is observed in the viscous-attenuation factor (α_{sv}) mainly in the rainy extreme event observed in October/18, where it has dominated more than 50% of the solid attenuation term ($\alpha_s = \alpha_{ss} + \alpha sv$).

Table 13 – Comparison between the solid attenuation coefficients per campaign: α_s, total solid attenuation; α_{ss}, scattering attenuation and α_{sv}, viscous attenuation.

	May/17	Apr/18	Aug/18	18Oct/18	20Oct/18	Average
α_{sv}	0.08	0.10	0.14	4.22	0.64	0.97
α_{ss}	2.21	2.85	3.82	3.96	0.60	2.33
α_s	2.29	2.95	3.95	8.18	1.24	3.31

5.2.2 Mapping of Total Suspended Solid Concentration

Similar to Taquari River results, after establishing a correlation curve, it was possible to obtain the TSS distribution throughout the cross-section within the extrapolated values.

Since it was shown the extrapolation importance at Taquari River analysis, here, for Passauna River it was decided do not show the intermediate step which would be comparable with the TSS without extrapolations.

In the Tables 14 and 15 are shown the difference associated to the cross-section plots and the laboratory analysis.

On average the $TSS_{Laboratory}$ was about 2% lower than the $TSS_{Extrapolated}$. The largest difference was on October 20th, followed by Aug/18, when the values obtained in the laboratory were 26% greater and 25% lower than the TSS cross-section average obtained by the ADCP signal corrections, respectively.

Table 14 – Difference between the TSS from laboratory and the TSS obtained from ADCP correlation at Passauna River. Units in mg/L.

	Campaigns					
	May/17	Apr/18	Aug/18	18Oct/18	20Oct/18	
$TSS_{Laboratory}$	10.3	13.31	17.67	209	31.5	
$TSS_{extrapolated}$	9.94	16.05	23.43	209.7	24.98	
Difference	4%	−17%	−25%	0%	26%	−2%

In terms of flow discharge, on average the laboratory values were 17% lower than the values obtained by the ADCP.

Table 15 – Difference between the Qss from laboratory and the Qss obtained from ADCP correlation at Passauna River. Units in Ton/day.

	Campaigns					
	May/17	Apr/18	Aug/18	18Oct/18	20Oct/18	
$Qss_{Laboratory}$	0.8481	1.8296	0.7878	203.9606	5.2636	
$Qss_{extrapolated}$	0.82	2.21	1.4	227.88	4.17	
Difference	3%	−17%	−44%	−10%	26%	17%

Whereas in average the differences were about −2% and 17%, for TSS and Qss, respectively, the mapping of these parameters throughout the cross-section (Figure 42) indicates that the point sampling has neglected the TSS, and therefore the Qss gradients towards to the bed. This situation was also observed in Aug/18, but in a lower percentage, since the gradient in Aug/18 was about $40mg/L$ and the gradient observed in 18Oct/18 was about $1000mg/L$.

Although in the conventional analysis is recommended that the point samples should be taken at different depths, respecting the theoretical profile (the Rouse Profile). In practice, due to safety issues, it is not always possible to even sample. But, when conducted even under extreme flood situations, it is usually taken only one sample close to the surface, which can result in unrealistic concentrations, especially in these situations when it is really important to know the incoming load.

Many studies related to reservoir sedimentation and expected life-time are based on the upstream yield data, such conventional issues can lead to a biased historical data series and when applied to these studies can lead to wrong estimations. This is an important statement if it is taken into account that there is an official Gauge Station with solid and flow discharge monitoring located in this cross-section (See Figure 21).

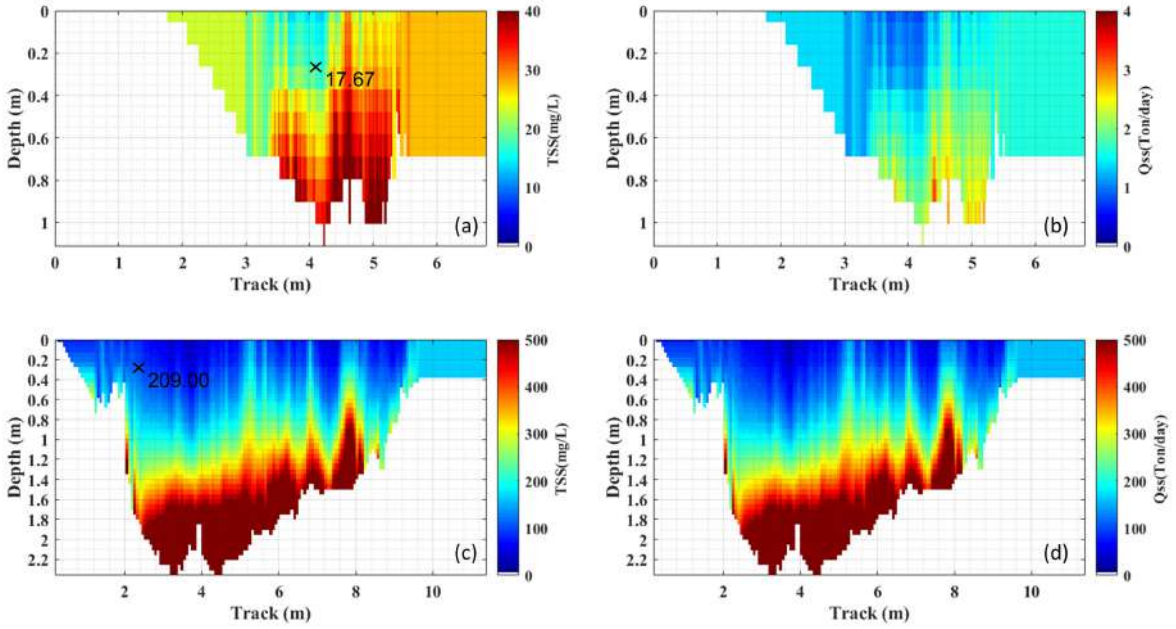

Figure 42 – Mapping throughout the cross-section: (a) TSS from Aug/18 and (b) Qss from Aug/18, (c) TSS from 18Oct/18 and (d) Qss from 18Oct/18.

5.2.3 Summary

In this section, it was obtained the correlation curve for Passauna River. The correlation has presented a good agreement, even if we consider all the different characteristics at this place than the ones observed at Taquari River — such as lower flow velocities and cohesive particles. So, the use as this place as a transitional area to test the methodology for the lentic system has been successfully accomplished.

5.3 Passauna Reservoir

As stated at Chapter 4 Passauna Reservoir is a lentic environment located at the same watershed as Passauna River, therefore it has the same sedimentologic characteristic as well it is subjected to the same weather conditions as the river.

For this environment it wasn't obtained the $TSSxQ$ relation, therefore the suspended load, because since it has low velocities the equipment wasn't capable to obtain the discharge measurements, except for the extreme rainy event monitoring when the discharge reaches $12m^3/s$ and the associated suspended solid concentration was about $160.71mg/L$.

At Ferraria Bridge the water sampling was done considering the point method, and in most of the field campaigns it was done with high spatial resolution: between 3 to 9 water samples per measurement campaign (Figure 43).

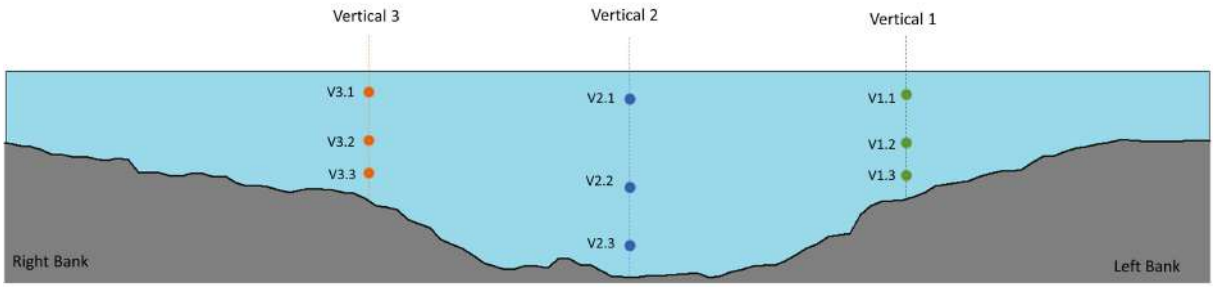

Figure 43 – Ferraria Bridge point sampling points location.

Table 16 shows the number of water samples that were possible to collect per field campaign. In October/18 was the extreme event monitoring and the sampling was done only in the middle of the cross-section (V2.1 and V2.2) because due the high velocities we assume that the cross-section would be mixed[1]. Usually, the variations on the number of collected samples were due to the hydraulic conditions at the measurement day, for example, the water level was one of the parameters taken into account in this decision.

As in Passauna River, the LISST measurements didn't cover all field campaigns. But, in fact, the measurement campaigns happened in an ideal weather situation because it covered the drought and rainy season and also the extreme rainy event, which made possible the extrapolation to the other field campaigns without granulometric data.

[1] afterwards, as shown in the Passauna River results and as will be shown here for Passauna reservoir, this assumption didn't agree with the TSS distribution obtained by the ADCP.

Table 16 – Mean parameters measured in the V2 vertical.

Campaign day	Sampling point spacial resolution
8/24/2017	9 sampling points: 3 points/vertical
8/14/2018	9 sampling points: 3 points/vertical
10/18/2018	2 sampling points: V2.1 and V2.2
10/20/2018	2 sampling points: V2.1 and V2.2
2/4/2019	3 sampling points: V1.1, V2.1 and V2.2
2/5/2019	3 sampling points: V1.1, V2.1 and V2.2
4/2/2019	2 sampling points: V2.1 and V2.2

Table 17 shows the D50 variation within the TSS (only considering the measurements made in the central vertical, V2, in the surface, and in the bottom points). The whole granulometric curve obtained for each campaign per vertical and depth is given in Figure 44.

Table 17 – Ferraria Bridge spatial resolution water sampling points per campaign.

Campaign Day	Depth(m)	Designation	D50(μm)	$TSS_{Laboratory}(mg/L)$
Oct/18	0.12	Surface	13.23	44.00 ± 4.2
	1.58	Bottom	42.01	29.67 ± 7.1
Feb/19	0.23	Surface	13.60	51.00 ± 1.4
	0.75	**Bottom**	16.01	56.67 ± 10.4
Apr/19	0.30	Surface	48.47	8.50 ± 0.3
	2.70	**Bottom**	47.98	11.50 ± 0.7

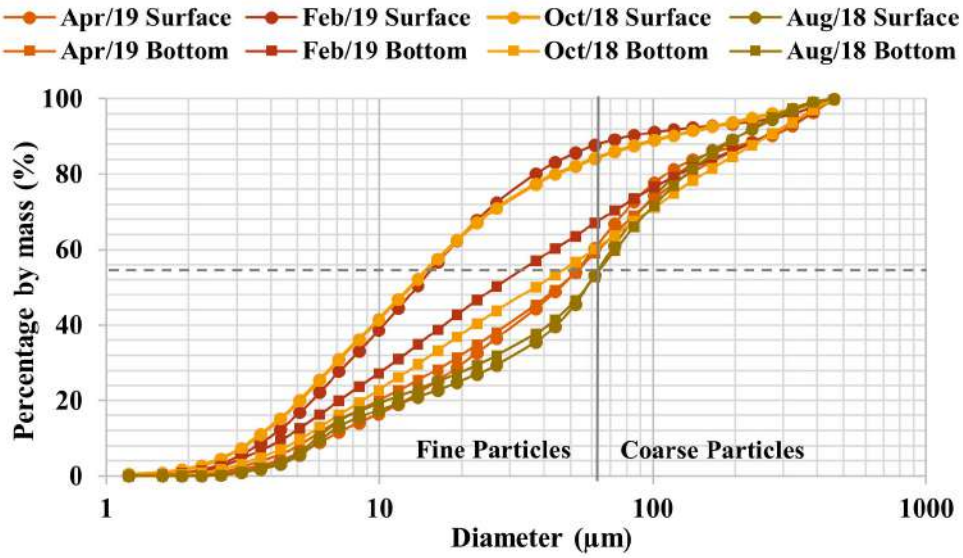

Figure 44 – Granulometric Curve at Ferraria Bridge.

From the exposed, it is possible to observe a pattern in the drought season measurements, where the D50 was similar throughout the water column (surface measure-

ments and bottom measurements). On the other hand, the TSS was different with higher concentrations close to the bottom and lower concentrations on the surface.

In the rainy season, particularly in the extreme event in Oct/18, the distribution was different and it has presented greater particles in the bottom and, different from what was expected it showed an inversion in the TSS values with a gradient varying from $29 mg/L$ in the bottom to $44 mg/L$ in the surface.

The measurement from Feb/19 showed one pattern where the TSS and D50 values can be considered uniform in the entire profile, with D50 values slightly ranging from $16 \mu m$ in the bottom to $13 \mu m$ in the surface and the TSS values ranging from $56 mg/L$ in the bottom to $51 mg/L$ in the surface.

Such patterns confirm the fact that in a medium situation the finest grains tend to aggregate and when exposed to a high energy situation, as in the turbulent flow induced by the rainy events the flocs are destroyed into small particles.

Considering the weather situation before the field measurement campaigns and the TSS determination (Figure 45), the granulometric data gaps were filled with the mean of the measured data on a given day. The measured parameters distribution over the campaigns, as well as the filled values (for the central vertical), are shown in Figure 45.

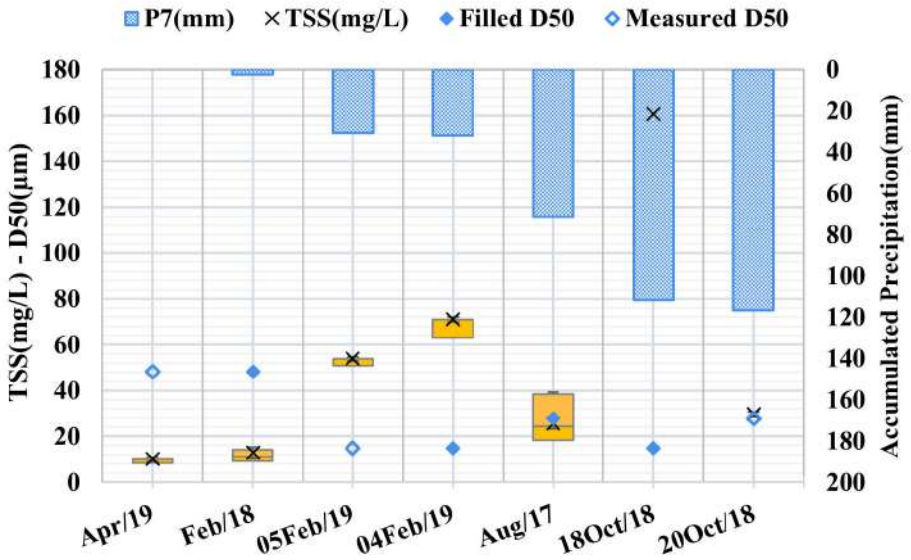

Figure 45 – Relation between the parameters obtained during the campaigns. P7 is the accumulated precipitation registered from 7 days before the measurement campaign and the yellow boxes represent the upper and lower limits of the TSS laboratory analysis in each campaign, considering the sampling distribution presented at Figure 43. All parameters's values were arranged from the lowest measured precipitation data to the highest measured precipitation data.

Here, as also observed in the lotic environment, there is a trend involving the D50 where the higher the precipitation, the lower the D50.

On the other hand, since the lentic system can take longer to answer some forcing

and inputs, the TSS pattern was different from the previously observed: there wasn't observed a straight relation between TSS and precipitation. One possible explanation for this fact is a possible lag between the sampling moment regarding the recorded precipitation data.

After all the granulometric and TSS analysis, the point values[2] were used to make the corrections considering the same formulations applied to Taquari and Passauna River and its implementation, as exposed at Figure 31 in Chapter 4.

The following section will present the backscatter corrections considering the data and assumptions presented.

5.3.1 Backscatter Corrections

Figure 46 shows the correlation curve at the Passauna reservoir through the point analysis methodology. The low agreement ($R^2 = 0.5066$) obtained in this place, when compared to Passauna and Taquari River correlations, can be due to the high uncertainty associated with the measurements and sampling of the parameters.

Even though the measurements were carefully conducted, as well as the laboratory analysis and the post-processing data, these uncertainties are most related to low velocities and low TSS concentrations. In these kinds of systems, a minimal disturbance caused by a small leaf, or by wind, or the simple movement of the boat can create noise that will be easily computed by the ADCP signal and therefore in the ADCP corrections and correlations.

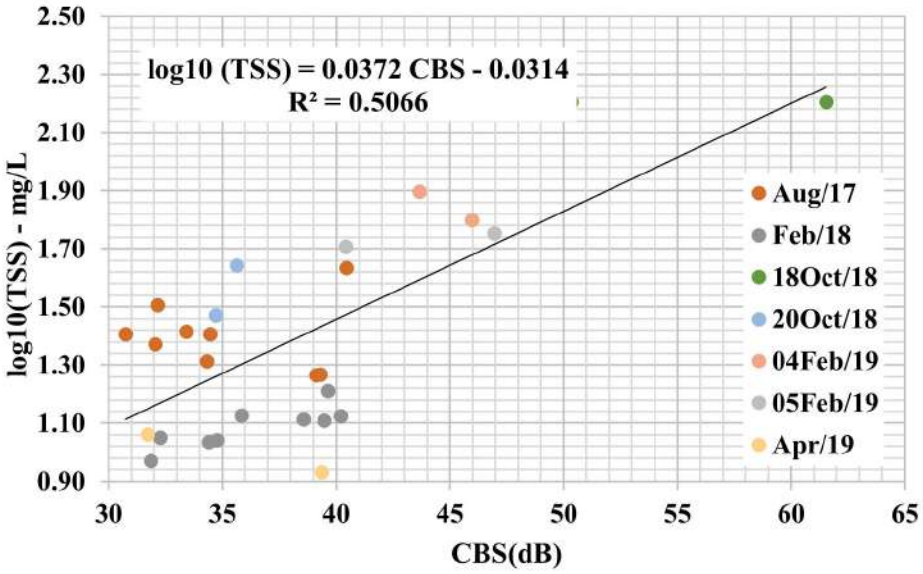

Figure 46 – Correlation curve between SSC and ADCP corrected signal at Ferraria Bridge.

[2] to simplify at this section it was shown the average value of these parameters, but for all calculations, it was considered the point values

Regarding the analysis of the solid attenuation term, due to the granulometric content, was noticed that the finest material plays an important role in the signal attenuation (Table 18), mainly during the rainy situation.

When we analyse together the values from Table 18 and Figure 45, we notice that in the rainy measurement campaigns the viscous attenuation term (α_{sv}) has the most representative effect, with values that varied from $1.26dB/m$ (which is about 78% of the total solid attenuation coefficient, $\alpha_s = \alpha_{ss} + \alpha_{sv}$), in 20Oct/18 to $2.93dB/m$ and $6.64dB/m$ in 04Feb/19 and 18Oct/18, respectively, both about 97% from α_{ss}.

The contribution of the scattering attenuation term (α_{ss}) was more evident in the drought situation (low precipitation) with values ranging from $0.43dB/m$ to $0.66dB/m$ (about 79% to 83% of the α_{ss}) in Apr/19 and Feb/18, respectively.

Table 18 – Comparison between the solid attenuation coefficients per campaign: α_s, total solid attenuation; α_{ss}, scattering attenuation and α_{sv}, viscous attenuation.

	Aug/17	Feb/18	18Oct/18	20Oct/18	04Feb/19	05Feb/19	Apr/19
α_{sv}	0.64	0.14	6.64	1.26	2.93	2.23	0.11
α_{ss}	0.15	0.66	0.24	0.35	0.10	0.08	0.43
α_s	0.79	0.80	6.88	1.61	3.04	2.31	0.55

5.3.2 Mapping of Total Suspended Solid Concentration

This section shows an overall discussion about the cross-section and the longitudinal measurement mapping. Different from the lotic environment, it wasn't considered the surface, banks and bed extrapolations.

As the lentic system is subject to the hydrodynamics forcings, such as temperature stratification, pressure variations and chemical and biologic forces, would not be possible to fit a single model to all campaigns without losing the nuances of the TSS distributions. Also, it wasn't calculated the suspended load, since the flow velocities are low which doesn't make it possible.

Figure 47 sketches the extrapolations at Passauna Reservoir, where we can see that the extrapolations would affect the TSS variations mainly on the drier days Figure 47a and Figure 47b. On rainy days, the extrapolation (Figure 47d) doesn't change too much the previous representation (Figure 47c, without extrapolation), although it is not possible to ensure that it will be well performed every time we have this situation.

Table 19 shows the comparison between the average of the $TSS_{Laboratory}$ and the average of the TSS obtained in the mapping of the cross-section was only 1% bigger than the observed by the ADCP, the differences had a big variation around the average.

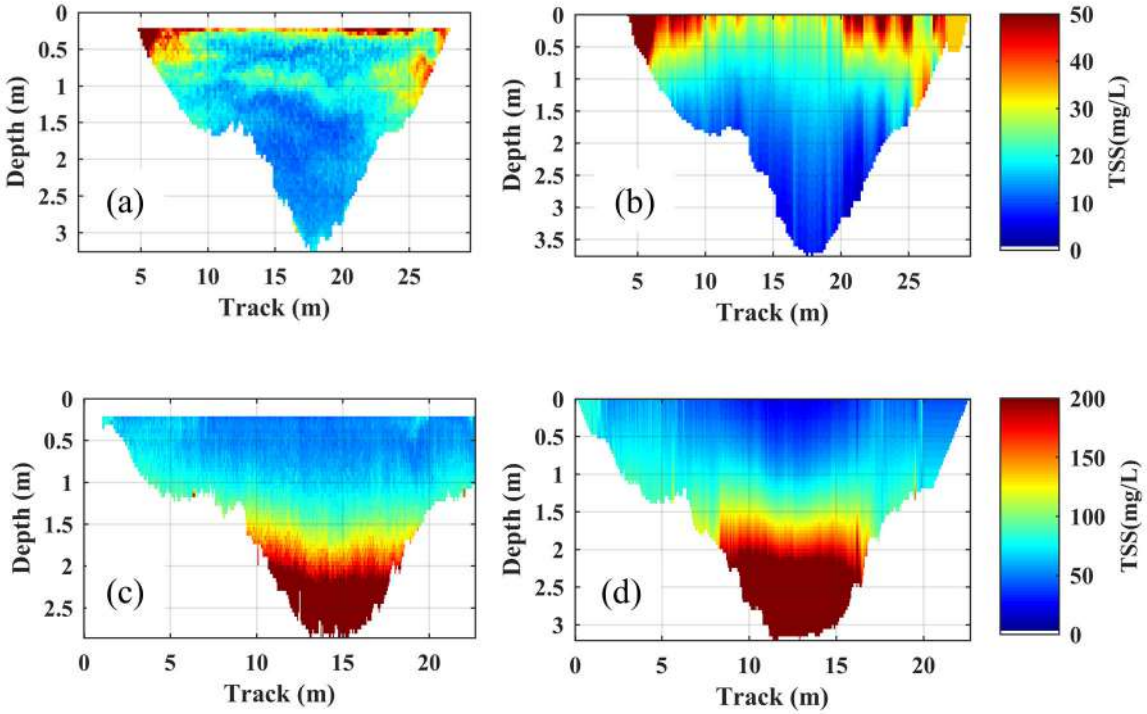

Figure 47 – Comparison between extrapolated and no-extrapolated TSS at Ferraria Bridge in Aug/17 (dry situation) and in 18Oct/18 (rainy situation).

The best TSS estimative was represented in Aug/17, when the difference was about only 4% between the laboratory analysis and the ADCP average. The biggest differences happened mainly in the rainy situation: in Feb/19, the TSS_{ADCP} was about 62% bigger than the $TSS_{Laboratory}$ and in Oct/18 (in both campaigns) the TSS_{ADCP} was about 78% lower than the $TSS_{Laboratory}$.

It is important to emphasize that the measurement from 20Oct/18 and Apr/19 count with additional uncertainty related to the field campaign and sampling. In both of the cited campaigns, the vessel used to do the measurements was launched from the left bank close to the measured cross-section, which caused erosion of the bank that spread across the cross-section. — this disturbances are evident in the mapped cross-section (see Figures 68 at Appendix D. Also, in Apr/19 the samples were collected about 3h hours difference of the ADCP, before the disturbance caused by the vessel.

Table 19 – Difference between the TSS from laboratory and the TSS obtained from ADCP correlation at Passauna Reservoir. Units in mg/L.

	Campaigns							
	Aug/17	Feb/18	18Oct/18	20Oct/18	04Feb/19	05Feb/19	Apr/19	Average
$TSS_{Laboratory}$	25.88	12.34	160.71	36.83	53.49	52.89	10.00	
TSS_{ADCP}	24.82	15.83	90.40	20.67	33.49	40.54	26.58	
Difference	4%	−22%	78%	78%	60%	30%	−62%	1%

5.3.2.1 Longitudinal transects

When performed, the longitudinal transects were made right after the cross-section measurements at Ferraria Bridge, throughout the area that involves the forebay (upstream the Ferraria Bridge location) until the area immediately downstream the Ferraria Bridge location.

From the starting point until the end, the transect covers another two monitoring points: Buffer and PPA points, as shown in Figure 48.

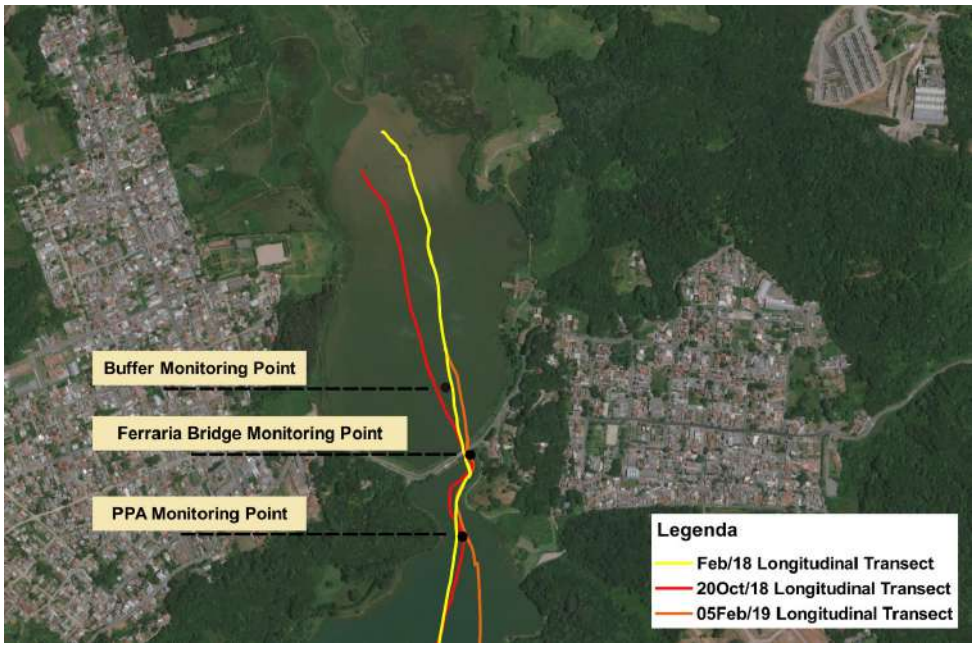

Figure 48 – Longitudinal transects and point measurements througout the transects.

From now on the idea is to cross the information from both measurement results — the Ferraria Bridge cross-section and the longitudinal transection monitoring. It is expected that the results from the longitudinal measurements reflects the results found at the Ferraria Bridge cross-section. The results are presented as following:

- Feb/18 during the rainy season, Ferraria Bridge cross-section and longitudinal transect measurement - Figure 49;
- 18Oct/18 during the extreme event, only Ferraria Bridge cross-section - Figure 50;
- 20Oct/18 two days after the pick of the extreme event, Ferraria Bridge cross-section and longitudinal transect measurement - Figure 51;
- and in 02/05/19 during the rainy season, Ferraria Bridge cross-section and longitudinal transect measurement - Figure 52;

Figure 49 shows the TSS mapping from Feb/18, where we can see the evolution of the stratification from the Buffer and FB points, with no apparent stratification until

reach the PPA point, with a gradient about $2°C$ from the top to the bottom. This situation presents a possible density current formation driven by temperature right after the Ferraria Bridge towards the PPA point. Within the density current, it is possible to notice also a gradient in the TSS and its evolution (with a variation around 20 to $50 mg/L$) towards the reservoir.

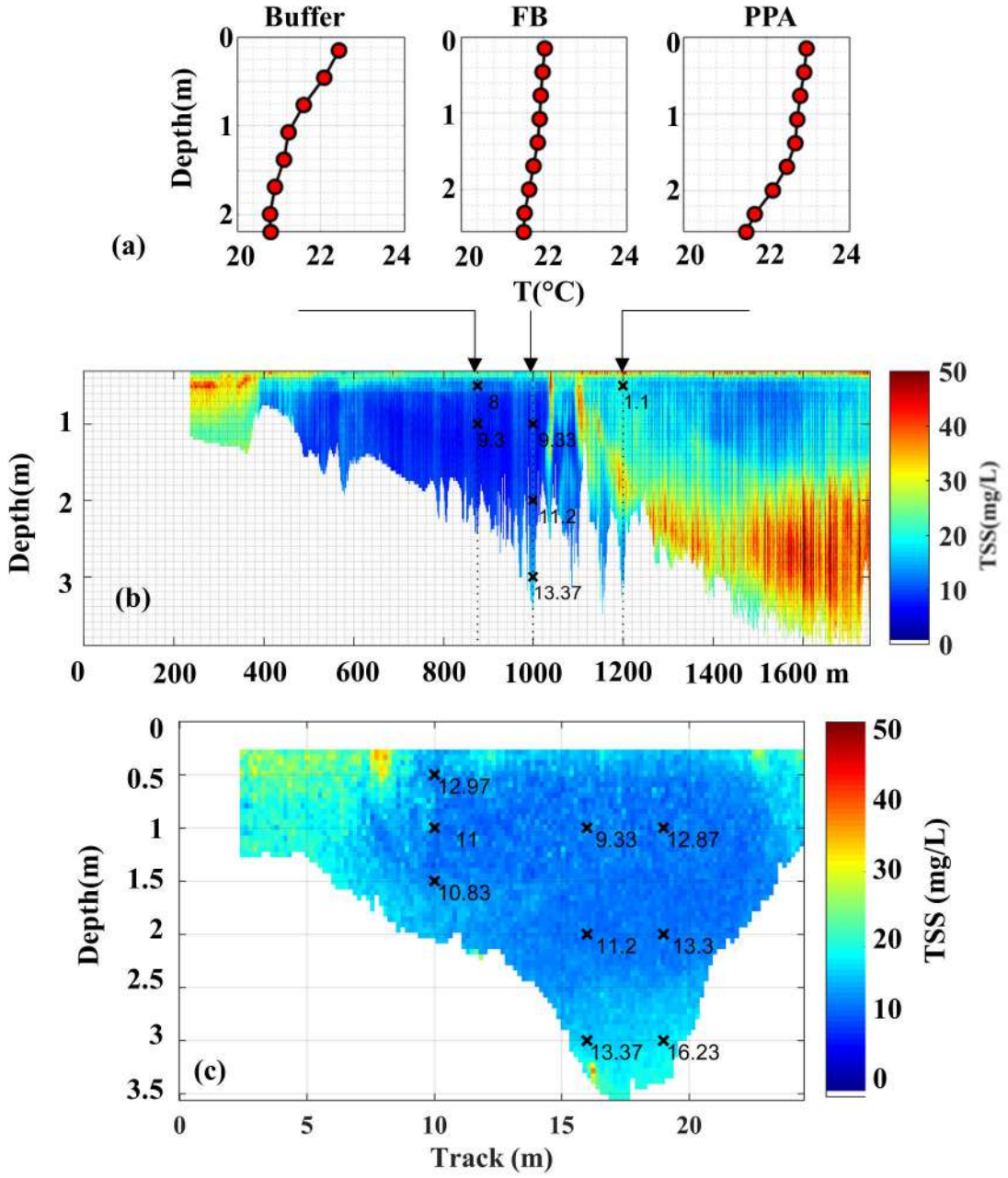

Figure 49 – Feb/18 monitoring campaign: (a) Temperature Profiles from Buffer, Ferraria bridge (FB) and PPA points, (b) Longitudinal Transect and (c) Ferraria Bridge Cross-Section. All values exposed in the transects are TSS in mg/L.

In 18Oct/18 (Figure 50), although the temperature profiles indicate a very well mixed situation (the temperature variation is lower than $1°C$), in terms of TSS the cross-

section mapping shows a strong TSS gradient over the depth — with higher concentrations values in the bed, the variation goes from about $50mg/L$ up to $200mg/L$ which can indicate an underflow turbidity density current (when the density current isn't driven by temperature but by TSS differences).

This measurement was taken during the extreme event when the Ferraria Bridge cross-section presented a lotic situation and a flow discharge about $12m^3/s$ (in a place where it is usually lower than $1m^3/s$).

Regarding the longitudinal transect, unfortunately for the extreme event, the longitudinal transect was not performed, so the density current couldn't be tracked.

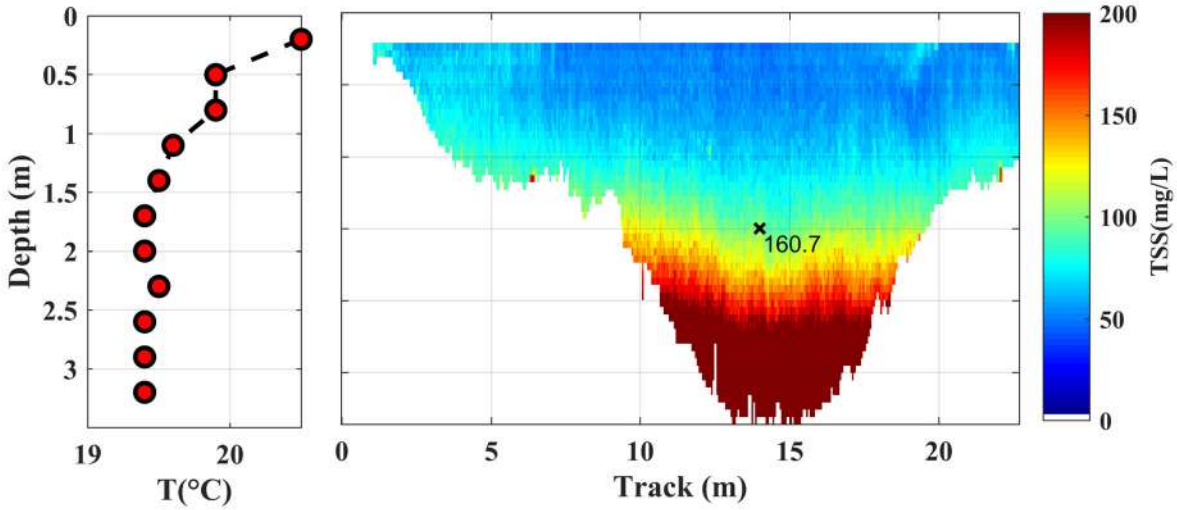

Figure 50 – 18Oct/18 monitoring campaign: Ferraria Bridge Cross-Section Mapping and Temperature Profile.

Even though Figure 51 represents the reservoir only two days after the peak of the event, it shows a situation completely different from that one observed before. Although the laboratory results indicate an inverted gradient in the cross-section mapping (Figure 51c), with higher TSS values close to the surface ($44mg/L$) and lower TSS (about $30mg/L$) close to the bed, the ADCP mapping didn't show any pronounced gradient and, in fact, the results show a low TSS concentration and a weak temperature stratification (Figure 51a).

This mixed situation is also observed in the longitudinal transect mapping (Figure 51b), where the water column has presented an almost constant $5mg/L$ TSS concentration with some variation in the deepest part from 10 to $20mg/L$. The strong and local variation observed in the Ferraria Bridge area, close to the surface can be accounted for some disturbance caused by the boat moving or the handling of the equipment in the measurement point.

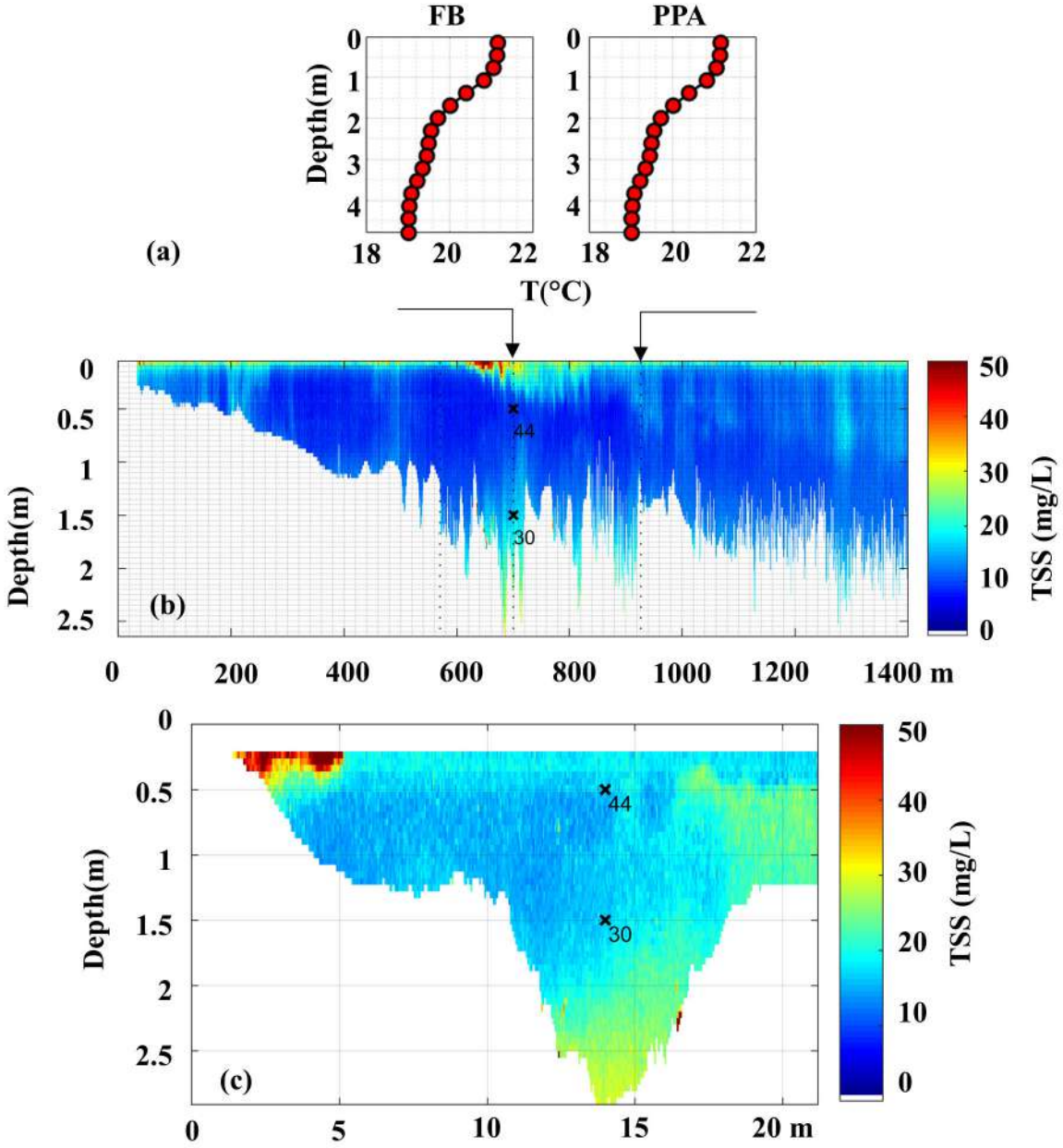

Figure 51 – 20Oct/18 monitoring campaign: (a) Temperature Profiles from Ferraria bridge (FB) and PPA points, (b) Longitudinal Transect and (c) Ferraria Bridge Cross-Section. All values exposed in the transects are TSS in mg/L.

As in Figure 49, in the measurement performed in 05Feb/19 (Figure 52) it is possible to observe the Temperature stratification evolution from the Buffer and FB points to PPA point, where first the situation wasn't stratified and then it starts to present a gradient about $2°C$ in only $1.5m$ deep. Within this variation, comes the TSS variation which leaves the Ferraria Bridge in a very well mixed situation (with TSS values ranging around $50mg/L$) and starts to spread towards the reservoir as a submerged density current with a TSS gradient from about $50mg/L$ up to $100mg/L$.

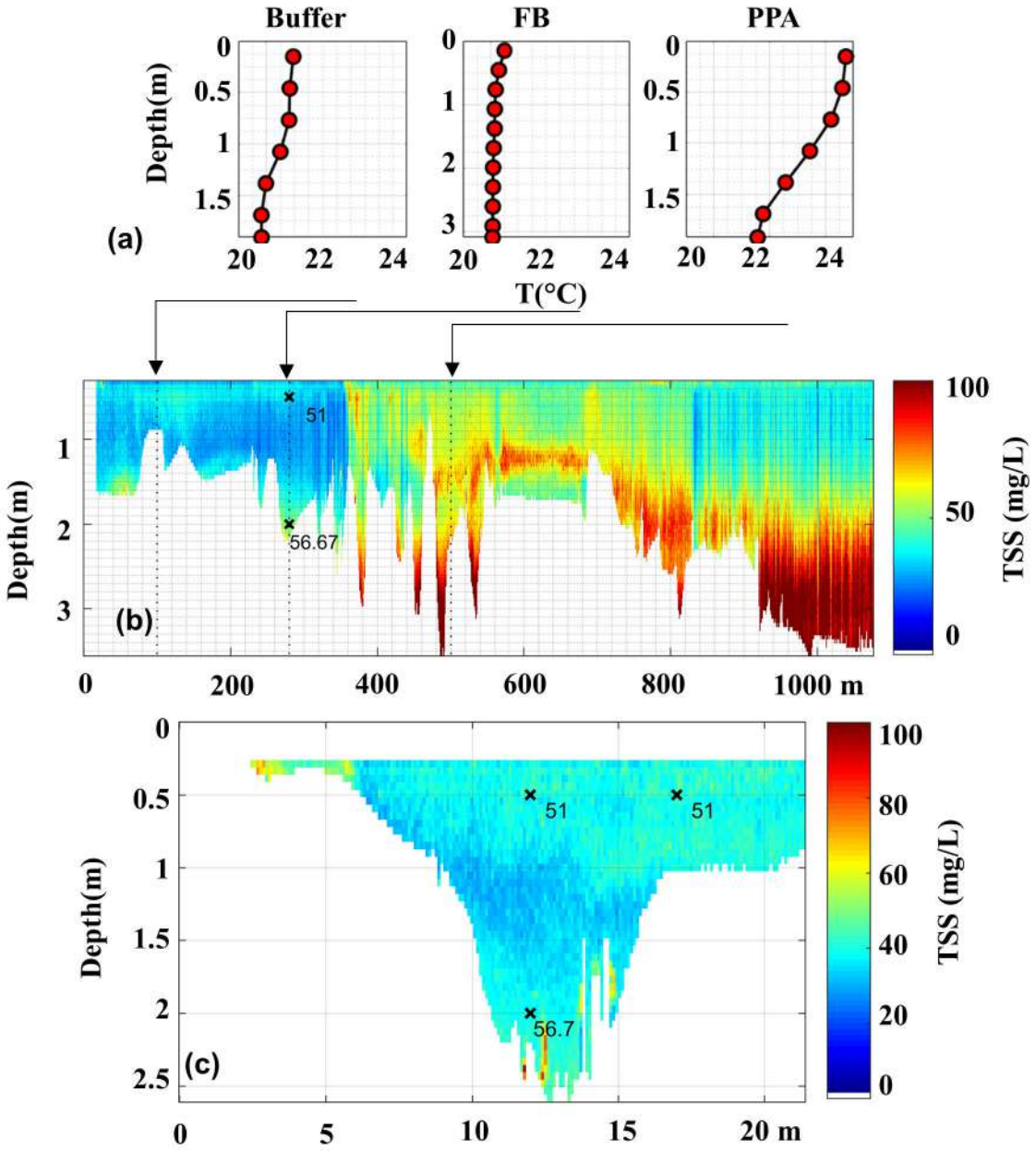

Figure 52 – 05Feb/19 monitoring campaign: (a) Temperature Profiles from Ferraria bridge (FB) and PPA points, (b) Longitudinal Transect and (c) Ferraria Bridge Cross-Section. All values exposed in the transects are TSS in mg/L.

The existence of the density currents observed by the ADCP in the results can be confirmed by the comparison with the analysis of the results from two recent studies regarding the bed solid throughout the talweg and the sedimentation rate downstream the bridge, close to PPA point.

Sotiri, Hilgert and Fuchs (2019) analyzed the bed solid content from upstream to downstream at Passauna reservoir and have found that before the bridge, in the forebay, the solid is majority composed by a silt-clay fraction (C12) — Figure 53. Under the

Bridge, it is replaced by almost 15% sand and 45% clay-silt fraction and right after the bridge (G7), close to the PPA point, where Ono (2019) has found a sedimentation rate up to $180 g/m^2$ (the higher sedimentation rate observed in her study), the sand fraction goes up to almost 45% and the silt-clay fraction drops to almost 15%, and then after all this dynamics, the silt-clay fraction establishes again along the talweg in the reservoir.

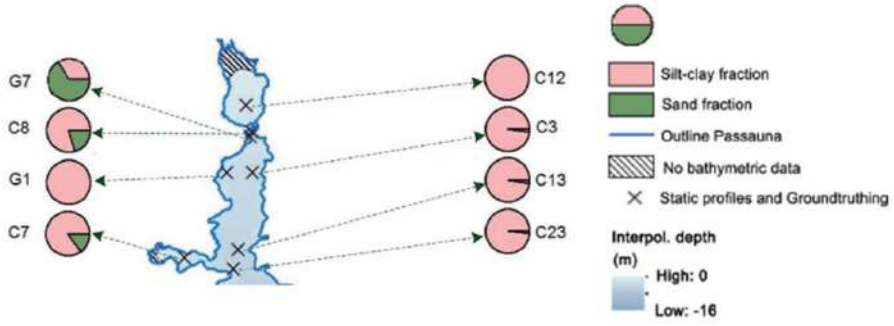

Figure 53 – Granulometry from Grab (G) and Cores (C) obtained by Sotiri, Hilgert and Fuchs (2019) at Passauna Reservoir. Adapted from: Sotiri, Hilgert and Fuchs (2019).

As exposed by Morris and Fan (1998) this solid dynamic can be related to the density current development and in a reservoir, most of the deposition is focused along the talweg where the density current usually develops. According to them, the solid begins depositing from turbidity currents right after the plunge point — possibly the point where it was observed the highest sedimentation rate associated with the highest particle size (G7 point).

To conclude, the authors highlighted that deposits from turbidity currents consist of fine material, finer than the observed in the delta deposits, even in reservoirs where most of the inflow load consists of fine fractions, as in the Passauna system.

5.3.3 Comparison within other TSS studies conducted at Passauna Reservoir

In the frame of the Mudak Project, several studies are being conducted in order to understand the system and also to reduce the complexity of the measurements with the proposition of advanced monitoring tools. This section sketches the comparison of the mapping results in the lentic environment with results obtained by other researchers. It is important to mention that the majority of these findings are still being constructed and investigate by the researchers and were given as a courtesy by the responsible. Therefore they were not published yet.

Figure 54 shows the comparisons from the extreme rainy event from Oct/18. On 18Oct/18 it is possible to see that after pass through the Ferraria Bridge cross-section the temperature variation (Figure 54a) establishes a pattern that travels toward the reservoir until reach the dam. Apparently, this variation in temperature does not play a role in the tracer spreading (Figure 54b), since it has present a different shape after the bridge cross-section. Also, such observations match with the ADCP measurement result within the cross-section with a very pronounced gradient that ranged from about $100 mg/L$ up to $200 mg/L$.

Regarding the measurements conducted in 20Oct/18, Figure 55, the numerical modeling results indicate a mixed situation (two days after the peak of the event) mainly close to the bridge, reflecting the uniform pattern observed in the TSS throughout the measurement of the longitudinal transect.

Figure 56 shows the comparisons from the whole reservoir and the mapped cross-section at Ferraria Bridge on 04Feb/19 considering numerical modeling (Figure 56a and b) and remote sensing techniques (Figure 56 c and d) to describe the spreading of the solids in the reservoir. Although for this day the longitudinal transect made with the ADCP was not performed it is possible to see that the variations observed at the cross-section were connected to the variations observed upstream of the Ferraria Bridge.

At Figure 57, it is shown the measurements from 05Feb/19. Both the results of the numerical simulation (Figure 57a 57b) and the results of the remote sensing(Figure 57c) confirm the dispersion pattern of the plume of solids observed in the longitudinal transect made with the ADCP(Figure 57d and 57e), the measurement of ADCP matches with the ranges of values on the surface found by the hyperspectral camera.

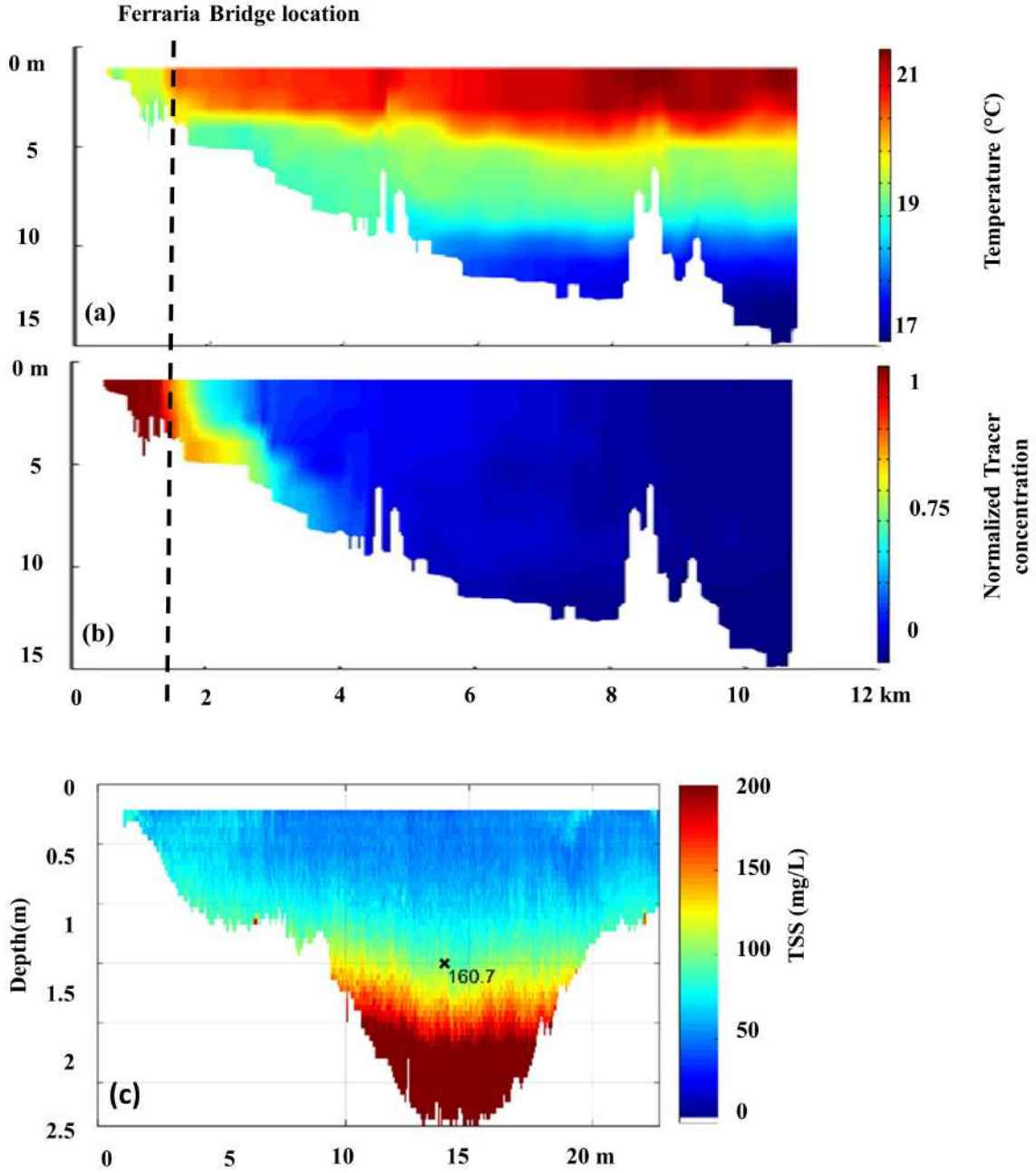

Figure 54 – Comparisons of the measurements performed on 18Oct/18 among numerical modeling for (a) Temperature and (b) Tracer Normalized Concentration (courtesy from Wendy Gonzales) and (c) the mapped cross-section made with the ADCP already discussed at Figure 50.

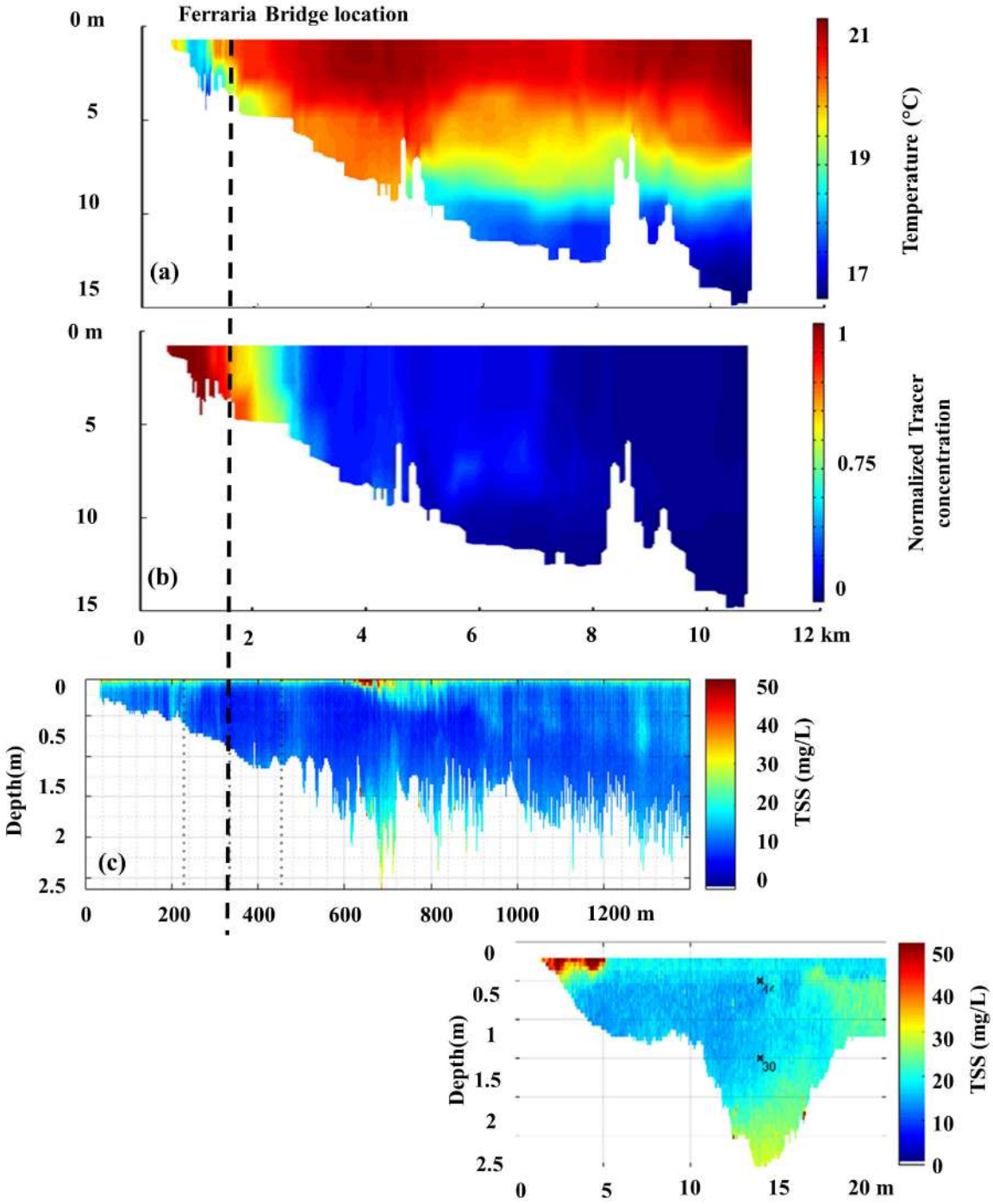

Figure 55 – Comparisons of the measurements performed on 20Oct/18 among numerical modeling for (a) Temperature and (b) Tracer Normalized Concentration (courtesy from Wendy Gonzales) the mapped longitudinal transect and (d) the mapped cross-section made with the ADCP, both already discussed at Figure 51.

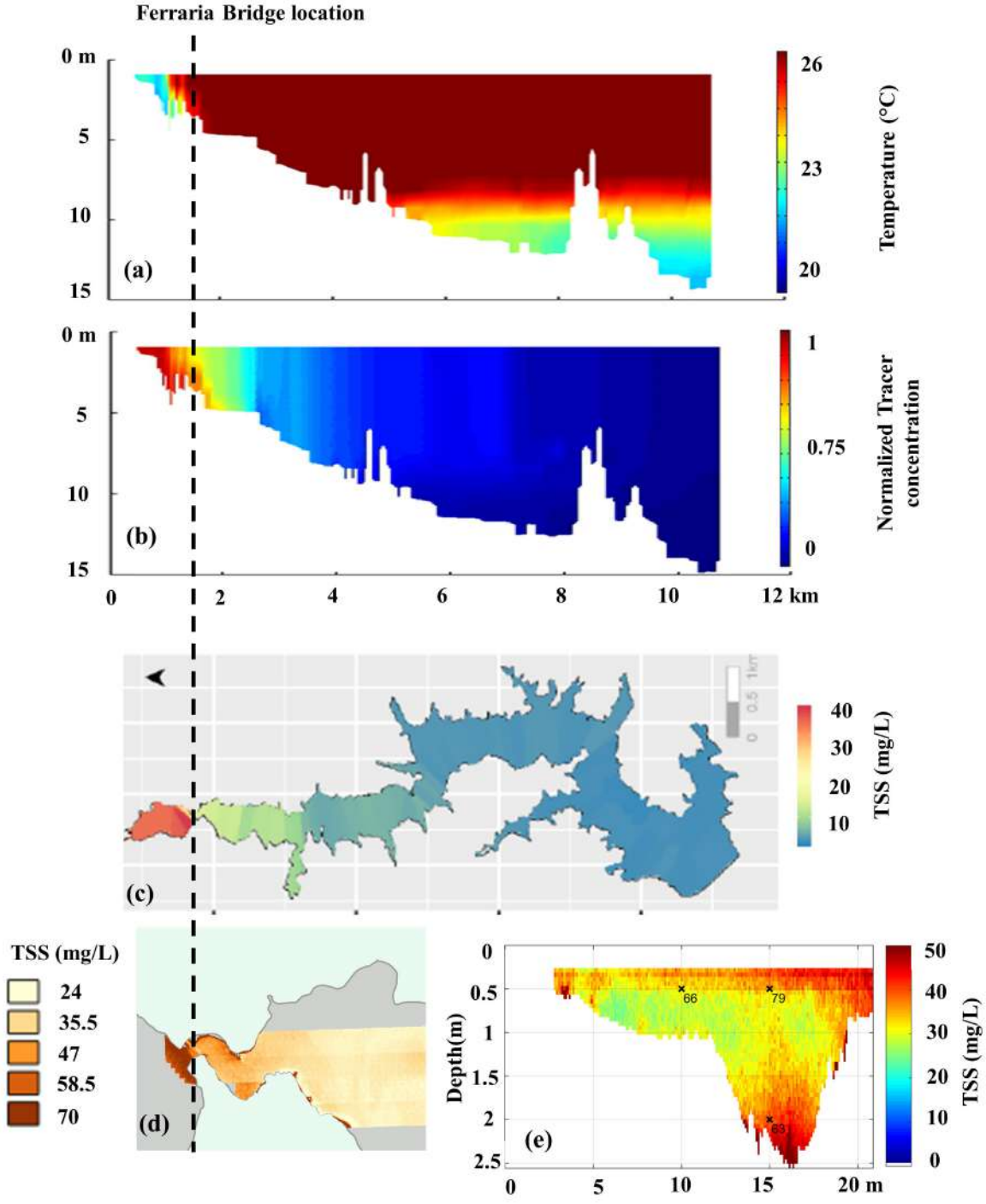

Figure 56 – Comparisons of the measurements performed on 04Feb/19 among numerical modelling for (a) Temperature and (b) Tracer Normalized Concentration (courtesy from Wendy Gonzales), (c) the TSS in the water surface obtained by close remote sensing, after Wagner (2019), (d) a composition obtained by drone images (courtesy from Jens Kern) and (e) the ADCP mapped cross-setion obtained at the presented study.

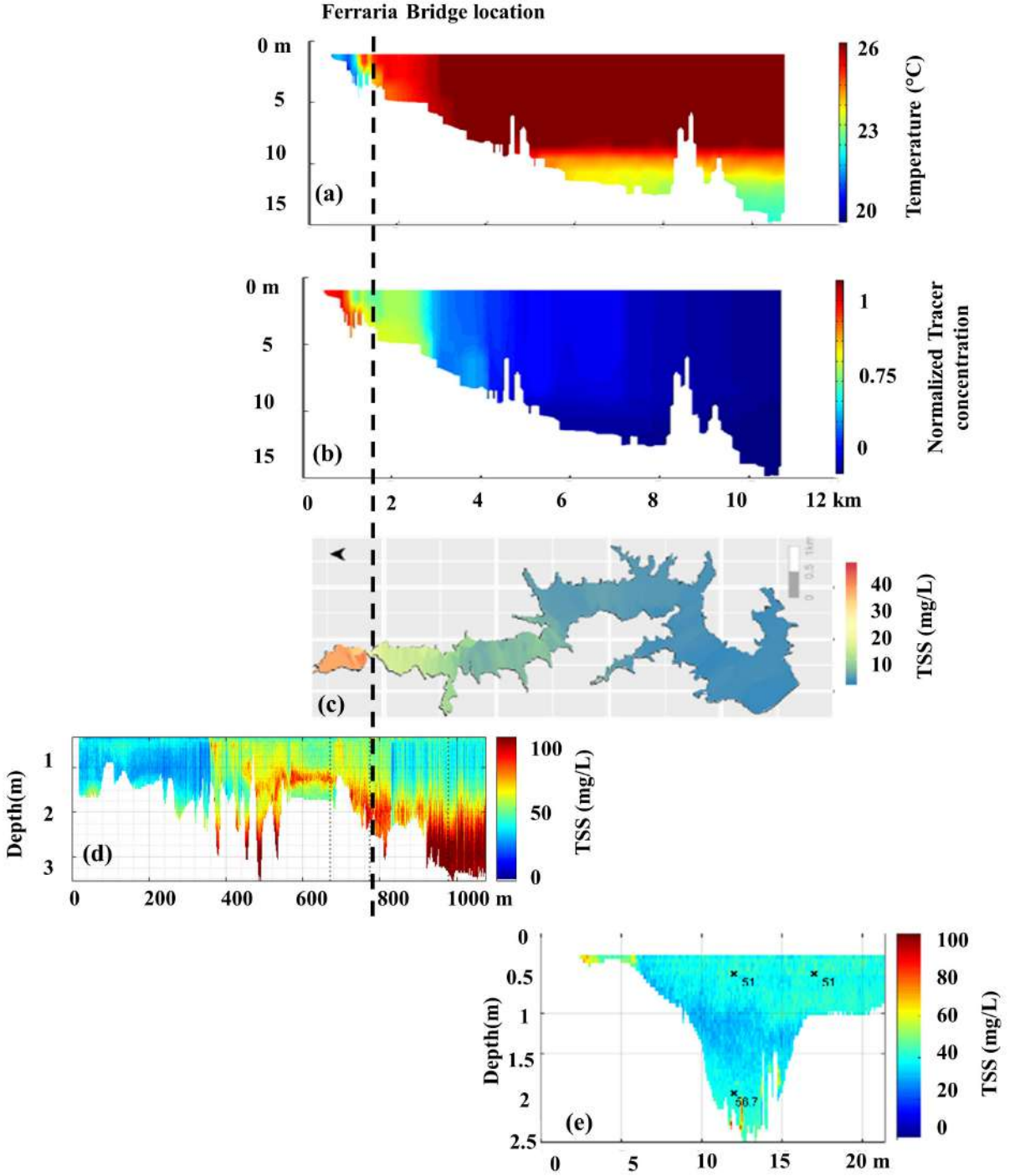

Figure 57 – Comparisons of the measurements performed on 05Feb/19 among numerical modeling for (a) Temperature and (b) Tracer Normalized Concentration (courtesy from Wendy Gonzales), (c) the TSS in the water surface obtained by close remote sensing, after Wagner (2019), (d) the mapped longitudinal transect and (e) the mapped cross-section made with the ADCP, both already discussed at Figure 52.

5.4 Discussion

From the exposed the differences between measured solids and in the solid estimated by the ADCP calibration in all analyzed environments can be accounted for several factors. Among them, it is possible to cite questions related to operational issues regarding field measurements, equipment setup and divergence between the sampling point and the measured signal. Also, the variation on temperature and in the solid concentration during the measurement campaign (SZUPIANY et al., 2019). The solid and diameter determination (whether in-situ or not) and the bias related to laboratory analysis.

In this context, the most challenging factor in laboratory analysis was regarding the low solid concentration in most of the campaigns in the Passauna system (which were about $10mg/L$ to $70mg/L$, with a spike during the rainy event of $160mg/L$ and $209mg/L$, in the reservoir and in the river, respectively). On the other hand, although laborious in Taquari River the laboratory analysis didn't represent a challenge due to its high solid concentration and mostly sand content.

Although it is known that the transmitted power can influence on the emitted signal, thus in the corrections, this factor was not considered in the calibrations because the differences in the voltage of the ADCP within the campaigns were considered low: $1.8volts$ at Taquari River measurements, $4.48volts$ at Passauna River measurements and $5.83volts$ at Passauna Reservoir measurements. Nevertheless, this is an important parameter to take into account, since differences observed by Szupiany et al. (2019) was in the order of $17.76volts$, which combined to the electric current variation has produced an underestimation of 68% in the sand concentration estimative.

In rivers, extrapolations play an important role in the TSS estimative. This was also observed by Haun and Lizano (2016) in a lentic environment, although any operational extrapolation was conducted by that study, due to the difficulties also founded at Passauna reservoir on the establishment and operationalization of such extrapolations, due different patterns intrinsic to lentic places. Also, another factor that must be considered by following Taquari River results is that even when sand content is more expressive the correction for fines must be taken into account in the calibration, such finds were also highlighted by Moore et al. (2013) and Szupiany et al. (2019).

From Passauna Reservoir results, it is possible to understand that mainly in lentic environments the average of the mapping at the cross-section it is not a good metric to determine the differences between laboratory measurements and the estimate of the concentration of solids obtained by ADCP. From each mapping (see the whole set of mapping result Figures at Appendix D)it is possible to observe that most of the laboratory analysis matches, not only in relative terms but also in absolute terms (in some points), to the equivalent depth point within the mapped cross-section. This is true mainly when

major variations are observed (by the ADCP) in the cross-section, reinforcing the fact that point measurements are not able to indicate solid variations, therefore characterize the whole cross-section.

Lentic systems are ruled by hydrodynamic forces, such as temperature variations due to interactions between atmospheric factors (pressure, heat, wind, etc) and the water column or between the water column and the bed, among others. Since it is not a flow velocity driven system, any disturbance can influence and cause different patterns in the solid distribution in the water column. These kinds of variations may have an effect on the acoustic signal, as observed in the mapped situation on $20Oct/18$ and $Apr/19$, when the vessel was launched from the margin.

Because water density variations (driven either by temperature or solid) can affect the acoustic signal (SZUPIANY et al., 2019), it was possible to observe variations in the longitudinal transections. The solid concentration gradient identified was about $50mg/L$ in Feb/18 to about $100mg/L$ in Feb/19 and the observation of some nuances (about $20mg/L$) in the longitudinal transect of 20Oct/18. Such values were different from other studies observed by Morris and Fan (1998), where the density current was characterized also by a high solid concentration ($41000mg/L$ and $72000mg/L$).

Although it is difficult to establish a quantitative threshold in the density or turbidity current definition, it is a fact that there is a solid plume identified by the ADCP coming into the reservoir and driven by the velocities produced by differences in temperature of the incoming flow. Such a statement is supported by the temperature profiles measured in the field campaigns (showed from Figures 49 to 52) and in the findings produced by others researches at Passauna reservoir in the frame of Mudak Project (see the previous section).

Also, the comparison within other findings, indicate that the technologies can complement each other. Considering that vertical profiles can detect variations within the water column and fill the information that it is missing with remote sensing. The opposite statement is also true because remote sensing provides information about the water surface that is not possible with the ADCP or another local sensor. In addition, the combination of these technologies can be used for calibration and validation of numerical models that further can be set for diagnostic and scenario models.

5.4.1 Summary

In this section, considering the methodology adopted for the rivers, it was presented the results for Passauna Reservoir.

The reservoir is considered a lentic environment with different conditions of the previously analyzed systems — a combination of hydraulic and hydrodynamic conditions,

highly cohesive solid fractions (silt-clay), the presence of organic matter, among others. Such characteristics can influence the formation of the aggregates (among these aggregates have also the combination of mineral+organic matter) that will behave differently from the essential solid composed only by mineral particles in lotic environments.

As observed in the mapping results, and confirmed by the comparison of other researchers in the same area, the ADCP and the adopted correction methods applied were able to see the gradients in the Ferraria Bridge cross-section and in the longitudinal transects.

6 Conclusion and Outlook

The objective of this study was to assess the feasibility and limitations of using acoustic surrogate technologies using a down-looking moving ADCP to map solid concentration and transport characteristics in a lentic environment.

It has been presented a correlation method between acoustic measurements and solid concentrations to obtain and compare solid concentration information within lotic and lentic environments. The main idea was to check if the lotic environment methodology could be enhanced and extended to the lentic environment in order to study its dynamics – such as turbidity or density current formation, considering all the differences between the presented systems.

Main outcomes of this study were:

- Improvements of using down-looking moving ADCP measurements for solid transport analysis in lotic environments
- Development of a post-processing methodology for down-looking moving ADCP measurements for solid transport analysis in lentic environments.
- Development of mapping algorithms of concentration distributions measured by ADCPs
- Description of dominant solid transport characteristics and flow paths

6.1 Improvements for solid measurements in a Lotic Environment

Considering that the ADCP measurements have met the quality criteria for discharge evaluation, such as the measurement of vertical profiles for moving bed evaluation and correct cross-section measurement settings, it was possible to apply the methodology described at Landers et al. (2016) and Guerrero et al. (2016), both based on the modified sonar equation proposed by Urick (1975), to obtain the correlation between the corrected ADCP signal and the measured SS.

Lessons learned, limitations and findings for the river environments were:

- Besides the corrections applied to the raw signal, it was noticed that the difference of 5% in SNR estimated using the ADCP's Fixed Frequency and Smart-Pulse modes did not significantly affect the correlation curve and resulting estimated SSC.
- Regarding the mapping extrapolations (bed, surface, and banks) applied to the ADP measurements, the results indicated a small difference in the SSC, about 3%

between $CBS_{extrapolated}$ and $CBS_{no-extrapolated}$. On the other hand, such differences were much greater when comparing sediment load, about 63% different, which indicates the importance of considering the extrapolations mainly when estimating suspended load, showing the importance of considering the extrapolation on the non-measured areas.

- The results also indicated that past survey data can be post-processed to map suspended solid concentration patterns over the measured cross-section. In addition, obtained correlations can be used when future ADCP measurements are made at the same cross-sections, even without sampling.

- The application of the methodology for the Passauna river showed the importance of the analysis and consideration of the viscous term, in the solid corrections, mainly during the extreme event monitoring, when the presence of fines was more significant. Regarding the comparison between a surrogate and conventional TSS, it was observed that on average the differences were about 2% between laboratory and TSS from ADCP. The differences were bigger in the suspended load estimative, about 17% between laboratory and ADCP.

6.2 Development of the method for Lentic Environment

In the lentic system, with mostly fine and cohesive solid content and a totally different dynamics compared to the lotic system, the results showed that the ADCP was able to detect different gradients related to the suspended solids within the monitored cross-section and longitudinal transects. However, for this environment, a weaker agreement between the surrogate and conventional analysis was observed.

A major finding was the ability of the method being able to detect a solid plume driven by a density current formation, which allows describing the interflow and underflow characteristics as dominant solid transport pathway.

Such outcomes are supported by the comparison with thermal variations from upstream to downstream, wherein most of the campaigns it was observed a stratification pattern that comes from the inflow to the reservoir, and by the observation of the sedimentation rates and patterns observed by Ono (2019) and Sotiri, Hilgert and Fuchs (2019).

The weaker agreement between conventional and surrogate technology in the lentic system can be associated with uncertainties when comparing in-situ with sampled laboratory, especially when related to low solid concentrations. Furthermore, uncertainties related to the system and the application of the sensor analysis should be considered: due to the low concentrations and low flow velocities, a minimal disturbance caused by a small leaf, or by wind, or the simple movement of the boat can create noise that will be

easily computed by the ADCP signal and therefore in the corrections and correlations. To overcome those sensitivities, several repetitions of stationary measurements showed advantages by using statistical analysis in post-processing, which was not possible with the few conventional samples.

Also, it is necessary to consider that the solid content in the lentic environment is composed mostly of fine and cohesive particles which will favor the aggregation. Although the fine particles are considered in the formulations as the viscous term (α_{sv}), still the effects of the interaction between sound waves and the flocs are not fully known.

Lessons learned and limitations and advantages are:

- One difficulty of the ADCP application to this place was the extrapolation of the unmeasured zones (surface, banks and bed), as it was done in the lotic environments. Also, information about velocities in the reservoir were often not reliable, due to low flow velocities characteristic of those places, which made impossible to compute load values that coming into the reservoir.

- Due to the use of moving ADCP, the spatial, as well as the temporal resolution, could be increased in all study sites. In the reservoir, moving ADCP has the advantage to track the solid plume and follow its development into the system.

- In addition, obtained correlations can be used when future ADCP measurements are made at the same cross-sections, even without sampling, either in the lotic or lentic environment. Overall, though, care should be taken to only apply the correlation and estimate suspended solids characteristics (particularly grain size) and sources are reasonably similar to those present when the correlation was developed. The mapping also allows for an improved understanding of solid transport processes, as it includes highly resolved velocity and geometrical information, all measured at the same instant of time.

- Also, since it is a site-specific methodology, each method will have a particular application case and probably will be difficult to apply the same developed methodology to all environments in the natural environment. Thinking of it, it is not the aim of the development of the surrogate technologies to replace entirely the conventional analysis, but to complement it in order to obtain more temporal and spatial data resolution.

- Although initially this technology requires some investment to be established, once the state, the manager or the responsible institutions know some particularities of its environments, with a trained staff and setup devices, the applicability of such methods for a long term will become cheap, reducing time and efforts and increasing the information access. Which will allow a faster and accurate decision making.

6.3 Recommendation for future work

The analysis done in this study indicated that the fine solid fractions and therefore its flocculation dynamics between aggregation and disaggregation play an important role in the ADCP response. For instance, the solid particle formed by a floc is not as rigid as a solid formed by a pure mineral, and probably, it will represent a different interaction between the sound wave and the floc. Certainly, more studies need to be addressed to the interaction between the aggregates and the ADCP signal as well the fine fraction, taking into account the solid attenuation factor in order to improve the ADCP response in places where fine contents are more expressive.

In this sense, regarding the sampling collection itself it is indicated that, if possible, the granulometric analysis be done in-situ right after the ADCP static measurements, mainly in environments with high cohesive content. Due to its cohesiveness, when subjected to sampling, transportation and laboratory analysis preparation, the flocs that were previously observed in-situ by the ADCP, can be destroyed and therefore the correction will be done for another diameter, different from the diameter captured by the ADCP.

Also, more efforts should be addressed to the obtention of the sensitivity analysis and uncertainties on the solid concentration estimated from ADCP, such analysis and estimative could make it more reliable in the way of its operational application.

Bibliography

ANA. Hidroweb: Hydrological information system (snirh). *Brazilian Nacional Water Agency*, 2019. Available at: <http://www.snirh.gov.br/hidroweb/>.

ANA. National hydrometheorological network (rede hidrometeorológica nacional). *Brazilian Nacional Water Agency*, 2020. Access on July 20th, 2020. Available at: <http://dadosabertos.ana.gov.br/datasets/8014bf6e92144a9b871bb4136390f732_0-/data)>.

APHA. *Standard Methods for the Examination of Water and Wastewater*. [S.l.]: Amer Public Health Assn, 1999. ISBN 0875532357.

BAGNOLD, R. A. An approach to the sediment transport problem for general physics. *USGS Professional Paper*, 1966.

BARANYA, S.; JÓZSA, J. Estimation of suspended sediment concentrations with adcp in danube river. *Journal of Hydrology and Hydromechanics*, Walter de Gruyter GmbH, v. 61, n. 3, p. 232–240, sep 2013.

BOCALON, T. S. *Estudos de sedimentos do Rio Passauna com enfase na determinação de metais pesados*. Dissertação (Mestrado) — Environmental Management, 2007.

CARVALHO, N. *Hidrossedimentologia prática*. Rio de Janeiro: Editora Intercieência, 2008. ISBN 9788571931817.

CARVALHO, N. de O. et al. *Reservoir sedimentation assesment guideline*. [S.l.], 2000.

CARVALHO, N. de O. et al. *Sedimentometric Practices Guide*. [S.l.], 2000.

COQUEMALA, V. *Variacao anual do fitoplancton no reservatorio do Passauna, Parana*. Dissertação (Mestrado) — Biologic Sciences, 2005.

CORTéS, A. C. *Splitting Gravity Currents in Stratified Systems*. Tese (Doutorado) — Departamento de Ingeniería Civil e Instituto de Investigación del Agua - Universidad de Granada, Granada, 2014.

CZUBA, J. A. et al. Comparison of fluvial suspended-sediment concentrations and particle-size distributions measured with in-stream laser diffraction and in physical samples. *Water Resources Research*, v. 51, p. 320–340, 2015.

DAVIES, E. J. et al. Scattering signatures of suspended particles: An integrated system for combining digital holography and laser diffraction. *Optical Express*, v. 19, n. 25, dez. 2011.

DEINES, K. L. Backscatter estimation using broadband acoustic doppler current profilers. In: *IEEE Working Conference on Current Measurement*. [S.l.: s.n.], 1999.

D.THORNE, P.; RAMAZANMERAL. Formulations for the scattering properties of suspended sandy sediments for use in the application of acoustics to sediment transport processes. *Continental Shelf Research*, v. 28, p. 309–317, 2008.

EDWARDS, T. K.; GLYSSON, D. G. *Field Methods for Measurement of Fluvial Hidrossedimentology*. [S.l.], 1988.

EMBRAPA. *Manual de métodos de análise de solo / Centro Nacional de Pesquisa de Solos*. 2. ed.. ed. [S.l.], 1997.

EMMANUEL, B. O. S. S. et al. Validation of the particle size distribution obtained with the laser in-situ scattering and transmission (lisst) meter in flow-through mode. *Optics Express*, v. 26, n. 9, abr. 2018.

ENGELUND, F.; HANSEN, E. *A Monograph on Sediment Transport in Alluvial Streams*. [S.l.]: Teknisk Forlag, 1967.

FELIX, D.; ALBAYRAK, I.; BOES, R. Laboratory investigation on measuring suspended sediment by portable laser diffractometer (lisst) focusing on particle shape. *Geo-Marine Letters*, v. 33, p. 485–498, 2013.

FELIX, D.; ALBAYRAK, I.; BOES, R. In-situ investigation on real-time suspended sediment measurement techniques: Turbidimetry, acoustic attenuation, laser diffraction (lisst) and vibrating tube densimetry. *International Journal of Sediment Research*, v. 33, p. 3–17, 2017. Available at: <https://doi.org/10.1016/j.ijsrc.2017.11.003>.

FISCHER, H. B. et al. *Mixing in Inland and Coastal Waters*. [S.l.]: Academic Press, 1979.

FLAMMER, G. H. *Ultrasonic Measurement of Suspended Sediment*. [S.l.], 1962.

GALLOWAY, J. M.; EVANS, D. A.; GREEN., W. R. *Comparability of Suspended-sediment Concentration and Total Suspended-solids Data for Two Sites on the L'anguille River, Arkansas, 2001 to 2003*. [S.l.], 2005.

GAMARO, P. E. *Medidores Acústicos Doppler de Vazão*. [S.l.]: Iatipu Binacional, 2012. ISBN ISBN 978-85-85263-07-2.

GARTNER, J. W. Estimating suspended solids concentrations from backscatter intensity measured by acoustic doppler current profiler in san francisco bay, california. *Marine Geology*, v. 211, p. 169–187, 2004.

GODOY, R. F. B. *Dinamica Da Qualidade Da Agua Em Reservatorio De Abastecimento Publico: Estudo De Caso Do Passauna,PR*. Dissertação (Mestrado) — Water Resources and Environmental Engineering Graduate Program, 2017.

GRAF, W. H. *Hydraulics of Sediment Transport*. [S.l.]: Water Resources Publications, 1984.

GRAF, W. H. *Fluvial Hydraulics - Flow and Transport Processes in Channel of Simple Geometry*. [S.l.]: John Wiley & Sons Ltd, 1998.

GUERRERO, M. et al. The acoustic properties of suspended sediment in large rivers: consequences on adcp methods applicability. *Water*, v. 8, n. 1, p. 13, jan. 2016.

GUERRERO, M.; RüTHER, N.; SZUPIANY, R. N. Laboratory validation of acoustic doppler current profiler (adcp) techniques for suspended sediment investigations. *Flow Measurement and Instrumentation*, 2012.

GUERRERO, M.; SZUPIANY, R.; AMSLER, M. Comparison of acoustic backscattering techniques for suspended sediments investigation. *Flow Measurement and Instrumentation*, Elsevier BV, v. 22, n. 5, p. 392–401, oct 2011.

HALLIDAY, D.; RESNICK, R. *Fundamentals of Physics*. 8th. ed. [S.l.]: LTC, 2009. v. 2.

HAUN, S.; LIZANO, L. River flow. I n: . London: Taylor & Francis, 2016. cap. Evaluation of a density currenty by using ADCP backscatter data and LISST measurements, p. 875,881.

HAUN, S.; LIZANO, L. Sensitivy analysis of sediment flux derived by laser diffraction and acoustic backscatter within reservoir. *International Journal of Sediment Research*, p. 18–26, 2018.

KLASSEN, I. *Three-dimensional Numerical Modeling of Cohesive Sediment Flocculation Processes in Turbulent Flows*. Tese (Doutorado) — Civil Engineer-, Geo and Environmental Sciences - Karlsruhe Institute of Technology, 2017.

LANDERS, M. N. et al. *Sediment Acoustic Index Method for Computing Continuous Suspended Sediment Concentrations*. [S.l.], 2016. Available at: <http://dx.doi.org/10-.3133/tm3C5.>

LANE, E. W. Report of the subcommittee on sediment terminology. *Transactions, American Geophysical Union*, American Geophysical Union (AGU), v. 28, n. 6, p. 936, 1947.

LATRUBESSE, E.; STEVAUX, J.; SINHA, R. Tropical rivers. *Geomorphology*, Elsevier BV, v. 70, n. 3-4, p. 187–206, sep 2005.

LIMA, J. E. F. W. et al. *Diagnostico do fluxo de sedimentos em suspensao na Bacia do Rio Sao Francisco*. [S.l.], 2001.

MEGER, D. G. *Material Particulado Suspenso e Macroconstituintes Ionicos em um Reservatorio de Abastecimento: o caso do Rio Passauna, Curitiba, Parana,Brasil.* Dissertação (Mestrado) — Positivo University, 2007.

MEYER-PETER, E.; MüELLER, R. Formulas for bed-load transport. In: *International Association for Hydaraulic Structures Research*. [S.l.: s.n.], 1948.

MONTANHER, O. C.; NOVO, E. M. L. ao de M.; BARBOSA, C. C. F. Modelos para estimativa da concentração de sedimentos em suspensão em rios amazônicos de águas brancas via sensoriamento remoto. In: *Anais XVI Simpósio Brasileiro de Sensoriamento Remoto - SBSR*. [S.l.: s.n.], 2013.

MOORE, S. A. et al. Using multi-frequency acoustic attenuation to monitor grain size and concentration of suspended sediment in rivers. *The Journal of the Acoustical Society of America*, Acoustical Society of America (ASA), v. 133, n. 4, p. 1959–1970, apr 2013.

MORRIS, G. L.; FAN, J. *Reservoir Sedimentation Handbook: Desining and Management of Dams, Reservoirs and Watershed for Sustainable Use*. [S.l.]: The McGraw-Hill Companies, Inc, 1998.

MOSBRUCKER, A. R. et al. *Estimating Concentrations of Fine-grained and Total Suspended Sediment from Close-range Remote Sensing Imagery*. [S.l.], 2015.

MUELLER, D. S. et al. Measuring discharge with acoustic doppler current profilers from a moving boat - techniques and methods. In: _____. [S.l.]: USGS, 2013. cap. 22, p. 116.

OLIVETTI, D. *CÂMERAS MULTI E HIPERESPECTRAL AEROTRANSPORTADAS: CONTRIBUIÇÕES PARA MONITORAMENTO DE QUALIDADE DE ÁGUAS CONTINENTAIS*. Tese (Doutorado) — Brasilia Federal University (UNB), 2020.

ONO, G. M. Monitoramento e análise da sedimentação no reservatório Passauna-PR. Document presented as partial exam to obtain the Master of Science degree. 2019.

PITRAT, D. M. J. J. *Avaliacao Da Contaminacao Por Metais Em Rios: Estudo De Caso Da Bacia Do Rio Passauna.* Dissertação (Mestrado) — Hydric resources and Environmental Engineering, 2010.

RAUEN, W. B.; CASTRO, C. O. de; SILVA, M. G. da. Caracterização hidrossedimentologica do rio passauna, pr, brasil, a partir de dados históricos. In: *XX Simposio Brasileiro de Recursos Hídricos*. [S.l.: s.n.], 2017.

RD-INSTRUMENTS. *Acoustic Doppler Current Profiler Principles of Operation a Practical Primer.* [S.l.], 2011.

RIJN, L. C. van. Sediment transport, part i: Bed load transport. *Journal of Hydraulic Engineering*, 1984.

ROIG, H. L. et al. Uso de câmeras de baixo custo acopladas a veículos aéreos leves no estudo do aporte de sedimentos no lago paranoá. In: INPE. *Anais XVI Simpósio Brasileiro de Sensoriamento Remoto - SBSR*. [S.l.], 2013.

RUBEN, L. D. et al. Acoustic sediment estimation toolbox (ASET): A software package for calibrating and processing TRDI ADCP data to compute suspended-sediment transport in sandy rivers. *Computers & Geosciences*, Elsevier BV, p. 104499, apr 2020.

SABESP. *Norma Técnica Interna SABESP-NTS13.* [S.l.], 1999.

SALGADO, M. S. K.; RAUEN, W. B. *Coleta E Analise De Sedimentos Do Reservatorio Do Passauna.* [S.l.], 2014.

SANEPAR. *Plano Diretor SAIC - Sistema de Abastecimento de água Integrado de Curitiba e Região Metropolitana.* [S.l.], 2013.

SANTOS, B. B. D. et al. Evaluation of the laser diffraction method for the measurement of suspended sediment concentration in mogi-guassu reservoir/sp. brazil. *International Journal of River Basin Management*, Informa UK Limited, v. 17, n. 1, p. 89–99, mar 2018.

SANTOS, I. dos et al. *Hidrometria Aplicada.* [S.l.]: CEHPAR - Centro de Hidráulica e Hidrologia Prof. Parigot de Souza, 2001.

SAUNITI, R. M.; FERNANDES, L. A.; BITTENCOURT, A. V. L. The study of passauna's river barrage with its reservoir sedimentation, curitiba-pr. *Boletim Paranaense de Geociências*, v. 54, p. 65–82, 2004.

SCHULKIN, M.; MARSH, W. H. Sound absorptionin sea water. *Journal of the Acoustical Society of America*, 1962.

SEQUOIA. *LISST-100x Particle Size Analyzer*. [S.l.], 2015.

SEQUOIA. *LISST-200x Particle Size Analyzer*. [S.l.], 2018.

SEQUOIASC. *Processing LISST-100 and LISST-100x Data in Matlab*. 2015. Online. Available at: <https://www.sequoiasci.com/article/processing-lisst-100-and-lisst-100x-data-in-matlab/>.

SEQUOIASC, I. *Laser Diffraction Principles*. 2017. Online. Available at: <http:/-/www.sequoiasci.com/article/laser-diffraction-principles/>.

SHIELDS, A. *Application of Similarity Principles and Turbulence Research to Bed-load Movement*. [S.l.], 1936.

SHOTBOLT, L. A.; THOMAS, A. D.; HUTCHINSON, S. M. The use of reservoir sediments as environmental archives of catchment inputs and atmospheric pollution. *Progress in Physical Geography: Earth and Environment*, v. 29, n. 3, p. 337–361, set. 2005.

SIH. Hydrological system information. *Parana State Water Agency*, 2019. Available at: <http://www.aguasparana.pr.gov.br/pagina-264.html>.

SONTEK. *RiverSurveyor S5/M9 System Manual Firmware Version 4.02*. [S.l.], 2016.

SOTIRI, K.; HILGERT, S.; FUCHS, S. Sediment Classification in a Brazilian Reservoir: Pros and Cons of Parametric Low Frequencies. *Advances in Oceanography and Limnology*, PAGEPress, v. 10, n. 1, may 2019.

SUEKAME, H. K. Avaliação dos processos hidrológicos e sedimentológicos de uma bacia hidrográfica. Thesis. 2020.

SZUPIANY, R. N. et al. Estimating sand concentrations using ADCP-based acoustic inversion in a large fluvial system characterized by bi-modal suspended-sediment distributions. *Earth Surface Processes and Landforms*, Wiley, v. 44, n. 6, p. 1295–1308, jan 2019.

TERABE, F. R. *Estudo Sobre O Uso Do Perfilador Acústico De Corrente Por Efeito Doppler (adcp) Para Medição Do Transporte Sólido Em Suspensão.* Dissertação (Mestrado) — Federal University of Parana, 2004.

UMEDA, M.; YOKOYAMA, K.; ISHIKAWA, T. Observation and simulation of floodwater intrusion and sedimentation in the shichikashuku reservoir. *Journal of Hydraulic Engineering*, p. 881–891, set. 2006.

URICK, R. J. *Principles of Underwater Sounds*. [S.l.]: Mc Graw Hill, 1975.

USBR. *Erosion and sedimentation manual*. [S.l.]: Denver, Colo. : U.S. Dept. of the Interior, Bureau of Reclamation, Technical Service Center, Sedimentation and River Hydraulics Group ; Washington, DC : For sale by the Supt. of Docs., U.S. G.P.O., 2006.

WAGNER, A. *Event-Based Measurement and Mean Annual Flux Assessment of Suspended Sediment in Meso Scale Catchments*. Tese (Doutorado) — Karlsruhe Institut für Technologie, 2019.

WOOD, M. Workshop at ii hydrosedimentology international conference. In: *The Sediment Acoustic Index Method and SAID Tool*. [S.l.: s.n.], 2017.

WOOD, M.; GARTNER, J. *Use of Acoustic Backscatter and Vertical Velocity to Estimate Concentration and Dynamics of Suspended Solids in Upper Klamath Lake, South-central Oregon: Implications for Aphanizomenon Flos-aquae.* [S.l.], 2010.

WOOD, M.; TEASDALE, G. N. *Use of Surrogate Technologies to Estimate Suspended Sediment in the Clearwater River, Idaho, and Snake River, Washington.* [S.l.], 2013.

WOOD, M. S. et al. Measuring suspended sediment in sand-bedded rivers using down-looking acoustic doppler current profilers. In: *Joint Federal Interagency Sedimentation and Hydrologic Modeling Conference*. [S.l.]: SEDHYD, 2019. p. 15.

WOSIACKI, L. F. et al. Suspended sediment estimate through an adcp analysis - study case: Taquari river, pantanal, brazil. In: *ANAIS III ENES/I PIA*. [S.l.]: ABRH, 2018.

YANG, C. T.; STALL, J. B. *Unit Stream Power for Sediment Transport in Natural Rivers.* [S.l.], 1974.

Appendix

APPENDIX A – ADP-M9 Backscatter Attenuation Corrections

At this appendix it is shown step-by-step the SNR attenuation model applied to the ADCP backscatter.

The ADCPs use the Sonar equation proposed by Urick (1975 apud GAMARO, 2012) to obtain the difference between emitted and reflected signal. This relation tells us the amount of sound reflected back towards the equipment until the emitted signal reaches a target, considering all the losses along the way — e.g. spreading, absorption and attenuation losses. After some arrangements, it can be written as the equation 2.5, presented at Chapter 2, as follow:

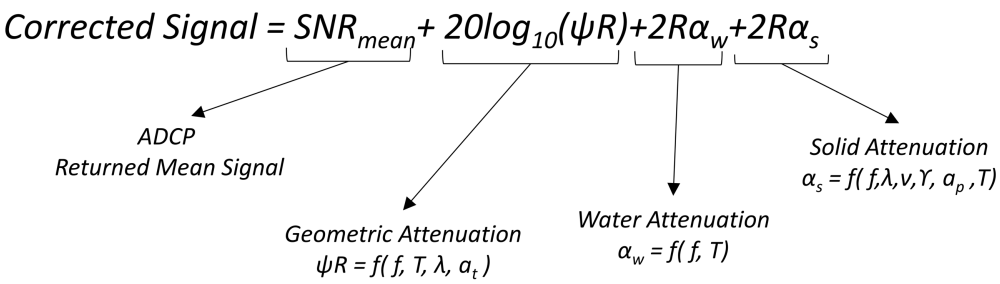

Here we have that the corrected signal is a function from the mean spread signal (geometric attenuation) and the attenuation due the water and solid. Each one of these attenuation terms can be expressed mathematically as function of the equipment, eg: frequency, wavelength, transducer ratio, or as a function of the medium, eg: water temperature, water viscosity, solid diameter, solid and water density (specific gravity).

At this equation, the SNR_{mean} is the simple average of the 4 ADCP transducers. The second term from the equation, given by $20\log(\psi R)$ is the geometrical attenuation term, related to the spherical spread of the beam — Baranya and Józsa (2013). R is the slant distance from transducert head to the measured bin, in meters. The coefficient ψ is a correction factor related to the effect of spherical spreading close to the transducer:

$$\psi = \left(\frac{1+1.35Z+(2.5Z)^{3.2}}{1.35Z+(2.5Z)^{3.2}}\right), \quad Z = \frac{R}{R_{critical}}, \tag{A.1}$$

where $R_{critical}$ is the critical range which is function of the transducer radius, a_t, in cm and the wave length, λ, as follows:

$$R_{critical} = \frac{\pi a_t^2}{\lambda} \tag{A.2}$$

The approach for water absorption (α_w) is given by the relation presented by Schulkin and Marsh (1962 apud BARANYA; JÓZSA, 2013) in the Equation A.3.

$$\alpha_w = 8.687 \left(\frac{3.38 \cdot 10^{-6} f^2}{f_T}\right), \quad f_T = 21.9 \cdot 10^{\left(6 - \frac{1520}{273+T}\right)}, \tag{A.3}$$

where f is the instrument frequency, f_T is the relaxation frequency, which depends on the Temperature, T, in $^{\circ}C$.

As pointed out by Flammer (1962), attenuation from suspended solid consists of a viscous-loss (α_{sv}) component and a scattering-loss (α_{ss}) component. Depending on the ADCP frequency the attenuation due to solid will play a role only in particle under certain diameters.

As highlighted by Baranya and Józsa (2013): the lower the particle diameter, the bigger the viscous loss. On the other hand: the bigger the particle diameter, the bigger the scattering loss.

The solid attenuation loss term,α_s can be estimated as presented by Guerrero et al. (2016), based on the formulation proposed by D.Thorne and RamazanMeral (2008):

$$\alpha_s = \alpha_{ss} + \alpha_{sv} \tag{A.4}$$

where:

$$\alpha_{ss} = \frac{3\chi \cdot SSC}{4 \cdot a_p \rho_s}, \tag{A.5}$$

$$\alpha_{sv} = TSS \cdot K \frac{(\sigma - 1)^2}{2\rho_s} \cdot \frac{S}{S^2 + (\sigma + \varsigma^2)} \tag{A.6}$$

where α_s is the solid attenuation, α_{ss} is the solid scattering attenuation and α_{sv} is the solid viscous attenuation all parameter in Db units. TSS is the total suspended solid in mg/L, a_p is particle radius, K is known as the wave number, given by:

$$K = \frac{2\pi}{\lambda}, \tag{A.7}$$

σ is the relative density given by the relation between solid density, ρ_s and the fluid density, in this case, water density, ρ_w, according to Equation A.8.

$$\sigma = \frac{\rho_s}{\rho_w}, \tag{A.8}$$

where ρ_w can be obtained by the UNESCO approach (equation A.9) presented at Fischer et al. (1979).

$$\rho_w = 999.842594 + 6.793952 \cdot 10^{-2} \cdot T - 9.09529 \cdot 10^{-3} \cdot T^2 + 1.001685 \cdot 10^{-4} \cdot T^3 - 1.120083 \cdot 10^{-6} \cdot T^4 + 6.536332 \cdot 10^{-9} \cdot T^5 \quad \text{(A.9)}$$

where T is the water temperature in $^{\circ}C$. χ, from equation A.10 is equal to:

$$\chi = \frac{0.29x^4}{0.95 + 1.28x^2 + 0.25x^4} \quad \text{(A.10)}$$

where:

$$x = K \cdot a_p \quad \text{(A.11)}$$

ς is equal to:

$$\varsigma = 0.5 + \frac{9}{4\gamma} \quad \text{(A.12)}$$

γ is equal to:

$$\gamma = \sqrt{\frac{\pi \cdot 1000f}{\nu}} \quad \text{(A.13)}$$

where $\nu = 1.0 \cdot 10^{-6}\ m^2/s$ is the water viscosity. The parameter S, from Equation A.5, is equal to:

$$S = \left[\frac{9}{(4\gamma \cdot a_p)}\right]\left[1 + \frac{4}{(\gamma \cdot a_p)}\right] \quad \text{(A.14)}$$

In the Equation A.4, the first term is related to the attenuation from viscous losses and the second term is related to the scattering losses.

APPENDIX B – LISST-200X Processing Analysis

At this Appendix it will be present the processing steps and analysis of the LISST-200x to obtain the granulomnetric curve.

B.1 In-situ technique and data treatment

The field practice for LISST-200x measurement require a background file for the correct field measurement. In this sence, the background file was measured only once, right before the beginning of the measurement campaign. During the field measurements, the LISSTs were released in the same depth where the water was sampled for laboratory analysis.

The measurements were done by leaving the equipment stand for some minutes (between 2 - 4 minutes) at each depth in order to stabilize the sensors to improve the measurements and create more data at the same location to be used in the final average for sediment estimative and characterization.

During operation, the output from the diffracted laser beam, optical transmission, pressure sensor and water temperature are recorded as raw data and can be downloaded and processed later on for granulometry and total volume concentration.

Together with the LISST instruments it is provided the SOP software that can be used for post-processing analysis. Also, the manufacturer provides specifics Matlab routines that make the inversions and all calculations to obtain the volumetric concentration and therefore the granulometric distribution over the classes of different types of the LISST instrument series.

Since the instrument can be affected by a range of factors intrinsic to the environment and the handling, it is necessary to consider some criteria and filtering to obtain better and reliable results. In this sense it is not uncommon to clear some data from the results if it is considered an outlier or if the measurement was done under suspisious circunstances – eg. too turbidy or too clean water.

B.2 Sensor Corrections

The filtering processing considered the instructions from the manufacturer regarding the Transmission parameter, T. According to Sequoia (2018), if the transmission is $0.100 > T > 0.995$, the data must to discarded. For T values lower than 0.300 and greater than 0.980, the manufacturer indicates wary on these data. So, in this study the criterion

was tighter and all T values: 0.300>T>0.980, were discarded. Figure 58 exemplifies the transmission for one data set from Passauna reservoir.

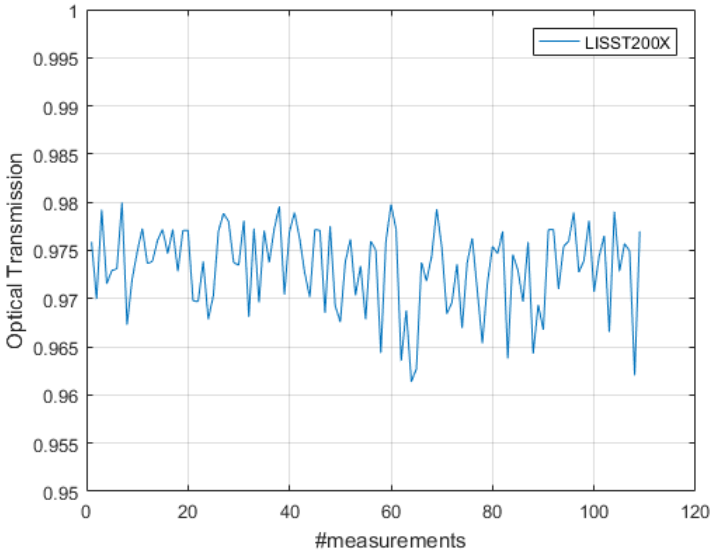

Figure 58 – Optical Transmission.

After filtering all data out of the T range, the quantile method (Q1 – 25% and Q3 – 75%) was applied to the data set, followed by the move mean technique, with a window length of 5, to avoid outliers and abrupt variations in the data to be analyzed (Figure 59).

These corrections are important to avoid possible non-representative particle that could cross the laser path during the measurement. For the post-processing analysis was considered the "random shaped" particles inversion model. The granulometric curve was

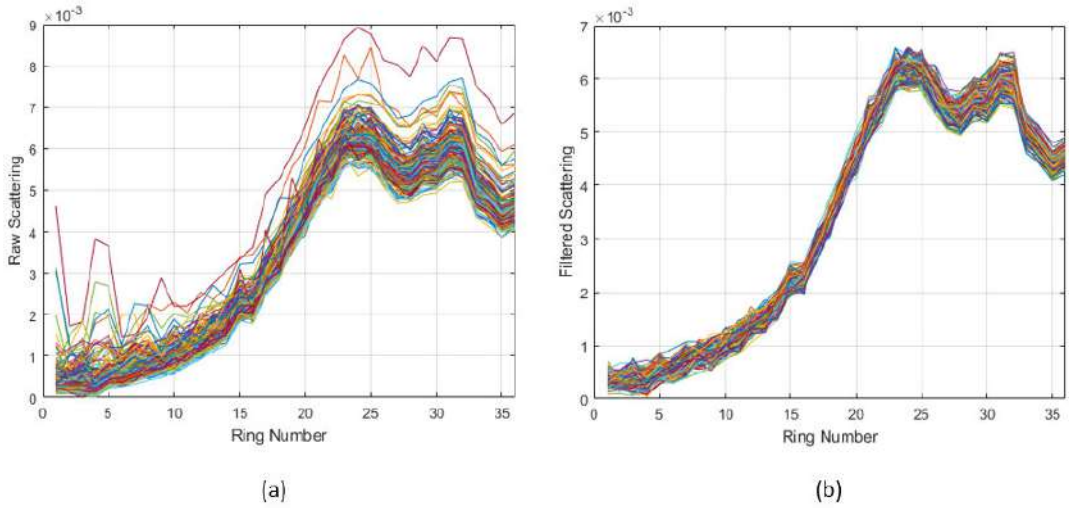

Figure 59 – Scattering Data for LISST200x (a) before and (b) after the filtering application.

computed by linear interpolation of the cumulated volumetric concentration values in each class for both equipment.

APPENDIX C – ADP-M9 Verification of frequency at different operation modes

At this appendix it is shown the relative error between the correlation obtained with the filtration of 3MHz frequency extrated from measurements made with Smart Pulse mode and the correlation obtained with 3MHz measurement (Fixed Frequency mode).

The static ADP measurements were conducted at 6 verticals over the Taquari River cross section in the SPM. During post-processing, only the data recorded by the 3MHz beams in each cross section and vertical were used in the solid determination calculations, avoiding all the 1MHz cells.

In order to test whether removing the 1MHz data had a significant impact on the amount of data available and quality of the solid correlations, one extra measurement was conducted during the last campaign (Jan/2018) using the FFM (3MHz) in addition to the regular measurement made with the SPM. The measurements made with the SPM was filtered to obtain only the 3MHz data.

Table 20 shows the mean signal (SNR_{mean}) for the FFM and SPM and the relative difference between them, which were about 5% on average. The results indicate that SNR_{mean} was higher using the SPM than the FFM in all verticals.

Table 20 – Relative Error between the Smart Pulse and Fixed mode – comparison between 3MHz.

Vertical	Frequency Mode	Mean SNR (dB)	Mean Difference
V1	3 MHz – Fixed Mode	64.53	4%
	3 MHz – Smart Pulse	67.28	
V2	3 MHz – Fixed Mode	59.13	8%
	3 MHz – Smart Pulse	64.10	
V3	3 MHz – Fixed Mode	65.35	3%
	3 MHz – Smart Pulse	67.59	
V4	3 MHz – Fixed Mode	64.68	4%
	3 MHz – Smart Pulse	67.31	
V5	3 MHz – Fixed Mode	63.09	5%
	3 MHz – Smart Pulse	66.37	
V6	3 MHz – Fixed Mode	60.38	5%
	3 MHz – Smart Pulse	63.71	
Average	-	-	5%

These results itself indicated that if the measurements were taken with the FFM (as usually done in all aforementioned studies), on average, the corrected signal strength would be lower than those collected in the SPM. Thus, as will be further explained, test scenarios were created considering the subtraction of 5% over the SNR_{mean}, in order to check its influence on the correlation curve and on the estimated SSC.

It was created two scenarios two evaluate the influence of this 5% difference on the correlation curve:

- Figure 60a is the regression line built with all corrections mentioned: Smart Pulse filtering and total solid attenuation — hereinafter called CBS1
- Figure 60b considered the same approach as in Figure 60a, but with a -5% correction applied to the raw measured mean SNR data due the Smart Pulse filtering — hereinafter called CBS2.

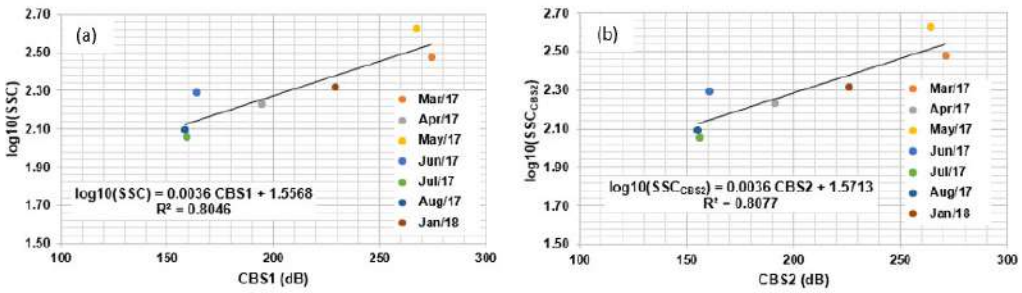

Figure 60 – Mean discharge and mean solid concentration during the field campaigns.

As we can observe from the equations of the regression lines in fig.6, there is no significant difference between CBS1 and CBS2 regressions, meaning that the SmartPulse filtering had little effect on the final results.

Which means that using only the 3MHz from the SPM doesn't produce any significative difference in the correlation curve, therefore in the SS obtained from the ADCP.

APPENDIX D – Mapping Results

At this appendix is shown the mapping of all measured cross-section at Taquari River, Passauna River and Passauna Reservoir.

D.1 Taquari River Mapped cross-setion

Sample integrated collection and Laboratory Analysis by Settling tube Method

- SSC in March/17 = $300.3 mg/L$
- SSC in April/17 = $169.90 mg/L$
- SSC in May/17 = $422.50 mg/L$
- SSC in June/17 = $195.40 mg/L$
- SSC in Jul/17 = $113.60 mg/L$
- SSC in Aug/17 = $124.10 mg/L$
- SSC in Jan/18 = $207.80 mg/L$

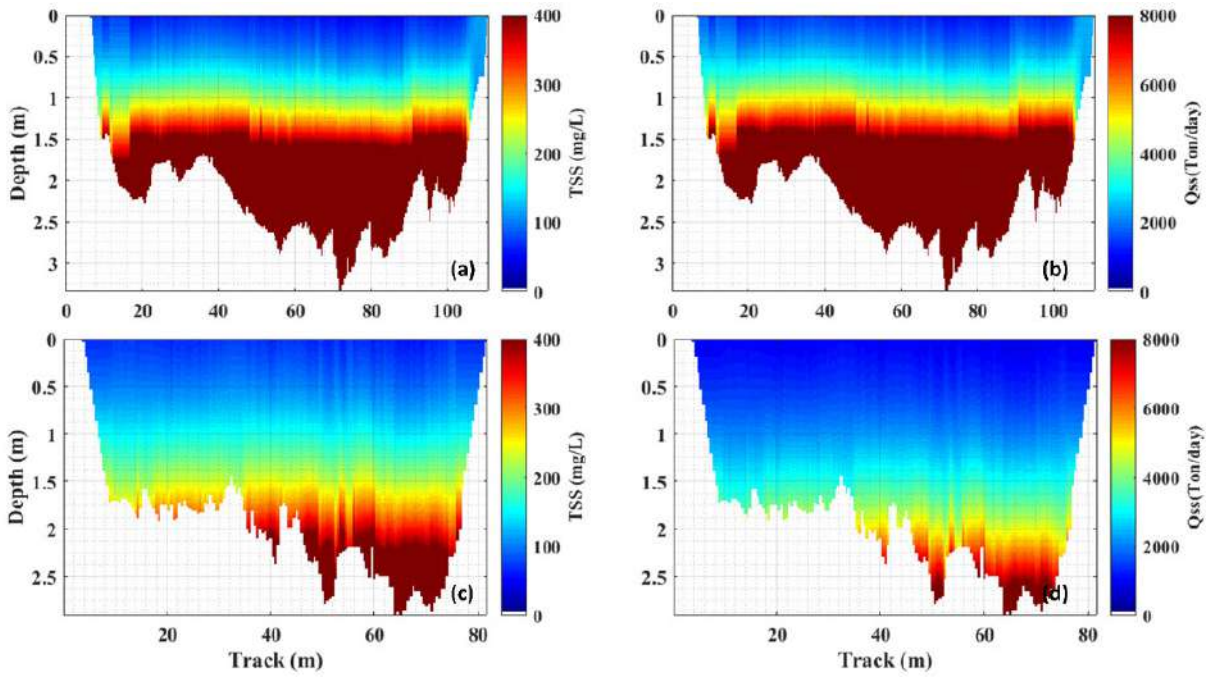

Figure 61 – Mapped cross-section in Mar/17 (a) TSS, (b)Qss and in Apr/17 (c) TSS, (d) Qss.

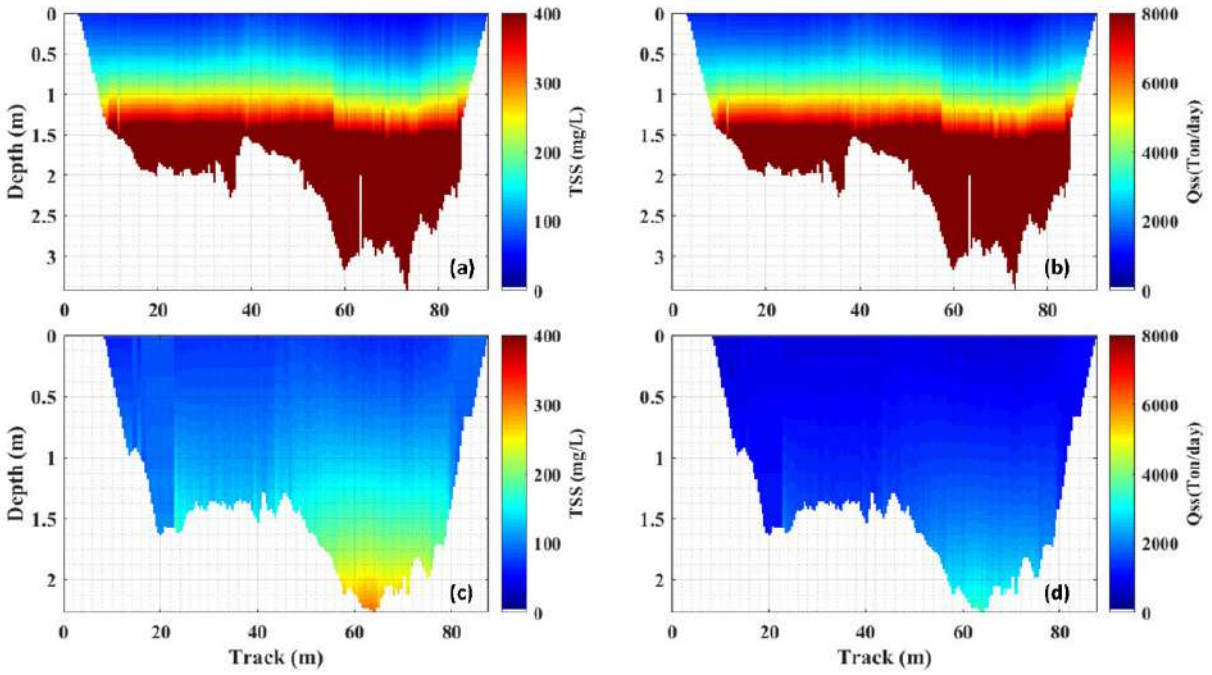

Figure 62 – Mapped cross-section in May/17 (a) TSS, (b)Qss and in June/17 (c) TSS, (d) Qss.

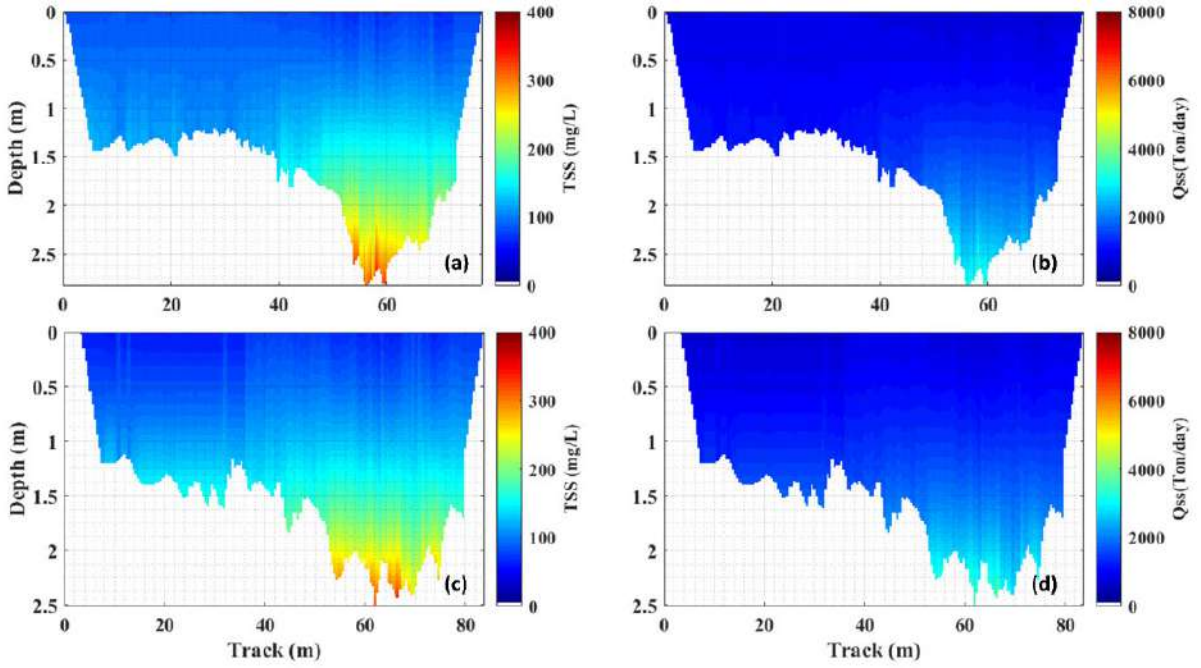

Figure 63 – Mapped cross-section in July/17 (a) TSS, (b)Qss and in August/17 (c) TSS, (d) Qss.

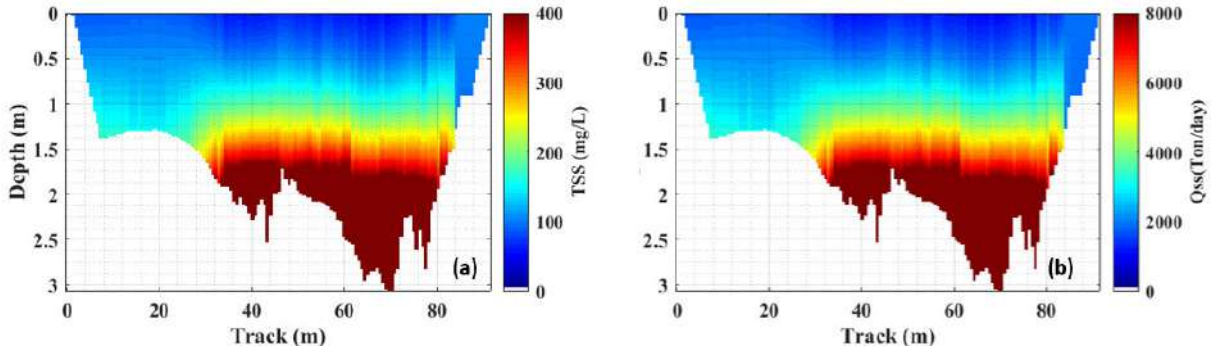

Figure 64 – Mapped cross-section in Jan/18 (a) TSS, (b)Qss.

D.2 Passauna River Mapped cross-setion

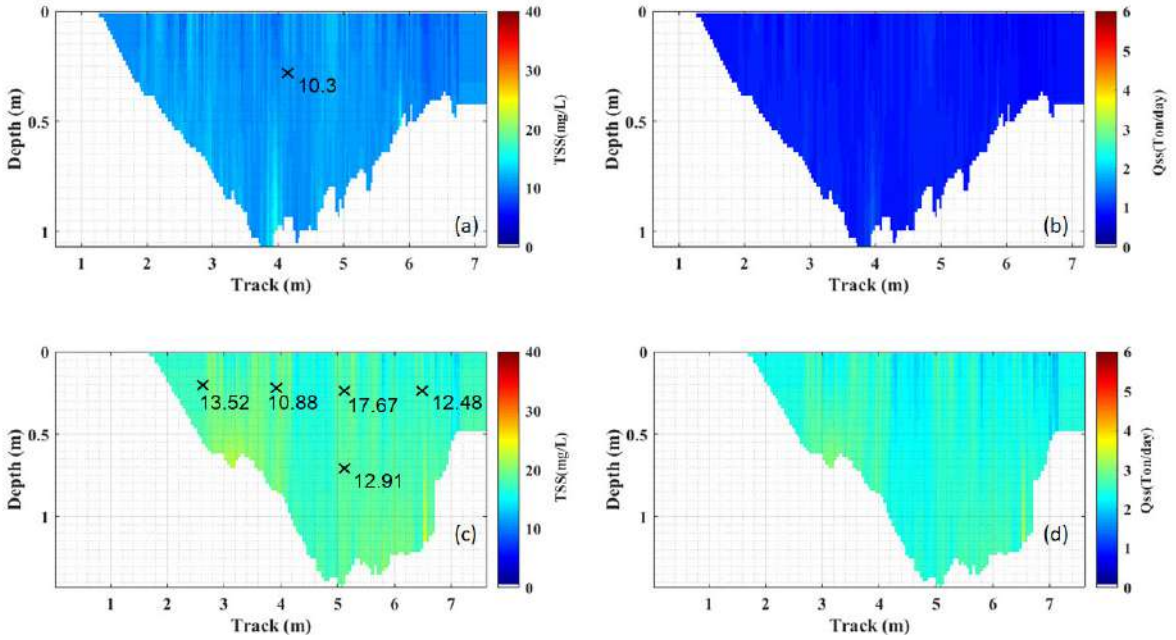

Figure 65 – Mapped cross-section in May/17 (a) TSS, (b)Qss and in Apr/18 (c) TSS, (d) Qss.

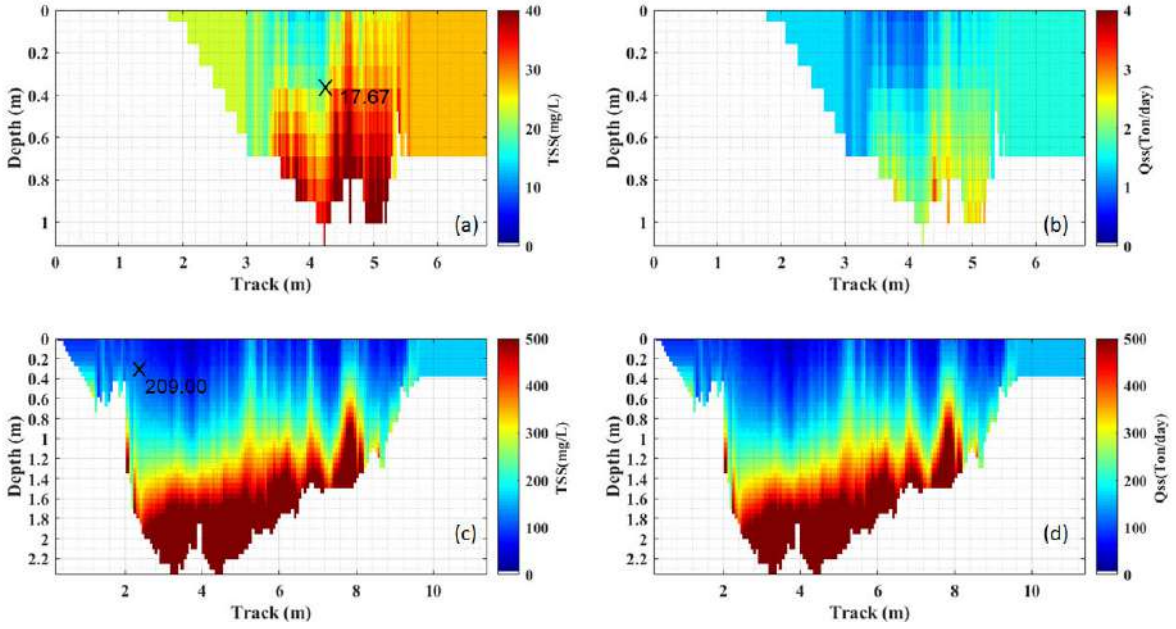

Figure 66 – Mapped cross-section in Aug/18 (a) TSS, (b)Qss and in 18Oct/18 (c) TSS, (d) Qss.

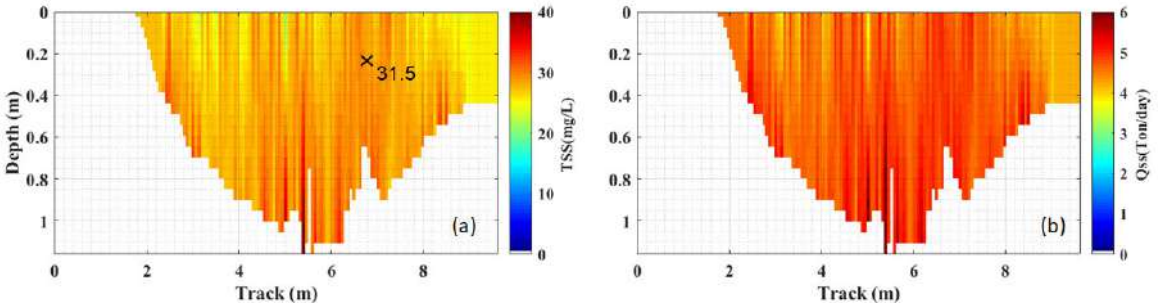

Figure 67 – Mapped cross-section in 20Oct/18 (a) TSS, (b)Qss.

D.3 Ferraria Bridge Mapped cross-setion

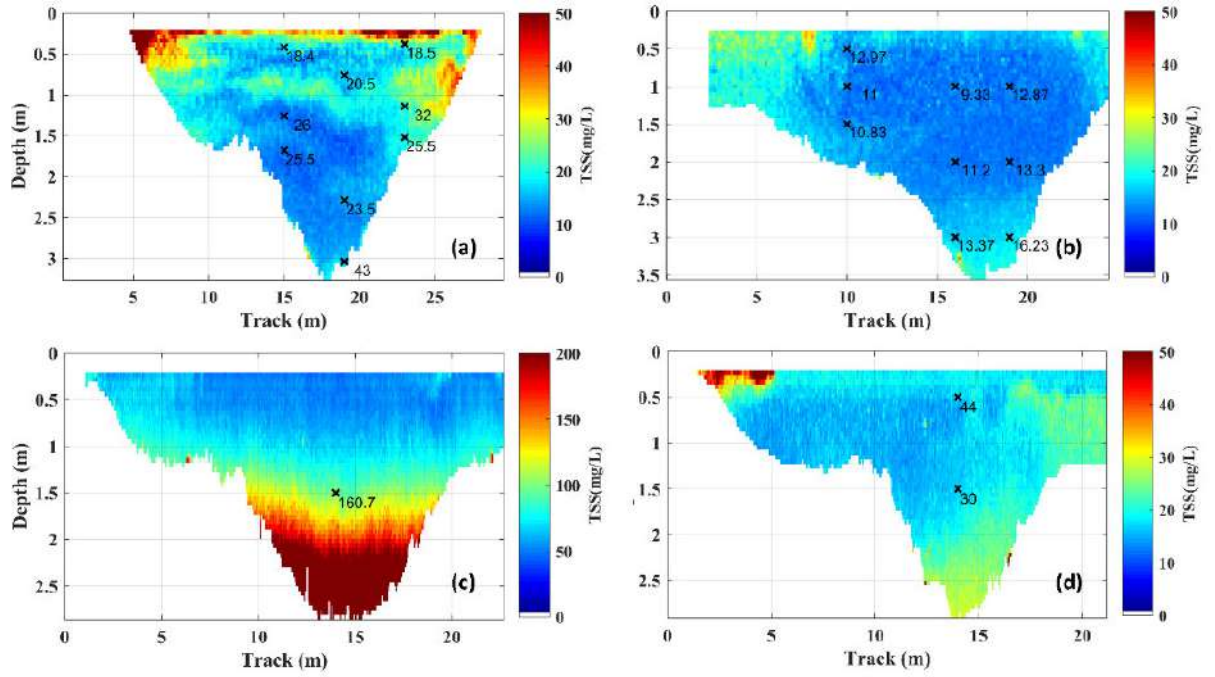

Figure 68 – Mapped cross-section in (a) Aug/17, (b) Feb/18, (c) 18Oct/18 and (d) 20Oct/18.

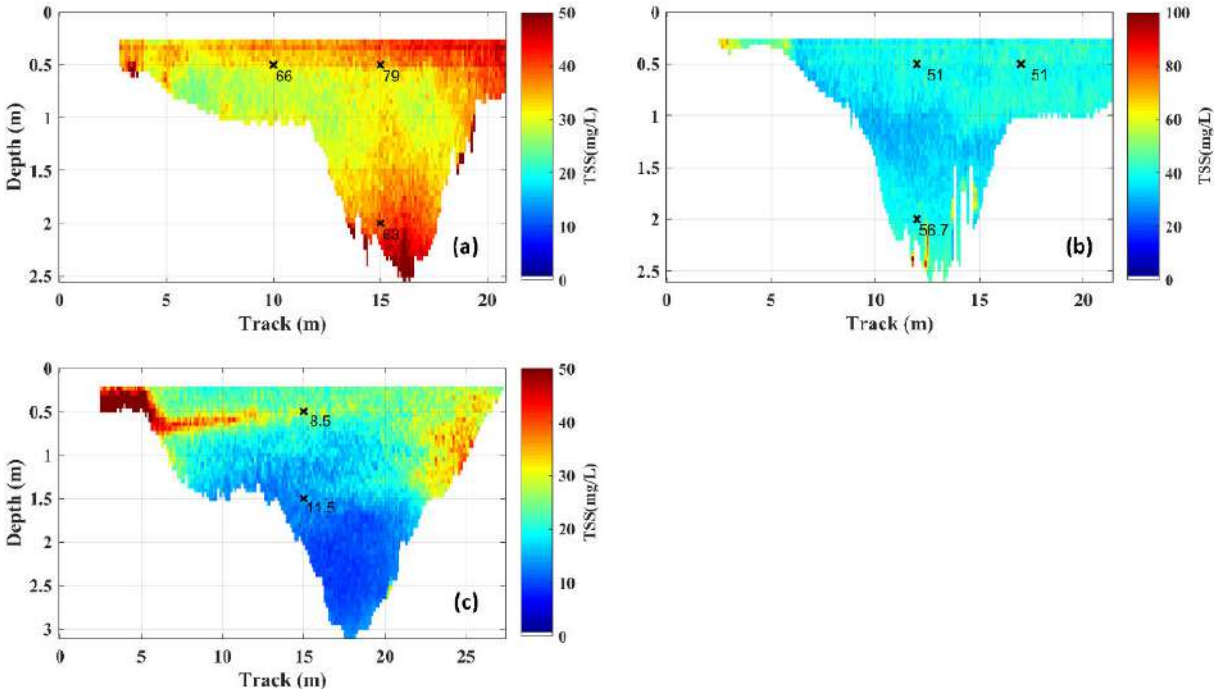

Figure 69 – Mapped cross-section in (a) 04Feb/19, (b) 05Feb/19 and (c) Apr/19.

This document is licensed under a Creative Commons
Attribution-ShareAlike 4.0 International License (CC BY-SA 4.0):
https://creativecommons.org/licenses/by-sa/4.0/deed.en

Surrogate technologies for suspended Solid dynamics assessment in surface Waters

Zur Erlangung des akademischen Grades einer

DOKTORIN DER NATURWISSENSCHAFTEN (Dr.Ing)

bei der Fakultät für
Bauingenieur-, Geo- und Umweltwissenschaften
des Karlsruher Instituts für Technologie (KIT)

eingereichte

DISSERTATION

von

Liege Fernanda Koston Wosiacki, Dipl.-Ing., M.Sc

aus Curitiba (Brasilien)
Tag der MündlichenPrüfung: 20.08.2020

Referent: Prof. Dr-Ing. Tobias Bleninger
Korreferent: Prof. Dr-Ing. Stephan Fuchs

Karlsruhe (Deutschland) und Curitiba (Brasilien)
2020

FEDERAL UNIVERSITY OF PARANÁ

LIÉGE FERNANDA KOSTON WOSIACKI

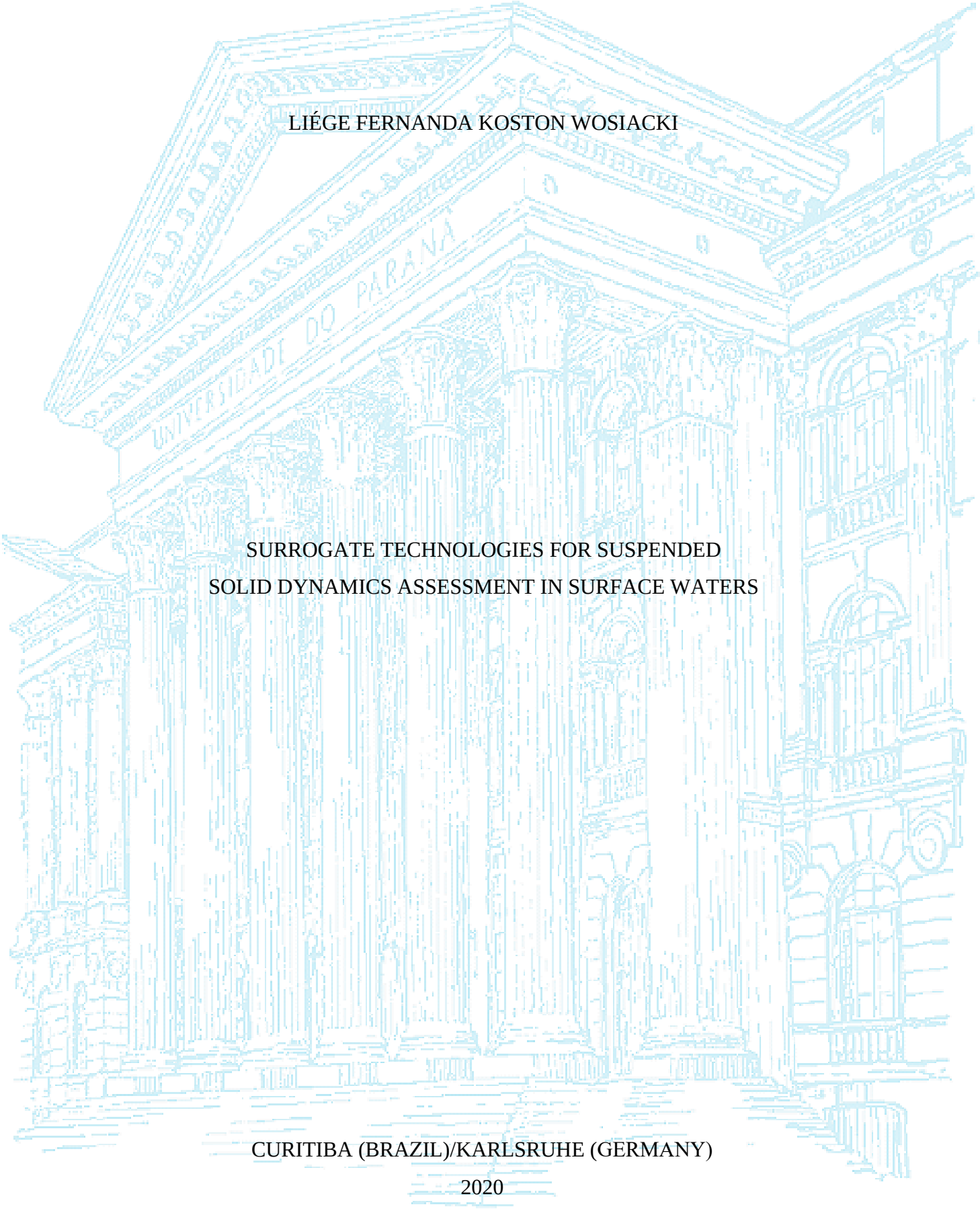

SURROGATE TECHNOLOGIES FOR SUSPENDED SOLID DYNAMICS ASSESSMENT IN SURFACE WATERS

CURITIBA (BRAZIL)/KARLSRUHE (GERMANY)

2020

LIÉGE FERNANDA KOSTON WOSIACKI

SURROGATE TECHNOLOGIES FOR SUSPENDED SOLID DYNAMICS ASSESSMENT IN SURFACE WATERS

Thesis submitted in partial fulfillment of the requirements of the Graduate Program on Water Resources and Environmental Engineering from Federal University of Paraná(UFPR), in Cotutelle Agreement between UFPR and KIT (Karlsruhe Institute of Technology, in Karlsruhe, Germany).

Supervisor: Dr-Ing. Tobias Bleninger (UFPR).

Co-Supervisor: Dr-Ing. Stephan Fuchs (KIT).

CURITIBA (BRAZIL)/KARLSRUHE (GERMANY)
2020

ACKNOWLEDGMENTS

First of all, I would like to thank my parents, Jeane and Wolney, for being always on my back, supporting me and lifting me up when things got difficult. Everything I do is to make you proud of me.

Special thanks go to Pedro, my husband, for all patience and support, even if it had costed my absence for long periods.

I also want to thank my colleagues from the "salinha", who become my friends — Felipe, Laís, Patrícia, Sabrina, Aninha and Lucas, for their support and for the funniest productivity environment, which made everything lighter.

Special thanks to Lediane and Luziadne, two gifts that this journey brought me. I have no words to thank you for being literaly at my side during the good and bad times. Thank you for your friendship and for always being there.

Thanks to my friend Lívia for all the coffee-breaks, partnership, friendship, advices, and for sharing the same passion for science with me.

Many thanks go to the entire PPGERHA family: Luciane and Prof. Heloíse and Carol Kozak for guiding me in my first steps in the lab. To Prof. Cristóvão for his kindness, his always exciting help in field campaigns and for many phylosophical questions. To Bruna Poli for your support and company when I first arrived in Germany. To all the amazing researchers that are part of this family who kindly shared their knowledge, their arms (on carrying all the equipment from the car to the lab, from the lab to the car) and their coffee (without coffee I don't know anything) during this journey.

Thanks to all my colleagues from Germany (from KIT and KLU - Koblenz-Landau University) and for the very good time I spent there with Mayra, Klajdi, Adrian, Stephan, Lisa, Jens, Wendy and Irina. Also, many thanks to Andreas Schenk, for helping me with the amazing opportunity to go to USGS/USA.

Thanks to my co-supervisor Prof. Stephan Fuchs for the brainstorming and revisions of manuscripts/thesis and for the efforts to make the double-degree possible. Thanks to my supervisor Prof. Tobias Bleninger for all patience, advices, support in difficult times and for sharing his knowledge and experience — either in the University or during the happy-hours.

This thesis and experiences wouldn't be possible without financial support from CAPES (Brazil) and GRACE (Germany).

"Todos temos dentro de nós
uma insuspeita reserva de força
que emerge quando a vida nos põe à prova."
(do livro A Ilha Sob o Mar — Isabel Allende)

ABSTRACT

In general, solids refer to the matter that is suspended or dissolved in water. It can result from the erosive processes in the watershed, such as runoff, bank erosion or from the riverbed, it can be formed by mineral, organic particles or a combination of both. Its dynamics in surface waters is bound to natural and anthropic processes within the watershed, as weathering or land use. Besides the environmental issues, the knowledge about solid dynamics is a fundamental tool in the assessment of the economic viability of several projects, such as the establishment and/or maintenance of a hydro way, a harbor, an irrigation canal or even the construction of a dam, for energy or water supply. However, despite all efforts and investments to obtain solid information through a robust sedimentometric network, conventional methods still do not always supply the needed information, either by operational, analytical or safety issues and because of it, the use of alternative technologies to obtain solid information in surface waters has been encouraged. Among them, it has been rising the use of acoustic methods, which are a non-intrusive technique that allows indirect quantification of suspended solids in high temporal and spatial resolution. Therefore, the proposed research aims to apply the existent methods based on the formulations proposed by Urick (1975), of the modified SONAR equation and validate a field-scale solid mapping technology using acoustic measurements with an ADCP (Acoustic Doppler Current Profiler) to obtain sedimentometric data in lotic and lentic systems. The main idea was to apply the solid-acoustic correlation methodology in two rivers (Taquari River in Mato Grosso do Sul State and at Passauna River, in Parana) and then apply the established settings first developed for the lotic environment, in a lentic environment: Passauna Reservoir (in the same watershed as Passauna River). Results have shown that the methods applied to lotic environments, with mostly non-cohesive content and high solid concentration, can be extended to a lentic environment, with mostly cohesive content and low solid concentration. Also, the results shown that the method applied has accomplished the objectives and it was possible to measure and identify solid variation throughout the water column, in all study sites, and longitudinal measurements at the lentic environment.

Key-words: Solids. ADCP. Surrogate-Tecnologies. Lentic-Environment.

ZUSAMMENFASSUNG

Feststofftransport im Wasser bezieht sich im Allgemeinen auf gelöste oder suspendierte Stoffe. Diese können aus erosiven Prozessen des Einzugsgebiets stammen, von Ufererosion oder auch aus dem Flussbett. Es handelt sich hierbei um mineralische, organische Partikel oder eine Kombination aus beiden. Die Feststoffdynamik in Oberflächengewässern ist an natürliche und anthropogene Prozesse innerhalb des Einzugsgebiets, wie Verwitterung oder Landnutzung gebunden. Neben den Umweltaspekten ist das Wissen über die Feststoffdynamik ein grundlegendes Instrument für die Beurteilung der Wirtschaftlichkeit mehrerer Projekte, z. B. der Errichtung und Instandhaltung einer Wasserstraße, eines Hafens, eines Bewässerungskanals oder des Baus eines Damms, zur Energie- oder Wasserversorgung. Herkömmliche Methoden zur Bestimmung der Konzentrationen und deren Verteilung entsprechen jedoch oft nicht den Erfordernissen in zeitlicher und räumlicher Auflösung. Eine vielversprechende Alternative basierend auf akustischen Methoden wurde in dieser Arbeit untersucht. Akustische Messungen können eine indirekte Quantifizierung suspendierter Feststoffe in hoher zeitlicher und räumlicher Auflösung ermöglichen. Daher zielt die vorgeschlagene Forschung darauf ab, die vorhandenen Methoden, die auf den von citeonline urick1975 vorgeschlagenen Formulierungen der modifizierten Schallausbreitungsgleichung basierend, anzuwenden. Ziel ist es Feststoffkonzentrationen flächig im Feldmaßstab zu erfassen. Hierfür wurde Messungen mit einem akustischen ADCP (Acoustic Doppler Current Profiler) durchgeführt. Zur Validierung wurden konventionelle Messungen zur Feststoffkonzentrationsbestimmung durchgeführt. Untersuchungen wurden in Fliessgewässern und einem Stausee, somit unter unterschiedlichen Strömungsbedingungen durchgeführt. Die Untersuchungsgebiete waren im Taquari-Fluss (Pantanal, Brasilien) und Passauna Fluss (Curitiba, Brasilien), sowie dem Passauna Stausee (Curitiba, Brasilien). Die Ergebnisse haben gezeigt, dass die Methoden, die auf Fließgewässer mit größtenteils nicht kohäsivem Material und hohen Feststoffkonzentrationen angewendet wurden, auch auf ein stehendes Gewässer mit größtenteils kohäsivem Material und niedrigeren Feststoffkonzentrationen ausgedehnt werden können. Die angewandte Methodik wurde dann herangezogen, um die Messergebnisse hochaufgelöst über Fließquerschnitte darzustellen, oder über Transekte im Falle der Stauhaltung. Diese gaben Aufschluss über Transportwege und Bereiche mit höherer und niedriger Konzentration.

Schlüsselworte: Feststoffe. ADCP. Ersatztechnologien. Sedimenttransport.

RESUMO

De maneira geral, o termo sólidos refere-se à matéria que encontra-se suspensa ou dissolvida na água, resultante dos processos erosivos que ocorrem na bacia hidrográfica, pela erosão do leito e das margens ou que são carreados por escoamento superficial. Os sólidos podem ser formados por partículas minerais, orgânicas ou por uma combinação desses, e sua dinâmica em águas superficiais está vinculada a processos naturais e antrópicos na bacia, tais como intemperismo ou pelas diferentes formas de uso do solo. Além de questões relativas ao meio ambiente, o conhecimento sobre sua dinâmica é uma ferramenta fundamental na avalição da viabilidade econômica de diferentes projetos, tais como implantação ou manutenção de uma hidrovia, de um porto, de um canal de irrigação, na construção de barramentos, entre outros. No entanto, apesar de todos os esforços e investimentos para que seja estabelecida uma robusta rede de monitoramento, os métodos convencionais implantados na maioria dos postos nem sempre suprem a necessidade de informações, seja por questões operacionais, analíticas ou de segurança. Dessa forma, nos últimos anos o uso de tecnologias alternativas para obter informações de sólidos em águas superficiais vem sendo estimulado. Entre elas, tem-se o uso de métodos acústicos, uma técnica não intrusiva que permite quantificar indiretamente os sólidos em suspensão em alta resolução temporal e espacial. Assim sendo, propôs-se no presente estudo o desenvolvimento de uma tecnologia do mapeamento dos sólidos em suspensão usando medidas acústicas com um ADCP (Perfilador Acústico Doppler) para obter dados hidrosedimentológicos em sistemas lóticos e lênticos, tendo como base o modelo da equação modificada do SONAR proposta por Urick (1975). A ideia principal foi aplicar a metodologia que correlaciona a concentração dos sólidos suspensos com o sinal acústico em dois rios (rio Taquari, no Mato Grosso do Sul e no rio Passauna, no Paraná) e, em seguida, aplicar as configurações previamente estabelecidas nesses ambientes ao reservatório do Rio Passauna (à jusante da seção considerada como ambiente lótico do Rio Passauna). Os resultados mostraram que os métodos aplicados a ambientes lóticos, com um teor significativo de sólidos não coesivos e alta concentração de sólidos, podem ser estendidos ao ambiente lêntico, com teor significativo de sólidos mais finos (mais coesivos, propensos aos processos de agregação e desagregação) e baixa concentração de sólidos. Além disso, os resultados mostraram que foi possível medir e identificar variações de sólidos ao longo da coluna de água dentro da seção transversal, em todos os locais de estudo e nas medições longitudinais, de montante para jusante, no ambiente lêntico.

Palavras-chave: Sólidos. ADCP. Tecnologias-Alternativas. Ambientes-Lênticos.

LIST OF FIGURES

Figure 1 – Modes and mechanisms of solid transport, where τ is the streamflow shear stress. . . . 24
Figure 2 – Suspended load transport profiles. . . . 25
Figure 3 – Solid Deposit Formation in the transitional zone between lotic and lentic environments. . . . 26
Figure 4 – Density Current Formation: a transition from non-stratified to stratified flow. . . . 28
Figure 5 – The behavior of a gravity current in a two-layered stratified environment: (a) interflows (b) underflows, and (c) split flows. . . . 29
Figure 6 – (a) Sampling by Equal Width Increment (EWI), where the sampled volume (V_{EWI}) is proportional to the discharge and the Transitional Rate (TR_{EWI}, which is the sampling velocity) is constant at each vertical and (b) Sampling by Equal Discharge Increment(EDI), where the sampled volume (V_{EDI}) is equal and the Transitional Rate (TR_{EDI}, which is the sampling velocity) is different, proportional to water velocity, at each vertical. . . . 30
Figure 7 – Solid Series. . . . 31
Figure 8 – Wave sound propagation and related parameters. . . . 32
Figure 9 – Emitted pulse and reflected backscatter. . . . 34
Figure 10 – Velocity components measurement. . . . 35
Figure 11 – Measured Area and Cross-Section component. . . . 36
Figure 12 – Operating scheme of LISST equipment series - diffraction laser. . . . 38
Figure 13 – Examples of bias in the LISST volumetric concentrations produced by the presence of out-of-range particles (for LISST-100X, version). . . . 39
Figure 14 – Water-solid system described with a cycle of erosion, transport, deposition and consolidation, involved in particle aggregation/disaggregation and sorption/adsorption of contaminants. Below the scheme, the corresponding influence factors and the respective properties are presented. 39
Figure 15 – Spatial distribution of a) flow velocity, b) SSC and c) Suspended Load. Adapted from: Baranya and Józsa (2013). . . . 43
Figure 16 – Density current formation recognized by Haun and Lizano (2016) at Peñas Blancas reservoir, in Costa Rica. . . . 44
Figure 17 – Density current formation measured by Umeda, Yokoyama and Ishikawa (2006) by echosounder and ADCP measurements at Shichikashuku reservoir, in Japan. . . . 45

Figure 18 – Summary of the proposed methodology to be presented in the following sections. 49
Figure 19 – Taquari River Location and the Monitored Cross-section. 50
Figure 20 – Mean Precipitation and Discharge at Taquari River at Coxim Station (Code:1854004). 51
Figure 21 – Passauna Basin Location. 52
Figure 22 – Mean Precipitation and Discharge at Passauna River at Colonia Dom Pedro Station (Precipitation Data) and BR-277-Campo Largo Station (Discharge Data). 53
Figure 23 – Study Area. 54
Figure 24 – Comparison of the water color in the study area among different days: (a)March 5th, 2019 and (b) January 21th, 2018 55
Figure 25 – Longitudinal Transect and Cross-section sketch at Passauna Reservoir. 56
Figure 26 – ADP-M9 features. Adapted from: Sontek (2016). 57
Figure 27 – LISST-200x with the battery attached. 59
Figure 28 – Water Sampler Devices (a) USD-49 and (b) Van Dorne. 60
Figure 29 – Filtration System and Filters after analysis at Vertical 3 at Ferraria's Bridge from the 4th campaign (04/23/2018). 61
Figure 30 – Backscatter correction flowchart. 64
Figure 31 – Operational scheme used in the algorithm point sampling method analysis. 65
Figure 32 – LISST processing flowchart. 67
Figure 33 – (a) Mean velocity profiles during all measurement campaigns, Horizontal velocities during the measurement campaigns of (b) May/17 and (d) July/17 and Mean Backscatter Signal obtained during the measurement campaigns of (c) May/17 and (e) July/17. 69
Figure 34 – Relation between the parameters obtained during the campaigns. P7 is the accumulated precipitation registered from 7 days before the measurement campaign. All parameters's values were arranged from the lowest measured discharge to the highest measured discharge. 70
Figure 35 – Granulometric Curve for Taquari River. 71
Figure 36 – Correlation curve between SSC and ADCP corrected backscatter signal (CBS) at Taquari River. 72
Figure 37 – Measured ADCP signal in the cross-section: (a) without the 1MHz measured cells and (b) with the 1MHz cells filled with the extrapolations obtained by the average of the signal measured by the 3MHz cells. . . . 73
Figure 38 – Non-Extrapolated and Extrapolated Cross-Section, data from April/17: (a) Non-Extrapolated SSC, (b) Extrapolated SSC, (c) Non-Extrapolated Qss, (d) Extrapolated Qss. 76

Figure 39 – Granulometric Curve for Passauna River. 78
Figure 40 – Relation between the parameters obtained during the campaigns. P7 is the accumulated precipitation registered from 7 days before the measurement campaign. All parameters's values were arranged from the lowest measured discharge to the highest measured discharge. 79
Figure 41 – Correlation curve between SSC and ADCP corrected signal at Passauna River. 79
Figure 42 – Mapping throughout the cross-section: (a) TSS from Aug/18 and (b) Qss from Aug/18, (c) TSS from 18Oct/18 and (d) Qss from 18Oct/18. 82
Figure 43 – Ferraria Bridge point sampling points location. 83
Figure 44 – Granulometric Curve at Ferraria Bridge. 84
Figure 45 – Relation between the parameters obtained during the campaigns. P7 is the accumulated precipitation registered from 7 days before the measurement campaign and the yellow boxes represent the upper and lower limits of the TSS laboratory analysis in each campaign, considering the sampling distribution presented at Figure 43. All parameters's values were arranged from the lowest measured precipitation data to the highest measured precipitation data. 85
Figure 46 – Correlation curve between SSC and ADCP corrected signal at Ferraria Bridge. 86
Figure 47 – Comparison between extrapolated and no-extrapolated TSS at Ferraria Bridge in Aug/17 (dry situation) and in 18Oct/18 (rainy situation). . . 88
Figure 48 – Longitudinal transects and point measurements througout the transects. 89
Figure 49 – Feb/18 monitoring campaign: (a) Temperature Profiles from Buffer, Ferraria bridge (FB) and PPA points, (b) Longitudinal Transect and (c) Ferraria Bridge Cross-Section. All values exposed in the transects are TSS in mg/L. 90
Figure 50 – 18Oct/18 monitoring campaign: Ferraria Bridge Cross-Section Mapping and Temperature Profile. 91
Figure 51 – 20Oct/18 monitoring campaign: (a) Temperature Profiles from Ferraria bridge (FB) and PPA points, (b) Longitudinal Transect and (c) Ferraria Bridge Cross-Section. All values exposed in the transects are TSS in mg/L. 92
Figure 52 – 05Feb/19 monitoring campaign: (a) Temperature Profiles from Ferraria bridge (FB) and PPA points, (b) Longitudinal Transect and (c) Ferraria Bridge Cross-Section. All values exposed in the transects are TSS in mg/L. 93

Figure 53 – Granulometry from Grab (G) and Cores (C) obtained by Sotiri, Hilgert and Fuchs (2019) at Passauna Reservoir. Adapted from: Sotiri, Hilgert and Fuchs (2019). 94
Figure 54 – Comparisons of the measurements performed on 18Oct/18 among numerical modeling for (a) Temperature and (b) Tracer Normalized Concentration (courtesy from Wendy Gonzales) and (c) the mapped cross-section made with the ADCP already discussed at Figure 50. 96
Figure 55 – Comparisons of the measurements performed on 20Oct/18 among numerical modeling for (a) Temperature and (b) Tracer Normalized Concentration (courtesy from Wendy Gonzales) the mapped longitudinal transect and (d) the mapped cross-section made with the ADCP, both already discussed at Figure 51. 97
Figure 56 – Comparisons of the measurements performed on 04Feb/19 among numerical modelling for (a) Temperature and (b) Tracer Normalized Concentration (courtesy from Wendy Gonzales), (c) the TSS in the water surface obtained by close remote sensing, after Wagner (2019), (d) a composition obtained by drone images (courtesy from Jens Kern) and (e) the ADCP mapped cross-setion obtained at the presented study. . . 98
Figure 57 – Comparisons of the measurements performed on 05Feb/19 among numerical modeling for (a) Temperature and (b) Tracer Normalized Concentration (courtesy from Wendy Gonzales), (c) the TSS in the water surface obtained by close remote sensing, after Wagner (2019), (d) the mapped longitudinal transect and (e) the mapped cross-section made with the ADCP, both already discussed at Figure 52. 99

Figure 58 – Optical Transmission. 118
Figure 59 – Scattering Data for LISST200x (a) before and (b) after the filtering application. 118

Figure 60 – Mean discharge and mean solid concentration during the field campaigns. 121

Figure 61 – Mapped cross-section in Mar/17 (a) TSS, (b)Qss and in Apr/17 (c) TSS, (d) Qss. 122
Figure 62 – Mapped cross-section in May/17 (a) TSS, (b)Qss and in June/17 (c) TSS, (d) Qss. 123
Figure 63 – Mapped cross-section in July/17 (a) TSS, (b)Qss and in August/17 (c) TSS, (d) Qss. 123
Figure 64 – Mapped cross-section in Jan/18 (a) TSS, (b)Qss. 124
Figure 65 – Mapped cross-section in May/17 (a) TSS, (b)Qss and in Apr/18 (c) TSS, (d) Qss. 125

Figure 66 – Mapped cross-section in Aug/18 (a) TSS, (b)Qss and in 18Oct/18 (c) TSS, (d) Qss. 125
Figure 67 – Mapped cross-section in 20Oct/18 (a) TSS, (b)Qss. 126
Figure 68 – Mapped cross-section in (a) Aug/17, (b) Feb/18, (c) 18Oct/18 and (d) 20Oct/18. 127
Figure 69 – Mapped cross-section in (a) 04Feb/19, (b) 05Feb/19 and (c) Apr/19. . 127

LIST OF TABLES

Table 1 – Density of Water and Solid Mixtures (kg/L) as a function of Temperature and Solid Concentration (mg/L). Adapted from Morris and Fan (1998). 27
Table 2 – Wave sound velocities at $1atm$. Adapted from Halliday and Resnick (2009). 33
Table 3 – Most recent studies regarding surrogate technologies application for SS and density currents determination. 46
Table 4 – Summary of the instrumentation and related measured parameters in each Study Area. 62
Table 5 – Backscatter correction functions descriptions. 63
Table 6 – Mean parameters evaluated during the Moving bed analysis. 68
Table 7 – Mean discharge and mean solid concentration during the field campaigns. 70
Table 8 – Comparison between the solid attenuation coefficients per campaign: α_s, total solid attenuation; α_{ss}, scattering attenuation and α_{sv}, viscous attenuation. 72
Table 9 – Comparison between the SSC obtained from the laboratory analysis and the SSC obtained from the CBS regression and 1MHz-measured areas filled in with nearby 3MHz data — SSC units in mg/L. 74
Table 10 – Difference between the measured SSC and the SSC obtained from ADCP correlation - considering the results without any extrapolations and with extrapolations — SSC units in mg/L. 74
Table 11 – Difference between the measured Qss and the Qss obtained from ADCP correlation - considering the results without any extrapolations and with extrapolations — Qss units in $10^3 Ton/day$ 75
Table 12 – Mean discharge and solid parameters during the field campaigns. 77
Table 13 – Comparison between the solid attenuation coefficients per campaign: α_s, total solid attenuation; α_{ss}, scattering attenuation and α_{sv}, viscous attenuation. 80
Table 14 – Difference between the TSS from laboratory and the TSS obtained from ADCP correlation at Passauna River. Units in mg/L. 80
Table 15 – Difference between the Qss from laboratory and the Qss obtained from ADCP correlation at Passauna River. Units in Ton/day. 81
Table 16 – Mean parameters measured in the V2 vertical. 84
Table 17 – Ferraria Bridge spatial resolution water sampling points per campaign. . 84

Table 18 – Comparison between the solid attenuation coefficients per campaign: α_s, total solid attenuation; α_{ss}, scattering attenuation and α_{sv}, viscous attenuation. 87
Table 19 – Difference between the TSS from laboratory and the TSS obtained from ADCP correlation at Passauna Reservoir. Units in mg/L. 88
Table 20 – Relative Error between the Smart Pulse and Fixed mode – comparison between 3MHz. 120

TABLE OF CONTENTS

1 Introduction . . . 19
1.1 Hypothesis and Objectives . . . 21
1.1.1 Structure of the work . . . 21

2 Theoretical Background . . . 23
2.1 Solid Dynamics . . . 23
2.1.1 Lotic Environments . . . 23
2.1.2 Lentic Environments . . . 25
2.2 Suspended Solids Monitoring Techniques . . . 29
2.2.1 Conventional Methods . . . 29
2.2.2 Surrogates Technologies . . . 31

3 Recent Publications Overview . . . 41
3.1 The use of combined surrogate technologies to determine Solid Concentration 41
3.2 Surrogate technologies applied to a lentic environment . . . 44
3.3 Summary of the combined surrogate technologies . . . 45
3.4 Summary . . . 46

4 Materials and Methods . . . 48
4.1 Site Description . . . 49
4.1.1 Lotic Environments: Taquari River and Passauna River . . . 49
4.1.1.1 Taquari River . . . 49
4.1.1.2 Passauna River . . . 52
4.1.2 Lentic Environment: Passauna Reservoir . . . 54
4.2 Instrumentation and field procedures . . . 56
4.2.1 Acoustic Doppler Current Profiler (ADCP) — ADP-M9 . . . 57
4.2.2 Laser In-Situ Scattering Transmissiometer - LISST . . . 58
4.2.3 Water Sampling Instruments and Laboratory Analysis . . . 59
4.3 Data Processing . . . 61
4.3.1 Backscatter Correction — dB2SS code . . . 62
4.3.2 LISST data processing and analysis . . . 65

5 Results and Discussions . . . 68
5.1 Taquari River . . . 68
5.1.1 Velocity, backscatter and SSC distribution . . . 68
5.1.2 Backscatter Correlation for Taquari River . . . 71
5.1.3 Mapping of Suspended Solid Concentration . . . 72

5.1.3.1 Extrapolation for non-measured regions . . . 73
5.1.4 Summary . . . 76
5.2 Passauna River . . . 77
5.2.1 Backscatter Correction . . . 79
5.2.2 Mapping of Total Suspended Solid Concentration . . . 80
5.2.3 Summary . . . 82
5.3 Passauna Reservoir . . . 83
5.3.1 Backscatter Corrections . . . 86
5.3.2 Mapping of Total Suspended Solid Concentration . . . 87
5.3.2.1 Longitudinal transects . . . 89
5.3.3 Comparison within other TSS studies conducted at Passauna Reservoir . . . 95
5.4 Discussion . . . 100
5.4.1 Summary . . . 101

6 Conclusion and Outlook . . . 103
6.1 Improvements for solid measurements in a Lotic Environment . . . 103
6.2 Development of the method for Lentic Environment . . . 104
6.3 Recommendation for future work . . . 106

Bibliography . . . 107

Appendix 113

APPENDIX A ADP-M9 Backscatter Attenuation Corrections . . . 114

APPENDIX B LISST-200X Processing Analysis . . . 117
B.1 In-situ technique and data treatment . . . 117
B.2 Sensor Corrections . . . 117

APPENDIX C ADP-M9 Verification of frequency at different operation modes 120

APPENDIX D Mapping Results . . . 122
D.1 Taquari River Mapped cross-setion . . . 122
D.2 Passauna River Mapped cross-setion . . . 125
D.3 Ferraria Bridge Mapped cross-setion . . . 127

1 Introduction

The sedimentological dynamics in surface waters is a complex phenomenon and it is bound to the ecological and anthropic processes within the watershed. The sediments present in a water body are solid particles resulting from the erosive processes in the watershed, bank erosion or from the riverbed itself which can be formed by mineral or organic particles (e.g. pieces of shells, leaves, animals, etc.). With this in mind, from now on the term sediment will be replaced by the term solid through this document.

In the social context, along with populational growth, it is also observed the rising pressure on water resources. Therefore, the knowledge about erosion, movement, and sedimentation processes within a watershed is important not only for environmental studies but also to assess the economic feasibility of numerous engineering projects (LIMA et al., 2001) which are planned especially in the BRICS (Brazil, Russia, India, China, South Africa) countries. For instance, knowledge on solid transport dynamics is important for the planning and maintenance of a waterway, harbors, irrigation channels, and especially for hydropower and drinking water reservoirs.

The construction of a dam in a river causes an interruption of the river flux, resulting in flow velocity reduction and increase in solids deposition along the reservoir, which will lose its storage capacity and increase system degradation. Hence, knowledge about solids (quantification and transport characteristics) in these environments makes possible to understand how to proceed in the soil conservation practice programs, check dams safety and the mechanisms of bypass and sluicing, practices often used to reduce solids inflow or remove settled solids from a reservoir (USBR, 2006). So, regardless of the ending purpose of such constructions, the knowledge of its lifetime and water quality is bounded to the sediment load in the water.

Measurements of solids in water bodies, however, are a challenge when requiring results for large regions (all over a reservoir or a river branch) and in addition to sufficient temporal resolutions to be able to describe dominant solid transport mechanisms. Therefore, knowledge is important for engineering measures, such as river training methods, dredging, bank protection, reservoir and dam design, etc. Current techniques are based on taking water samples, which are analyzed for solid concentrations in the laboratory. For example, Brazil has nowadays about 1685 sedimentometric monitoring stations (ANA, 2020). However, high uncertainties are usually reported and several research questions arise:

- Are the measurement frequencies and methods sufficient for describing solid dynamics?

- Are there differences between in-situ concentrations and results obtained by sampling and laboratory analysis?
- Are there reliable techniques for in-situ analysis?
- Are there methods to allow measurements over large regions and subsequent mapping of the results?
- Can those methods detect phenomena such as turbidity currents or sediment plumes in reservoirs?

A very promising approach to tackle those questions is the use of surrogate technologies (alternative in-situ methods) to measure solid transport dynamics.

Some of the current trends are related to the use of Remote Sensing Analysis on large scale by using satellite images (MONTANHER; NOVO; BARBOSA, 2013), on a medium scale, by using airborne photogrammetry (ROIG et al., 2013; OLIVETTI, 2020) or on a local scale by using, for example, a hyper-spectrometer sensor or a common camera (MOSBRUCKER et al., 2015; WAGNER, 2019). The disadvantages of those are their limitations on water surface measurements only. Other optical-based surrogate technologies overcoming this limitation are turbidimeters or optical diffraction devices (e.g. the LISST equipment — Laser In-situ Scattering Transmissiometer), which however are limited to point measurements and are not easily applicable for mapping applications. In that sense the use of acoustic profilers, e.g. ADCPs, are the most considered, offering an additional advantage in providing not only results for solid concentration, but also 3D velocity profiles and turbulence characteristics.

Acoustic profiling techniques are considered non-intrusive and allow indirect quantification of suspended solids in high temporal and spatial resolution (Guerrero et al., 2016). They also can be an important tool to obtain sediment information during extreme rain events, when it is not safe to measure with conventional techniques (SZUPIANY et al., 2019).

As described by Wood and Teasdale (2013), Landers et al. (2016), and Szupiany et al. (2019), surrogate technologies can be a cost-effective component of a long-term solid monitoring program. Once a regression model is developed between surrogate data and suspended solid obtained in the laboratory, samples can be collected in less spatial or temporal resolution, reducing long-term operation and maintenance costs.

However, so far, this methodology has become operational only for side-looking ADCPs (MOORE et al., 2013; LANDERS et al., 2016) and only in river cross-sections, where it is possible to assume that the solid concentration is uniform at the same depth within a measured cross-section. In the past few years, interest has risen in using down-looking moving ADCP measurements to capture the variation of solid concentrations in

the water column and all along the driven trajectory. First tests are reported in, first — Guerrero, Szupiany and Amsler (2011); Baranya and Józsa (2013); Guerrero et al. (2016) and Haun and Lizano (2018), however mainly related to applications in lotic environments with high flow velocities associated to high solid concentrations with mostly sand content. This thesis thus aims to fill the gaps and assess the feasibility of solid concentration mapping in lentic environments, using an ADCP.

1.1 Hypothesis and Objectives

Considering that the solid-acoustic analysis has already been developed for lotic environments (i.e. river cross-sections), this study's objective is to assess the feasibility and limitations to using acoustic measurements (by down-looking moving ADCP measurements) to map solid concentration and transport information in a lentic environment.

Expected results are mapped solid concentrations in different environments including information on solid characteristics (fine and cohesive solid particles and lower concentrations) and comparisons with rivers (coarser solid content and higher concentrations). In addition, the mapped concentration is used to describe dominant transport processes and pathways for river inflows into reservoirs (turbidity currents or density currents).

In order to achieve those objectives, a field-scale solid mapping technology using acoustic measurements to obtain hydro sedimentological data at reservoir inflows will be developed and validated.

The specifics objectives are:

- To apply and validate the ADCP backscatter processing method to obtain suspended solid concentrations (SSC) and transport characteristics in fluvial (lotic) environments.
- Extension and enhancement of the ADCP backscatter processing method to obtain total solids concentration (TSS) in a reservoir (lentic) environment including density effects (reservoir stratification and turbidity or density current).
- Development of a mapping technology applying the backscatter processing to longitudinal and transversal section measurements to identify and quantify turbidity/density current formations.

1.1.1 Structure of the work

This document, is structured in 6 chapters including:

- The present Chapter: Introduction (Chapter 1), where it is presented the problematics around solids monitoring and where it is given an overview about the current study and also presented the hypothesis and objectives.
- Chapter 2, where it is going to be presented the theoretical background about the subject, presenting some concepts of the that have been widely studied.
- Chapter 3 presents the most recent contributions in the proposed subject, presenting some studies related to lotic and lentic environments in the past feel years.
- Chapter 4 explains extensively the methodology applied in the field measurement campaigns, the laboratory procedures and the acoustic post-processing analysis to obtain the correlations and mapping of the monitored cross-sections.
- At Chapter 5 it is presented the results and discussions about the results obtained in these environments.
- And finally, Chapter 6 where is presented the closure of the work with a summary of the main findings and an outlook for future researches to improve the acoustics analysis.

2 Theoretical Background

Often, the dynamic of solids is pointed out as the cause of many engineering problems, such as shortening of reservoirs lifetime, soil losses, mud related to flood events, among others.

Although there is evidence in history that men built systems of canals for many purposes (the irrigation canals in Mesopotamia, reservoirs in Egypt, rivers regulations in China and many other hydraulics constructions in Greece, Persia, India and Roman Empire) the influence of the solid over the flow has been studied only recently. According to Graf (1984), solids influence and interaction were first scientifically noticed only during the Renaissance period, when many scientists tried to describe the flow resistance as a solid-liquid interfacial problem.

2.1 Solid Dynamics

2.1.1 Lotic Environments

Solid transport in rivers is a complex phenomenon and is bound to the ecological and anthropical processes within the watershed, such as the presence of agricultural activities, urbanization, the presence of highways, waterways, harbors, among others. All of these processes can contribute to solid yield, which can be up to 200 $ton/km^2/year$ in tropical countries (LATRUBESSE; STEVAUX; SINHA, 2005).

According to APHA (1999), which gives the guidelines for laboratory analysis, solids refer to matter suspended or dissolved in water or wastewater and can be characterized by: its concentration (massic concentration — mass per volume: mg/L, or volumetric concentration — volume of solids per water volume: mL/L, μ/L), size (radius or diameter, in μm or mm) and load (usually given in mass per time: kg/sec, Ton/day). The methods to determine each one of the aforementioned characteristics are going to be deeply discussed further.

The path of a solid particle involves processes related to the *disaggregation* of a consolidated material (eg. soil or rock), in small particles with different sizes. Therefore, these particles will be carried out from an *erosion* process influenced by the stream-flow. According to Rijn (1984), a solid particle will be carried out if the sedimentation velocity is lower than the vertical eddy velocity, caused by turbulence, responsible to maintains it in suspension.

In hydraulic systems, the transport of solid matter can be classified in different modes and mechanisms. According to Figure 1, in a streamflow, the particles can be carried on the bottom (*bedload*) or suspended in the water column (*suspended load* and

wash load[1]), depending on the size of the particle and the flow conditions.

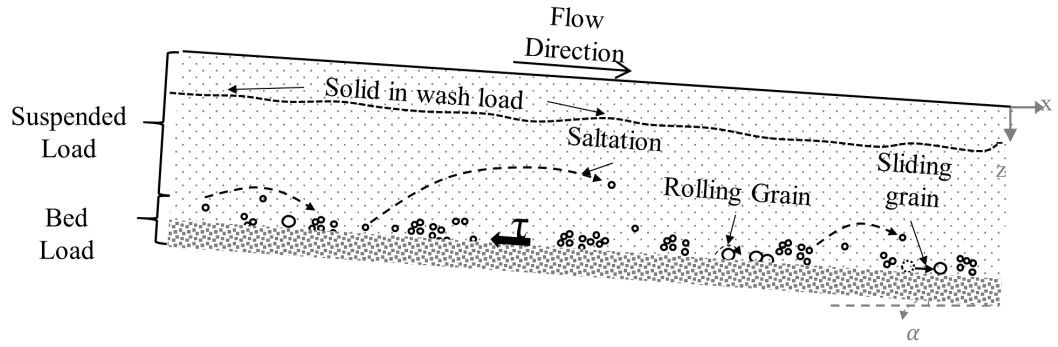

Figure 1 – Modes and mechanisms of solid transport, where τ is the streamflow shear stress.

Adapted from: Graf (1998).

Bedload is related to the larger particles and the transport mechanism can occur by a successive motion of rolling, sliding and saltating processes. The suspended load is related to the smaller particles and in this kind of transport the particles stay occasionally in contact with the bed, but most of the time the particles are suspended in the water column. As a result, in practical terms, the sum of these two kinds of mechanisms gives the Total Load.

To quantify solid transportation a great number of formulations and methods have been studied and applied throughout the years, most of them based on experimental results. Some of them are related only to the bed-load, the suspended load or the total load, which are in general the result of the sum of bed-load and suspended load.

If we are interested in the erosion/deposition process it is necessary to apply bed-load equations with different considerations. For example, a group of formulations given by Meyer-Peter and Müeller (1948) and Shields (1936), take into account the shear stress (τ) over the bed and the mean flow velocity. A second, and more complex group, considers turbulence as the main flow characteristic that leads to solid transportation in the bed. A third group, with proposed formulations by Bagnold (1966), Engelund and Hansen (1967) and Yang and Stall (1974), considers a relation between bed-load and flow potential.

At this point it is important to highlight that the equations describe the cross-sectional averaged transport, using cross-sectional averaged hydrodynamic parameters, which do not allow to map the transport characteristics, as proposed in this study.

It is important to consider that, although the use of such equations depends on a good field data collection, each formulation was developed for a specific flow range and morphological conditions, so their use must respect their hypothesis, simplifications and characteristics to be applied to the study location (SANTOS et al., 2001).

[1] This kind of load does not depend on the streamflow, it is part of an unpredictable load.

Regarding suspended load (Qss), we consider that particles are kept suspended by turbulence. As highlighted by Graf (1984) suspended load is always accompanied by bedload and the transition between the two modes of transport is gradual.

To predict the suspended load it is necessary to obtain the velocities and the solids concentration in the water column. Assuming a steady flow development, Figure 2 shows the profiles of both parameters and therefore the suspended load resulting profile.

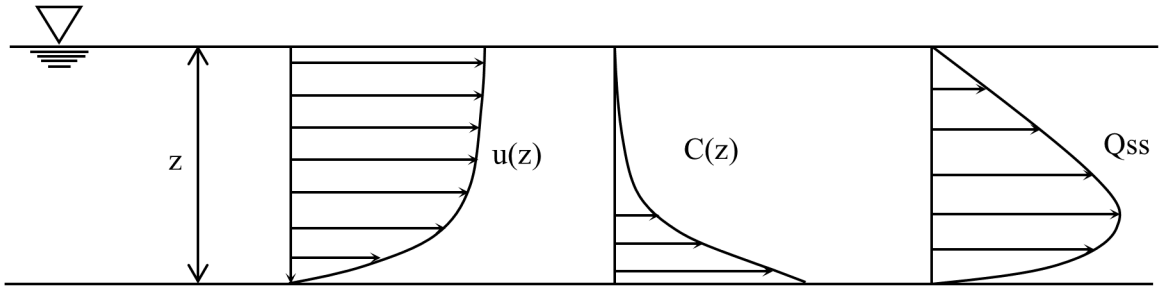

Figure 2 – Suspended load transport profiles.

Adapted from: Carvalho et al. (2000b)

As pointed out by Santos et al. (2001), the temporal solid distribution is related to the flow discharge: the larger the discharge the bigger the concentration of solids in the water column (equation 2.1). Although this relation is not always linear, it is possible to describe it as a solid rating curve, which makes possible to estimate the suspended load over time — so the bigger the amount of solid and discharge data available, the more reliable the suspended load estimative.

$$Qss = \int_{z_0}^{z} \int_{y_0}^{y} \int_{x_0}^{x} C_s(x, y, z) \cdot u(x, y, z) dx dy dz, \tag{2.1}$$

where Q_{ss} is the suspended load, $C_s(x, y, z)$ is the concentration and $u(x, y, z)$ is the velocity profile. Both vary in all dimensions: over the depth, from z_0 to z and in the both directions (x and y): from x_0 to x and from y_0 to y.

2.1.2 Lentic Environments

As the river flows into a lake or a reservoir the cross-sectional area enlarged and the flow velocity decreases. These characteristics reduce the stream solid transport capacity and lead to a sedimentation process that can happen immediately in the river mouth and throughout the reservoir length. Figure 3 sketches the transitional zone — from the lotic to the lentic environment, indicating the morphological changes of the region that are going to be briefly described in the sequence.

According to Shotbolt, Thomas and Hutchinson (2005) sedimentation processes, in a lentic environment, can be classified into primary and secondary processes, where primary processes refer to the initial deposition at the entrance of the reservoir (the topset bed and foreset bed formation from Figure 3) and the secondary processes are related to the resuspension and redistribution of previously deposited solids.

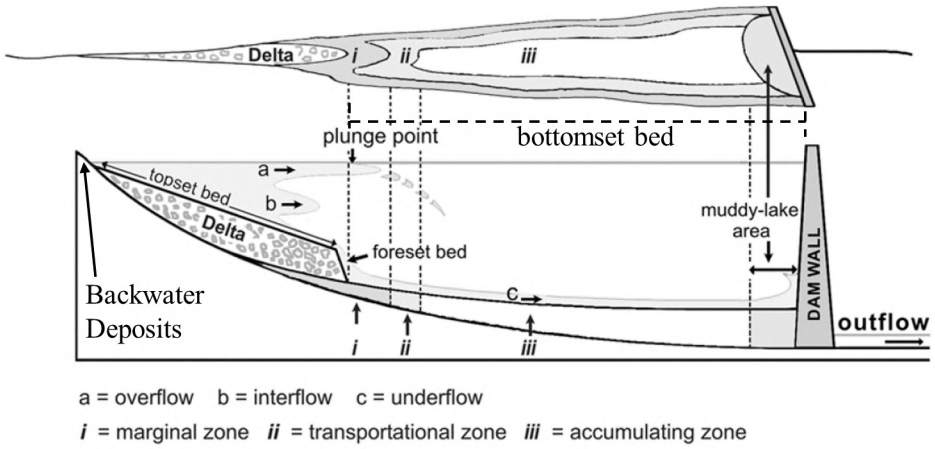

Figure 3 – Solid Deposit Formation in the transitional zone between lotic and lentic environments.

Adapted from Carvalho et al. (2000b),Morris and Fan (1998) and Shotbolt, Thomas and Hutchinson (2005).

As enumerated by Morris and Fan (1998), the topset bed corresponds to delta deposits due to the settling of the solid material that comes with the flow. The settled material can vary from coarse solids (sand) or may also contain a large fraction of finer solids (as silt and clay). Still, according to Morris and Fan (1998), the foreset bed represents the face of the delta advancing into the reservoir with a steeper slope and finest material.

Carvalho et al. (2000a) consider an additional morphodynamics formation, which is also part of the topset bed, called backwater deposit. This formation configures a deposit formation still in the fluvial system before it enters the reservoir. The authors also point out that this kind of formation can be responsible for flood events in the upstream, while those deposit formations inside the reservoir, cited by Morris and Fan (1998), are responsible to decrease the reservoir storage capability.

Another formation that happens after the delta, in the bottomset zone, is the bed deposits, which is also part of the delta formation. Depending on the length and configuration of the reservoir that formation can reach the dam and cause damages in its components (Morris and Fan (1998)).

Considering the system dynamics, these zones are not temporal or spatial stable. During flood events, for instance, the delta can accumulate large volumes of solids and

after that, during a drawdown situation, the deposits can be reworked into an equilibrium state due to a typical situation of morphodynamic-flow interaction.

As the water goes from the river towards the reservoir, besides the aforementioned changes in the morphodynamics of the water body there are some phenomena related to hydrodynamics, such as density current formations that can be responsible for the sedimentation pattern and spread over the reservoir.

Density Currents

Density currents occur due to the density difference between two fluids. According to Morris and Fan (1998), differences in both: temperature and solid concentration contribute to stratification in a reservoir, Table 1 shows the effect of the suspended solid on density and how it can vary with temperature. Still, according to the same authors, turbidity density currents occurs when the solid enters in a reservoir and plunge in clean water and travels down along the talweg in the reservoir.

Table 1 – Density of Water and Solid Mixtures (kg/L) as a function of Temperature and Solid Concentration (mg/L). Adapted from Morris and Fan (1998).

Temperature	Pure Water	Water + Solid		
		1000 mg/L	10 000 mg/L	100 000 mg/L
0	0.9998	1.0004	1.0061	1.0621
4	1.0000	1.0006	1.0062	1.0622
10	0.9997	1.0003	1.0059	1.0620
20	0.9982	0.9989	1.0044	1.0605
30	0.9957	0.9963	1.0019	1.0581

The zone where the inflowing turbid water entering a reservoir plunges beneath the clear water, thereby producing stratified flow, is called the plunge point or plunge line (MORRIS; FAN, 1998). As reviewed by Haun and Lizano (2016) density currents, can be defined as a layer of water that plunges and continues moving as stratified flow in equilibrium with the fluid.

As exposed by Graf (1984), in a lake or reservoir, the finer material will be carried for long distances, depending on the size of the particles, without settling. In this case, if the current reaches the dam it will produce a submerged muddy lake with a high concentration of fine solid (see: Figure 3).

Figure 4 shows the transition from non-stratified to stratified flow and the plunge point line. Although its location is after the delta zone, the plunge point is limited by the pool level, the discharge, the suspended solid concentration and the reservoir geometry.

The determination of the plunge point can be estimated based on the densimetric Froud number (equation 2.2).

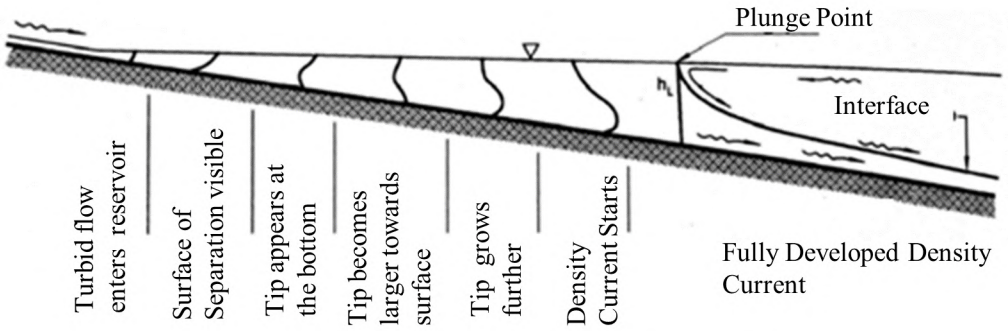

Figure 4 – Density Current Formation: a transition from non-stratified to stratified flow. Adapted from Morris and Fan (1998).

$$F_p = \frac{u}{\sqrt{\frac{\Delta\rho}{\rho'} g h}}, \tag{2.2}$$

where u is the mean velocity, h is the water depth at the plunge point, ρ is the density of the clear water, ρ' is the density of the turbid water, and $\Delta\rho = \rho' - \rho$.

According to Morris and Fan (1998), flume tests and reservoir measurements indicate that the densimetric Froude number has a value of about 0.78 at the plunge point.

As observed by Cortés (2014) and showed in Figure 5 the density current can behave in different ways:

(a) interflow, when the density current is lighter than the lower layer, then it will behave as an intrusion form on the thermocline;

(b) split flows, which occurs when the density current splits into a density step to form two intrusions;

(c) underflows, when the inlet is denser than the middle and

(d) overflows, as the situation showed in Figure 3-a, when the density current enters the reservoir before reaching the plunge point.

After it sinks, it can follow the talweg of the reservoir and as reviewed by Haun and Lizano (2016), the travel time of a density current can range between 0.03 and 0.05 m/s.

As reviewed by Shotbolt, Thomas and Hutchinson (2005), turbidity flows are important during storm events, but the non-stratified flow is dominant under normal flow

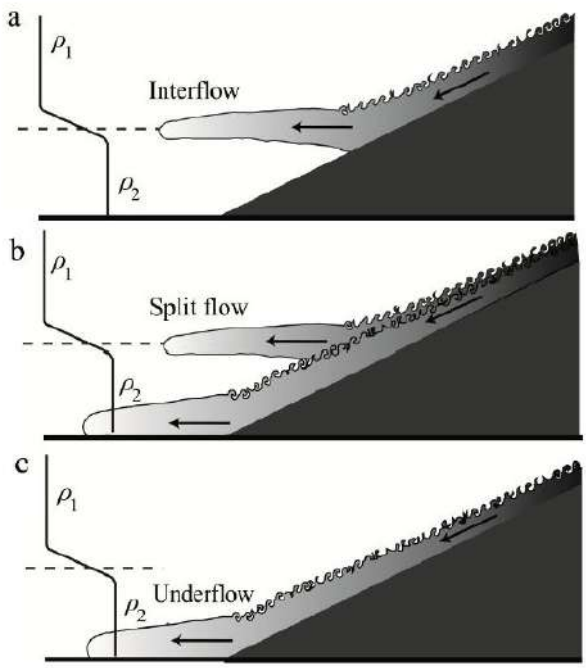

Figure 5 – The behavior of a gravity current in a two-layered stratified environment: (a) interflows (b) underflows, and (c) split flows.

Adapted from:Cortés (2014).

conditions when low-energy inputs are not capable to penetrating far into the water body and carry solids and substances.

2.2 Suspended Solids Monitoring Techniques

So far, it is clear that solids monitoring is a key to decision making. So, the choice of an appropriated method and the monitoring practice will give to the manager an indication of the temporal and spatial variation of the solids. This section will describe the conventional methods and the presentation of the most applied surrogate methods for solid determination.

2.2.1 Conventional Methods

The main purpose of sampling is to obtain solid concentration and grain size distribution in the water column. The samples obtained for suspended load determination are composed of a mix of dissolved[2] and suspended solids.

The conventional methods for sampling solids in the water column are usually classified as *point samples* or *vertical integration samples*.

The method can be performed considering different depths in each sampled vertical, for example, for stables cross-sections, the sampling can be taken as 1 single point at

[2] in this study the dissolved part is the solid fraction lower than $0.6\mu m$

0.6 from total depth; 2 points at 0.6 and 0.2 from total depth; and for 3 points at 1, 0.5 from the total depth and another one near the bottom. Carvalho et al. (2000b) suggests 5 vertical points at 0.1, 0.3, 0.5, 0.7 and 0.9 from total depth, if there is solid variation throughout the water column.

For vertical integration Carvalho (2008) presents two methodologies:

- Method of Equal Width Increment (*EWI*), where the cross-section is divided into equal width segments for sampling, in which all the samples can be mixed and then only a single analysis is performed, representing an average from the whole cross-section — Figure 6a.
- Method of Equal Discharge Increment (*EDI*), for this application it is necessary to know the discharge distribution along the cross-section. The method consists of sampling in the middle of each vertical. As in the EIW method, all the samples can be mixed and then only a single analysis is performed, representing an average from the whole cross-section — Figure 6b.

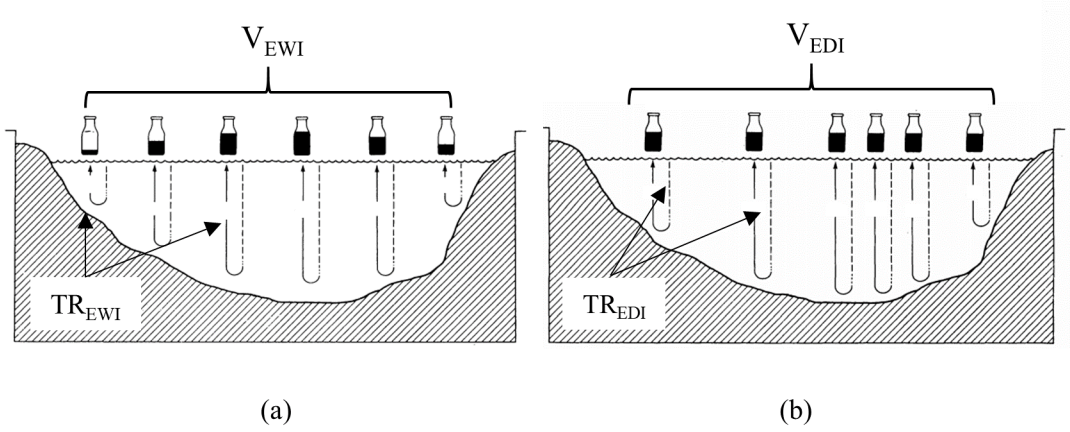

Figure 6 – (a) Sampling by Equal Width Increment (EWI), where the sampled volume (V_{EWI}) is proportional to the discharge and the Transitional Rate (TR_{EWI}, which is the sampling velocity) is constant at each vertical and (b) Sampling by Equal Discharge Increment(EDI), where the sampled volume (V_{EDI}) is equal and the Transitional Rate (TR_{EDI}, which is the sampling velocity) is different, proportional to water velocity, at each vertical.

Adapted from: Edwards and Glysson (1988).

After sampling the water for solid estimative it is necessary to proceed for laboratory analysis. However, before showing the conventional laboratory analysis, at this stage, it is important to rise and clarify the conceptual difference between suspended solids concentration (SSC) and total suspended solids (TSS).

As reviewed by Galloway, Evans and Green. (2005), SSC and TSS commonly are used to quantify concentrations of suspended solid-phase material in surface water. But

the analytical method to determine one or another can differ. The basic idea is that the SSC is obtained from the total sampled volume, which means if a bottle of 1 liter was collected, the whole bottle will be analyzed. The TSS analytical method uses a volume fraction, from the original water sample, obtained immediately after the sample has been well mixed.

According to Galloway, Evans and Green. (2005), the analytical methods differ and the two may not be equivalent when solid-phase material, especially sand, becomes more concentrated (this fact was also observed in some analysis conducted in this present study). It happens mainly due to the fast settling velocity of the coarser materials. In the presented study the analytical method regarding the finer fractions was obtained as TSS. For samples with a high amount of coarse materials (eg. sand), the solid concentration was determined as SSC.

The most common analytical process to obtain solid concentration is based on the gravimetric methods. Hence, the different forms of solid determination can be obtained by drying and wet weight difference of the remained solid, over a certain sampling volume. Figure 7 shows a flow-chart with different fractions of solids that can be determined during the analytical process in the laboratory.

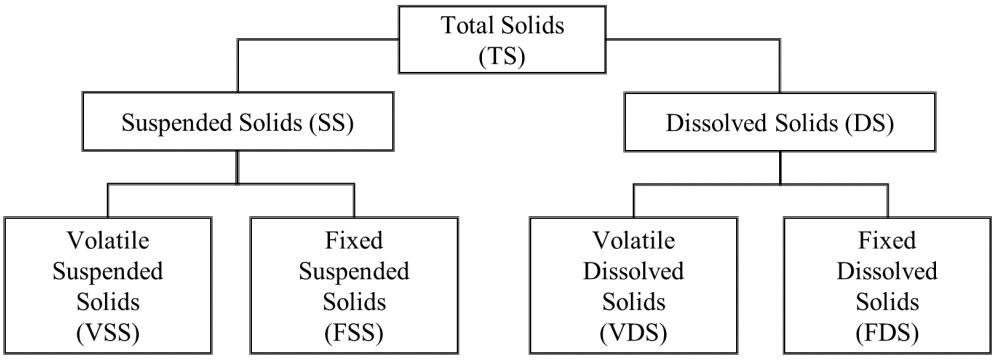

Figure 7 – Solid Series.

After APHA (1999).

In this study, for finer solids, the required fraction will be SS. This fraction, according to APHA (1999) is the remained amount of solid retained by a glass fiber filter of 2 μm or smaller. Considering the same definition, SABESP (1999) assumes a minimum filter porosity of 1.2 μm for this analysis. In this study was used a glass fiber filter of 0.6 μm.

2.2.2 Surrogates Technologies

In this Section will be presented the acoustic and the optical instruments proposed as surrogate technologies to obtain suspended solids (SS) and granulometry, respectively.

Acoustic Method

The Acoustic Doppler Current Profiler (ADCP) [3] was first developed to measure the water velocity and the discharge from a river cross-section by measuring the velocity of particles in the water. The acoustic method follows the velocity-area methodology for discharge estimation and its mechanism is based on the sound-wave propagation emitted by transducers that operate in frequencies that can vary depending on the type of the equipment. In this study, the ADP-M9, from Sontek-Xylem, will be used and more details about it will be given in Chapter 4.

The sound wave consists of a pressure wave that travels in an elastic environment, such as liquid, solids or gases. The wavelength (λ) is the consecutive distance between two regions of high or low pressure. In a bi-dimensional representation, when a source emits a pulse, the sound initiates its propagation in concentric circles around the source. These circles are known as the front wave - surfaces where the fluid oscillates. Near the source, the front waves are spherical. As they travel further, they become larger and can be approached as flat waves. In Figure 8, it is possible to observe the wave propagation from a point source and the associated wave parameters.

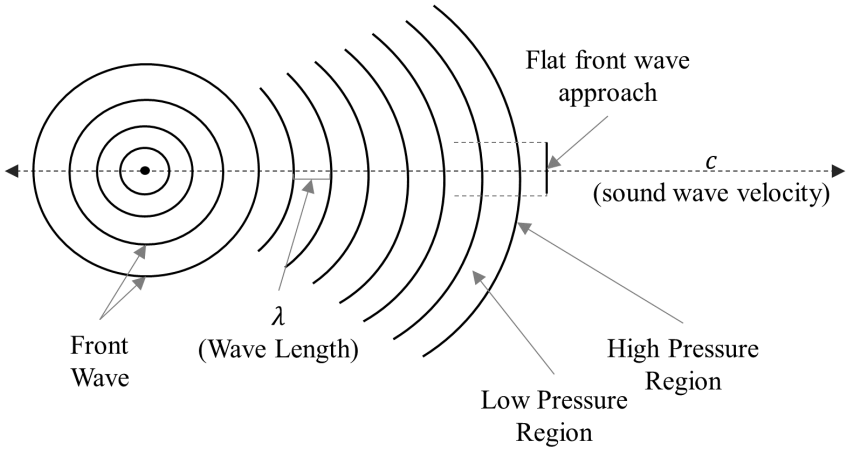

Figure 8 – Wave sound propagation and related parameters.

Adapted from Halliday and Resnick (2009).

Additionally to Figure 8, there is also the frequency, f, which is the number of waves that pass through a point in a certain time and C, which is the sound wave velocity. The relation for frequency can be written as (equation 2.3):

[3] As observed by Gamaro (2012), the device that measures the discharge by using the doppler effect is widely known by the acronym: ADCP. But, in fact, this is a specific name given by the manufacturer that makes it commercial. The name for this device will vary from one manufacture to another, for example: ADP, ADVM and Workhorse.

$$C = f\lambda. \tag{2.3}$$

Sound can travel at different speeds depending on the temperature or salinity at the medium. Table 2 shows the sound wave velocity in different mediums.

Table 2 – Wave sound velocities at $1atm$. Adapted from Halliday and Resnick (2009).

Medium	Velocity (m/s)
Air $(0\ ^{\circ}C\ )$	331
Air $(20\ ^{\circ}C)$	343
Water $(0\ ^{\circ}C)$	1402
Water $(20^{\circ}C)$	1482
Sea Water $(20^{\circ}C)$ and 35% of salinity	1522

The Doppler technology uses a sensor that is continuously transmitting ultrasonic signals at some frequency. The particles in the medium reflect this signal and depending on its position and velocity it will shift the frequency of the reflected signal. The shift in the frequency is detected by the sensor and used to estimate the flow velocity according to equation 2.4. To estimate the velocity the main assumption is that the suspended particles are moving at the same velocity as the water flow.

$$\Delta f = 2f\left(\frac{V}{C}\right), \tag{2.4}$$

where Δf is the frequency change, f is the emitted frequency and V is the relative velocity between the source and the particle.

As quoted by Wood (2017), the lower the frequency, the longer the distance that the sound can travel, however, the resolution of velocity data will decrease. On the other hand, the higher the frequency, the shorter the distance or range that the sound can travel, and in this case, the resolution of the velocity data will increase. Still, according to Wood (2017) a higher frequency is more appropriate for vertically oriented acoustic devices, particularly when flow depths are shallow and higher resolution is needed over short distances.

In Figure 9, it is possible to observe the wave behavior when it is emitted by the transducer and reflected by the suspended matter (a mixture of solids and organic particles), when it returns as a backscatter signal to the transducer.

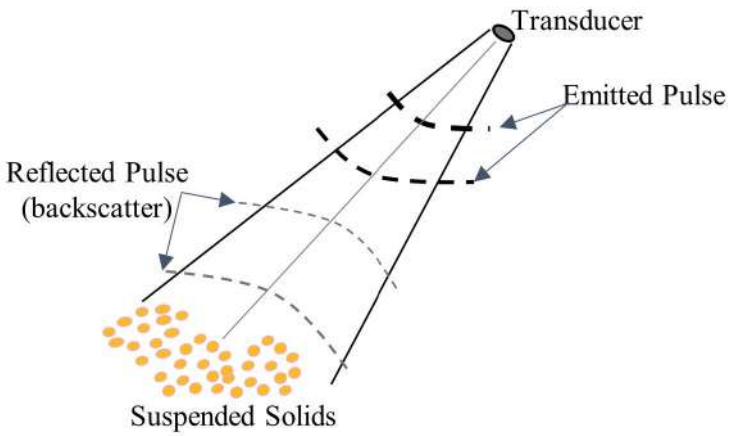

Figure 9 – Emitted pulse and reflected backscatter.

Adapted from: Gamaro (2012).

The ADCP measures the velocity straight from the emitted pulse directions, considering: (a) the duration of the acoustic return to determine the position of the particles; (b) the Doppler shift to computing the particle velocity, thus the water velocity and (c) the determination of the signal noise to ratio (SNR), which is a measure on the number of reflections, thus the quantity of the particles in the flow.

Generally, the device has at least three transducers with the same frequency, some devices have the fourth transducer in order to obtain the error estimation. The error can be obtained by the difference between the estimated vertical velocity component in each direction. Two pairs of transducers are aligned with the North-South direction and the other is aligned with the East-West direction, as it can be observed in Figure 10. where Δf is the frequency change, f is the emitted frequency and V is the relative velocity between the source and the particle.

For continuum measurements, the ADCP divides the water column into depth cells (known as bins) and for each one of these cells, the device calculates the average velocity and their directions. As pointed out by Mueller et al. (2013) on the surface, the ADCP cannot measure velocities due to the required *blanking* distance. On the bed, it also cannot be done due to *side-lobe* interference. In these layers, where it is not possible to measure the velocity, the estimation is usually done by the extrapolation of a theoretical profile.

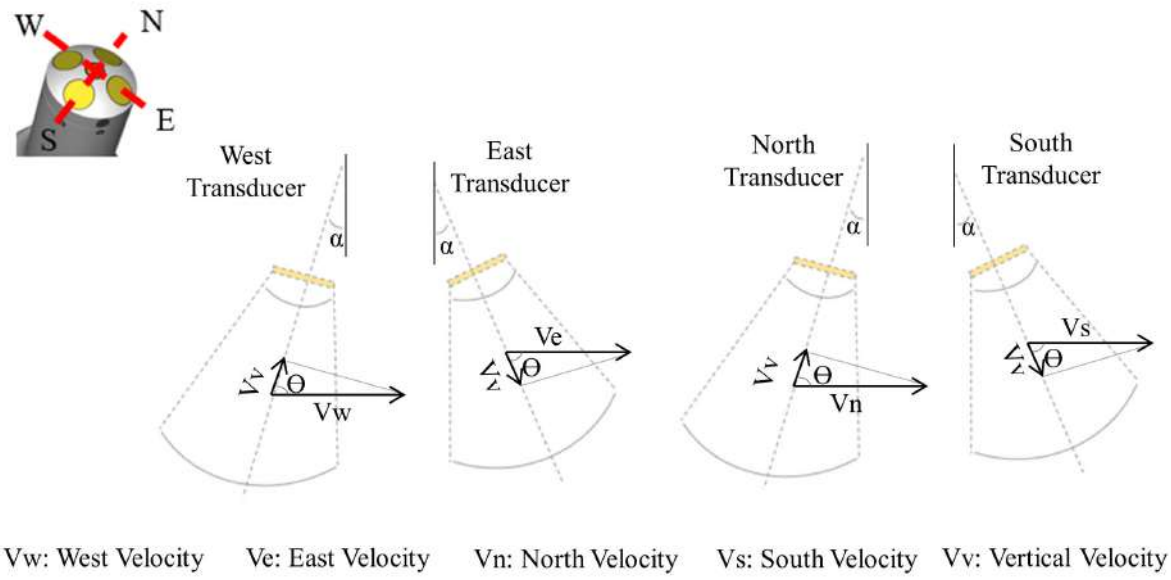

Figure 10 – Velocity components measurement.

Adapted from: Gamaro (2012).

The blank is a device's limitation produced by the transducer vibration. Where the transducer is at the same time the transmitter and the receiver, a short distance (blank) is needed after the signal transmission to allow the transducer to adjust itself to receive the shifted signal. The side-lobe is a parallel beam emitted by the device which reaches the bed before the main beam, producing a strong noise in the bed. There are also no measured areas near the banks, due to the low depth and the reflection caused by the edges. In this case, the velocity is obtained by keeping the device measuring in a fixed position at a certain distance from the edge, in order to obtain an average profile for further software extrapolation.

Finally, after all these considerations, the discharge is obtained in a similar procedure as in conventional estimation, considering the channel area, A, (obtained during the crossing) and the measured velocity, v — $Q = v.A$ (Figure 11).

For the signal attenuation and relation with suspended solids, the mechanism is based on the quantification of the backscatter by the suspended particles. This quantification allows us to estimate a correlation between the received signal and the distribution of suspended matter in the measured area. Hence, the larger the concentration, the larger the difference between the emitted and reflected signals.

According to Terabe (2004), the main advantage of its application is the possibility to make continuum measurements, without cause interference in the local condition of streamflow, because the equipment is not introduced into the water as the manual equipment.

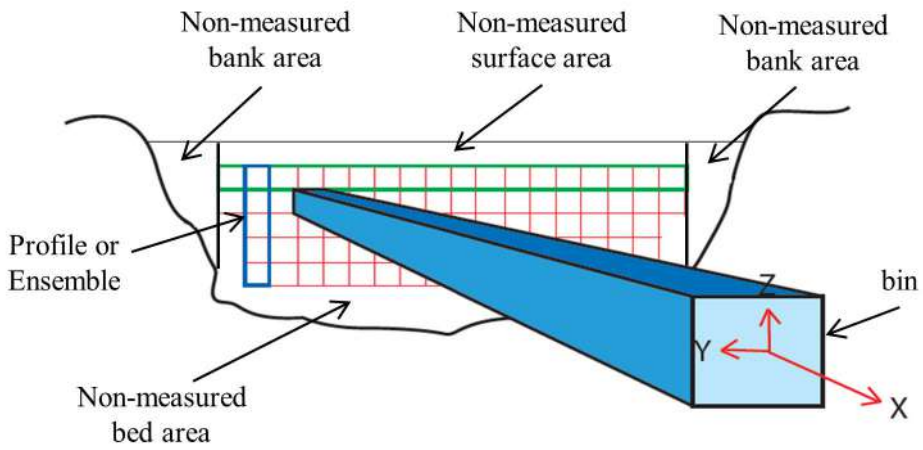

Figure 11 – Measured Area and Cross-Section component.

After Sontek (2016).

The determination of SSC by the reflected beam in the water requires some knowledge about several variables (Deines (1999)), such as:

1. The power transmitted into the water;
2. The acoustic characteristics from the equipment and its response;
3. The signal attenuation caused by propagation losses - water and solid attenuation, reflection and beam spread;

All of these factors can be mathematically translated into models that can be described by solid, hydrodynamics and device characteristics. Equation 2.5 shows the applied equation, where SNR_{mean} is the mean of the 4 beams of the ADCP throughout each vertical. $20\log(\psi R)$ is the spread attenuation, $2\alpha_w R$ is the water absorption and $2\alpha_s R$ is the solid attenuation term.

$$CBS = SNR_{mean} + 20\log(\psi R) + 2\alpha_w R + 2\alpha_s R, \tag{2.5}$$

where CBS is the corrected backscatter (in dB), the coefficient ψ is a near field correction factor related to the effect of spherical spreading, close to the transducer (adimensional), R is the slant range from the transducer head to the measured ADCP cell (in meters), α_w is the absorption energy by the water (in dB/m) and α_s is the attenuation due to the suspended matter (in dB/m).

The models applied in this study are based on the models presented by Guerrero et al. (2016) – for water absorption and for solid attenuation.

After the corrections it is possible to obtain an adjusted curve from the form presented at Equation 2.5, that correlates the corrected backscatter (CBS) in dB with the $Log10$ of SS in mg/L.

$$log(SS) = a.CBS + b, \tag{2.6}$$

$$SS = 10^{(a+b \cdot CBS)} \tag{2.7}$$

where a and b are the angular and linear coefficient of the adjusted curve.

Optical Method

The Laser In-situ Scattering Transmissometry (LISST) [4] is an optical technique that involves not only the estimative of SS, but also the granulometry, both *in-situ*. It is a submersible multi-parameter system for point measurements of the particle size distribution (PSD) and volumetric concentration (VC).

The LISSTs equipment are based on laser diffraction. Which consists of a collimated laser beam (L) (Figure 12) sent through an amount of suspended solid that is traveling with the flow. The intercepted light from the collimated beam will scatter (R) at a particular angle, based on particle diameter and will be detected by a silicon ring detector (D). Behind the ring-detector is placed a photodiode (P). A hole in the center of the ring-detector (D) allows the tightly focused laser beam to pass through. The photodiode P senses the power in this beam. A reduction in this power due to particles constitutes a measure of attenuation. This attenuation is used only to de-attenuate the light on rings. Following this de-attenuation, and after then subtracting a background (i.e. light on rings with filtered water), an inversion procedure produces the 36-element PSD (SEQUOIASC, 2017).

All this detection process on PSD will vary from 32 to 36 small forward angles, which corresponds to the particle size ranges between 2.5 to 500 μm and 1 to 500 μm, depending on the LISST version: LISST-100x and LISST-200x, respectively.

The equipment measures internally at $20Hz$, but due to data logger limitations, the individual measurements are averaged into a sample, and it is this sample average that is stored at a maximum sample rate of $1Hz$. As a default, the instrument operates in the Fixed Sample Rate mode at a $1Hz$ rate with 10 measurements per average. This average is obtained in 0.53 and 0.34 seconds, for LISST-200x and LISST-100x respectively (Sequoia (2015) and Sequoia (2018)).

[4] from Sequoiasc, Inc.

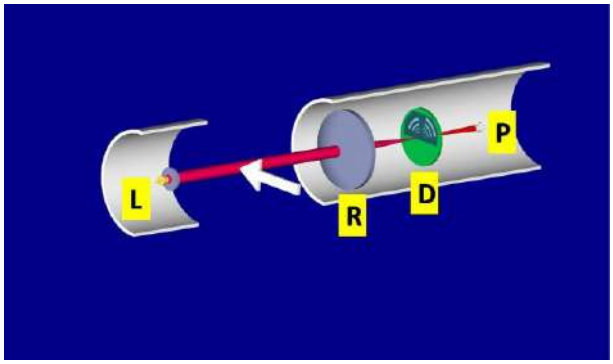

Figure 12 – Operating scheme of LISST equipment series - diffraction laser.
After SequoiaSc (2017).

According to Czuba et al. (2015) limitations on the use and application of the devices are related to the particle shape, particle composition, the range of the particle sizes, strong thermal stratifications and density fluctuations.

Depending on the application, some of the mentioned limitations can affect mainly the volume concentration determination. For example, as highlighted by Felix, Albayrak and Boes (2017), highly non-spherical particle shapes lead to overestimated LISST concentrations. Laboratory analysis (FELIX; ALBAYRAK; BOES, 2013) showed that the smallest irregular particles scatter more light than equivalent spheres (for feldspar and mica minerals) overestimating the SSC in 1.5 and 8 times the known value.

The composition of the particles is another factor that can affect the measurements. For particles $< 20\ \mu m$ the color becomes an important factor, since it will interact differently with the light. Also for small particles, the proportion between organic matter and mineral is important. Regarding the size, as cited by Czuba et al. (2015) the measurements of particles smaller or larger than those that the instrument can detect can affect the concentration.

Figure 13 sketches the situation indicated by Felix, Albayrak and Boes (2017) regarding the LISST limitations, when eventually some PSD values need to be discarded (from bin 1 to 3, in gray) because of some environmental issues or equipment limitations, such as: non-spherical particle shapes, the presence of small out-of-range particles (since is a backward relation, small particles will scatter more in the upper angles and produce a fake result regarding concentration in the small bins) and effects of the refractive index.

Despite all limitations, this technique shows a very good alternative for granulometry determination. Granulometry is always a problematic parameter to be determined, because of all the factors that can affect the aggregation and disaggregation (Figure 14).

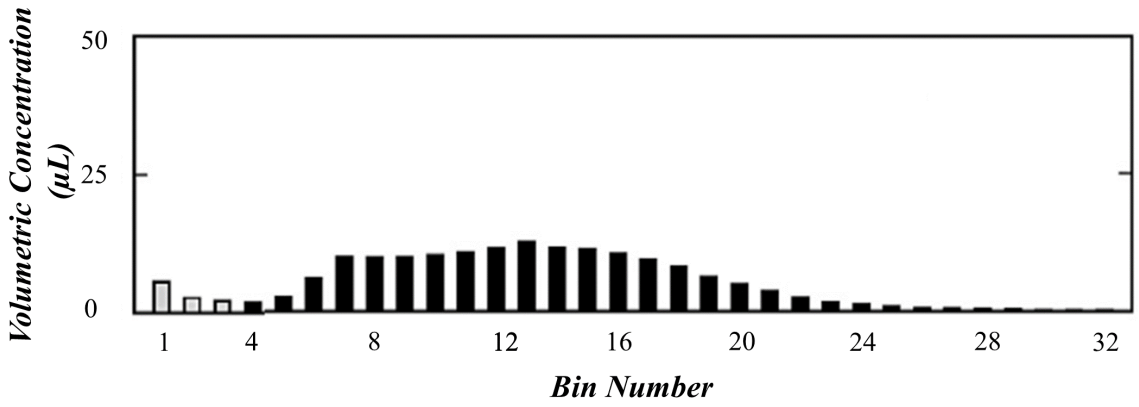

Figure 13 – Examples of bias in the LISST volumetric concentrations produced by the presence of out-of-range particles (for LISST-100X, version).

Adapted from Felix, Albayrak and Boes (2017).

As highlighted by Klassen (2017) factors as water sampling, storage, transportation (turbulence), temperature, pH variations and ultrasonic waves can change significantly the particle sizes and create a different granulometric curve in the laboratory than that one existing in the environment.

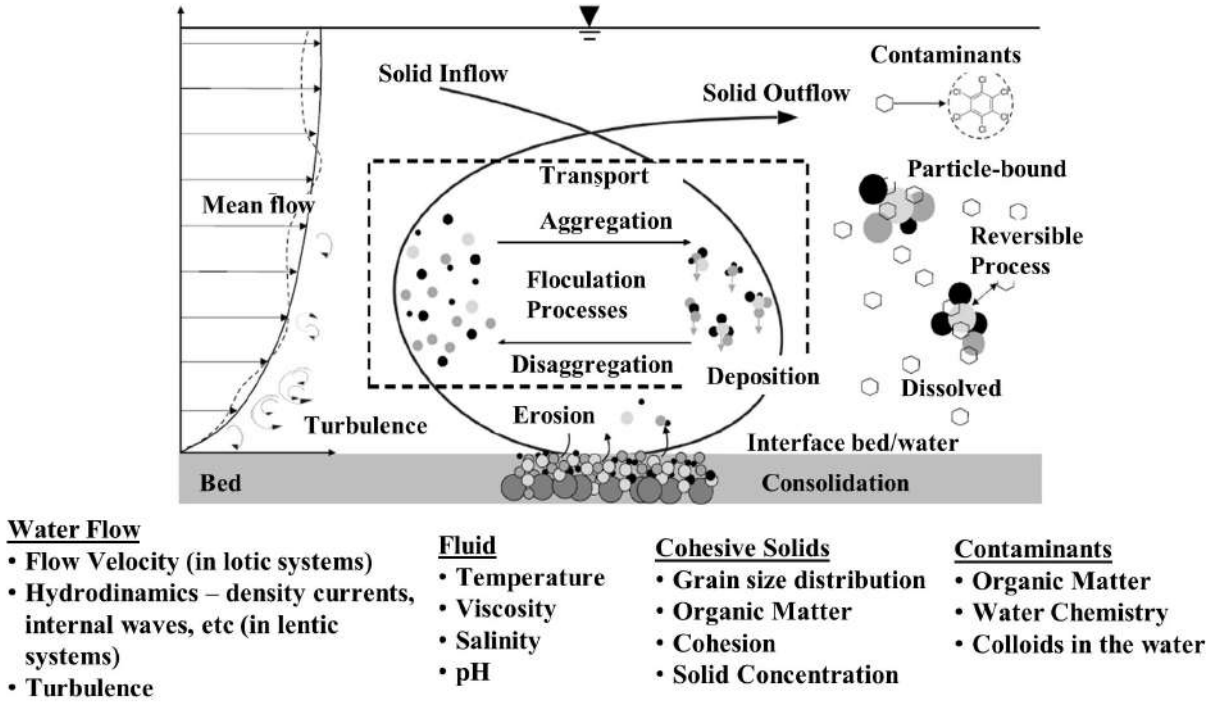

Figure 14 – Water-solid system described with a cycle of erosion, transport, deposition and consolidation, involved in particle aggregation/disaggregation and sorption/adsorption of contaminants. Below the scheme, the corresponding influence factors and the respective properties are presented.

Summary

Throughout this chapter it was briefly shown the theory to be applied in this study about solid dynamics in lotic and lentic environments and the sampling method, considering the conventional (sampling an laboratory analysis) and surrogate technologies, such as acoustic and optical measurements.

With this in mind, in the next chapter will be shown the most recent publications about the application of the cited equipment in solid studies followed by the methodology applied (Chapter 4) in this study to obtain SS information from surrogate technologies.

3 Recent Publications Overview

First developed for oceanic studies, the use of acoustic technology has been widely studied for a large number of applications. The first ADCP was produced in the $'70s$ as an adaptation of a Doppler speed log - an instrument that measures the speed of ships through the water or over the sea bottom (RD-INSTRUMENTS, 2011). In the $'80s$ the device was produced in a commercial scale and by the $'90s$ it became popular in the scientific community, with a wide range of studies related to its many options of applications, among them, the use of ADCP to estimate load (bed and suspended) and SS — Gamaro (2012).

This section will present the most recent and relevant contributions for the proposed study.

3.1 The use of combined surrogate technologies to determine Solid Concentration

Most publications related to surrogate technologies for solid dynamics studies are done in rivers, a system for which most of the models and devices were developed and which have a very good response. Related to ADCP applications, according to Deines (1999) (which gives us a very good contribution indicating a method that considers a proportional relation between the signal intensity and the solid concentration), when supported by careful calibration procedures, the acoustic signal can be used to obtain continuum measurement of discharges, loads and solid concentration, depending on the applied technique.

To reach reliable results, researches are combining different methods and comparing the results, in order to check the best approach. In this context, it has been common the combination of ADCP measurements and optical sensors (LISST, Tubidity-meters or OBS[1]) or water sampling and SSC correlations to study solid dynamics in the environment (GARTNER, 2004; GUERRERO; SZUPIANY; AMSLER, 2011; BARANYA; JÓZSA, 2013; WOOD; TEASDALE, 2013; GUERRERO et al., 2016; LANDERS et al., 2016; HAUN; LIZANO, 2018).

These combinations of techniques and devices were explored in the study proposed by Gartner (2004). He studied the solid dynamics comparing and correlating results from static ADCP, LISST and OBS measurements at different stations located in San Francisco Bay, USA. He considered the scattering for different particle sizes using the Rayleigh scattering model ($2\pi a_p/\lambda < 1$, where a_p is the particle diameter) as a criterion to define a range of suspended solid determination as a function of his ADCP frequencies. In his

[1] Optical Backscatter Sensor - a high intensity infra-red emitting diode (IRED), from Campbell Sci.

study, the author highlighted the backscatter intensity particle size dependency, stating that the method requires a steady size distribution for a good agreement.

This statement highlighted by Gartner (2004) was also mentioned by Wood and Teasdale (2013) and Guerrero et al. (2016), regarding the importance to take into account the medium characteristics, because the losses also depend on other parameters, such as temperature, salinity and SS.

Wood and Teasdale (2013) evaluated the use of acoustic surrogate technologies, such as: acoustic-backscatter, laser-diffraction and turbidity-meter to estimate real-time SSC at two rivers in the USA. At this study on the use of LISST, different from others cited studies, the authors did not assume a density value to convert volumetric concentration ($\mu L/L$) in massic concentration (mg/L), they applied a simple linear regression (SSC_v x SSC_m) to obtain real-time update about SSC variations. As a result, they obtained better correlations for the acoustic method that covers a larger part of the channel than the other evaluated surrogates technologies.

Guerrero, Szupiany and Amsler (2011) attempted for the first time, in scientific-practical terms, to characterize particle distribution and to determinate SSC in a large river, using a multi-frequency arrangement (two devices: 600 kHz and 1200 kHz).

Baranya and Józsa (2013) studied the ADCP x SSC correlation and quantified the lack of information related to the non-measured areas from ADCP. Also, they noted that the error in the SSC estimative can increase as the circumference of the particle approaches to the wavelength. In their study, they also mapped SSC at 7 cross-sections of 600 meters apart along of Danube River, the obtained results include interpolation along the water column at each cross-section, as shown in Figure 15. The authors estimated SSC based on a linear regression between the measured SSC and the relative backscatter. From sensitivity tests that analyzed how the solid flux will vary due to changes in the echo intensity, they observed that a variation of 20% in ADCP echo intensity can result in a variation of 10% in the estimation of SSC.

Based on these studies, later on, Guerrero et al. (2016) evaluated the acoustic properties of suspended solids and the consequences of the applicability of the ADCP correction methods. Take into account that Parana river represents a large sandy river and the Danube has characteristic of a sand-gravel bed and clay-silt particles being transported in the water column, comparing the results from each river they concluded that fine fractions resulted in appreciable viscous attenuation — it was greater in the Danube than in Parana, this was possible to observe due to application of a particle size distribution method.

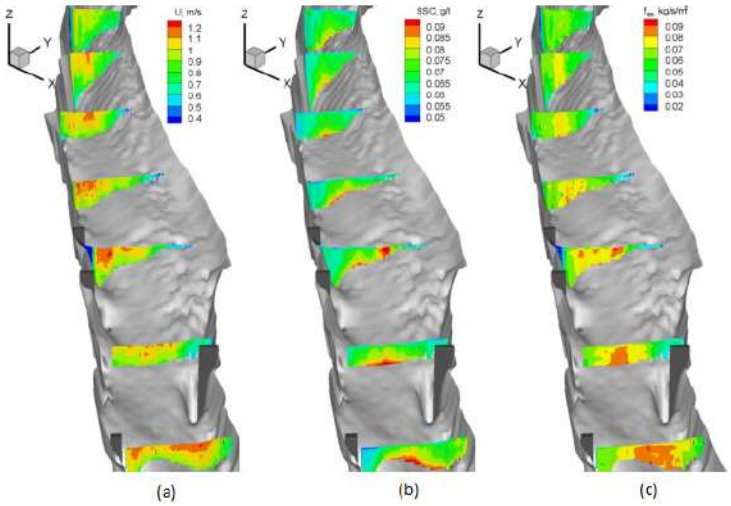

Figure 15 – Spatial distribution of a) flow velocity, b) SSC and c) Suspended Load. Adapted from: Baranya and Józsa (2013).

As a result of the operationalization efforts, for side-looking ADCPs, in 2016 USGS has published a manual of Techniques and Methods to guide the interested user through the process of establishing a station, collecting the data and developing the surrogate relation. In addition to this publication, researches from USGS are working on a proposal that aims to standardize the applied methodology and the obtained information (LANDERS et al., 2016).

Considering the aforementioned efforts on the operationalization of the use of the ADCP in the past years some specialists proposed two similar software to obtain SS information from down-looking ADCP and several point sampling within the cross-section: The STA software, proposed by Wood et al. (2019) and the ASET software proposed by Ruben et al. (2020). Both software are prepared to calibrate the RD Instrument ADCP, only.

All those already cited studies (and potential calibration software) have in common the application in river systems. There are not so many measurements and studies applied to a lentic environment (with low flow velocities) (HAUN; LIZANO, 2018). Some of the applications to these systems are related to density current formation (HAUN; LIZANO, 2016; UMEDA; YOKOYAMA; ISHIKAWA, 2006) or study of benthonic colonies (WOOD; GARTNER, 2010).

The next Section will present some of the studies that intend to apply a similar method proposed in this research to estimate solids concentration and density currents in a lentic environment.

3.2 Surrogate technologies applied to a lentic environment

The most recent application of surrogate technology to SS estimative in a reservoir was done by Haun and Lizano (2018) at Peñas Blancas reservoir in Costa Rica. They combined ADCP and LISST-SL[2] measurements in order to study the concentration of suspended solids all over the reservoir by establishing cross-sections over the lake.

With ADCP correlation and analysis they observed that the SS decreased during the campaign along the reservoir. According to the authors, the differences in the SS were not identified by conventional measurements that stated the same range of variation between the transects.

Besides the SS analysis along the reservoir, the authors aimed to evaluate the uncertainties related to the extrapolation of the ADCP signal near the bed and in the blanking zone using LISST-SL measurements for validation. They evaluated the differences on the SS when the extrapolations were not taken into account and found out that the differences increased as the depth increased, with values ranging from 0.6% up to 19.4% of difference (from the shallower to the deepest cross-section, in a reservoir).

Another application in a reservoir environment was done by Haun and Lizano (2016) when during a measurement campaign at Peñas Blancas reservoir they recognized a density current formation detected by the ADCP and decided to track it by doing longitudinal transects along the reservoir (Figure 16). The density current formation was confirmed by LISST-SL measurements that identified small differences in SS and granulometry.

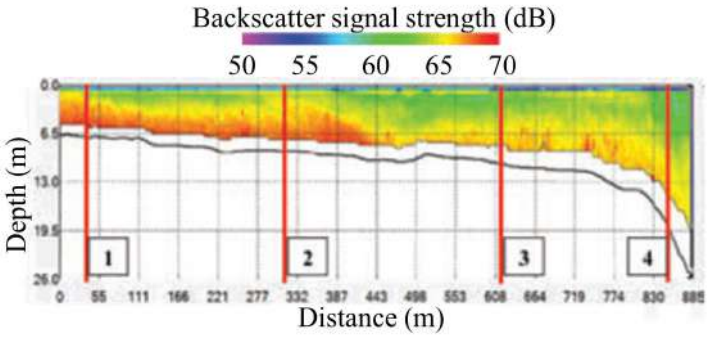

Figure 16 – Density current formation recognized by Haun and Lizano (2016) at Peñas Blancas reservoir, in Costa Rica.

Adapted from: Haun and Lizano (2016).

Umeda, Yokoyama and Ishikawa (2006) published a study that combined ADCP velocity measurement techniques to a reservoir longitudinal transect with turbidity and

[2] stream-line alined optical device from Sequoias Instrument Inc.

water quality parameters supported by echosounder measurements and numerical modeling (Figure 17). In their study, they obtained the density current field velocity in the water flow measurements at Shichikashuku reservoir, in Japan. From the field measurement validation for the numerical modeling simulation, they concluded that standard simulations models are capable of reproducing sedimentation phenomena considering only a few parameters.

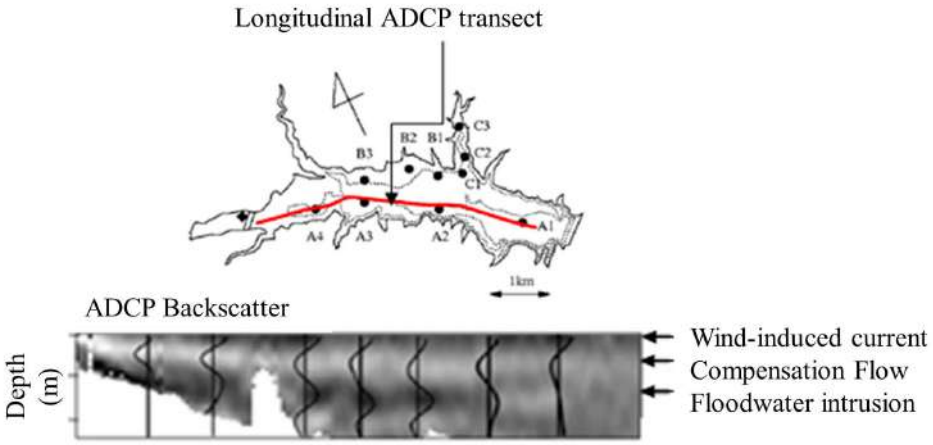

Figure 17 – Density current formation measured by Umeda, Yokoyama and Ishikawa (2006) by echosounder and ADCP measurements at Shichikashuku reservoir, in Japan.

Adapted from: Umeda, Yokoyama and Ishikawa (2006).

These three aforementioned studies were the only ones that used surrogate technologies to observe the development of a solid plume in lentic environments. Although the studies aimed to evaluate the density current velocity and visualize it through supersonic images and SS evaluations the studies did not report the ADCP correction and SS correlation applied to the density current evaluation.

3.3 Summary of the combined surrogate technologies

This section presents a summary (see Table 3) of the most recent studies to be considered in the application of the methods for rivers and lakes/reservoirs. As already mentioned, most of the studies were conducted mainly in rivers under standard conditions (significant flow velocities, SS concentration and granulometry).

Table 3 – Most recent studies regarding surrogate technologies application for SS and density currents determination.

Author(s)	Applycation Area	Main Driven Forces	Main Objective of the study
Gartner (2004)	Estuary - San Francisco Bay	Tides, Inlet rivers	ADCP x SSC correlation and comparison of estimated SSC from ADCP with OBS estimative.
Umeda, Yokoyama and Ishikawa (2006)	Reservoir - Shichikashuku	Inlet flows, Temperature, Wind, Atmospheric Pressure	The Study of washload sedimentation at Shichikashuku reservoir in Japan
Guerrero, Szupiany and Amsler (2011)	River - Parana River	River Flow	Used a two-frequency method to study SSC and grain size distribution.
Guerrero, Rüther and Szupiany (2012)	Laboratory Analysis	Laboratoy Controlled Discharge	Following the previous studies conducted by Guerrero, Szupiany and Amsler (2011), the authors carried out laboratory tests with the two frequencies method for grain size assesment using two ADCPs.
Baranya and Józsa (2013)	River - Danube River	River Flow	The authors studied the ADCP x SSC correlation and quantified the lack of information related to the non-measured areas from ADCP.
Guerrero et al. (2016)	Rivers - Parana and Danube	River flow	studied the acoustic properties of suspended solid and the consequences of the applicability of the ADCP correction methods
Haun and Lizano (2016)	Reservoir - Peñas Blancas	Inlet rivers, Temperature, Wind, Atmospheric Pressure	Track a density current formation during a flood event a Peñas Blancas Reservoir.
Haun and Lizano (2018)	Reservoir - Peñas Blancas	Inlet rivers, Temperature, Wind, Atmospheric Pressure	Study of suspended load within a tropical reservoir, by a week monitoring campaign in the rainy season stablishing cross-sections along the reservoir and observing the solid mass concentration decreasing along of it.

3.4 Summary

This Chapter has shown a summary of the most recent publications that based the presented research and its hypothesis and objectives.

Within the presented background around the surrogate technologies issues, specifically about the use of acoustics to estimate solid concentration, it has been clear that most of the researches were conducted mainly in lotic places with the presence of coarser

and non-cohesive solid content.

On the other hand, very few studies were conducted in order to study and support decisions making in lentic environments with the significative presence of finer solids and low flow velocities, such as reservoirs.

In order to accomplish the objectives presented in Chapter 1, the next chapter will present the methodology applied in this research to obtain SS information in lotic and lentic environments.

4 Materials and Methods

As presented in Chapter 3, most of the methods presented in literature are very well developed for lotic environments, with mostly non-cohesive particles. Therefore, the main idea will be first to understand and apply the methods at to these environments (to show the method domain) and then apply it to a lentic environment, with lower velocities and high cohesive particle content.

As summarized in the Figure 18, the general idea will be first to apply the methodology to a lotic environment, in a river (**step 1**) with high flow and high solid discharge — Taquari River, in order to test and understand the equipment and the correlations. Then the methodology will be applied to another lotic environment, at Passauna River considered a transitional area, with a lower discharge and different solid dynamics and characteristics, close to the lentic zone.

After that, in **step 2** the same methodology will be applied at Passauna Reservoir, a lentic environment, in order to estimate the TSS and visualize the TSS distribution over the depth and further (in the **step 3**), to analyze the density current inlet in a reservoir.

During the steps 1 and 2 will be tested the methods: *I-Field Measurements and Sampling*, *II-Data Processing and Laboratory Analysis* and *ADCP* x *SS Correlation*. Then, after the correlation establishment, at step 3: *the density current exploration* will be analyzed.

The proposed study is based on results produced within the SeWaMa Project (Innovative approaches for future solid and water management in Brazil) within the NoPa call (funded by CAPES and DAAD, 2015 - 2018) and the MUDAK project (Multidisciplinary data acquisition as the key for a globally applicable water resource management - http://www.mudak-wrm.kit.edu/) both are a consortium between Germany and Brazil, integrating Universities, municipal sanitation company and companies from the private sector. The projects involve researchers from different areas studying sedimentation in reservoirs, water quality aspects, land use and GHG production and emission in a water supply reservoir.

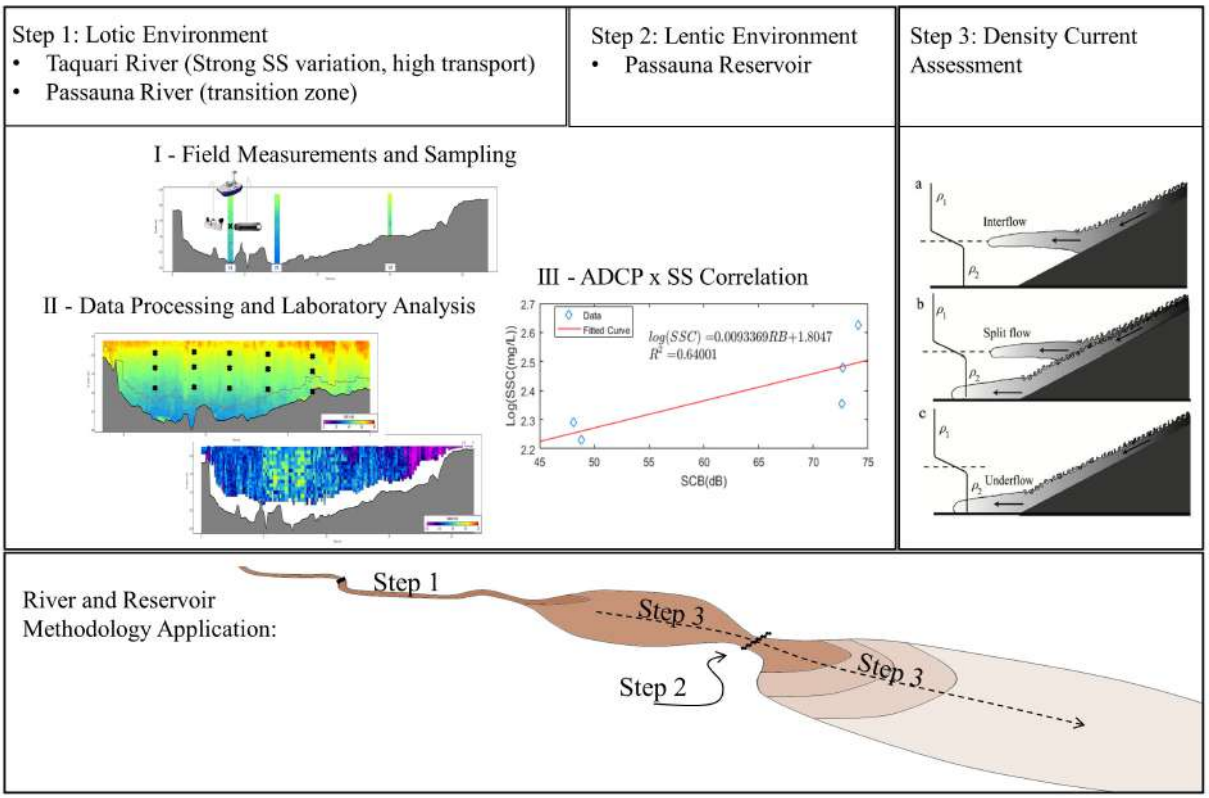

Figure 18 – Summary of the proposed methodology to be presented in the following sections.

4.1 Site Description

4.1.1 Lotic Environments: Taquari River and Passauna River

At this section will be given a short description of the lotic environments used to test the method for ADCP and suspended solid correlation. These two rivers were chosen because of their characteristics and their relation with the methods used in this research.

By its characteristics, Taquari River might be approximated as standard conditions for ADCP correlation found in the literature (discharge, granulometry, SS, etc.).

Passauna River presents different situation patterns (discharge, granulometry, SS, etc.) from those normally studied for ADCP correlation and will work as a transition environment (from lotic to lentic environment) in the application of the proposed method.

4.1.1.1 Taquari River

Taquari River is an important river from Paraguay Basin. It is located in the Pantanal Biome, the largest freshwater wetland system in the world, with a high diversity of flora and fauna. It is the main river from the Taquari Basin and one of the biggest tributaries of the Paraguay River Basin. The river is commonly known for its intense solid dynamics with high erosion and transport capacities.

Figure 19 shows the cross-section in the Taquari River before its confluence with Coxim River, at Coxim city, in a place where the streamlines can be consider aligned and the flux permanent and uniform. The cross-section has about 100 m width and between 3 m to 4 m deep, in the deepest part of the channel.

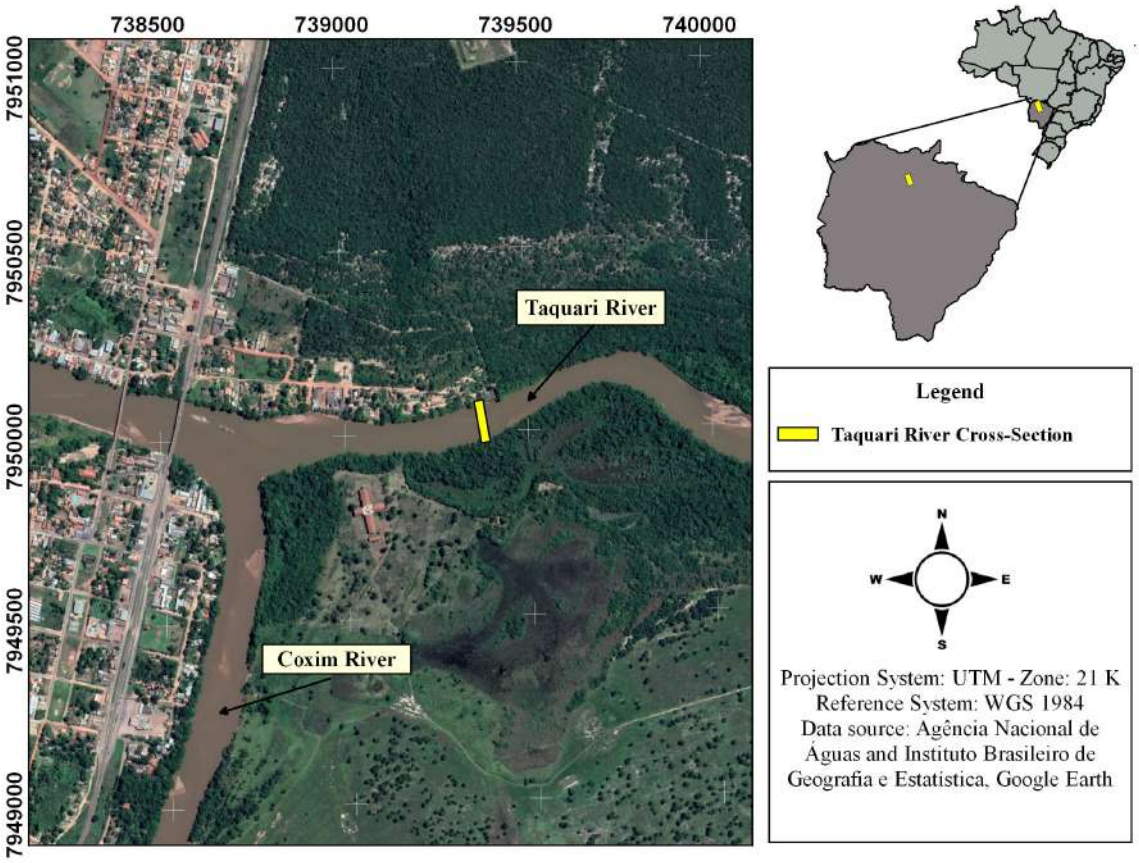

Figure 19 – Taquari River Location and the Monitored Cross-section.

After: Wosiacki et al. (2018).

According to Brazilian Water Institution (ANA - Agência Nacional de Águas - Coxim Station, Code: 1854004) data set, the discharge vary from about $300m^3/s$ up to $500m^3/s$ and the precipitation vary from about $25mm$ to up to $200mm$ in the dry and rainy season, respectively (total precipitation of $1200mm/yr$, in average) — Figure 20.

For this study it was done a total of 7 field campaigns in cooperation with UFMS[1] team. The campaigns happened between March of 2017 and January of 2018, when measurements were taken with the ADCP and water sampling to obtain SSC. The used devices and tools were: (a) ADP-M9 from Sontek-Xylem®, Figure 26, and (b) USD-49 Water Sampler, Figure 28a, which is a hand-line suspended solid sampler with about 27.5

[1] Federal University of Mato Grosso do Sul - HEroS: Hydrology, Erosion and Sedimentation Lab - https://heros.ufms.br

kg used to obtain integrated measurement from the water column — more details about the devices will be discussed thoroughly in the following sections.

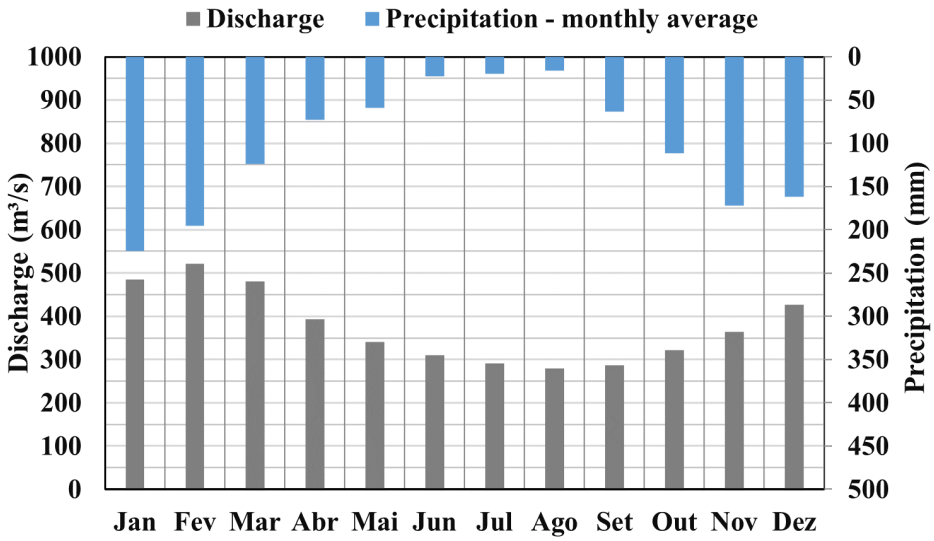

Figure 20 – Mean Precipitation and Discharge at Taquari River at Coxim Station (Code:1854004).

Source: ANA (2019).

To measure, the ADCP was setup for a Smart Pulse frequency mode, where the frequency is automatically chosen by the device based on the depth[2]. First were taken measurements along of the cross-section, to obtain the discharge. Since Taquari River has a strong bedload, was also taken a total of 6 static verticals, in every campaign, to correct the obtained velocities and avoid discharge's super-estimation when using the bottom track positioning. The 6 verticals were chosen based on the results of the Hidrossedimentos 3.1 tool, developed by Agricultural and Rural Extension Research Company from Santa Catarina State (EPAGRI -SC). Based on that the cross-section was divided according to the Equal Discharge Increment (EDI).

The water sampling was taken right after the static ADCP measurements, in the same verticals, to obtain a correlation between the received signal from ADCP and the SSC. For the 7 campaigns, all the 6 depth-integrated samples (400 mL per sample), were mixed to obtain one representative sample for the entire cross-section.

After each field campaign the samples were processed to analyze the granulometry and solid concentration. In a general way, the procedure was based on sieving of the largest grains (sand) according to the American Geophysical Union classification (LANE, 1947), considering a sieve granulometry as: 2.0, 1.0, 0.5, 0.25, 0.125 and 0.0063mm.

For the finest grains (silt and clay) the adopted procedure followed Carvalho

[2] Later on was adopted a single-frequency measurements, only applied for Passauna River and Passauna Reservoir — see next Section.

(2008), where the method is determined by solid concentration: if it is between 300 and 10000 (mg/L), the particle selection is done by a gravitational method where the fractions are divided according its sedimentation at a specific time (settling tube); if the concentration is between 3000 and 10000 (mg/L) it is used the pipetting method (CARVALHO, 2008). More details regarding laboratory analysis for the integrated samples can be obtained at Suekame (2020).

4.1.1.2 Passauna River

Passauna River is the main river of Passauna basin. It is located on the border of the cities of Araucaria, Campo Largo and Curitiba, in Parana State, Brazil (Figure 21). The monitoring cross-section is located at the bridge of BR277 highway and has about 15 m width and 1.5 m deep, in the deepst part of the channel.

At this location, were conducted a total of 5 field campaigns (from February of 2017 to Octobe of 2018), where 2 campaigns happened in October/2018 (Oct, 18th and Oct,20th)during an extreme event monitoring. At this situation was possible to obtain the highest flow velocities and TSS from the entire data set already monitored for this study.

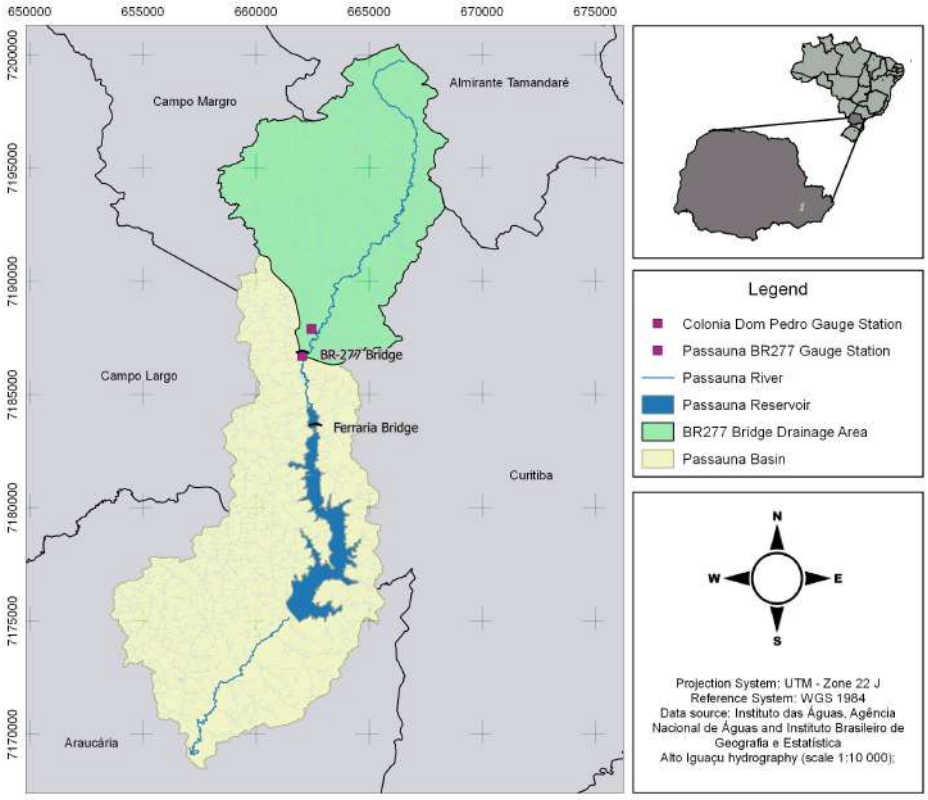

Figure 21 – Passauna Basin Location.

Also, at this cross-section is located one gauge station from ANA (BR-277 Campo

Largo Station, code: 65021800[3]). Additionaly there is another monitoring station from ANA located about 2.0 *km* of the BR277 bridge with precipitation data available (Colônia Dom Pedro Station, code: 65021770[4]).

The watershed is located in a climate region classified as *Cfb*[5] (Köppen-Geiger classification), with a few extremes of temperature and ample precipitation in all months. Figure 22 summarizes the mean precipitation and discharge throughout the year. It is possible to observe that mean precipitation varies from a minimum of about 74.63 *mm* in August to a maximum of 189.19 *mm* in January with a total annual precipitation about 1500 *mm* to 1600 *mm*.

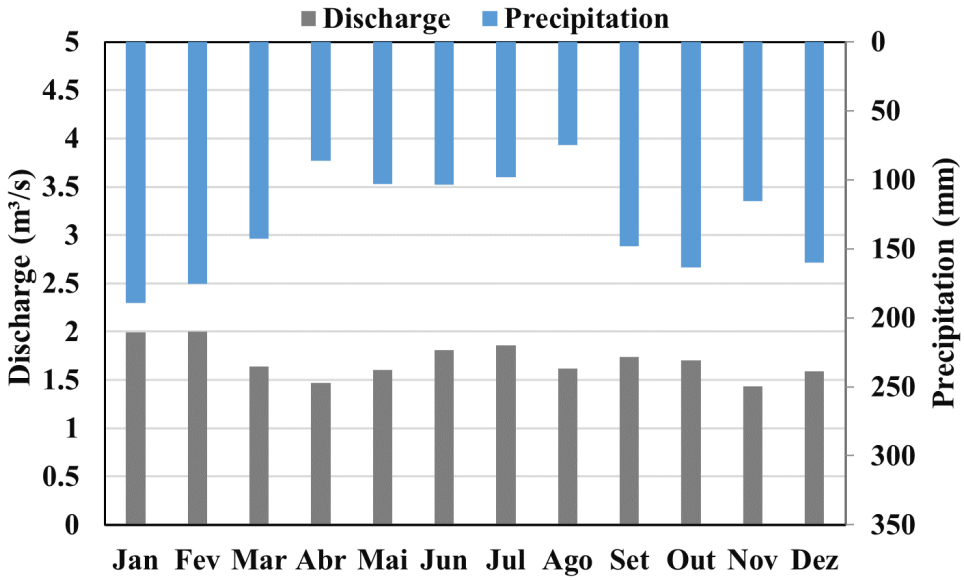

Figure 22 – Mean Precipitation and Discharge at Passauna River at Colonia Dom Pedro Station (Precipitation Data) and BR-277-Campo Largo Station (Discharge Data).

Source: SIH (2019).

The field procedures followed the same methods applied at Taquari River: first were taken measurements with ADCP (cross-section and static measurements) followed by water sampling. Different from Taquari River proceedures, here were made point sampling using the Van Dorne bottle. The granulometry data was measured *in-situ* with the LISST and to obtain temperature and sound velocity information it was used a CTD (also from Sontek-Xylem, to made the previously ADCP signal corrections).

Not all the measurements made with the LISST could be used due to technical problems related to *(a)* operational questions (the team was learning how to use the device), and then *(b)* related to the post-processing analysis (the comparison between two

[3] Sistema de Informações Hidrológicas (SIH) data base
[4] Sistema de Informações Hidrológicas (SIH) data base
[5] Marine West Coast Climate

versions of the same device presented different measurement results for TSS — LISST-100x and LISST-200x).

After each field campaign the water samples were analyzed in the laboratory in order to obtain the TSS — more details about the devices will be discussed thoroughly in the sequence.

4.1.2 Lentic Environment: Passauna Reservoir

Passauna Reservoir is located in the Passauna River basin (see Figure 21). The reservoir was full in the end of $'80s$ and according to Sanepar (2013), it produces a flow rate supply of 1800 L/s which corresponds roughly to 20% of all integrated supply system from Curitiba and its metropolitan area. It has a surface area around 11 km^2 and a volume of 71.6 hm^3.

This reservoir has a peculiarity related to its transitional area which differs from most of reservoirs. As showed in Figure 23, in the upstream – distant about 2 km from the entrance, the Passauna River loses the characteristic of a well fitted river and starts to flow in meanders. Depending on the period this meanders can be flooded (in rainy days) or not (in dry days) resulting in a *natural wetland* until reach the *forebay*.

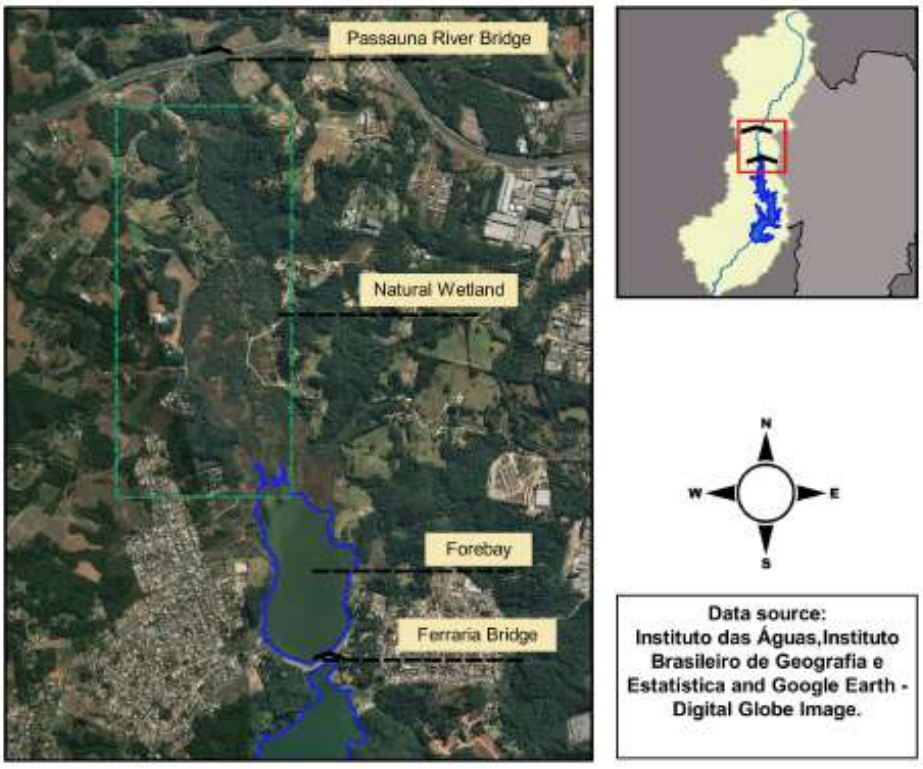

Figure 23 – Study Area.

At this location the main idea will be to apply the already tested methods (at Taquari and Passauna Rivers) at Ferraria Bridge and extrapolate it to longitudinal tran-

sects (from upstream to downstream) with ADCP, to evaluate the density current formations.

The study area will be concentrated in the upper part of the reservoir and it will include a region immediately downstream of the forebay, where some variations in the suspended plume were visually identified — Figure 24.

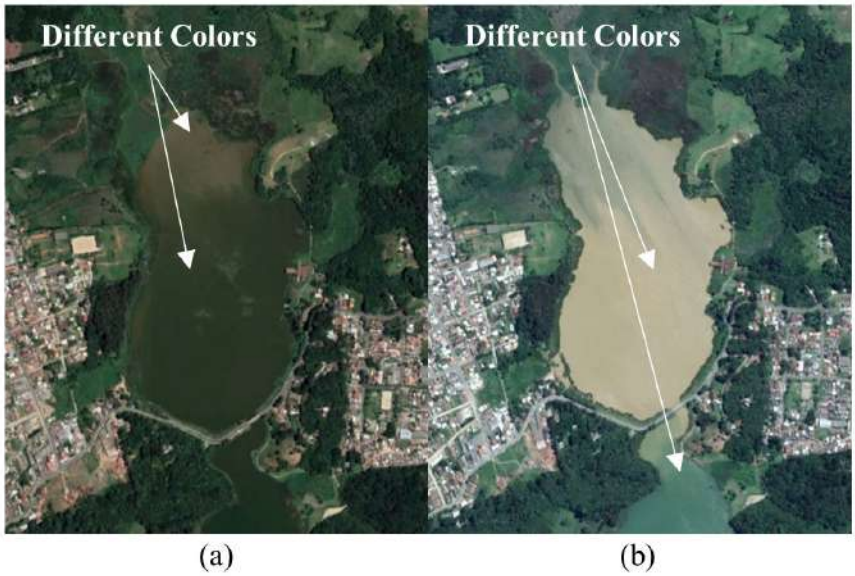

Figure 24 – Comparison of the water color in the study area among different days: (a)March 5th, 2019 and (b) January 21th, 2018

In terms of solid content, in the Passauna Reservoir Bocalon (2007) found a significative content of silt and clay fraction ($< 75\mu m$), around 63% during the raining season and around 53%, during the dry season for Ferraria Bridge. Pitrat (2010) found values around 80% to 90% for silt and clay during the dry and rainy seasons at Ferraria Bridge.

Sotiri, Hilgert and Fuchs (2019), analyzing bottom solids, has found that in more than 95% of the solid material the granulometry is lower than $63\mu m$ and assotiated bulk-wet density values ranging from $1.2g/cm^3$ up to $1.6g/cm^3$ in the bottom solid at Ferraria Bridge. They also find that the bottom solid content is mostly sand fraction, followed by silt-clay fraction, while the forebay is overwhelmingly composed by clay-silt fraction. The analysis done by these authors consisted in the laboratory sieving analysis for granulometry content estimative.

For this research, a total of 7 campaigns was conducted at Ferraria Bridge, from August of 2017 to February of 2019. As for Passauna River, two campaigns happened during an extreme rainy event, which were the campaigns that happened in October, 18th and 20th of 2018.

In all presented field campaigns were made point measurements at Ferraria's Bridge with ADCP, CTD and Water Sampling. The LISST measurements started from

August of 2018, with the aquisition of the LISST-200x by Federal University of Parana.

The measurement proceedures follow the measurements done in Taquari and Passauna River, with ADCP static measurements conducted in 3 verticals in the Ferraria Bridge cross-section, followed by point water sampling (with the Van Dorne bottle) and LISST measurements (Figure 25).

At 3 campaigns were made longitudinal transects, from upstream to downstream, in the reservoir using the ADCP, as shown Figure 25.

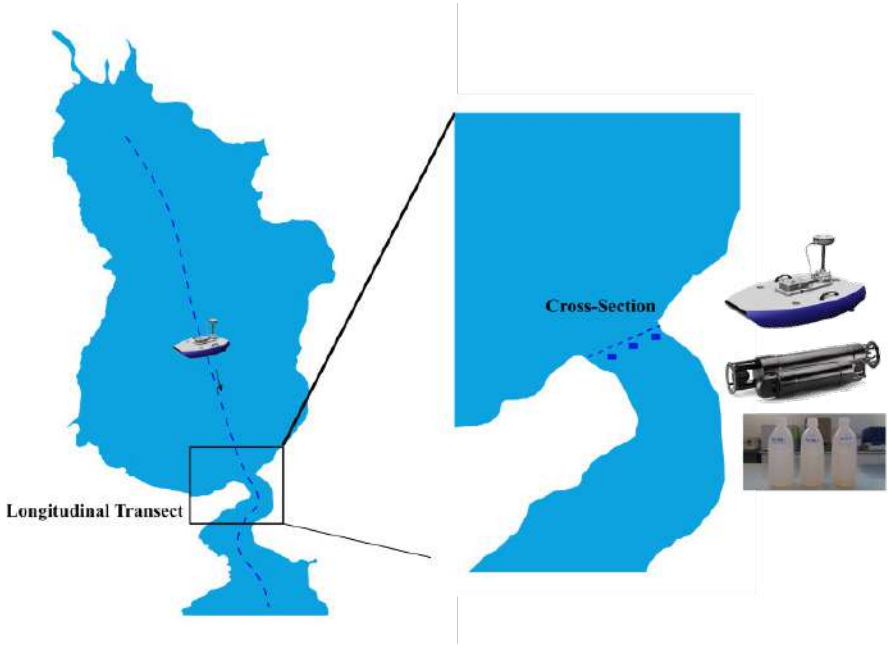

Figure 25 – Longitudinal Transect and Cross-section sketch at Passauna Reservoir.

The field procedures presented at this section were done to accomplish the **steps 2** and **3** from Figure 4.

4.2 Instrumentation and field procedures

As already mentioned, to obtain the data needed were used the ADP-M9 and the CTD instruments (from *Sontek/Xylem,Inc*) and the LISST-200x (from *Sequoia Scientific, Inc.*). For water sampling in the reservoir was used the Van Dorne bottle and a USD-49 sampler, from USGS[6] for water sampling at Taquari River. After the field measurements and water sampling, all the samples were taken to laboratory analysis for SS determination.

The ADP-M9 application is the one used to developed the whole technique presented in this study. On the other hand the LISST and the CTD devices, as well the sampling bottles, were used just as a tool to obtain the parameters for the application of the correlation methodology.

[6] United States Geological Survey

In the following will be described all cited equipments.

4.2.1 Acoustic Doppler Current Profiler (ADCP) — ADP-M9

The ADP-M9 is a multibeam acoustic probe composed of 9 beams: 2 sets with 4 transducer, operating at 1 MHz and 3 MHz, and 1 vertical transducer used to obtain the depth, operating at 0.5 MHz. The ADP-M9 has a profiling range distance from 0.06 m of up to 40 m and a profiling range velocity about ± 20 m/s, $\pm 25\%$ and a vertical resolution of 128 cells, from 0.02 m to 4 m size — Sontek (2016).

Usually, the user can choose the operating frequency mode, if Fixed Frequency Mode (FFM): 1 MHz or 3 MHz or SmartPulse Mode (SPM). The SPM is the most indicated to obtain discharge measurements because the device will automatically change to the appropriate frequency for the local depth. The FFM is only indicated if the user already knows the local conditions to set the device properly, for discharge measurements[7].

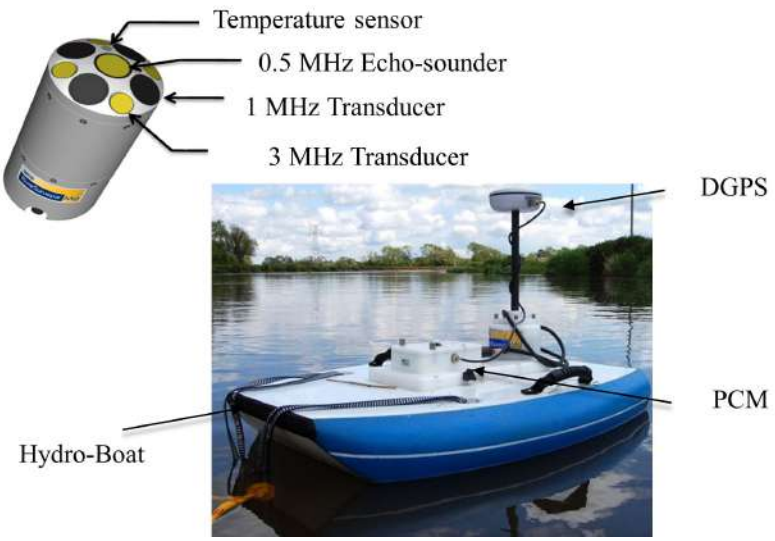

Figure 26 – ADP-M9 features. Adapted from: Sontek (2016).

As presented in Figure 26, it is also composed of an internal compass and a differential GPS (DGPS) used to rise the GPS precision and a PCM (Power and Communication Module), which provides power to the ADCP using a rechargeable battery pack.

The ADCP device was used in two different ways: *(a)* continuum measurement along the cross-section to obtain the discharge estimation and *(b)* static measurements along the cross-section.

At this study most of the measurements were taken considering a FFM of 3 MHz, the only exception was at Taquari River were all of the measurements (the static ones and the cross-sections) were done with the SPM – in this case, the post-processing methods

[7] Although to build the correlation CBSxSS is necessary a single frequency mode.

involved the application of a *filter*[8] to make possible the backscatter correction. This *filter* is responsible to select only the cells measured with 3 MHz frequency.

At Passauna River if the purpose was to obtain the ADCP signal for SSC correlation the measurements were done with FFM, if the purpose were to obtain the flow discharge the measurements were done with the SPM.

In the reservoir, it was identified that the crossing method with the ADCP along a cross-section would not be possible for discharge estimation, because even in a narrower section as at Ferraria Bridge, the flow velocity is too low.

4.2.2 Laser In-Situ Scattering Transmissiometer - LISST

In this study, the first intention was to use two LISSTs devices to do the SS and granulometry analysis: one called LISST-100x[9] in cooperation with Koblenz-Landau University and another one called LISST-200x recently acquired by Federal University of Parana.

However, different from what was expected, both equipment presented differences in measurements made at the same place. The manufacturer was sought to provide clarification and during its analysis, it was found a misalignment in the LISST-100x bin the LISST-200x had all components working fine. Because of it, specifically for this study, the LISST-100x measurements were discarded and only the LISST-200x were considered.

Furthermore, it was also noticed that these equipment weren't appropriated to obtain SS measurements. So, it was decided in this study to use it as a tool only to obtain granulometry information — specifically the D50 which is required to apply the proposed methodology.

The determining factor for this decision was that the LISST measures the SSC in volumetric units. Most of the applied formulation need it on massic units. In one way or another, a conversion factor (solid density) must be determined. Although there is an effort to create a calibration curve to obtain this conversion factor, which due the solid characteristics is not the common used in the literature (2.65 g/L), this is not part of this study. So far, the TSS will be determined only by laboratory analysis which is a well known and consolidated technique.

To make the measurements, the LISST was released in the same depth where the water was sampled for laboratory analysis, at Ferraria's Bridge and Passauna River Bridge. The measurements were done by leaving the equipment stand for some minutes (between 2 - 4 minutes) at each depth, in order to stabilize the sensors and the temperature.

[8] the filtering process consists basically on the replacement of the 1MHz cells by the average of the 3 MHz cells — this step will be deeply discussed later on.

[9] LISST-100x Type C

Figure 27 – LISST-200x with the battery attached.

During operation, the output from the diffracted laser beam, optical transmission, pressure sensor and water temperature are recorded as raw data and can be downloaded and processed later on for granulometry and total volume concentration (SEQUOIA, 2018).

After the field measurements, the data must be post-processed in Matlab script in order to obtain all the data provided to build the granulometric curve.

4.2.3 Water Sampling Instruments and Laboratory Analysis

The water sampling was done considering two methods depending on the site: at Taquari River the samples were taken with USD-49 sampler (Figure 28a), which is a medium-weight hand-line suspended-solid sampler used to collected integrated water samples. The sampler can be lowered and raised, hand over hand, with a flexible suspension line. As previously cited, the sampler cannot touch the bottom and it must be at least at 15 *cm* from the bottom, to guarantee that the sampling will be only of suspended solids.

At Passauna River and Reservoir, the sampling were taken with a Van Dorne Water Sampler (Figure 28b), which is a device used to collect instantaneous and discrete (point) samples. The device must be submerged until it reaches the desired depth and then the closure mechanism is activated by the user.

Figure 28 – Water Sampler Devices (a) USD-49 and (b) Van Dorne.

After each field campaign, the samples were taken to the laboratory to be analyzed. All the laboratory procedures related to the SSC were based on the gravimetric method, which is based on the weight difference. During the process, it is measured the difference between wet and dry weight related to a certain sampling volume considered for each analysis.

For the Taquari River, due to the high amount of suspended solids the concentration was obtained by the visual accumulation tube method which is first used for granulometry information and then through the weight and previous volume determination it is possible to obtain the SSC. All the laboratory procedures and analysis for the Taquari River were done in cooperation with the Federal University of Mato Grosso do Sul (UFMS) and is described in more details by Suekame (2020) that followed the methods described at Carvalho et al. (2000b). In a general way, the determination of SSC and granulometry at Taquari River is a simple task, since all the laboratory procedures are carefully taken, the number of solids generally provides good results.

The laboratory analysis and procedures for Passauna River and Reservoir were closely followed by the author and due to some particularities it demanded more careful and adaptation methods application in the lab.

The analysis followed the majority of the procedures indicated by APHA (1999) — see Chapter 2. Although the whole solid series was determined, for the proposed analysis only the Total Suspended Solid (TSS) fraction was considered.

For each sampling point, the samples were analyzed at least 3 times, where were considered a minimum of 1 liter per analysis. Considering the low concentrations presented in the reservoir and even in the Passauna River, usually, the samples were collected in 5 liters bottles and the triplicated were well homogenized and partitioned in 1 liter beaker each and then filtered, dried and weighed.

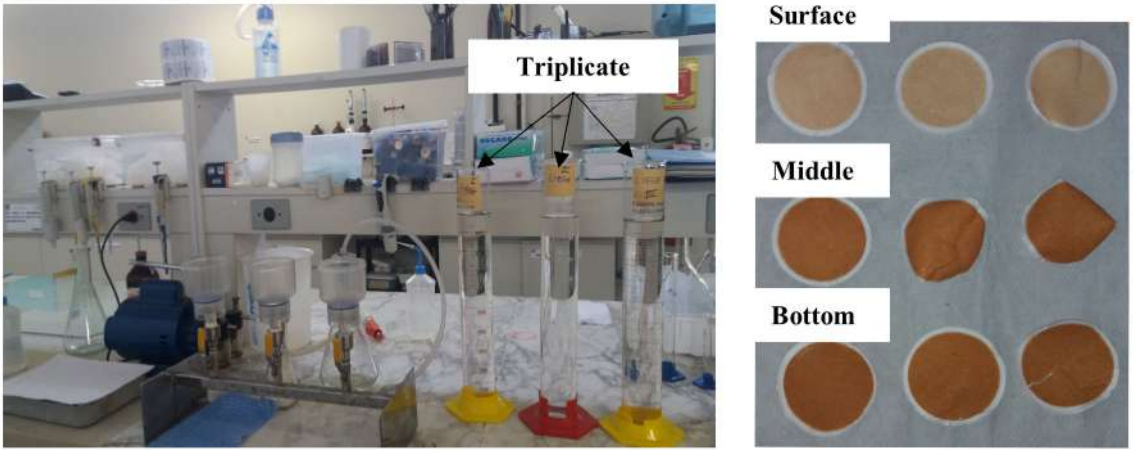

Figure 29 – Filtration System and Filters after analysis at Vertical 3 at Ferraria's Bridge from the 4th campaign (04/23/2018).

4.3 Data Processing

Most of data processing and analysis was done considering MATLAB and Excel algorithms. In a general way, the sensors already have an option to export their measured data as a MATLAB or ASCII format:

- The ADP-M9 provides the Sontek RyverSurveyor, a software designed to measure river discharge and depth from a moving or stationary vessel. The software can be used to observe the real-time measurement and also to post-processing analysis of discharge and flow velocities. However, it is not able to make the solid-ADCP corrections, so it is necessary to export the data in "ASCII format" or "*mat" extension to post-processing the variables.
- The LISST comes with the SOP software (Standard Operating Procedure functionality of the program) used to visualize and export the data in ***.RBN** extension that can be easy read by the Matlab routines supplied by the manufacturer: *getscat_L200X.m* and *invert_L200X.p* functions[10].

Regarding the ADCP, the backscatter processing algorithm had to follow two different processing ways due to the adopted setup measurement procedures, for Taquari and Passauna catchment.

[10] the functions are availabe at the 'Software and Downloads' tab on the LISST-200X webpage: http://www.sequoiasci.com/product/lisst-200x/. Noticed that when the function was used for the first time there was a problem in the algorithm that was easly solved by contacting the manufacturer: The variable returned by the function which contains **cscat** is actually named **RBNdata.cscat**, so instead *invert_L200X(**Cscat**,Random,Sharpen,ShowProgressBar)* used it as *invert_L200X(**RBNdata.cscat**,Random,Sharpen,ShowProgressBar)*

At Taquari River the measurements with ADCP were done with the SPM, also the static one used for SSC correlation. As already mentioned, the sampling procedures were different for this system. So, although the model application was the same, some particularities in the data treatment and processing were different.

At Passauna Catchment, the measurements with ADCP were done considering the FFM, and the sampling and laboratory analysis were also different from those one applied at Taquari River.

Table 4 summarizes the obtained parameters for each tool.

Table 4 – Summary of the instrumentation and related measured parameters in each Study Area.

Intrument/Tool	Parameter	Study Site Application
ADP-M9	Flow discharge (Q)	Taquari and Passauna River
	SS correlation	Taquari and Passauna River and Passauna Reservoir
	Temperature at the Surface	Taquari and Passauna River and Passauna Reservoir
LISST-200X	D50	Passauna River and Passauna Reservoir
CTD	Temperature and Sound Velocity Profiles	Passauna River and Passauna Reservoir
Laboratory Analysis	APHA (1999) procedures for SS	Passauna River and Passauna Reservoir
	Carvalho (2008) procedures for SS	Taquari River
	Carvalho (2008) procedures for D50	Taquari River

4.3.1 Backscatter Correction — dB2SS code

An algorithm created by the author called **dB2SS**, was written to extract and correct the Signal to Noise Ratio (SNR) and correlate it with SS data, by using the Modified Sonar Equation (Equation 2.5) to make the corrections and reach the form of Equation 2.7 to obtain the correlation — all the models and formulations of this step are presented at Appendix A.

Below the aforementioned equations were repeated to help the reader:

$$CBS = SNR_{mean} + 20\log(\psi R) + 2\alpha_w R + 2\alpha_s R,$$
$$log(SS) = a.CBS + b,$$
$$SS = 10^{(a+b\cdot CBS)}$$

Summarized at Table 5 and Figure 30 are the algorithm steps used to obtain the *SS* x *CBS* correlation. It was applied 5 functions (written in Matlab Environment), each one with different purposes during the calculations: *Func_mergefiles*, *Func_mean_speed*, *Func_bs_correction*, *Func_rmvoutlier* and *Func_LSRFit*.

Table 5 – Backscatter correction functions descriptions.

Function name	Description/Processing	Result
$Func_mergefiles$	It is a "pre-postprocessing" function used to merge the solid information and the ADCP data file structure, in order to produce a single file to be read in the main program	Data file with ADCP and solid content
$Func_mean_speed$	It calculates the mean velocity, mean signal and the corrected depth of each correspondent ADCP cell based. This function uses the function *rmvoutlier*, applied at the ADCP 4 beams (SNR).	It returns the mean Speed, Mean SNR, Depth and the corrected position of the 1st calculated cell
$Func_rmvoutlier$	It removes the outliers considering the quantile method (Q1 and Q3 limits) from the 4 transducers	It returns a matrix without outliers
$Func_bs_correction$	It makes all backscatter correction considering the steps presented at Appendix A	It rreturns the CBS for each campaing and/or measured point in the water column
$Func_LSRFit$	It fits a regression line based on Least-Square Regression.	It returns the angular and linear coefficient from the fitted curve.

During the processing it was important to remember that for Taquari River and Passauna system the field procedures were differents (the sampling methods and ADCP setup). To analyze such differences and to adapt the algorithm correction to the Passauna case, some differences during the post-processing analysis had to be taken into account.

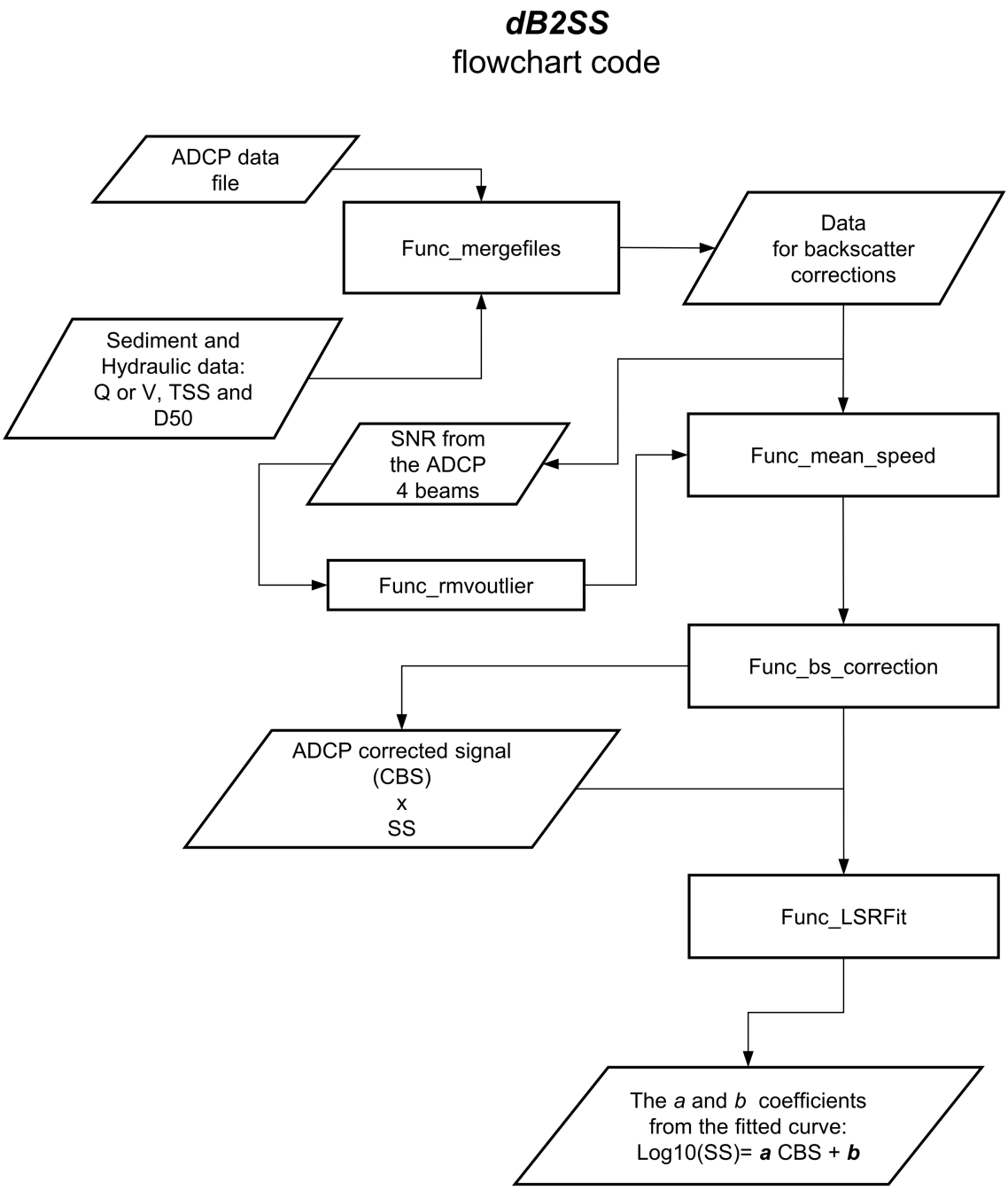

Figure 30 – Backscatter correction flowchart.

The main difference between the point and the integrated ADCP backscatter correction algorithm is that in the point analysis the backscatter correlation was done at the same depth where the water was sampled. So, the algorithm read the TSS at the corresponded depth and integrated the backscatter throughout the water until that depth.

In this way the water column is divided into the corresponding number of samples, eg. for Passauna Reservoir: the cross-section was divided into 3 verticals and were taken

3 water sampling points at each vertical. Then, in the algorithm, the water column is divided according to a given depth, and for each campaign (3 verticals, 3 measurement points at each vertical) the analysis will result in 9 pairs of TSS x CBS, as shown in Figure 31.

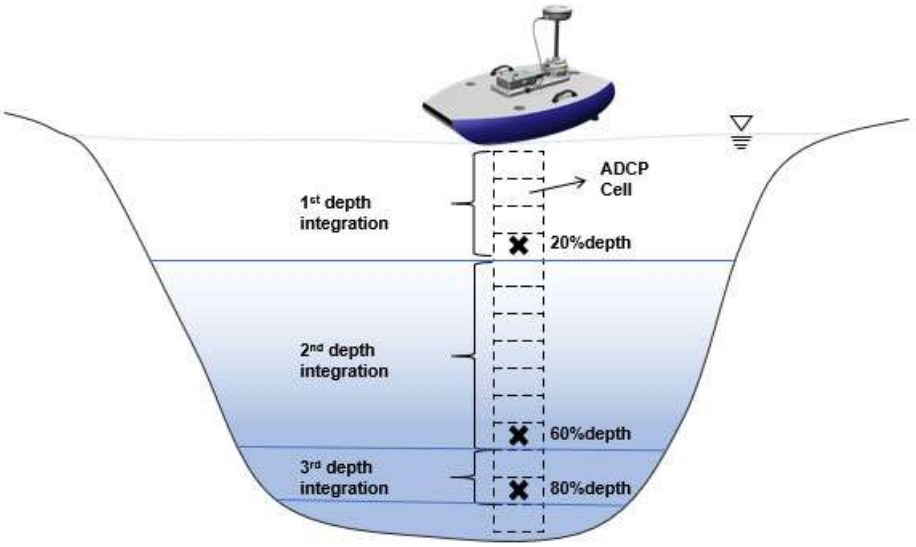

Figure 31 – Operational scheme used in the algorithm point sampling method analysis.

At the integrated analysis (Taquari River), the water sample was mixed and analyzed in a composed way and the correction was applied for the average of the SNR. Obtaining from this analysis only one pair of SSC x CBS at each campaign.

4.3.2 LISST data processing and analysis

The LISST analysis was based on the steps presented in Figure 32, which are described in detail in Appendix B.

As indicated by the manufacturer, considering a good device setup, calibration and field practice, it is possible to obtain the processed data through the application of the *getscat_L200X* and *invert_L200X* functions. However, during the post-processing analysis, it was noticed that would be necessary to apply a filter and a smooth method in order to avoid outlier influence.

Since the instrument can be affected by a range of factors intrinsic to the environment and the handling, it is necessary to consider some criteria and filtering to obtain better and reliable results. In this sense it is not uncommon to clear some data from the results if it is considered an outlier or if the measurement was done under suspicious circumstances – eg. too turbid or too clean water.

The first measurement criteria to be taken into account is the transmission power (T) data value, which is the proportion of light being transported in a turbid medium. With this mind, for a reliable data set obtaining, T should be between 0.1 and 0.995

(SEQUOIA, 2018) — the greater the T, the means that more light is passing through the medium, so the clear the water and the lower T value, the more turbid the water. In fact, the manufacturer advises being aware of the transmission data lower than 0.3 and greater than 0.98. Therefore, if the data is out of this range it should be discarded.

Additionally, the data were analyzed according to its average and all data out of the $1st$ and the $3rd$ quantile (25% and 75%, respectively) was not considered. Similar data treatment was adopted by EMMANUEL et al. (2018), considering only data between the $15th$ and $75th$ percentiles, this procedure was taken by them in order to avoid outlying data, mainly the positive spikes due to bubbles.

Another step was the addition of a move mean filter to all data, in order to smooth the data and avoid abrupt variations from one size to another, throughout the entire class analysis.

Besides the post-processing already mentioned, additionally, the *getscat_L200X* and *invert_L200X* functions are provided by the manufacturer and are used to obtain raw scattering data (scattering and transmission) from the binary device data file and to return the uncalibrated volume distribution in μL, respectively (SEQUOIASC, 2015).

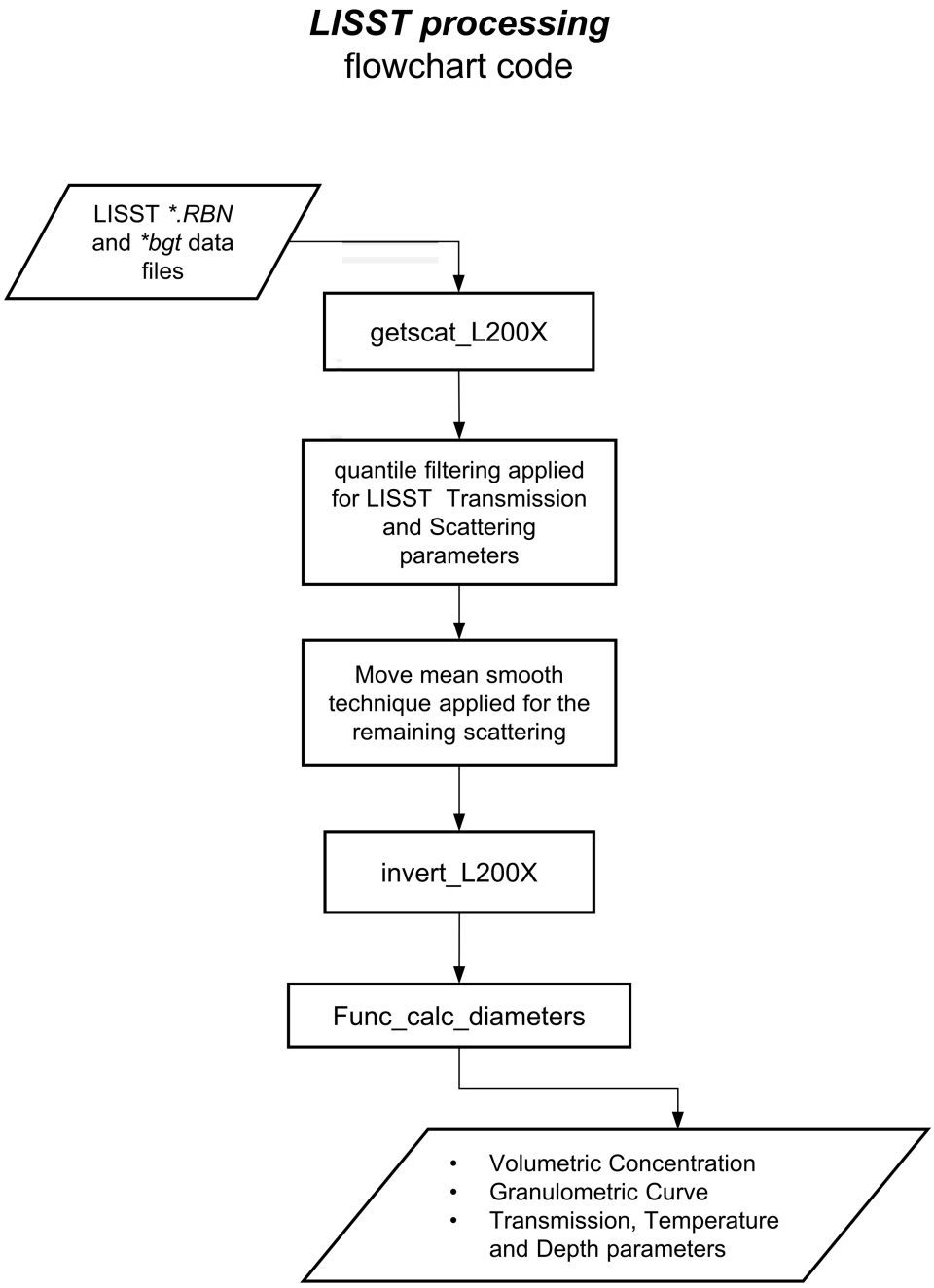

Figure 32 – LISST processing flowchart.

5 Results and Discussions

This section presents the results regarding the measurements done with the tools and steps presented in Chapter 4, for Taquari and Passauna Rivers and Passauna Reservoir. The data for Taquari River was produced by the Federal University of Mato Grosso do Sul (in Brazil) - Environmental Technologies Graduate Program and the data for Passauna system was obtained in the frame of NoPa and Mudak Project coordinated by a consortium between Federal University of Parana (in Brazil) and Karlsruhe Institute of Technology (in Germany).

The results are presented starting with the analysis of the measured parameters and the mapping of the raw data over the cross-section, as well as for some profiles. This is followed by the results for correcting the backscatter signal, and the correlation for SSC or TSS. In the end, the processed results for the profiles are mapped over the whole cross-section and longitudinal profiles (at Passauna reservoir, only).

5.1 Taquari River

5.1.1 Velocity, backscatter and SSC distribution

To obtain discharge and velocity measurements, the procedures during the field campaign and the post-processing analysis followed the guidelines indicated at Mueller (2013). Since the Taquari River has dynamic solid transport conditions, the procedures also included an evaluation of the presence of the moving bed, which indicated a possible error in the estimated velocity from 3% in July/17 up to 12% in March/17 (Table 6).

Table 6 – Mean parameters evaluated during the Moving bed analysis.

	Campaigns						
	Mar	Apr	May	Jun	Jul	Aug	Jan
Mean Moving-Bed velocity (m/s)	0.15	0.07	0.07	0.05	0.03	0.06	0.11
Mean Water Velocity (m/s)	1.27	1.00	1.00	0.95	0.91	0.96	0.99
Potential error	12%	7%	7%	5%	3%	6%	11%

The velocity profiles in all measurement campaigns are shown in Figure 33. To illustrate, it is also shown the horizontal velocities and backscatter signal (mean SNR) from May/17 and Jul/17, in a rainy and in a dry situation, respectively.

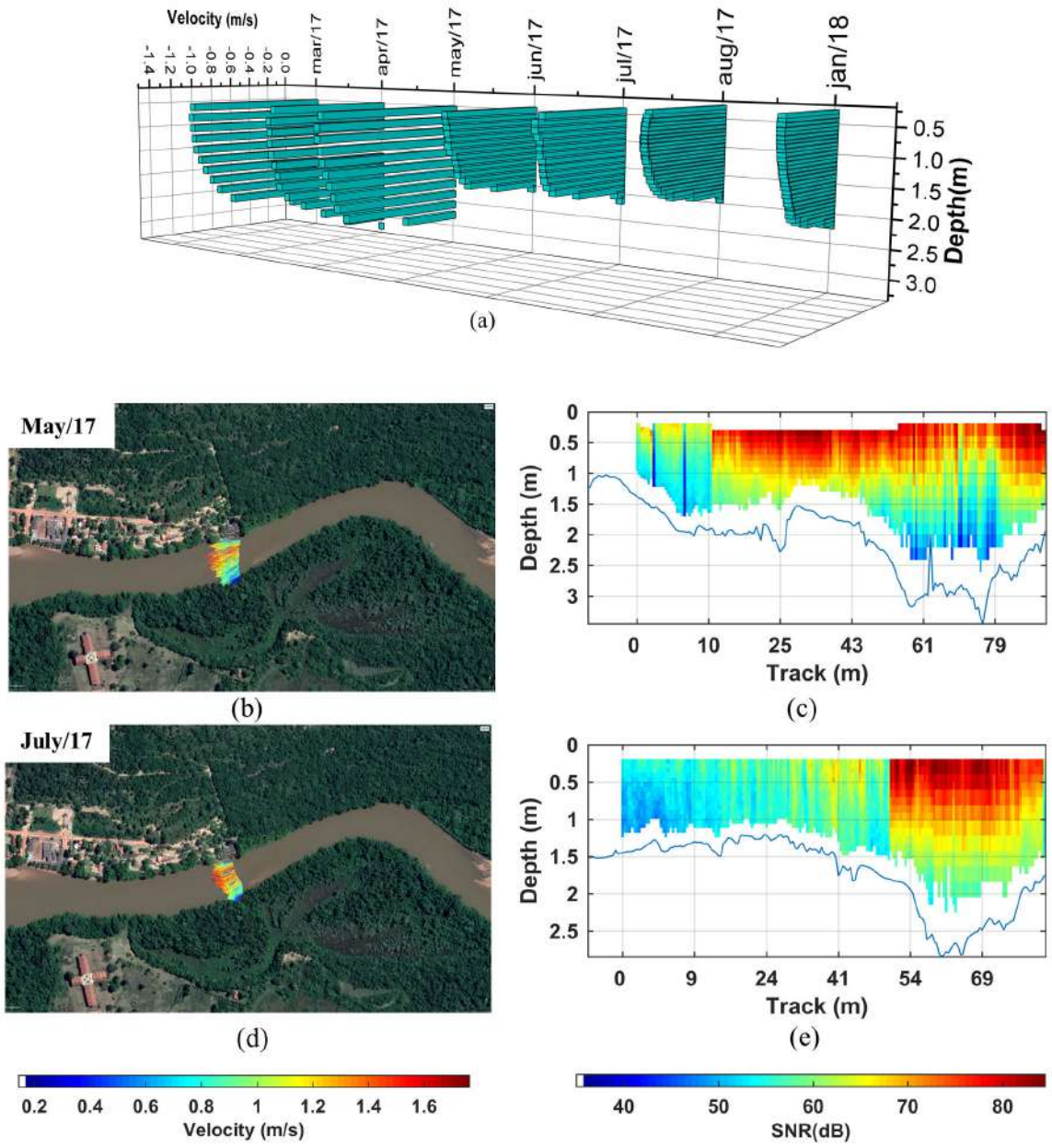

Figure 33 – (a) Mean velocity profiles during all measurement campaigns, Horizontal velocities during the measurement campaigns of (b) May/17 and (d) July/17 and Mean Backscatter Signal obtained during the measurement campaigns of (c) May/17 and (e) July/17.

The velocities varied from $0.64m/s$ in Jan/18 to up to $1.28m/s$ in May/17. Although in May the measurements didn't have the largest discharge value, the SSC was highest when compared to all other sample dates due to the amount of precipitation in the previous day before the measurement campaign (as presented in Table 7 and Figure 34).

Table 7 – Mean discharge and mean solid concentration during the field campaigns.

	Campaigns						
	Mar	Apr	May	Jun	Jul	Aug	Jan
$Q(m^3/s)$	252.25	162.96	221.66	129.82	117.16	131.28	227.57
$D50(mm)$	120	134	104	107	134	135	136
SSC Laboratory (mg/L)	300.3	169.9	422.5	195.4	113.6	124.1	207.8

Figure 34 shows the relation among the parameters measured during the campaigns and the accumulated precipitation registered from 7 days before the measurement campaign. As we can see the variation of the parameters showed that the SSC increases with the discharge and the precipitation. The highest SSC was observed in May/17, suggesting a washload influence due to the high precipitation rate in the period — Figure 34 is arranged from the lowest measured discharge, in Jul/17, to the highest measured discharge, in Mar/17.

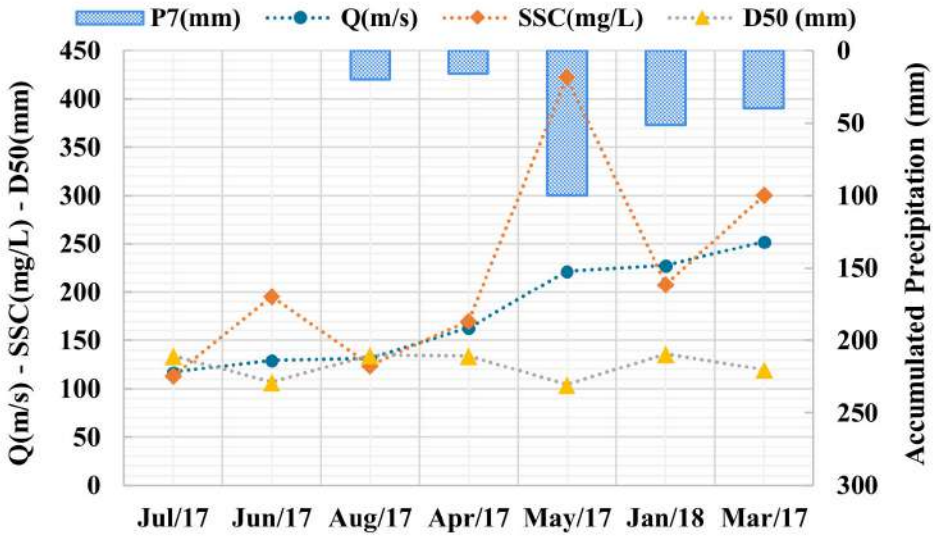

Figure 34 – Relation between the parameters obtained during the campaigns. P7 is the accumulated precipitation registered from 7 days before the measurement campaign. All parameters's values were arranged from the lowest measured discharge to the highest measured discharge.

For all the field campaigns, D50 stayed uniform so it had a poor correlation with other measured parameters. The particle size distribution curves for all sampling events are shown in Figure 35 and it is possible to confirm the presence of the fine fractions that tend to aggregate. As an average of all campaigns, the sampled suspended solid

was comprised of 83% of sand and 17% of silt and clay particles. The presence of fine particles is significant in most campaigns following precipitation events, mainly in May/17, corroborating the washload assumption previously mentioned.

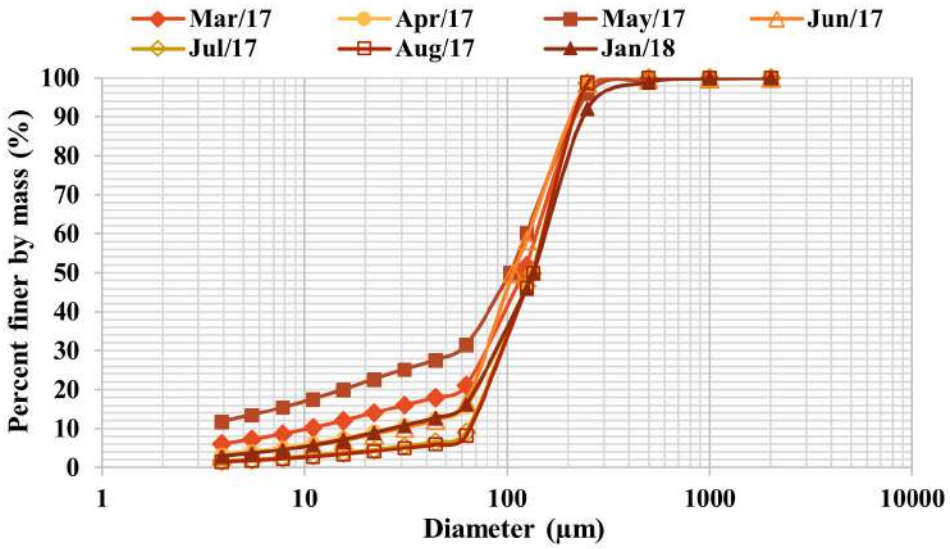

Figure 35 – Granulometric Curve for Taquari River.

5.1.2 Backscatter Correlation for Taquari River

As mentioned, the measurements at Taquari River considered the SPM and the depth-integrated water sampling to obtain SSC information. So, to be sure about the differences caused by the use of SPM instead of the FFM, it was evaluated both modes. All details about this procedure can be found in Appendix C, where it was found that it caused a difference of only 5% in the SSC, on average. Which can be considered insignificant, taking into account the amount of SSC present in Taquari River.

After all the corrections and the aforementioned analysis, Figure 36 shows the correlation between SSC and the corrected backscatter obtained for Taquari River.

Also, during the correction processing, it was evaluated the influence of the particles in the signal attenuation. It was possible by the assessment of the total solid attenuation term given by the third term from the Equation 2.5, where $\alpha_s = \alpha_{ss} + \alpha_{sv}$, a combination of scattering (α_{ss}) and viscous (α_{sv}) attenuation.

The contribution of both terms is summarized in Table 8, where it is possible to notice that, for Taquari River, sand attenuation plays an important role in the solid attenuation backscatter. In fact, considering all campaigns the sand attenuation accounted for up to 95% of the total solid attenuation. The biggest contribution of the fines in the total solid attenuation happened mainly in May and accounted only for 5% of the total solid backscatter attenuation.

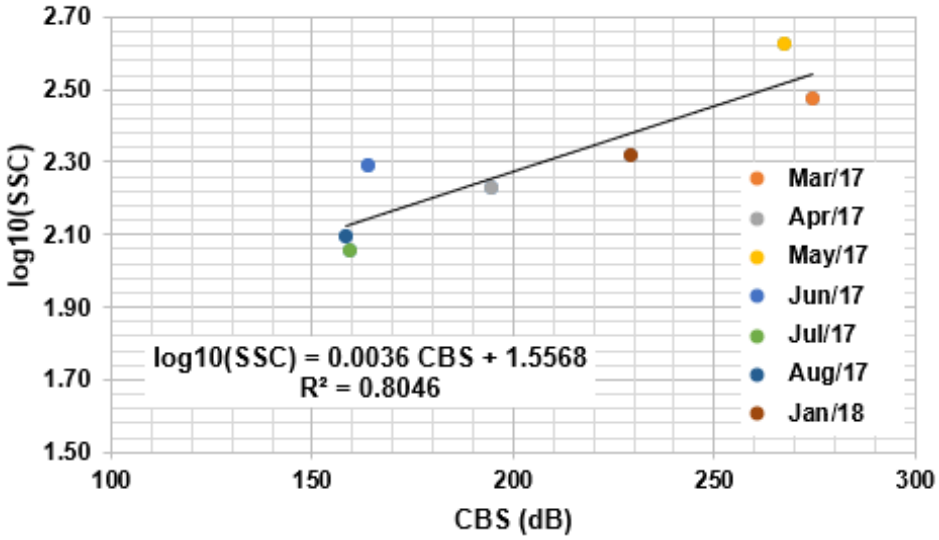

Figure 36 – Correlation curve between SSC and ADCP corrected backscatter signal (CBS) at Taquari River.

Table 8 – Comparison between the solid attenuation coefficients per campaign: α_s, total solid attenuation; α_{ss}, scattering attenuation and α_{sv}, viscous attenuation.

	Mar/17	Apr/17	May/17	jun/17	jul/17	Aug/17	jan/18	Average
α_{sv}	2.57	1.3	4.19	1.9	0.88	0.95	1.56	1.91
α_{ss}	75.06	52.88	78.85	39.84	36.46	39.52	65.61	55.46
α_s	77.63	54.19	83.04	41.73	37.34	40.47	67.17	57.37

In one analysis made by Guerrero et al. (2016), at Parana River (Argentina), they found that the attenuation coefficient for sand suspended from the riverbed was two orders of magnitude higher than the backscattering coefficient for the washload content (usually the finest particles). The goal of the solid backscatter attenuation analysis was to check how the fine solids could influence the final SSC average.

In this study, we found that the difference in these coefficients was one order of magnitude, on average the attenuation coefficient for suspended sand was 55.43 dB/m and the backscattering coefficient for the fine fraction was about 1.9 dB/m.

5.1.3 Mapping of Suspended Solid Concentration

The advantage of ADCP measurements against the manual sampling is that the ADCP measurements can rapidly provide a much higher spatial resolution of SSC in a cross-section than is possible with manual samples alone. The correlations obtained for different ADCP measured SNR intensities with the sampled and analyzed laboratory results can be used to compute SSC concentrations for each measured ADCP cell when measuring the full cross-section, thus showing and quantifying SSC variations over the cross-section.

5.1.3.1 Extrapolation for non-measured regions

As pointed out by Mueller et al. (2013), ADCPs cannot measure the whole cross-section. Non-measured regions are close to the surface (ADCP transducer draft and required blanking distance caused by the ringing of transducers), close to the banks (insufficient depths to measure with ADCP), and close to the bed (due to the acoustic side-lobe effect). The near-surface blanking distance is due to the limitation produced by the transducer vibration. As the transducer is both the transmitter and the receiver, a short distance (blank) is needed after the signal transmission to allow the transducer to adjust itself to receive the shifted signal. The side-lobe is an area of weak acoustic energy parallel to the main acoustic beams emitted by the device which reaches the bed before the main beam, producing interference when the device interprets the acoustic reflection from the main beam.

Before starting the extrapolation procedures near the bed, banks, and surface, it was necessary to fill part of the cross-section area where data collected using the 1MHz beams were removed (Figure 37). To do so, those cells were replaced by the average values of the ADCP corrected signal measured with the 3MHz frequency beams, since all signal corrections were done for this frequency, only.

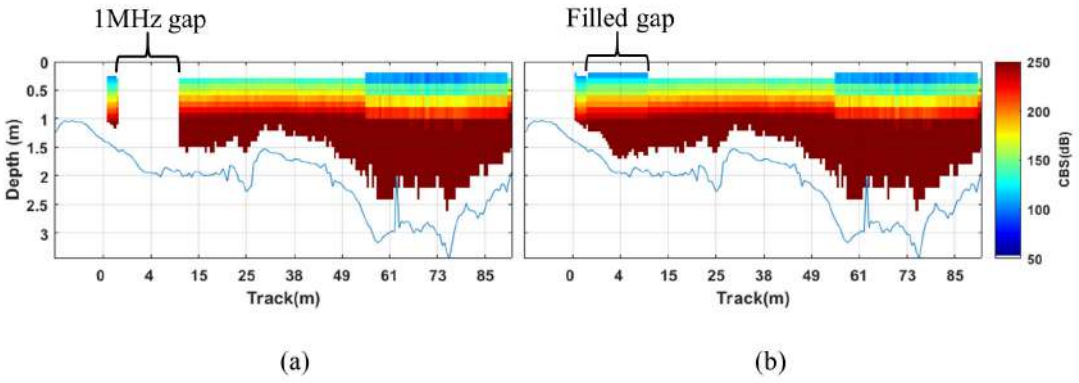

Figure 37 – Measured ADCP signal in the cross-section: (a) without the 1MHz measured cells and (b) with the 1MHz cells filled with the extrapolations obtained by the average of the signal measured by the 3MHz cells.

The comparison between the SSC obtained from laboratory ($SSC_{Laboratory}$) and the ADCP filled cross section ($SSC_{No-Extrapolated}$), as shown in Figure 37, indicate that, on average, the $SSC_{No-Extrapolated}$ was 9% lower than the $SSC_{Laboratory}$. The biggest differences were observed for May and Jun/2017 samples, where the $SSC_{No-Extrapolated}$ was 18% and 42% lower than the $SSC_{Laboratory}$ (Table 9).

Such differences were expected when we considered the representation given in the correlation curve (Figure 36), as already mentioned the correlation points from May

and June had the worst representation, with the greatest absolute difference among all correlated points.

Table 9 – Comparison between the SSC obtained from the laboratory analysis and the SSC obtained from the CBS regression and 1MHz-measured areas filled in with nearby 3MHz data — SSC units in mg/L.

	Campaigns							
	Mar/17	Apr/17	May/17	Jun/17	Jul/17	Aug/17	Jan/18	Avg
$SSC_{Laboratory}$	300.30	169.90	422.50	195.40	113.60	124.10	207.80	
$SSC_{No-Extrapolated}$	318.60	180.94	347.98	112.74	117.11	113.76	206.07	
Difference	6%	6%	−18%	−42%	3%	−8%	−1%	−9%

After filling in the measured portions of the cross-section with nearby 3MHz data, it was proceeded with extrapolating data in the unmeasured areas: near the bed, surface and banks. The near-bed extrapolation was done using an SSC x Depth exponential fitted curve. The curve was fitted to the measured ADCP data in each ensemble (in the full cross-section measurement) and extended to the bed as determined by the ADCP-measured depth. The near-banks extrapolation was done for the unmeasured areas between the last ADCP measured vertical and the edge of the water on each bank. The extrapolated area was considered triangular (with a uniform slope). A constant SSC value was assumed to be present from the first/last, valid ADCP-measured vertical to each bank. The near-surface extrapolation was simply done by extending a constant SSC value from the first measured ADCP cell in an ensemble to the water surface.

Table 10 shows the comparison between the SSC obtained from Laboratory analysis ($SSC_{Laboratory}$) and both SSC obtained by the ADCP x SSC correlation: $SSC_{No-Extrapolated}$ mapping with no extrapolation and $SSC_{Extrapolated}$ with all mentioned extrapolations (1MHz + Bed + Surface + Bank extrapolations). Also, Table 11 shows the comparison between the Suspended Load, Qss: $Qss_{Laboratory}$, $Qss_{No-Extrapolated}$ mapping with no extrapolation and $Qss_{Extrapolated}$ with all mentioned extrapolations.

In terms of suspended load (Qss) the differences between $Qss_{No-Extrapolated}$ and $Qss_{Extrapolated}$ indicated that, on average, including the extrapolated areas resulted in a 63% increase in load.

Table 10 – Difference between the measured SSC and the SSC obtained from ADCP correlation - considering the results without any extrapolations and with extrapolations — SSC units in mg/L.

	Campaigns							
	Mar/17	Apr/17	May/17	Jun/17	Jul/17	Aug/17	Jan/18	Avg
$SSC_{Laboratory}$	300.30	169.90	422.50	195.40	113.60	124.10	207.80	
$SSC_{No-Extrapolated}$	318.60	180.94	347.98	112.74	117.11	113.76	206.07	
$SSC_{Extrapolated}$	365.93	179.61	417.91	108.30	113.23	109.24	216.58	
Difference[1]	6%	6%	−18%	−42%	3%	−8%	−1%	−8%
Difference[2]	22%	6%	−1%	−45%	0%	−12%	4%	−4%

[1]Difference between $SSC_{Laboratory}$ and $SSC_{No-Extrapolated}$.

[2]Difference between $SSC_{Laboratory}$ and $SSC_{Extrapolated}$.

Table 11 – Difference between the measured Qss and the Qss obtained from ADCP correlation - considering the results without any extrapolations and with extrapolations — Qss units in $10^3 Ton/day$

	Campaigns							
	Mar/17	Apr/17	May/17	Jun/17	Jul/17	Aug/17	Jan/18	Avg
$Qss_{Laboratory}$	6.5	2.3	8.0	2.2	1.1	1.4	4.0	
$Qss_{No-Extrapolated}$	4.2	1.6	4.2	0.81	0.8	0.8	2.5	
$Qss_{Extrapolated}$	7.9	2.5	8.0	1.2	1.1	1.2	4.3	
Difference[1]	−35%	−29%	−48%	−63%	−31%	−43%	−38%	−41%
Difference[2]	22%	6%	−1%	−45%	0%	−12%	4%	−4%
Difference[3]	86%	49%	89%	50%	44%	56%	69%	63%

[1]Difference between $Qss_{Laboratory}$ and $Qss_{No-Extrapolated}$.

[2]Difference between $Qss_{Laboratory}$ and $Qss_{Extrapolated}$.

[3]Difference between $Qss_{No-Extrapolated}$ and $Qss_{Extrapolated}$.

The comparison with the $Qss_{Laboratory}$ indicates that, on average, the loads estimated using the extrapolation methods were only 4% lower than the average sampled loads ($Qss_{Laboratory}$). On the other hand, ignoring the extrapolated areas resulted in an average estimated load that was 41% lower than the $Qss_{Laboratory}$.

Differences due the extrapolation were also observed by Haun and Lizano (2018), they notice that the differences were increasing as the depth was increasing with values that range from 0.6% up to 19.4% of difference (from the shallower to the deepest cross-section, in a reservoir).

As we can observe in Figure 38, which illustrates both, the SSC and Qss extrapolated, in the whole cross-section in April/2017 (the measurement campaign with SSC values that best fit the correlation curve), most of the differences were observed for the concentrations close to the bed which (following the theoretical profile for SSC in rivers – Rouse profile), are higher than the concentrations observed throughout the water column.

Also, the corrected backscatter presented in Figure 38 matches the expected and mapped patterns SSC and therefore the Qss, presented in Figure 37, which shows that the corrected SNR and resulting estimated SSC and Qss increase with depth.

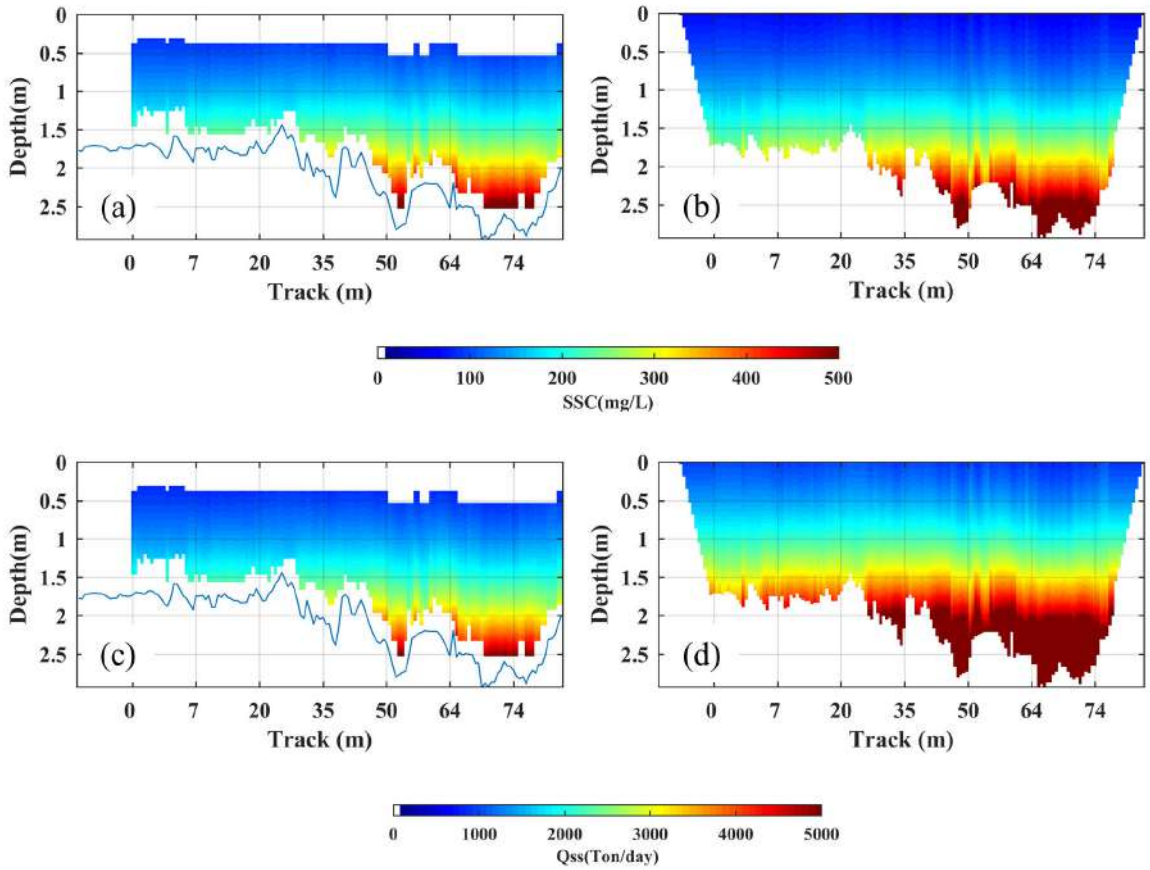

Figure 38 – Non-Extrapolated and Extrapolated Cross-Section, data from April/17: (a) Non-Extrapolated SSC, (b) Extrapolated SSC, (c) Non-Extrapolated Qss, (d) Extrapolated Qss.

5.1.4 Summary

In this section, it was performed the ADCP correction for Taquari River. Due to some particularities during the field campaigns and also due to the solid characteristics, before obtaining the CBS it was performed corrections regarding the frequency in the SPM and due to the solid attenuation coefficient. The final correlation has presented a determination coefficient (R^2) as 0.8046.

So, the final SSC and Qss mapping and average values were obtained after the extrapolation from the blanking zones: bed, bank and surface extrapolations.

The corrections techniques applied at Taquari River were used as a validation of the method in order to prove that under *ideal* conditions, such as: lotic environment, high flow velocities, high solid concentration and non-cohesive particles (silt and sand diameters), the formulations are suitable to the proposed methodology.

5.2 Passauna River

In the frame of the presented research, the Passauna River can be considered as a transitional environment for the corrections technique application. It is a lotic environment and it is the main tributary of the Passauna Reservoir, which means that the conditions to be found here will be very close to those to be found at the reservoir, but higher velocities and particle diameters.

Table 12 shows the TSS and discharge fluctuations along the field campaigns. The extreme event is evident in October, 2018 where the discharge was about 12 m^3/s and the associated TSS concentration was 209 mg/L, equivalent to 70% of the maximum concentration value $TSS_{max} = 294\ mg/L$ and 70% above the concentration average obtained during the whole time serie for this region (RAUEN; CASTRO; SILVA, 2017).

Table 12 – Mean discharge and solid parameters during the field campaigns.

	Campaigns				
	May/17	Apr/18	Aug/18	18Oct/18	20Oct/18
Q(m^3/s)	0.95	1.59	0.52	11.3	1.93
D50(μm)	93.17[1]	93.17[1]	93.17	37.22[2]	37.22
$TSS_{Laboratory}$	10.3 ± 0.4	13.31 ± 1.6	17.67 ± 6.1	209 ± 1.4	31.5 ± 2.1

[1]Filled with D50 data from Aug/18

[2]Filled with D50 data from 20Oct/18

Regarding the diameter determination, as exposed in Table 12, not all the campaigns had granulometric data. Due to some operational questions related to inappropriate use of the equipment in the field, it was decided do not to use some measurements (from April/18 and 18Oct/18) measurements due to the production of suspicious data.

Figure 39 shows the granulometric curve for 2 campaigns when the LISST was used to obtain the particle size measurements. From these two campaigns, we can observe that Passauna River presents a high content of fine and cohesive material, silt and clay, which is about 65% and about 35% of sand.

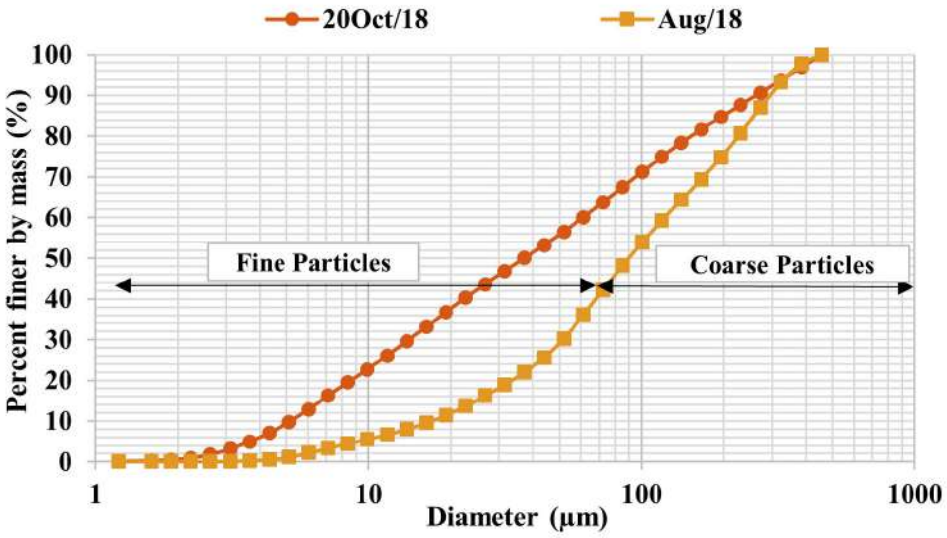

Figure 39 – Granulometric Curve for Passauna River.

To the other campaigns, it was used the available granulometric data to replace the missing values. To do so, it was considered the hydraulic and meteorological situation of the campaign day.

Figure 40 shows the relation among the parameters measured during the campaigns and the accumulated precipitation registered on the day of the measurement campaign. As we can see the variation of the parameters showed that the higher the discharge, the higher the SSC (notice that Figure 34 is arranged from the lowest measured discharge, in Aug/18, to the highest measured discharge, in 18Oct/18).

The granulometric analysis indicates that the largest diameters happened during the drought season (Aug/18) and the smallest during the rainy season (20Oct/18). As explained by Klassen (2017), cohesive particles (as the one we are leading at Passauna River), in the natural environment is subject to a great number of factors that can influence the aggregation and disaggregation of the particles. For example, one of these factors is the high velocities produced by turbulence. During the rainy events, the high turbulence may be responsible for the disaggregation of the flocs and during the drought situation may favor the formation of aggregates and therefore particles with larger diameters.

Another question related to the particle characteristics is the solid density from the suspended solids, that due their characteristics differ from the common values found in the literature (usually about $2.65 kg/L$). At Passauna River, the solids are finer presenting a medium diameter of around $D50 = 50 \mu m$, with a solid density of $1.91 \pm 0.2 kg/m^3$, according to the laboratory analysis results.

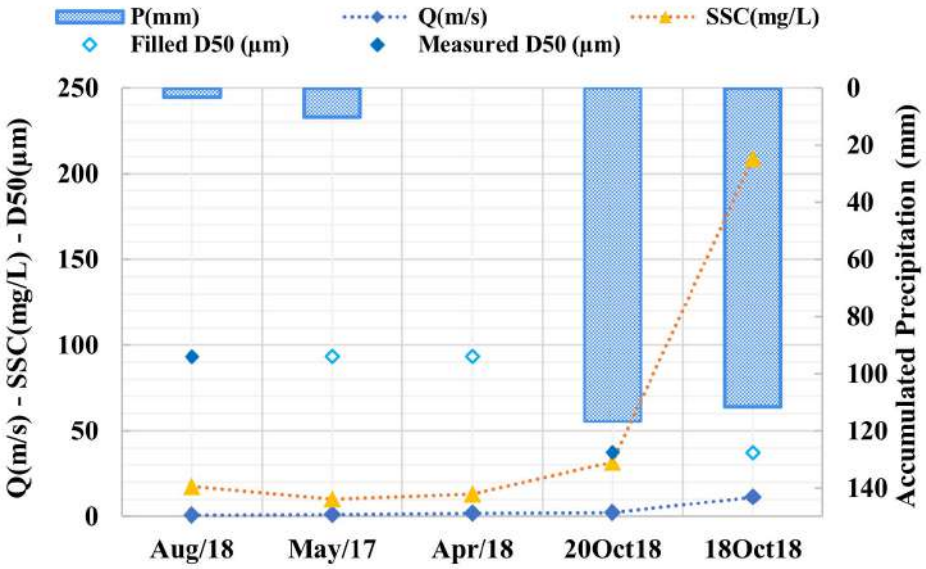

Figure 40 – Relation between the parameters obtained during the campaigns. P7 is the accumulated precipitation registered from 7 days before the measurement campaign. All parameters's values were arranged from the lowest measured discharge to the highest measured discharge.

5.2.1 Backscatter Correction

Figure 41 shows the correlation curve obtained for Passauna River, with an agreement of $R^2 = 0.9401$. Here was made point sampling and the number of samples was random in each campaign. Because of it, the corrections considered only the middle sampled point as well only the related ADCP vertical throughout the cross-section. In this context, most of the settings used for Taquari River (integrated analysis), was also applied here, but with different solids characteristics and TSS.

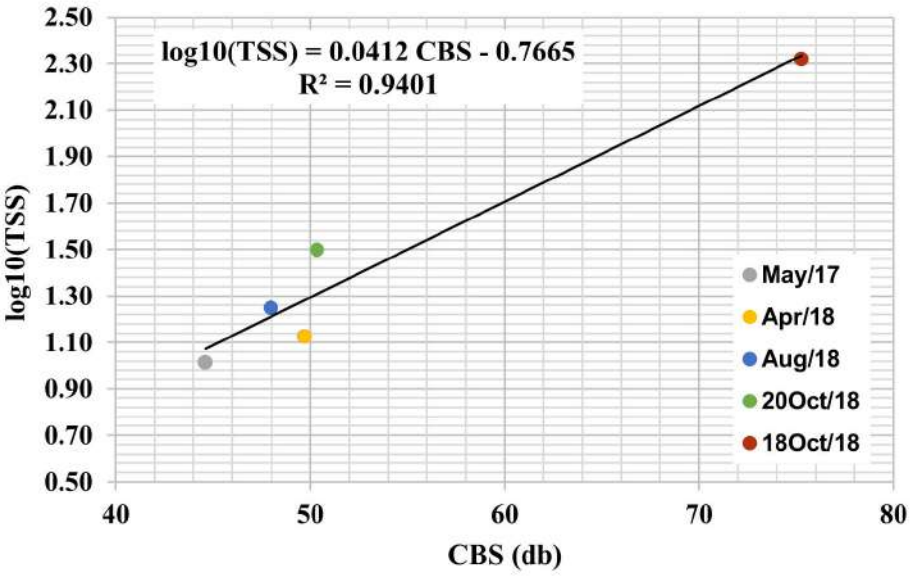

Figure 41 – Correlation curve between SSC and ADCP corrected signal at Passauna River.

Regarding the analysis of the solid attenuation term, as expected due to the granulometric content, it was noticed that the finest material plays an important role in the signal attenuation (Table 13).

Its importance is observed in the viscous-attenuation factor (α_{sv}) mainly in the rainy extreme event observed in October/18, where it has dominated more than 50% of the solid attenuation term ($\alpha_s = \alpha_{ss} + \alpha sv$).

Table 13 – Comparison between the solid attenuation coefficients per campaign: α_s, total solid attenuation; α_{ss}, scattering attenuation and α_{sv}, viscous attenuation.

	May/17	Apr/18	Aug/18	18Oct/18	20Oct/18	Average
α_{sv}	0.08	0.10	0.14	4.22	0.64	0.97
α_{ss}	2.21	2.85	3.82	3.96	0.60	2.33
α_s	2.29	2.95	3.95	8.18	1.24	3.31

5.2.2 Mapping of Total Suspended Solid Concentration

Similar to Taquari River results, after establishing a correlation curve, it was possible to obtain the TSS distribution throughout the cross-section within the extrapolated values.

Since it was shown the extrapolation importance at Taquari River analysis, here, for Passauna River it was decided do not show the intermediate step which would be comparable with the TSS without extrapolations.

In the Tables 14 and 15 are shown the difference associated to the cross-section plots and the laboratory analysis.

On average the $TSS_{Laboratory}$ was about 2% lower than the $TSS_{Extrapolated}$. The largest difference was on October 20th, followed by Aug/18, when the values obtained in the laboratory were 26% greater and 25% lower than the TSS cross-section average obtained by the ADCP signal corrections, respectively.

Table 14 – Difference between the TSS from laboratory and the TSS obtained from ADCP correlation at Passauna River. Units in mg/L.

	Campaigns					
	May/17	Apr/18	Aug/18	18Oct/18	20Oct/18	
$TSS_{Laboratory}$	10.3	13.31	17.67	209	31.5	
$TSS_{extrapolated}$	9.94	16.05	23.43	209.7	24.98	
Difference	4%	−17%	−25%	0%	26%	−2%

In terms of flow discharge, on average the laboratory values were 17% lower than the values obtained by the ADCP.

Table 15 – Difference between the Qss from laboratory and the Qss obtained from ADCP correlation at Passauna River. Units in Ton/day.

	Campaigns					
	May/17	Apr/18	Aug/18	18Oct/18	20Oct/18	
$Qss_{Laboratory}$	0.8481	1.8296	0.7878	203.9606	5.2636	
$Qss_{extrapolated}$	0.82	2.21	1.4	227.88	4.17	
Difference	3%	−17%	−44%	−10%	26%	17%

Whereas in average the differences were about −2% and 17%, for TSS and Qss, respectively, the mapping of these parameters throughout the cross-section (Figure 42) indicates that the point sampling has neglected the TSS, and therefore the Qss gradients towards to the bed. This situation was also observed in Aug/18, but in a lower percentage, since the gradient in Aug/18 was about $40mg/L$ and the gradient observed in 18Oct/18 was about $1000mg/L$.

Although in the conventional analysis is recommended that the point samples should be taken at different depths, respecting the theoretical profile (the Rouse Profile). In practice, due to safety issues, it is not always possible to even sample. But, when conducted even under extreme flood situations, it is usually taken only one sample close to the surface, which can result in unrealistic concentrations, especially in these situations when it is really important to know the incoming load.

Many studies related to reservoir sedimentation and expected life-time are based on the upstream yield data, such conventional issues can lead to a biased historical data series and when applied to these studies can lead to wrong estimations. This is an important statement if it is taken into account that there is an official Gauge Station with solid and flow discharge monitoring located in this cross-section (See Figure 21).

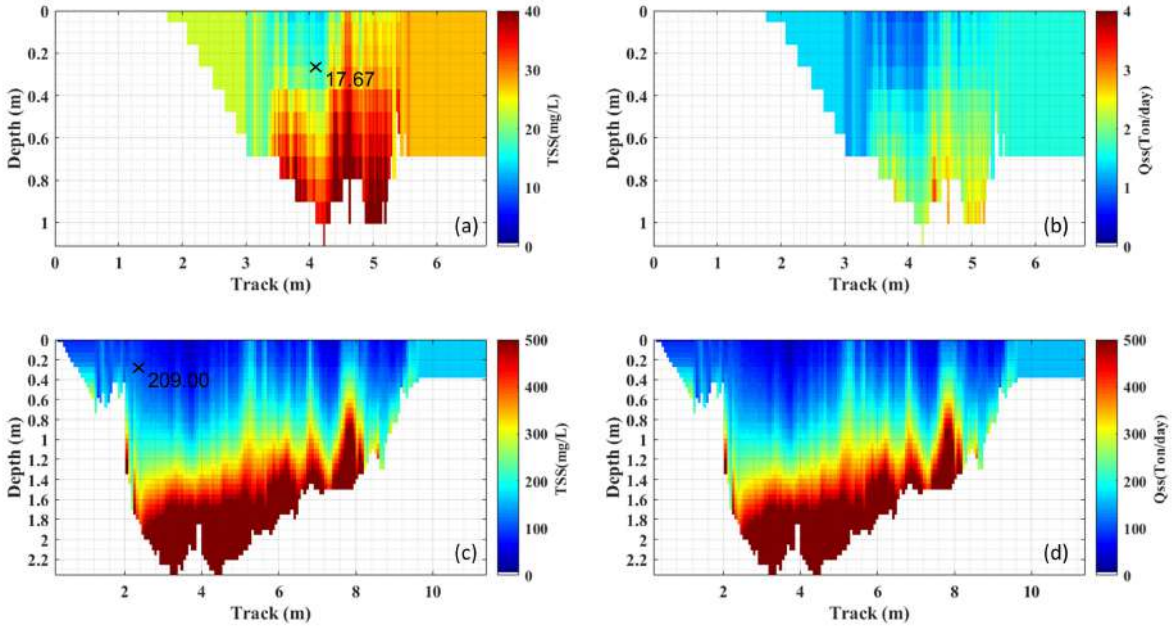

Figure 42 – Mapping throughout the cross-section: (a) TSS from Aug/18 and (b) Qss from Aug/18, (c) TSS from 18Oct/18 and (d) Qss from 18Oct/18.

5.2.3 Summary

In this section, it was obtained the correlation curve for Passauna River. The correlation has presented a good agreement, even if we consider all the different characteristics at this place than the ones observed at Taquari River — such as lower flow velocities and cohesive particles. So, the use as this place as a transitional area to test the methodology for the lentic system has been successfully accomplished.

5.3 Passauna Reservoir

As stated at Chapter 4 Passauna Reservoir is a lentic environment located at the same watershed as Passauna River, therefore it has the same sedimentologic characteristic as well it is subjected to the same weather conditions as the river.

For this environment it wasn't obtained the $TSSxQ$ relation, therefore the suspended load, because since it has low velocities the equipment wasn't capable to obtain the discharge measurements, except for the extreme rainy event monitoring when the discharge reaches $12m^3/s$ and the associated suspended solid concentration was about $160.71mg/L$.

At Ferraria Bridge the water sampling was done considering the point method, and in most of the field campaigns it was done with high spatial resolution: between 3 to 9 water samples per measurement campaign (Figure 43).

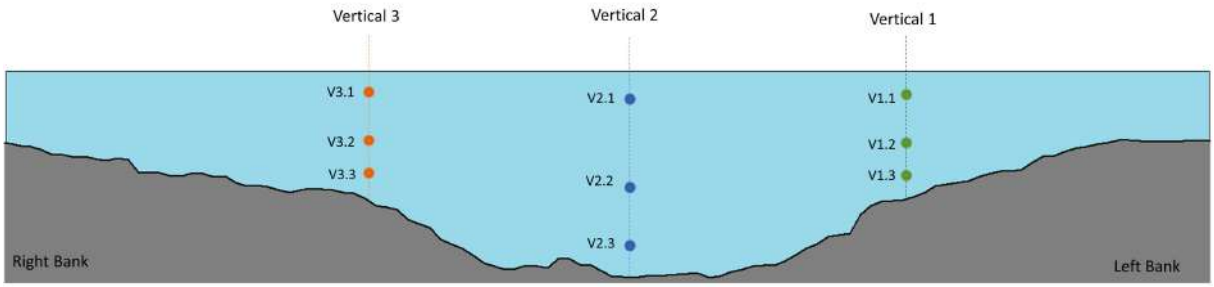

Figure 43 – Ferraria Bridge point sampling points location.

Table 16 shows the number of water samples that were possible to collect per field campaign. In October/18 was the extreme event monitoring and the sampling was done only in the middle of the cross-section (V2.1 and V2.2) because due the high velocities we assume that the cross-section would be mixed[1]. Usually, the variations on the number of collected samples were due to the hydraulic conditions at the measurement day, for example, the water level was one of the parameters taken into account in this decision.

As in Passauna River, the LISST measurements didn't cover all field campaigns. But, in fact, the measurement campaigns happened in an ideal weather situation because it covered the drought and rainy season and also the extreme rainy event, which made possible the extrapolation to the other field campaigns without granulometric data.

[1] afterwards, as shown in the Passauna River results and as will be shown here for Passauna reservoir, this assumption didn't agree with the TSS distribution obtained by the ADCP.

Table 16 – Mean parameters measured in the V2 vertical.

Campaign day	Sampling point spacial resolution
8/24/2017	9 sampling points: 3 points/vertical
8/14/2018	9 sampling points: 3 points/vertical
10/18/2018	2 sampling points: V2.1 and V2.2
10/20/2018	2 sampling points: V2.1 and V2.2
2/4/2019	3 sampling points: V1.1, V2.1 and V2.2
2/5/2019	3 sampling points: V1.1, V2.1 and V2.2
4/2/2019	2 sampling points: V2.1 and V2.2

Table 17 shows the D50 variation within the TSS (only considering the measurements made in the central vertical, V2, in the surface, and in the bottom points). The whole granulometric curve obtained for each campaign per vertical and depth is given in Figure 44.

Table 17 – Ferraria Bridge spatial resolution water sampling points per campaign.

Campaign Day	Depth(m)	Designation	D50(μm)	$TSS_{Laboratory}(mg/L)$
Oct/18	0.12	Surface	13.23	44.00 ± 4.2
	1.58	Bottom	42.01	29.67 ± 7.1
Feb/19	0.23	Surface	13.60	51.00 ± 1.4
	0.75	**Bottom**	16.01	56.67 ± 10.4
Apr/19	0.30	Surface	48.47	8.50 ± 0.3
	2.70	**Bottom**	47.98	11.50 ± 0.7

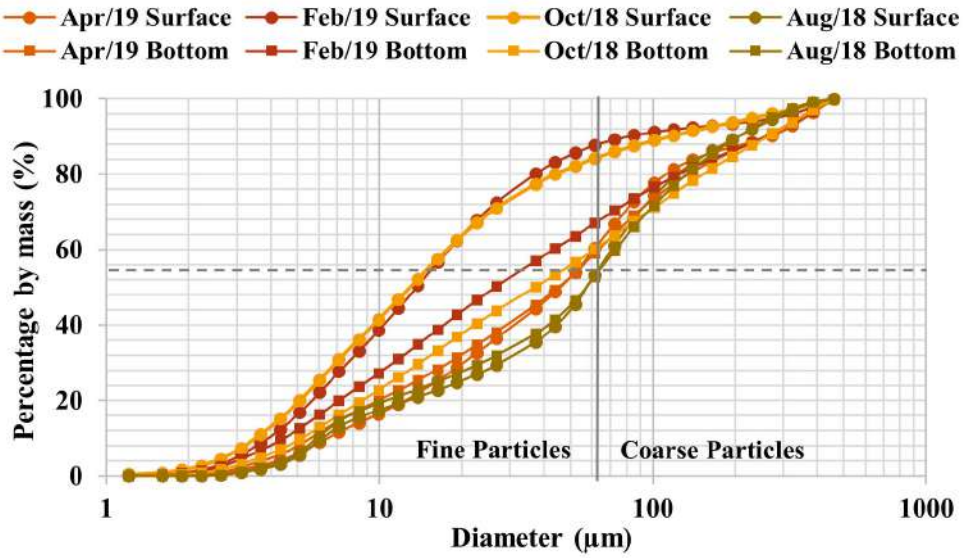

Figure 44 – Granulometric Curve at Ferraria Bridge.

From the exposed, it is possible to observe a pattern in the drought season measurements, where the D50 was similar throughout the water column (surface measure-

ments and bottom measurements). On the other hand, the TSS was different with higher concentrations close to the bottom and lower concentrations on the surface.

In the rainy season, particularly in the extreme event in Oct/18, the distribution was different and it has presented greater particles in the bottom and, different from what was expected it showed an inversion in the TSS values with a gradient varying from $29 mg/L$ in the bottom to $44 mg/L$ in the surface.

The measurement from Feb/19 showed one pattern where the TSS and D50 values can be considered uniform in the entire profile, with D50 values slightly ranging from $16 \mu m$ in the bottom to $13 \mu m$ in the surface and the TSS values ranging from $56 mg/L$ in the bottom to $51 mg/L$ in the surface.

Such patterns confirm the fact that in a medium situation the finest grains tend to aggregate and when exposed to a high energy situation, as in the turbulent flow induced by the rainy events the flocs are destroyed into small particles.

Considering the weather situation before the field measurement campaigns and the TSS determination (Figure 45), the granulometric data gaps were filled with the mean of the measured data on a given day. The measured parameters distribution over the campaigns, as well as the filled values (for the central vertical), are shown in Figure 45.

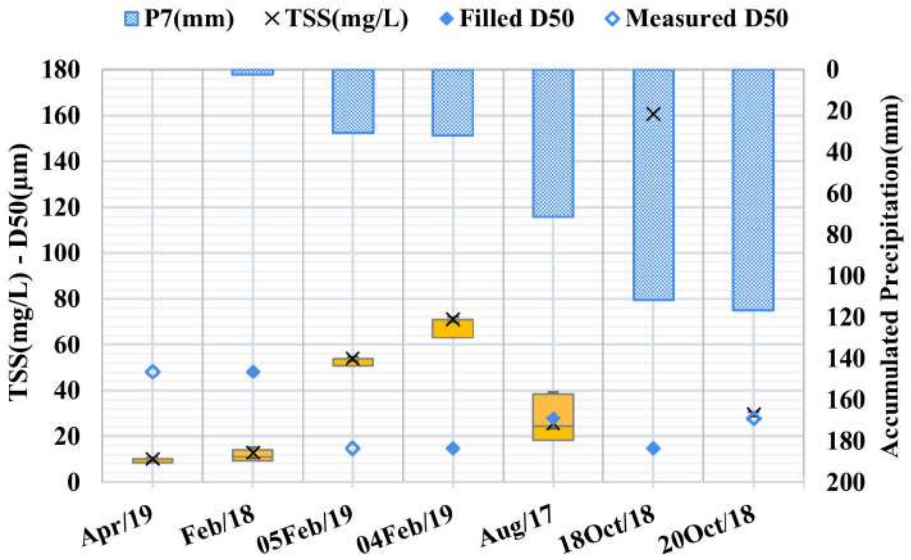

Figure 45 – Relation between the parameters obtained during the campaigns. P7 is the accumulated precipitation registered from 7 days before the measurement campaign and the yellow boxes represent the upper and lower limits of the TSS laboratory analysis in each campaign, considering the sampling distribution presented at Figure 43. All parameters's values were arranged from the lowest measured precipitation data to the highest measured precipitation data.

Here, as also observed in the lotic environment, there is a trend involving the D50 where the higher the precipitation, the lower the D50.

On the other hand, since the lentic system can take longer to answer some forcing

and inputs, the TSS pattern was different from the previously observed: there wasn't observed a straight relation between TSS and precipitation. One possible explanation for this fact is a possible lag between the sampling moment regarding the recorded precipitation data.

After all the granulometric and TSS analysis, the point values[2] were used to make the corrections considering the same formulations applied to Taquari and Passauna River and its implementation, as exposed at Figure 31 in Chapter 4.

The following section will present the backscatter corrections considering the data and assumptions presented.

5.3.1 Backscatter Corrections

Figure 46 shows the correlation curve at the Passauna reservoir through the point analysis methodology. The low agreement ($R^2 = 0.5066$) obtained in this place, when compared to Passauna and Taquari River correlations, can be due to the high uncertainty associated with the measurements and sampling of the parameters.

Even though the measurements were carefully conducted, as well as the laboratory analysis and the post-processing data, these uncertainties are most related to low velocities and low TSS concentrations. In these kinds of systems, a minimal disturbance caused by a small leaf, or by wind, or the simple movement of the boat can create noise that will be easily computed by the ADCP signal and therefore in the ADCP corrections and correlations.

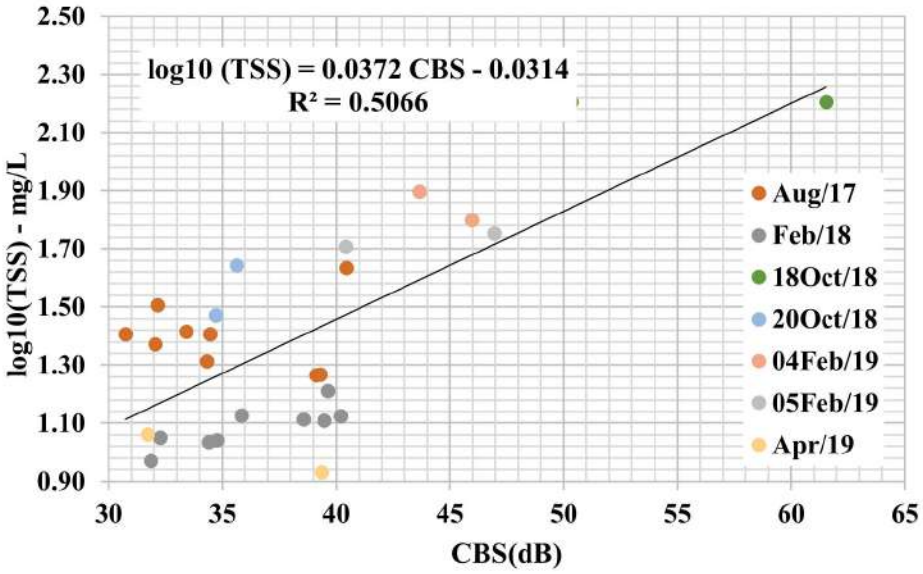

Figure 46 – Correlation curve between SSC and ADCP corrected signal at Ferraria Bridge.

[2] to simplify at this section it was shown the average value of these parameters, but for all calculations, it was considered the point values

Regarding the analysis of the solid attenuation term, due to the granulometric content, was noticed that the finest material plays an important role in the signal attenuation (Table 18), mainly during the rainy situation.

When we analyse together the values from Table 18 and Figure 45, we notice that in the rainy measurement campaigns the viscous attenuation term (α_{sv}) has the most representative effect, with values that varied from $1.26dB/m$ (which is about 78% of the total solid attenuation coefficient, $\alpha_s = \alpha_{ss} + \alpha_{sv}$), in 20Oct/18 to $2.93dB/m$ and $6.64dB/m$ in 04Feb/19 and 18Oct/18, respectively, both about 97% from α_{ss}.

The contribution of the scattering attenuation term (α_{ss}) was more evident in the drought situation (low precipitation) with values ranging from $0.43dB/m$ to $0.66dB/m$ (about 79% to 83% of the α_{ss}) in Apr/19 and Feb/18, respectively.

Table 18 – Comparison between the solid attenuation coefficients per campaign: α_s, total solid attenuation; α_{ss}, scattering attenuation and α_{sv}, viscous attenuation.

	Aug/17	Feb/18	18Oct/18	20Oct/18	04Feb/19	05Feb/19	Apr/19
α_{sv}	0.64	0.14	6.64	1.26	2.93	2.23	0.11
α_{ss}	0.15	0.66	0.24	0.35	0.10	0.08	0.43
α_s	0.79	0.80	6.88	1.61	3.04	2.31	0.55

5.3.2 Mapping of Total Suspended Solid Concentration

This section shows an overall discussion about the cross-section and the longitudinal measurement mapping. Different from the lotic environment, it wasn't considered the surface, banks and bed extrapolations.

As the lentic system is subject to the hydrodynamics forcings, such as temperature stratification, pressure variations and chemical and biologic forces, would not be possible to fit a single model to all campaigns without losing the nuances of the TSS distributions. Also, it wasn't calculated the suspended load, since the flow velocities are low which doesn't make it possible.

Figure 47 sketches the extrapolations at Passauna Reservoir, where we can see that the extrapolations would affect the TSS variations mainly on the drier days Figure 47a and Figure 47b. On rainy days, the extrapolation (Figure 47d) doesn't change too much the previous representation (Figure 47c, without extrapolation), although it is not possible to ensure that it will be well performed every time we have this situation.

Table 19 shows the comparison between the average of the $TSS_{Laboratory}$ and the average of the TSS obtained in the mapping of the cross-section was only 1% bigger than the observed by the ADCP, the differences had a big variation around the average.

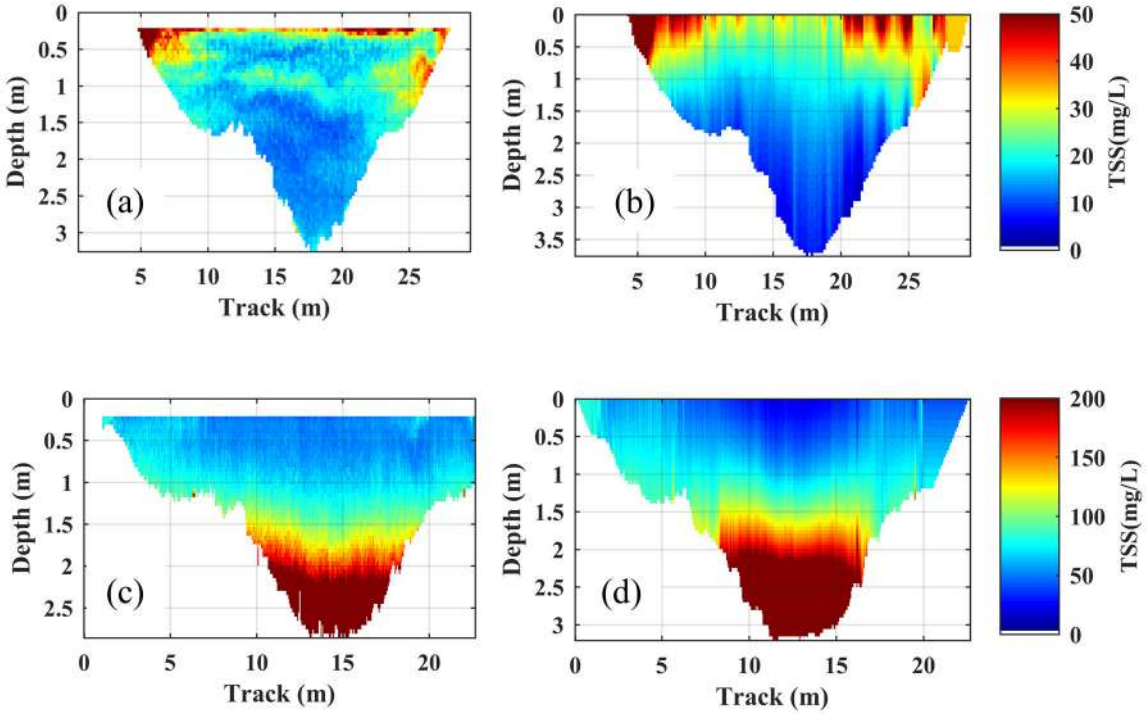

Figure 47 – Comparison between extrapolated and no-extrapolated TSS at Ferraria Bridge in Aug/17 (dry situation) and in 18Oct/18 (rainy situation).

The best TSS estimative was represented in Aug/17, when the difference was about only 4% between the laboratory analysis and the ADCP average. The biggest differences happened mainly in the rainy situation: in Feb/19, the TSS_{ADCP} was about 62% bigger than the $TSS_{Laboratory}$ and in Oct/18 (in both campaigns) the TSS_{ADCP} was about 78% lower than the $TSS_{Laboratory}$.

It is important to emphasize that the measurement from 20Oct/18 and Apr/19 count with additional uncertainty related to the field campaign and sampling. In both of the cited campaigns, the vessel used to do the measurements was launched from the left bank close to the measured cross-section, which caused erosion of the bank that spread across the cross-section. — this disturbances are evident in the mapped cross-section (see Figures 68 at Appendix D. Also, in Apr/19 the samples were collected about 3h hours difference of the ADCP, before the disturbance caused by the vessel.

Table 19 – Difference between the TSS from laboratory and the TSS obtained from ADCP correlation at Passauna Reservoir. Units in mg/L.

	Campaigns							
	Aug/17	Feb/18	18Oct/18	20Oct/18	04Feb/19	05Feb/19	Apr/19	Average
$TSS_{Laboratory}$	25.88	12.34	160.71	36.83	53.49	52.89	10.00	
TSS_{ADCP}	24.82	15.83	90.40	20.67	33.49	40.54	26.58	
Difference	4%	−22%	78%	78%	60%	30%	−62%	1%

5.3.2.1 Longitudinal transects

When performed, the longitudinal transects were made right after the cross-section measurements at Ferraria Bridge, throughout the area that involves the forebay (upstream the Ferraria Bridge location) until the area immediately downstream the Ferraria Bridge location.

From the starting point until the end, the transect covers another two monitoring points: Buffer and PPA points, as shown in Figure 48.

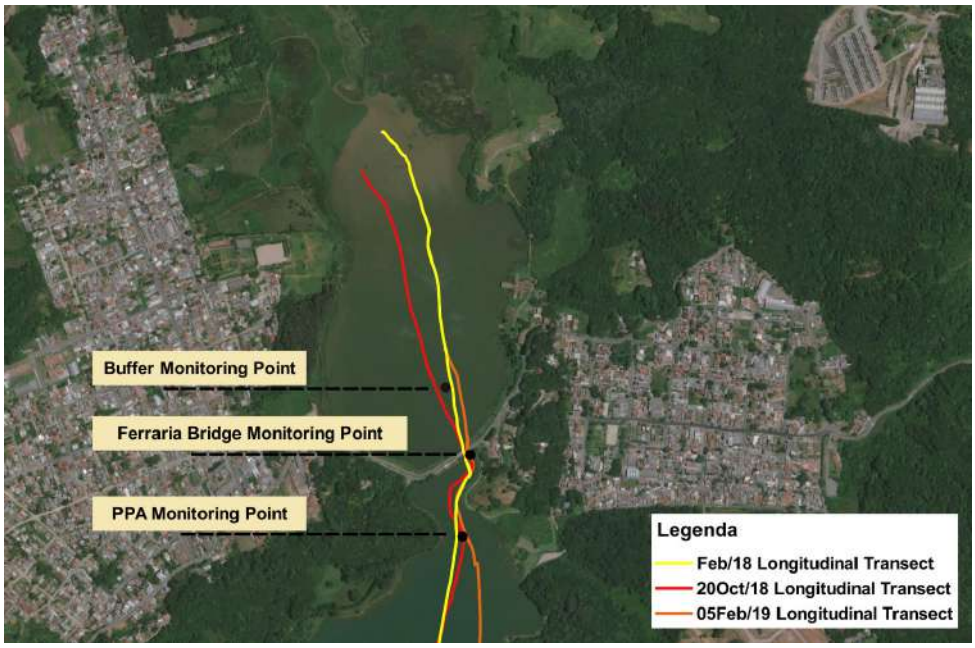

Figure 48 – Longitudinal transects and point measurements througout the transects.

From now on the idea is to cross the information from both measurement results — the Ferraria Bridge cross-section and the longitudinal transection monitoring. It is expected that the results from the longitudinal measurements reflects the results found at the Ferraria Bridge cross-section. The results are presented as following:

- Feb/18 during the rainy season, Ferraria Bridge cross-section and longitudinal transect measurement - Figure 49;
- 18Oct/18 during the extreme event, only Ferraria Bridge cross-section - Figure 50;
- 20Oct/18 two days after the pick of the extreme event, Ferraria Bridge cross-section and longitudinal transect measurement - Figure 51;
- and in 02/05/19 during the rainy season, Ferraria Bridge cross-section and longitudinal transect measurement - Figure 52;

Figure 49 shows the TSS mapping from Feb/18, where we can see the evolution of the stratification from the Buffer and FB points, with no apparent stratification until

reach the PPA point, with a gradient about $2°C$ from the top to the bottom. This situation presents a possible density current formation driven by temperature right after the Ferraria Bridge towards the PPA point. Within the density current, it is possible to notice also a gradient in the TSS and its evolution (with a variation around 20 to $50 mg/L$) towards the reservoir.

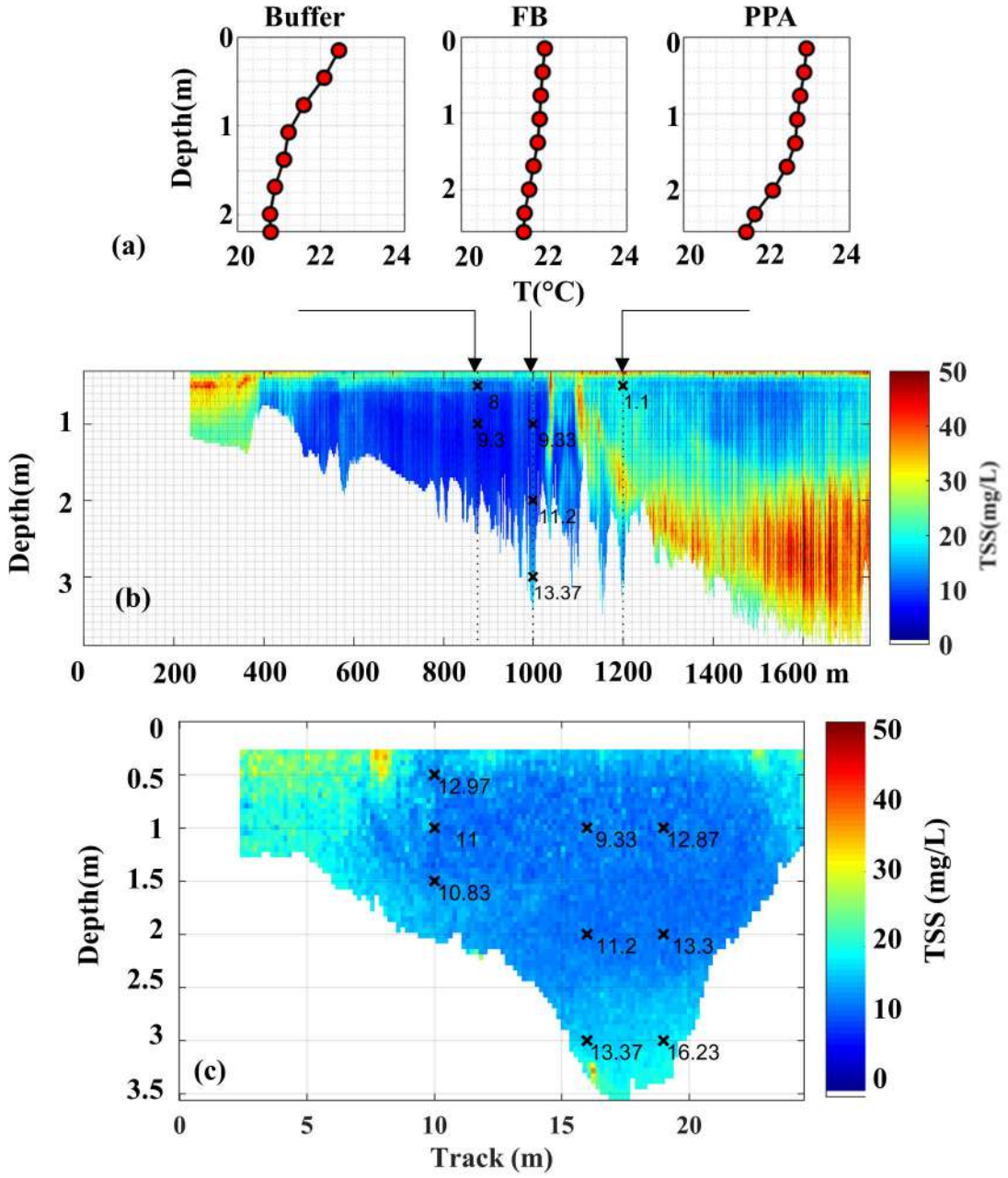

Figure 49 – Feb/18 monitoring campaign: (a) Temperature Profiles from Buffer, Ferraria bridge (FB) and PPA points, (b) Longitudinal Transect and (c) Ferraria Bridge Cross-Section. All values exposed in the transects are TSS in mg/L.

In 18Oct/18 (Figure 50), although the temperature profiles indicate a very well mixed situation (the temperature variation is lower than $1°C$), in terms of TSS the cross-

section mapping shows a strong TSS gradient over the depth — with higher concentrations values in the bed, the variation goes from about $50mg/L$ up to $200mg/L$ which can indicate an underflow turbidity density current (when the density current isn't driven by temperature but by TSS differences).

This measurement was taken during the extreme event when the Ferraria Bridge cross-section presented a lotic situation and a flow discharge about $12m^3/s$ (in a place where it is usually lower than $1m^3/s$).

Regarding the longitudinal transect, unfortunately for the extreme event, the longitudinal transect was not performed, so the density current couldn't be tracked.

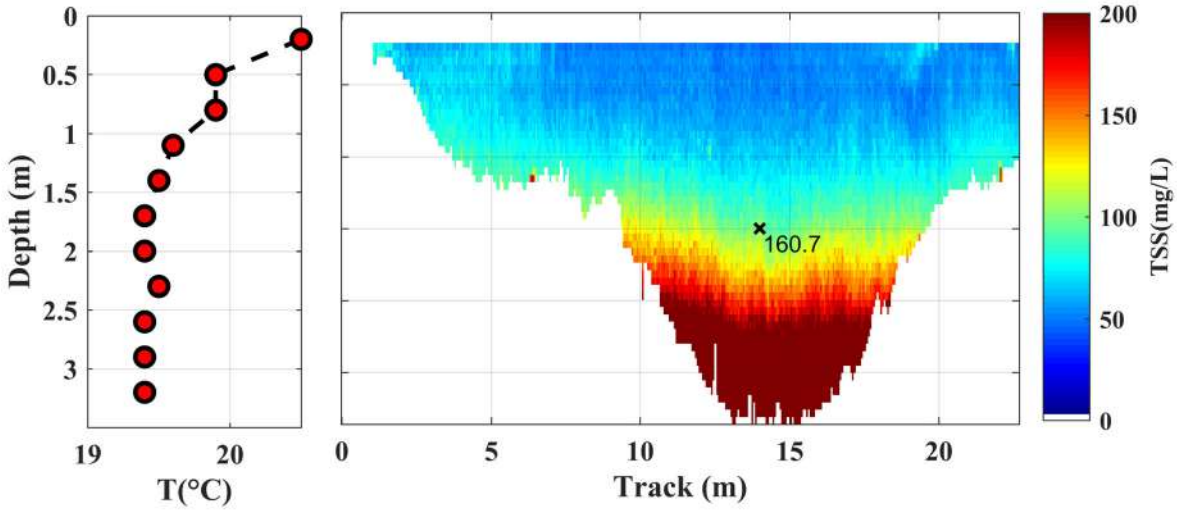

Figure 50 – 18Oct/18 monitoring campaign: Ferraria Bridge Cross-Section Mapping and Temperature Profile.

Even though Figure 51 represents the reservoir only two days after the peak of the event, it shows a situation completely different from that one observed before. Although the laboratory results indicate an inverted gradient in the cross-section mapping (Figure 51c), with higher TSS values close to the surface ($44mg/L$) and lower TSS (about $30mg/L$) close to the bed, the ADCP mapping didn't show any pronounced gradient and, in fact, the results show a low TSS concentration and a weak temperature stratification (Figure 51a).

This mixed situation is also observed in the longitudinal transect mapping (Figure 51b), where the water column has presented an almost constant $5mg/L$ TSS concentration with some variation in the deepest part from 10 to $20mg/L$. The strong and local variation observed in the Ferraria Bridge area, close to the surface can be accounted for some disturbance caused by the boat moving or the handling of the equipment in the measurement point.

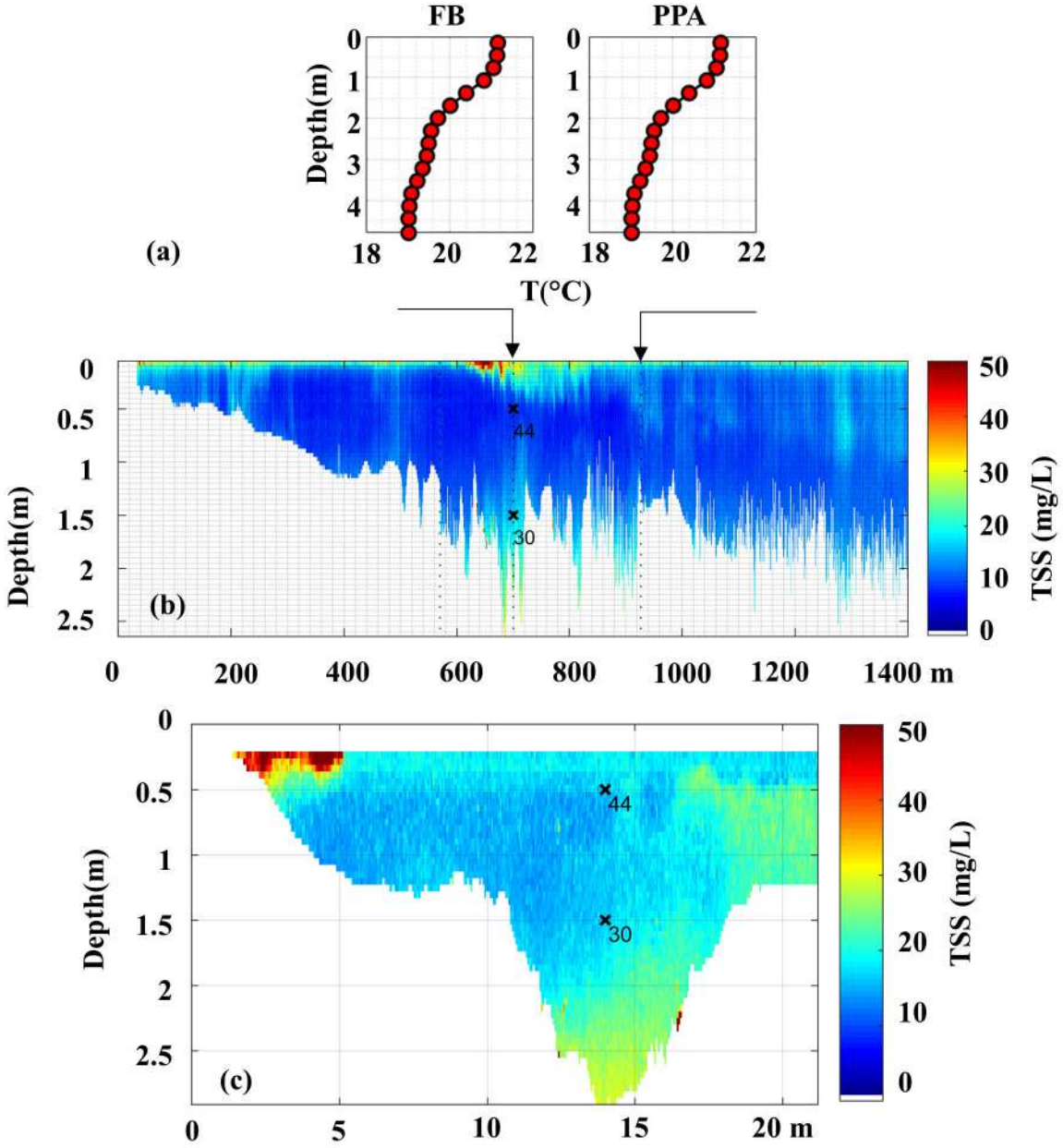

Figure 51 – 20Oct/18 monitoring campaign: (a) Temperature Profiles from Ferraria bridge (FB) and PPA points, (b) Longitudinal Transect and (c) Ferraria Bridge Cross-Section. All values exposed in the transects are TSS in mg/L.

As in Figure 49, in the measurement performed in 05Feb/19 (Figure 52) it is possible to observe the Temperature stratification evolution from the Buffer and FB points to PPA point, where first the situation wasn't stratified and then it starts to present a gradient about $2°C$ in only $1.5m$ deep. Within this variation, comes the TSS variation which leaves the Ferraria Bridge in a very well mixed situation (with TSS values ranging around $50mg/L$) and starts to spread towards the reservoir as a submerged density current with a TSS gradient from about $50mg/L$ up to $100mg/L$.

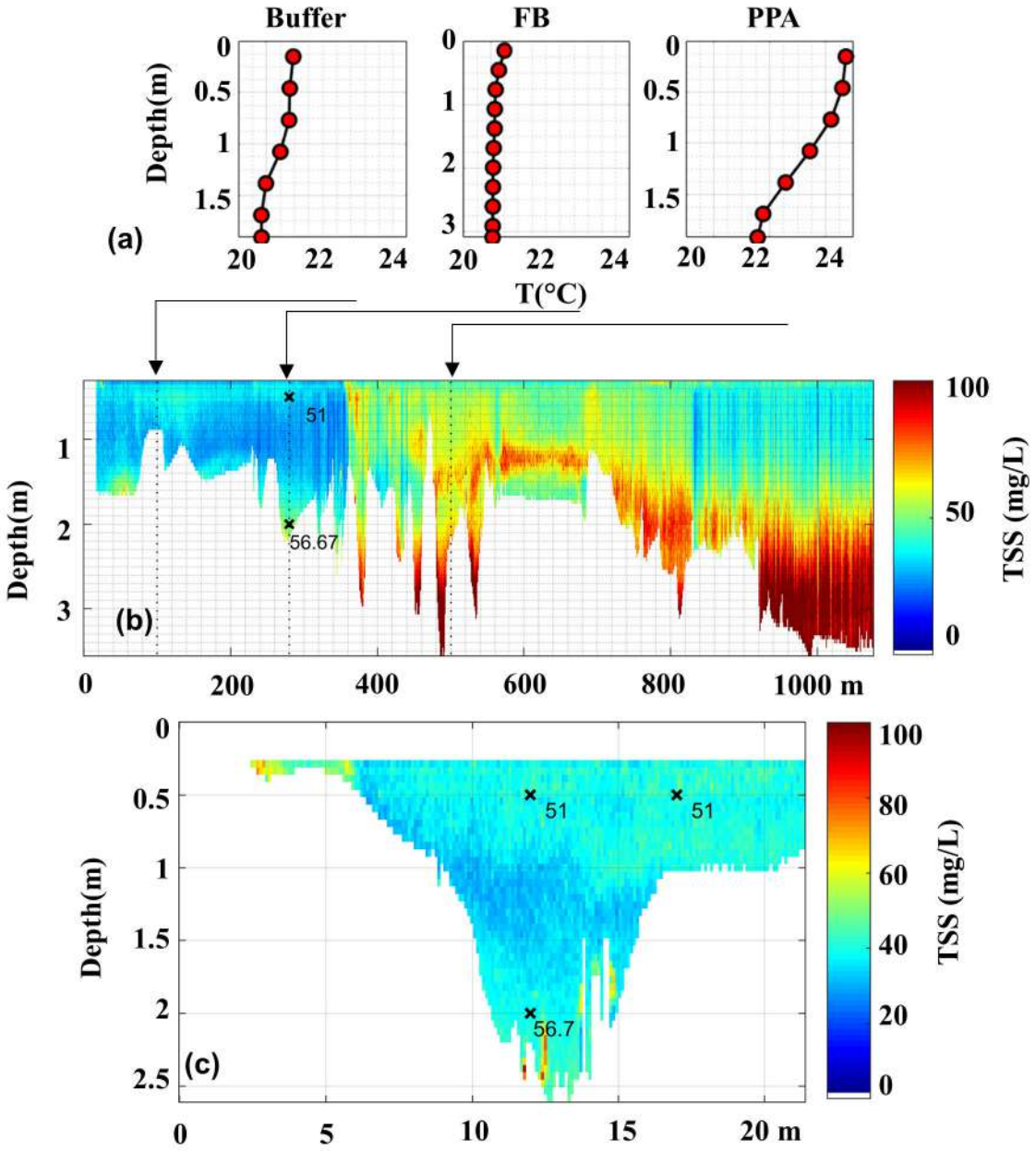

Figure 52 – 05Feb/19 monitoring campaign: (a) Temperature Profiles from Ferraria bridge (FB) and PPA points, (b) Longitudinal Transect and (c) Ferraria Bridge Cross-Section. All values exposed in the transects are TSS in mg/L.

The existence of the density currents observed by the ADCP in the results can be confirmed by the comparison with the analysis of the results from two recent studies regarding the bed solid throughout the talweg and the sedimentation rate downstream the bridge, close to PPA point.

Sotiri, Hilgert and Fuchs (2019) analyzed the bed solid content from upstream to downstream at Passauna reservoir and have found that before the bridge, in the forebay, the solid is majority composed by a silt-clay fraction (C12) — Figure 53. Under the

Bridge, it is replaced by almost 15% sand and 45% clay-silt fraction and right after the bridge (G7), close to the PPA point, where Ono (2019) has found a sedimentation rate up to $180 g/m^2$ (the higher sedimentation rate observed in her study), the sand fraction goes up to almost 45% and the silt-clay fraction drops to almost 15%, and then after all this dynamics, the silt-clay fraction establishes again along the talweg in the reservoir.

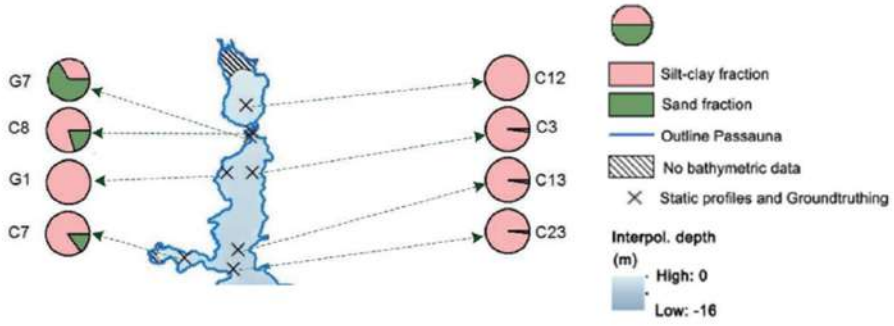

Figure 53 – Granulometry from Grab (G) and Cores (C) obtained by Sotiri, Hilgert and Fuchs (2019) at Passauna Reservoir. Adapted from: Sotiri, Hilgert and Fuchs (2019).

As exposed by Morris and Fan (1998) this solid dynamic can be related to the density current development and in a reservoir, most of the deposition is focused along the talweg where the density current usually develops. According to them, the solid begins depositing from turbidity currents right after the plunge point — possibly the point where it was observed the highest sedimentation rate associated with the highest particle size (G7 point).

To conclude, the authors highlighted that deposits from turbidity currents consist of fine material, finer than the observed in the delta deposits, even in reservoirs where most of the inflow load consists of fine fractions, as in the Passauna system.

5.3.3 Comparison within other TSS studies conducted at Passauna Reservoir

In the frame of the Mudak Project, several studies are being conducted in order to understand the system and also to reduce the complexity of the measurements with the proposition of advanced monitoring tools. This section sketches the comparison of the mapping results in the lentic environment with results obtained by other researchers. It is important to mention that the majority of these findings are still being constructed and investigate by the researchers and were given as a courtesy by the responsible. Therefore they were not published yet.

Figure 54 shows the comparisons from the extreme rainy event from Oct/18. On 18Oct/18 it is possible to see that after pass through the Ferraria Bridge cross-section the temperature variation (Figure 54a) establishes a pattern that travels toward the reservoir until reach the dam. Apparently, this variation in temperature does not play a role in the tracer spreading (Figure 54b), since it has present a different shape after the bridge cross-section. Also, such observations match with the ADCP measurement result within the cross-section with a very pronounced gradient that ranged from about $100 mg/L$ up to $200 mg/L$.

Regarding the measurements conducted in 20Oct/18, Figure 55, the numerical modeling results indicate a mixed situation (two days after the peak of the event) mainly close to the bridge, reflecting the uniform pattern observed in the TSS throughout the measurement of the longitudinal transect.

Figure 56 shows the comparisons from the whole reservoir and the mapped cross-section at Ferraria Bridge on 04Feb/19 considering numerical modeling (Figure 56a and b) and remote sensing techniques (Figure 56 c and d) to describe the spreading of the solids in the reservoir. Although for this day the longitudinal transect made with the ADCP was not performed it is possible to see that the variations observed at the cross-section were connected to the variations observed upstream of the Ferraria Bridge.

At Figure 57, it is shown the measurements from 05Feb/19. Both the results of the numerical simulation (Figure 57a 57b) and the results of the remote sensing(Figure 57c) confirm the dispersion pattern of the plume of solids observed in the longitudinal transect made with the ADCP(Figure 57d and 57e), the measurement of ADCP matches with the ranges of values on the surface found by the hyperspectral camera.

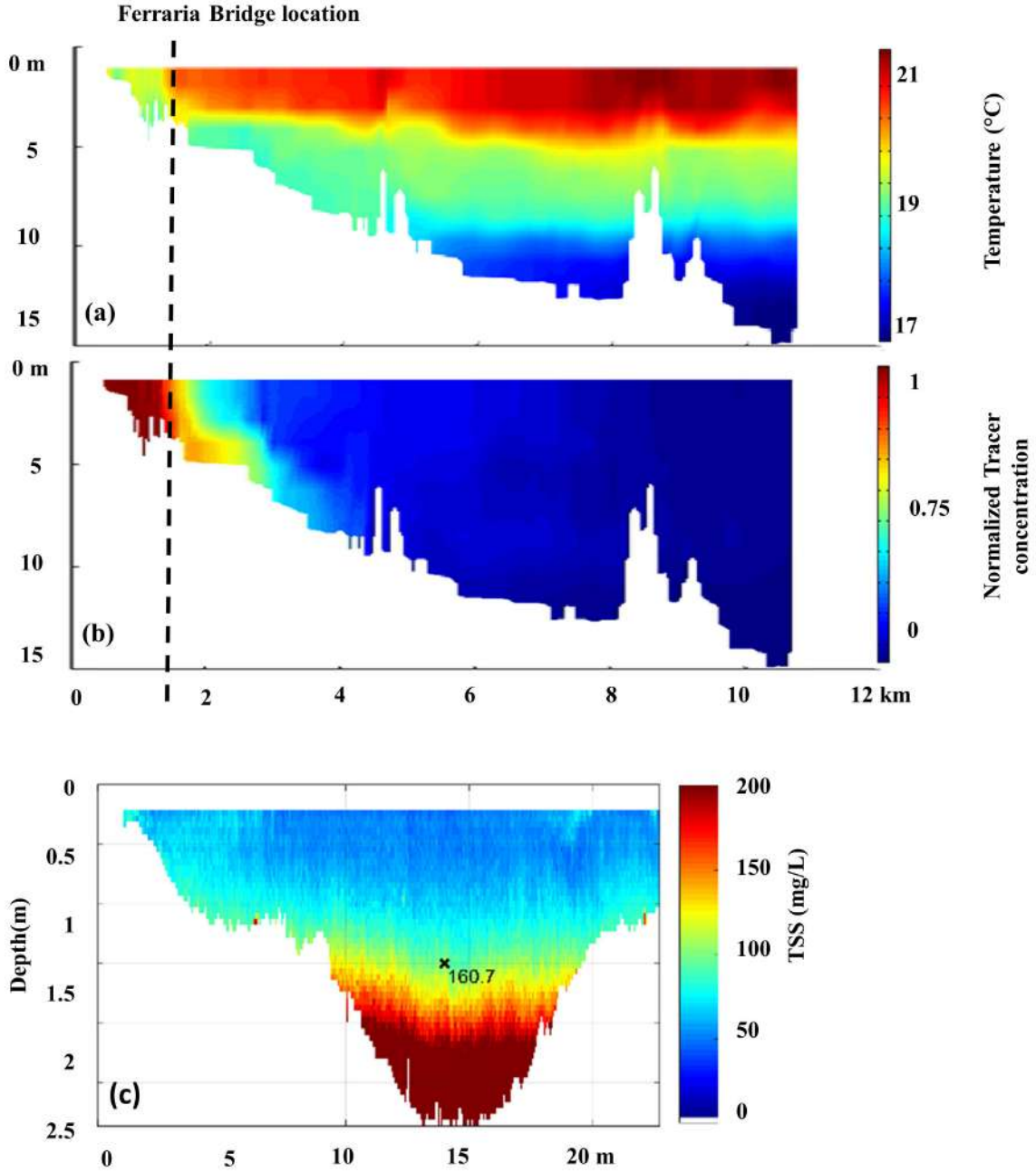

Figure 54 – Comparisons of the measurements performed on 18Oct/18 among numerical modeling for (a) Temperature and (b) Tracer Normalized Concentration (courtesy from Wendy Gonzales) and (c) the mapped cross-section made with the ADCP already discussed at Figure 50.

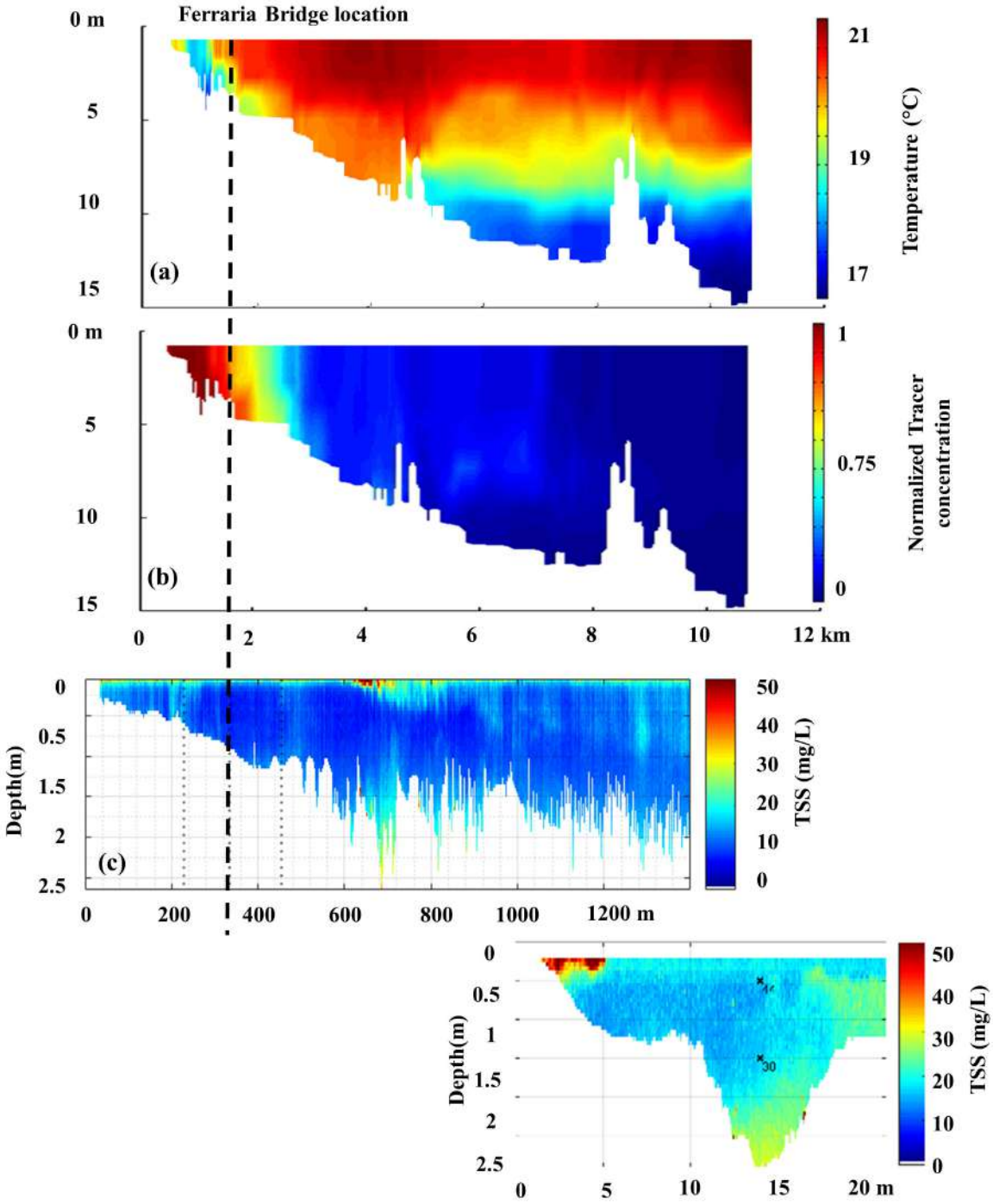

Figure 55 – Comparisons of the measurements performed on 20Oct/18 among numerical modeling for (a) Temperature and (b) Tracer Normalized Concentration (courtesy from Wendy Gonzales) the mapped longitudinal transect and (d) the mapped cross-section made with the ADCP, both already discussed at Figure 51.

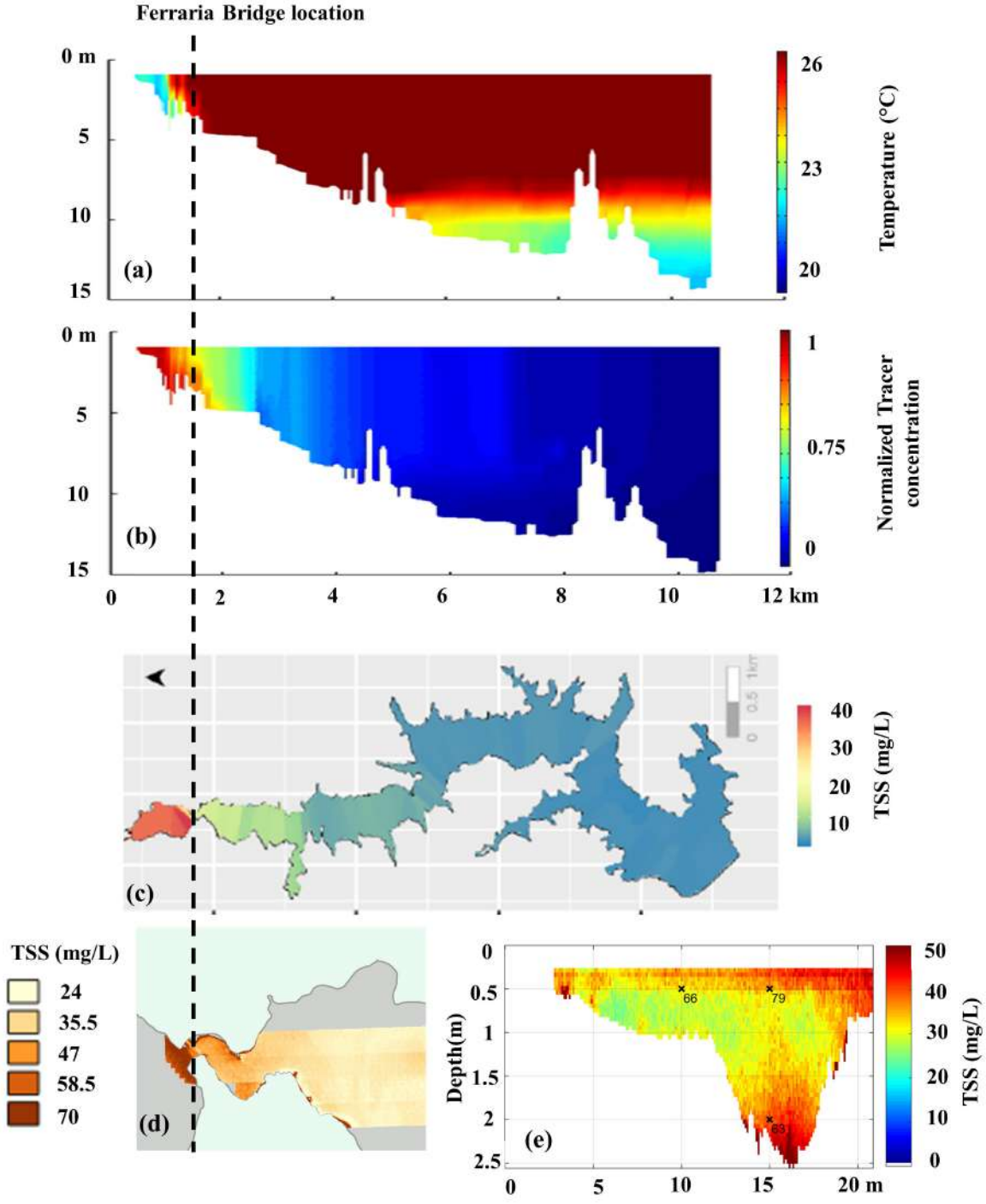

Figure 56 – Comparisons of the measurements performed on 04Feb/19 among numerical modelling for (a) Temperature and (b) Tracer Normalized Concentration (courtesy from Wendy Gonzales), (c) the TSS in the water surface obtained by close remote sensing, after Wagner (2019), (d) a composition obtained by drone images (courtesy from Jens Kern) and (e) the ADCP mapped cross-setion obtained at the presented study.

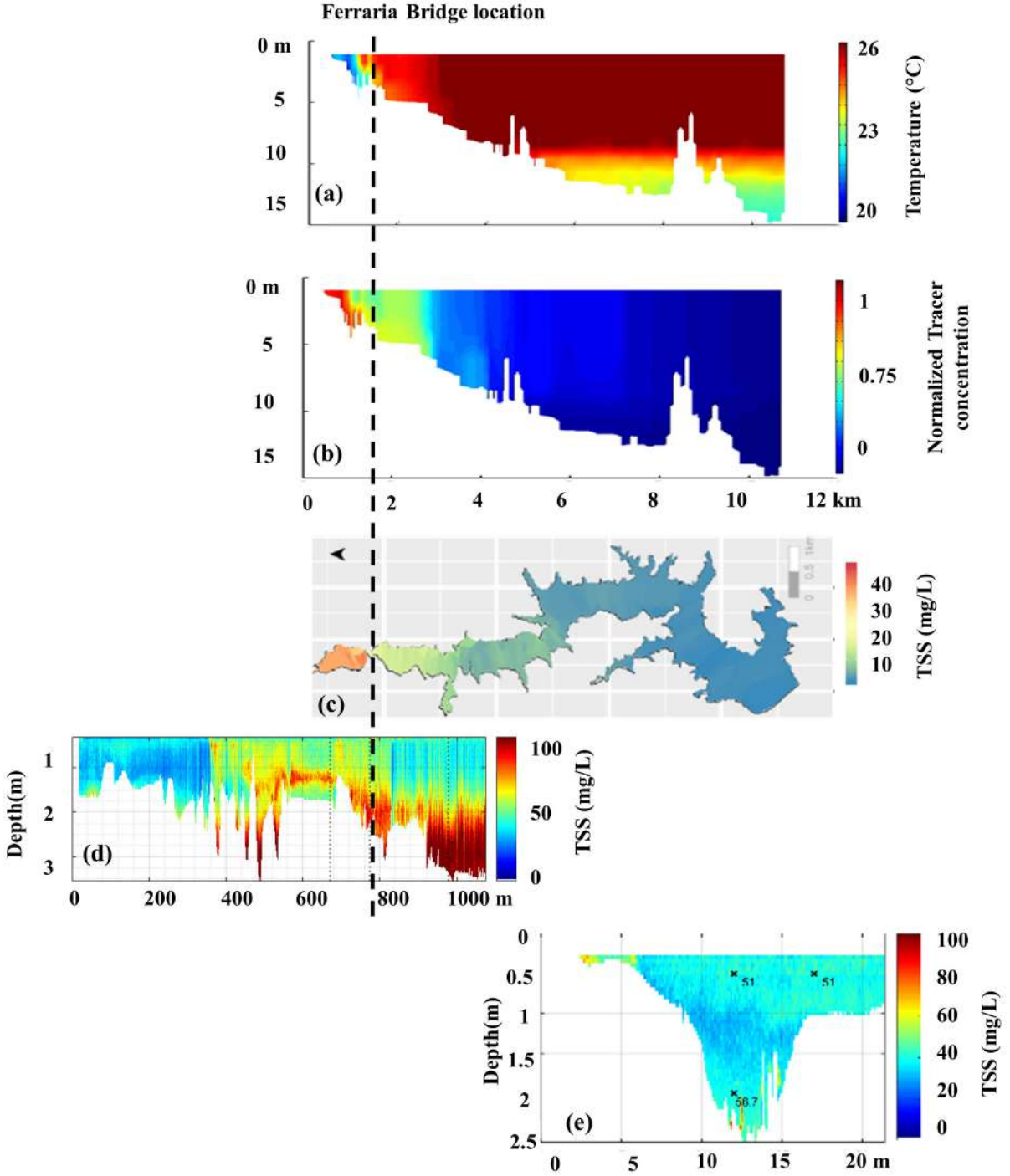

Figure 57 – Comparisons of the measurements performed on 05Feb/19 among numerical modeling for (a) Temperature and (b) Tracer Normalized Concentration (courtesy from Wendy Gonzales), (c) the TSS in the water surface obtained by close remote sensing, after Wagner (2019), (d) the mapped longitudinal transect and (e) the mapped cross-section made with the ADCP, both already discussed at Figure 52.

5.4 Discussion

From the exposed the differences between measured solids and in the solid estimated by the ADCP calibration in all analyzed environments can be accounted for several factors. Among them, it is possible to cite questions related to operational issues regarding field measurements, equipment setup and divergence between the sampling point and the measured signal. Also, the variation on temperature and in the solid concentration during the measurement campaign (SZUPIANY et al., 2019). The solid and diameter determination (whether in-situ or not) and the bias related to laboratory analysis.

In this context, the most challenging factor in laboratory analysis was regarding the low solid concentration in most of the campaigns in the Passauna system (which were about $10mg/L$ to $70mg/L$, with a spike during the rainy event of $160mg/L$ and $209mg/L$, in the reservoir and in the river, respectively). On the other hand, although laborious in Taquari River the laboratory analysis didn't represent a challenge due to its high solid concentration and mostly sand content.

Although it is known that the transmitted power can influence on the emitted signal, thus in the corrections, this factor was not considered in the calibrations because the differences in the voltage of the ADCP within the campaigns were considered low: $1.8volts$ at Taquari River measurements, $4.48volts$ at Passauna River measurements and $5.83volts$ at Passauna Reservoir measurements. Nevertheless, this is an important parameter to take into account, since differences observed by Szupiany et al. (2019) was in the order of $17.76volts$, which combined to the electric current variation has produced an underestimation of 68% in the sand concentration estimative.

In rivers, extrapolations play an important role in the TSS estimative. This was also observed by Haun and Lizano (2016) in a lentic environment, although any operational extrapolation was conducted by that study, due to the difficulties also founded at Passauna reservoir on the establishment and operationalization of such extrapolations, due different patterns intrinsic to lentic places. Also, another factor that must be considered by following Taquari River results is that even when sand content is more expressive the correction for fines must be taken into account in the calibration, such finds were also highlighted by Moore et al. (2013) and Szupiany et al. (2019).

From Passauna Reservoir results, it is possible to understand that mainly in lentic environments the average of the mapping at the cross-section it is not a good metric to determine the differences between laboratory measurements and the estimate of the concentration of solids obtained by ADCP. From each mapping (see the whole set of mapping result Figures at Appendix D)it is possible to observe that most of the laboratory analysis matches, not only in relative terms but also in absolute terms (in some points), to the equivalent depth point within the mapped cross-section. This is true mainly when

major variations are observed (by the ADCP) in the cross-section, reinforcing the fact that point measurements are not able to indicate solid variations, therefore characterize the whole cross-section.

Lentic systems are ruled by hydrodynamic forces, such as temperature variations due to interactions between atmospheric factors (pressure, heat, wind, etc) and the water column or between the water column and the bed, among others. Since it is not a flow velocity driven system, any disturbance can influence and cause different patterns in the solid distribution in the water column. These kinds of variations may have an effect on the acoustic signal, as observed in the mapped situation on $20Oct/18$ and $Apr/19$, when the vessel was launched from the margin.

Because water density variations (driven either by temperature or solid) can affect the acoustic signal (SZUPIANY et al., 2019), it was possible to observe variations in the longitudinal transections. The solid concentration gradient identified was about $50mg/L$ in Feb/18 to about $100mg/L$ in Feb/19 and the observation of some nuances (about $20mg/L$) in the longitudinal transect of 20Oct/18. Such values were different from other studies observed by Morris and Fan (1998), where the density current was characterized also by a high solid concentration ($41000mg/L$ and $72000mg/L$).

Although it is difficult to establish a quantitative threshold in the density or turbidity current definition, it is a fact that there is a solid plume identified by the ADCP coming into the reservoir and driven by the velocities produced by differences in temperature of the incoming flow. Such a statement is supported by the temperature profiles measured in the field campaigns (showed from Figures 49 to 52) and in the findings produced by others researches at Passauna reservoir in the frame of Mudak Project (see the previous section).

Also, the comparison within other findings, indicate that the technologies can complement each other. Considering that vertical profiles can detect variations within the water column and fill the information that it is missing with remote sensing. The opposite statement is also true because remote sensing provides information about the water surface that is not possible with the ADCP or another local sensor. In addition, the combination of these technologies can be used for calibration and validation of numerical models that further can be set for diagnostic and scenario models.

5.4.1 Summary

In this section, considering the methodology adopted for the rivers, it was presented the results for Passauna Reservoir.

The reservoir is considered a lentic environment with different conditions of the previously analyzed systems — a combination of hydraulic and hydrodynamic conditions,

highly cohesive solid fractions (silt-clay), the presence of organic matter, among others. Such characteristics can influence the formation of the aggregates (among these aggregates have also the combination of mineral+organic matter) that will behave differently from the essential solid composed only by mineral particles in lotic environments.

As observed in the mapping results, and confirmed by the comparison of other researchers in the same area, the ADCP and the adopted correction methods applied were able to see the gradients in the Ferraria Bridge cross-section and in the longitudinal transects.

6 Conclusion and Outlook

The objective of this study was to assess the feasibility and limitations of using acoustic surrogate technologies using a down-looking moving ADCP to map solid concentration and transport characteristics in a lentic environment.

It has been presented a correlation method between acoustic measurements and solid concentrations to obtain and compare solid concentration information within lotic and lentic environments. The main idea was to check if the lotic environment methodology could be enhanced and extended to the lentic environment in order to study its dynamics – such as turbidity or density current formation, considering all the differences between the presented systems.

Main outcomes of this study were:

- Improvements of using down-looking moving ADCP measurements for solid transport analysis in lotic environments
- Development of a post-processing methodology for down-looking moving ADCP measurements for solid transport analysis in lentic environments.
- Development of mapping algorithms of concentration distributions measured by ADCPs
- Description of dominant solid transport characteristics and flow paths

6.1 Improvements for solid measurements in a Lotic Environment

Considering that the ADCP measurements have met the quality criteria for discharge evaluation, such as the measurement of vertical profiles for moving bed evaluation and correct cross-section measurement settings, it was possible to apply the methodology described at Landers et al. (2016) and Guerrero et al. (2016), both based on the modified sonar equation proposed by Urick (1975), to obtain the correlation between the corrected ADCP signal and the measured SS.

Lessons learned, limitations and findings for the river environments were:

- Besides the corrections applied to the raw signal, it was noticed that the difference of 5% in SNR estimated using the ADCP's Fixed Frequency and Smart-Pulse modes did not significantly affect the correlation curve and resulting estimated SSC.
- Regarding the mapping extrapolations (bed, surface, and banks) applied to the ADP measurements, the results indicated a small difference in the SSC, about 3%

between $CBS_{extrapolated}$ and $CBS_{no-extrapolated}$. On the other hand, such differences were much greater when comparing sediment load, about 63% different, which indicates the importance of considering the extrapolations mainly when estimating suspended load, showing the importance of considering the extrapolation on the non-measured areas.

- The results also indicated that past survey data can be post-processed to map suspended solid concentration patterns over the measured cross-section. In addition, obtained correlations can be used when future ADCP measurements are made at the same cross-sections, even without sampling.

- The application of the methodology for the Passauna river showed the importance of the analysis and consideration of the viscous term, in the solid corrections, mainly during the extreme event monitoring, when the presence of fines was more significant. Regarding the comparison between a surrogate and conventional TSS, it was observed that on average the differences were about 2% between laboratory and TSS from ADCP. The differences were bigger in the suspended load estimative, about 17% between laboratory and ADCP.

6.2 Development of the method for Lentic Environment

In the lentic system, with mostly fine and cohesive solid content and a totally different dynamics compared to the lotic system, the results showed that the ADCP was able to detect different gradients related to the suspended solids within the monitored cross-section and longitudinal transects. However, for this environment, a weaker agreement between the surrogate and conventional analysis was observed.

A major finding was the ability of the method being able to detect a solid plume driven by a density current formation, which allows describing the interflow and underflow characteristics as dominant solid transport pathway.

Such outcomes are supported by the comparison with thermal variations from upstream to downstream, wherein most of the campaigns it was observed a stratification pattern that comes from the inflow to the reservoir, and by the observation of the sedimentation rates and patterns observed by Ono (2019) and Sotiri, Hilgert and Fuchs (2019).

The weaker agreement between conventional and surrogate technology in the lentic system can be associated with uncertainties when comparing in-situ with sampled laboratory, especially when related to low solid concentrations. Furthermore, uncertainties related to the system and the application of the sensor analysis should be considered: due to the low concentrations and low flow velocities, a minimal disturbance caused by a small leaf, or by wind, or the simple movement of the boat can create noise that will be

easily computed by the ADCP signal and therefore in the corrections and correlations. To overcome those sensitivities, several repetitions of stationary measurements showed advantages by using statistical analysis in post-processing, which was not possible with the few conventional samples.

Also, it is necessary to consider that the solid content in the lentic environment is composed mostly of fine and cohesive particles which will favor the aggregation. Although the fine particles are considered in the formulations as the viscous term (α_{sv}), still the effects of the interaction between sound waves and the flocs are not fully known.

Lessons learned and limitations and advantages are:

- One difficulty of the ADCP application to this place was the extrapolation of the unmeasured zones (surface, banks and bed), as it was done in the lotic environments. Also, information about velocities in the reservoir were often not reliable, due to low flow velocities characteristic of those places, which made impossible to compute load values that coming into the reservoir.

- Due to the use of moving ADCP, the spatial, as well as the temporal resolution, could be increased in all study sites. In the reservoir, moving ADCP has the advantage to track the solid plume and follow its development into the system.

- In addition, obtained correlations can be used when future ADCP measurements are made at the same cross-sections, even without sampling, either in the lotic or lentic environment. Overall, though, care should be taken to only apply the correlation and estimate suspended solids characteristics (particularly grain size) and sources are reasonably similar to those present when the correlation was developed. The mapping also allows for an improved understanding of solid transport processes, as it includes highly resolved velocity and geometrical information, all measured at the same instant of time.

- Also, since it is a site-specific methodology, each method will have a particular application case and probably will be difficult to apply the same developed methodology to all environments in the natural environment. Thinking of it, it is not the aim of the development of the surrogate technologies to replace entirely the conventional analysis, but to complement it in order to obtain more temporal and spatial data resolution.

- Although initially this technology requires some investment to be established, once the state, the manager or the responsible institutions know some particularities of its environments, with a trained staff and setup devices, the applicability of such methods for a long term will become cheap, reducing time and efforts and increasing the information access. Which will allow a faster and accurate decision making.

6.3 Recommendation for future work

The analysis done in this study indicated that the fine solid fractions and therefore its flocculation dynamics between aggregation and disaggregation play an important role in the ADCP response. For instance, the solid particle formed by a floc is not as rigid as a solid formed by a pure mineral, and probably, it will represent a different interaction between the sound wave and the floc. Certainly, more studies need to be addressed to the interaction between the aggregates and the ADCP signal as well the fine fraction, taking into account the solid attenuation factor in order to improve the ADCP response in places where fine contents are more expressive.

In this sense, regarding the sampling collection itself it is indicated that, if possible, the granulometric analysis be done in-situ right after the ADCP static measurements, mainly in environments with high cohesive content. Due to its cohesiveness, when subjected to sampling, transportation and laboratory analysis preparation, the flocs that were previously observed in-situ by the ADCP, can be destroyed and therefore the correction will be done for another diameter, different from the diameter captured by the ADCP.

Also, more efforts should be addressed to the obtention of the sensitivity analysis and uncertainties on the solid concentration estimated from ADCP, such analysis and estimative could make it more reliable in the way of its operational application.

Bibliography

ANA. Hidroweb: Hydrological information system (snirh). *Brazilian Nacional Water Agency*, 2019. Available at: <http://www.snirh.gov.br/hidroweb/>.

ANA. National hydrometheorological network (rede hidrometeorológica nacional). *Brazilian Nacional Water Agency*, 2020. Access on July 20th, 2020. Available at: <http://dadosabertos.ana.gov.br/datasets/8014bf6e92144a9b871bb4136390f732_0-/data)>.

APHA. *Standard Methods for the Examination of Water and Wastewater*. [S.l.]: Amer Public Health Assn, 1999. ISBN 0875532357.

BAGNOLD, R. A. An approach to the sediment transport problem for general physics. *USGS Professional Paper*, 1966.

BARANYA, S.; JÓZSA, J. Estimation of suspended sediment concentrations with adcp in danube river. *Journal of Hydrology and Hydromechanics*, Walter de Gruyter GmbH, v. 61, n. 3, p. 232–240, sep 2013.

BOCALON, T. S. *Estudos de sedimentos do Rio Passauna com enfase na determinação de metais pesados*. Dissertação (Mestrado) — Environmental Management, 2007.

CARVALHO, N. *Hidrossedimentologia prática*. Rio de Janeiro: Editora Intercieência, 2008. ISBN 9788571931817.

CARVALHO, N. de O. et al. *Reservoir sedimentation assesment guideline*. [S.l.], 2000.

CARVALHO, N. de O. et al. *Sedimentometric Practices Guide*. [S.l.], 2000.

COQUEMALA, V. *Variacao anual do fitoplancton no reservatorio do Passauna, Parana*. Dissertação (Mestrado) — Biologic Sciences, 2005.

CORTéS, A. C. *Splitting Gravity Currents in Stratified Systems*. Tese (Doutorado) — Departamento de Ingeniería Civil e Instituto de Investigación del Agua - Universidad de Granada, Granada, 2014.

CZUBA, J. A. et al. Comparison of fluvial suspended-sediment concentrations and particle-size distributions measured with in-stream laser diffraction and in physical samples. *Water Resources Research*, v. 51, p. 320–340, 2015.

DAVIES, E. J. et al. Scattering signatures of suspended particles: An integrated system for combining digital holography and laser diffraction. *Optical Express*, v. 19, n. 25, dez. 2011.

DEINES, K. L. Backscatter estimation using broadband acoustic doppler current profilers. In: *IEEE Working Conference on Current Measurement*. [S.l.: s.n.], 1999.

D.THORNE, P.; RAMAZANMERAL. Formulations for the scattering properties of suspended sandy sediments for use in the application of acoustics to sediment transport processes. *Continental Shelf Research*, v. 28, p. 309–317, 2008.

EDWARDS, T. K.; GLYSSON, D. G. *Field Methods for Measurement of Fluvial Hidrossedimentology*. [S.l.], 1988.

EMBRAPA. *Manual de métodos de análise de solo / Centro Nacional de Pesquisa de Solos*. 2. ed.. ed. [S.l.], 1997.

EMMANUEL, B. O. S. S. et al. Validation of the particle size distribution obtained with the laser in-situ scattering and transmission (lisst) meter in flow-through mode. *Optics Express*, v. 26, n. 9, abr. 2018.

ENGELUND, F.; HANSEN, E. *A Monograph on Sediment Transport in Alluvial Streams*. [S.l.]: Teknisk Forlag, 1967.

FELIX, D.; ALBAYRAK, I.; BOES, R. Laboratory investigation on measuring suspended sediment by portable laser diffractometer (lisst) focusing on particle shape. *Geo-Marine Letters*, v. 33, p. 485–498, 2013.

FELIX, D.; ALBAYRAK, I.; BOES, R. In-situ investigation on real-time suspended sediment measurement techniques: Turbidimetry, acoustic attenuation, laser diffraction (lisst) and vibrating tube densimetry. *International Journal of Sediment Research*, v. 33, p. 3–17, 2017. Available at: <https://doi.org/10.1016/j.ijsrc.2017.11.003>.

FISCHER, H. B. et al. *Mixing in Inland and Coastal Waters*. [S.l.]: Academic Press, 1979.

FLAMMER, G. H. *Ultrasonic Measurement of Suspended Sediment*. [S.l.], 1962.

GALLOWAY, J. M.; EVANS, D. A.; GREEN., W. R. *Comparability of Suspended-sediment Concentration and Total Suspended-solids Data for Two Sites on the L'anguille River, Arkansas, 2001 to 2003*. [S.l.], 2005.

GAMARO, P. E. *Medidores Acústicos Doppler de Vazão*. [S.l.]: Iatipu Binacional, 2012. ISBN ISBN 978-85-85263-07-2.

GARTNER, J. W. Estimating suspended solids concentrations from backscatter intensity measured by acoustic doppler current profiler in san francisco bay, california. *Marine Geology*, v. 211, p. 169–187, 2004.

GODOY, R. F. B. *Dinamica Da Qualidade Da Agua Em Reservatorio De Abastecimento Publico: Estudo De Caso Do Passauna,PR*. Dissertação (Mestrado) — Water Resources and Environmental Engineering Graduate Program, 2017.

GRAF, W. H. *Hydraulics of Sediment Transport*. [S.l.]: Water Resources Publications, 1984.

GRAF, W. H. *Fluvial Hydraulics - Flow and Transport Processes in Channel of Simple Geometry*. [S.l.]: John Wiley & Sons Ltd, 1998.

GUERRERO, M. et al. The acoustic properties of suspended sediment in large rivers: consequences on adcp methods applicability. *Water*, v. 8, n. 1, p. 13, jan. 2016.

GUERRERO, M.; RüTHER, N.; SZUPIANY, R. N. Laboratory validation of acoustic doppler current profiler (adcp) techniques for suspended sediment investigations. *Flow Measurement and Instrumentation*, 2012.

GUERRERO, M.; SZUPIANY, R.; AMSLER, M. Comparison of acoustic backscattering techniques for suspended sediments investigation. *Flow Measurement and Instrumentation*, Elsevier BV, v. 22, n. 5, p. 392–401, oct 2011.

HALLIDAY, D.; RESNICK, R. *Fundamentals of Physics*. 8th. ed. [S.l.]: LTC, 2009. v. 2.

HAUN, S.; LIZANO, L. River flow. I n: . London: Taylor & Francis, 2016. cap. Evaluation of a density currenty by using ADCP backscatter data and LISST measurements, p. 875,881.

HAUN, S.; LIZANO, L. Sensitivy analysis of sediment flux derived by laser diffraction and acoustic backscatter within reservoir. *International Journal of Sediment Research*, p. 18–26, 2018.

KLASSEN, I. *Three-dimensional Numerical Modeling of Cohesive Sediment Flocculation Processes in Turbulent Flows*. Tese (Doutorado) — Civil Engineer-, Geo and Environmental Sciences - Karlsruhe Institute of Technology, 2017.

LANDERS, M. N. et al. *Sediment Acoustic Index Method for Computing Continuous Suspended Sediment Concentrations*. [S.l.], 2016. Available at: <http://dx.doi.org/10-.3133/tm3C5.>

LANE, E. W. Report of the subcommittee on sediment terminology. *Transactions, American Geophysical Union*, American Geophysical Union (AGU), v. 28, n. 6, p. 936, 1947.

LATRUBESSE, E.; STEVAUX, J.; SINHA, R. Tropical rivers. *Geomorphology*, Elsevier BV, v. 70, n. 3-4, p. 187–206, sep 2005.

LIMA, J. E. F. W. et al. *Diagnostico do fluxo de sedimentos em suspensao na Bacia do Rio Sao Francisco*. [S.l.], 2001.

MEGER, D. G. *Material Particulado Suspenso e Macroconstituintes Ionicos em um Reservatorio de Abastecimento: o caso do Rio Passauna, Curitiba, Parana,Brasil.* Dissertação (Mestrado) — Positivo University, 2007.

MEYER-PETER, E.; MüELLER, R. Formulas for bed-load transport. In: *International Association for Hydaraulic Structures Research*. [S.l.: s.n.], 1948.

MONTANHER, O. C.; NOVO, E. M. L. ao de M.; BARBOSA, C. C. F. Modelos para estimativa da concentração de sedimentos em suspensão em rios amazônicos de águas brancas via sensoriamento remoto. In: *Anais XVI Simpósio Brasileiro de Sensoriamento Remoto - SBSR*. [S.l.: s.n.], 2013.

MOORE, S. A. et al. Using multi-frequency acoustic attenuation to monitor grain size and concentration of suspended sediment in rivers. *The Journal of the Acoustical Society of America*, Acoustical Society of America (ASA), v. 133, n. 4, p. 1959–1970, apr 2013.

MORRIS, G. L.; FAN, J. *Reservoir Sedimentation Handbook: Desining and Management of Dams, Reservoirs and Watershed for Sustainable Use*. [S.l.]: The McGraw-Hill Companies, Inc, 1998.

MOSBRUCKER, A. R. et al. *Estimating Concentrations of Fine-grained and Total Suspended Sediment from Close-range Remote Sensing Imagery*. [S.l.], 2015.

MUELLER, D. S. et al. Measuring discharge with acoustic doppler current profilers from a moving boat - techniques and methods. In: _____. [S.l.]: USGS, 2013. cap. 22, p. 116.

OLIVETTI, D. *CÂMERAS MULTI E HIPERESPECTRAL AEROTRANSPORTADAS: CONTRIBUIÇÕES PARA MONITORAMENTO DE QUALIDADE DE ÁGUAS CONTINENTAIS*. Tese (Doutorado) — Brasilia Federal University (UNB), 2020.

ONO, G. M. Monitoramento e análise da sedimentação no reservatório Passauna-PR. Document presented as partial exam to obtain the Master of Science degree. 2019.

PITRAT, D. M. J. J. *Avaliacao Da Contaminacao Por Metais Em Rios: Estudo De Caso Da Bacia Do Rio Passauna.* Dissertação (Mestrado) — Hydric resources and Environmental Engineering, 2010.

RAUEN, W. B.; CASTRO, C. O. de; SILVA, M. G. da. Caracterização hidrossedimentologica do rio passauna, pr, brasil, a partir de dados históricos. In: *XX Simposio Brasileiro de Recursos Hídricos*. [S.l.: s.n.], 2017.

RD-INSTRUMENTS. *Acoustic Doppler Current Profiler Principles of Operation a Practical Primer.* [S.l.], 2011.

RIJN, L. C. van. Sediment transport, part i: Bed load transport. *Journal of Hydraulic Engineering*, 1984.

ROIG, H. L. et al. Uso de câmeras de baixo custo acopladas a veículos aéreos leves no estudo do aporte de sedimentos no lago paranoá. In: INPE. *Anais XVI Simpósio Brasileiro de Sensoriamento Remoto - SBSR*. [S.l.], 2013.

RUBEN, L. D. et al. Acoustic sediment estimation toolbox (ASET): A software package for calibrating and processing TRDI ADCP data to compute suspended-sediment transport in sandy rivers. *Computers & Geosciences*, Elsevier BV, p. 104499, apr 2020.

SABESP. *Norma Técnica Interna SABESP-NTS13.* [S.l.], 1999.

SALGADO, M. S. K.; RAUEN, W. B. *Coleta E Analise De Sedimentos Do Reservatorio Do Passauna.* [S.l.], 2014.

SANEPAR. *Plano Diretor SAIC - Sistema de Abastecimento de água Integrado de Curitiba e Região Metropolitana.* [S.l.], 2013.

SANTOS, B. B. D. et al. Evaluation of the laser diffraction method for the measurement of suspended sediment concentration in mogi-guassu reservoir/sp. brazil. *International Journal of River Basin Management*, Informa UK Limited, v. 17, n. 1, p. 89–99, mar 2018.

SANTOS, I. dos et al. *Hidrometria Aplicada.* [S.l.]: CEHPAR - Centro de Hidráulica e Hidrologia Prof. Parigot de Souza, 2001.

SAUNITI, R. M.; FERNANDES, L. A.; BITTENCOURT, A. V. L. The study of passauna's river barrage with its reservoir sedimentation, curitiba-pr. *Boletim Paranaense de Geociências*, v. 54, p. 65–82, 2004.

SCHULKIN, M.; MARSH, W. H. Sound absorptionin sea water. *Journal of the Acoustical Society of America*, 1962.

SEQUOIA. *LISST-100x Particle Size Analyzer*. [S.l.], 2015.

SEQUOIA. *LISST-200x Particle Size Analyzer*. [S.l.], 2018.

SEQUOIASC. *Processing LISST-100 and LISST-100x Data in Matlab*. 2015. Online. Available at: <https://www.sequoiasci.com/article/processing-lisst-100-and-lisst-100x-data-in-matlab/>.

SEQUOIASC, I. *Laser Diffraction Principles*. 2017. Online. Available at: <http:/-/www.sequoiasci.com/article/laser-diffraction-principles/>.

SHIELDS, A. *Application of Similarity Principles and Turbulence Research to Bed-load Movement*. [S.l.], 1936.

SHOTBOLT, L. A.; THOMAS, A. D.; HUTCHINSON, S. M. The use of reservoir sediments as environmental archives of catchment inputs and atmospheric pollution. *Progress in Physical Geography: Earth and Environment*, v. 29, n. 3, p. 337–361, set. 2005.

SIH. Hydrological system information. *Parana State Water Agency*, 2019. Available at: <http://www.aguasparana.pr.gov.br/pagina-264.html>.

SONTEK. *RiverSurveyor S5/M9 System Manual Firmware Version 4.02*. [S.l.], 2016.

SOTIRI, K.; HILGERT, S.; FUCHS, S. Sediment Classification in a Brazilian Reservoir: Pros and Cons of Parametric Low Frequencies. *Advances in Oceanography and Limnology*, PAGEPress, v. 10, n. 1, may 2019.

SUEKAME, H. K. Avaliação dos processos hidrológicos e sedimentológicos de uma bacia hidrográfica. Thesis. 2020.

SZUPIANY, R. N. et al. Estimating sand concentrations using ADCP-based acoustic inversion in a large fluvial system characterized by bi-modal suspended-sediment distributions. *Earth Surface Processes and Landforms*, Wiley, v. 44, n. 6, p. 1295–1308, jan 2019.

TERABE, F. R. *Estudo Sobre O Uso Do Perfilador Acústico De Corrente Por Efeito Doppler (adcp) Para Medição Do Transporte Sólido Em Suspensão.* Dissertação (Mestrado) — Federal University of Parana, 2004.

UMEDA, M.; YOKOYAMA, K.; ISHIKAWA, T. Observation and simulation of floodwater intrusion and sedimentation in the shichikashuku reservoir. *Journal of Hydraulic Engineering*, p. 881–891, set. 2006.

URICK, R. J. *Principles of Underwater Sounds*. [S.l.]: Mc Graw Hill, 1975.

USBR. *Erosion and sedimentation manual*. [S.l.]: Denver, Colo. : U.S. Dept. of the Interior, Bureau of Reclamation, Technical Service Center, Sedimentation and River Hydraulics Group ; Washington, DC : For sale by the Supt. of Docs., U.S. G.P.O., 2006.

WAGNER, A. *Event-Based Measurement and Mean Annual Flux Assessment of Suspended Sediment in Meso Scale Catchments*. Tese (Doutorado) — Karlsruhe Institut für Technologie, 2019.

WOOD, M. Workshop at ii hydrosedimentology international conference. In: *The Sediment Acoustic Index Method and SAID Tool*. [S.l.: s.n.], 2017.

WOOD, M.; GARTNER, J. *Use of Acoustic Backscatter and Vertical Velocity to Estimate Concentration and Dynamics of Suspended Solids in Upper Klamath Lake, South-central Oregon: Implications for Aphanizomenon Flos-aquae.* [S.l.], 2010.

WOOD, M.; TEASDALE, G. N. *Use of Surrogate Technologies to Estimate Suspended Sediment in the Clearwater River, Idaho, and Snake River, Washington.* [S.l.], 2013.

WOOD, M. S. et al. Measuring suspended sediment in sand-bedded rivers using down-looking acoustic doppler current profilers. In: *Joint Federal Interagency Sedimentation and Hydrologic Modeling Conference*. [S.l.]: SEDHYD, 2019. p. 15.

WOSIACKI, L. F. et al. Suspended sediment estimate through an adcp analysis - study case: Taquari river, pantanal, brazil. In: *ANAIS III ENES/I PIA*. [S.l.]: ABRH, 2018.

YANG, C. T.; STALL, J. B. *Unit Stream Power for Sediment Transport in Natural Rivers.* [S.l.], 1974.

Appendix

APPENDIX A – ADP-M9 Backscatter Attenuation Corrections

At this appendix it is shown step-by-step the SNR attenuation model applied to the ADCP backscatter.

The ADCPs use the Sonar equation proposed by Urick (1975 apud GAMARO, 2012) to obtain the difference between emitted and reflected signal. This relation tells us the amount of sound reflected back towards the equipment until the emitted signal reaches a target, considering all the losses along the way — e.g. spreading, absorption and attenuation losses. After some arrangements, it can be written as the equation 2.5, presented at Chapter 2, as follow:

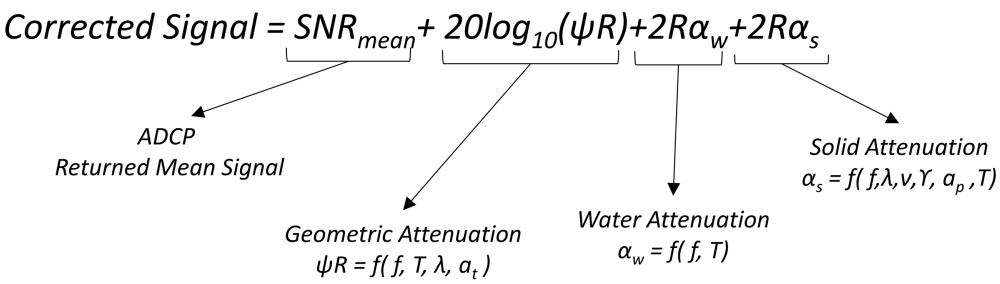

Here we have that the corrected signal is a function from the mean spread signal (geometric attenuation) and the attenuation due the water and solid. Each one of these attenuation terms can be expressed mathematically as function of the equipment, eg: frequency, wavelength, transducer ratio, or as a function of the medium, eg: water temperature, water viscosity, solid diameter, solid and water density (specific gravity).

At this equation, the SNR_{mean} is the simple average of the 4 ADCP transducers. The second term from the equation, given by $20\log(\psi R)$ is the geometrical attenuation term, related to the spherical spread of the beam — Baranya and Józsa (2013). R is the slant distance from transducert head to the measured bin, in meters. The coefficient ψ is a correction factor related to the effect of spherical spreading close to the transducer:

$$\psi = \left(\frac{1+1.35Z+(2.5Z)^{3.2}}{1.35Z+(2.5Z)^{3.2}}\right), \quad Z = \frac{R}{R_{critical}}, \tag{A.1}$$

where $R_{critical}$ is the critical range which is function of the transducer radius, a_t, in cm and the wave length, λ, as follows:

$$R_{critical} = \frac{\pi a_t^2}{\lambda} \tag{A.2}$$

The approach for water absorption (α_w) is given by the relation presented by Schulkin and Marsh (1962 apud BARANYA; JÓZSA, 2013) in the Equation A.3.

$$\alpha_w = 8.687 \left(\frac{3.38 \cdot 10^{-6} f^2}{f_T}\right), \quad f_T = 21.9 \cdot 10^{\left(6 - \frac{1520}{273+T}\right)}, \tag{A.3}$$

where f is the instrument frequency, f_T is the relaxation frequency, which depends on the Temperature, T, in $^{\circ}C$.

As pointed out by Flammer (1962), attenuation from suspended solid consists of a viscous-loss (α_{sv}) component and a scattering-loss (α_{ss}) component. Depending on the ADCP frequency the attenuation due to solid will play a role only in particle under certain diameters.

As highlighted by Baranya and Józsa (2013): the lower the particle diameter, the bigger the viscous loss. On the other hand: the bigger the particle diameter, the bigger the scattering loss.

The solid attenuation loss term,α_s can be estimated as presented by Guerrero et al. (2016), based on the formulation proposed by D.Thorne and RamazanMeral (2008):

$$\alpha_s = \alpha_{ss} + \alpha_{sv} \tag{A.4}$$

where:

$$\alpha_{ss} = \frac{3\chi \cdot SSC}{4 \cdot a_p \rho_s}, \tag{A.5}$$

$$\alpha_{sv} = TSS \cdot K \frac{(\sigma - 1)^2}{2\rho_s} \cdot \frac{S}{S^2 + (\sigma + \varsigma^2)} \tag{A.6}$$

where α_s is the solid attenuation, α_{ss} is the solid scattering attenuation and α_{sv} is the solid viscous attenuation all parameter in Db units. TSS is the total suspended solid in mg/L, a_p is particle radius, K is known as the wave number, given by:

$$K = \frac{2\pi}{\lambda}, \tag{A.7}$$

σ is the relative density given by the relation between solid density, ρ_s and the fluid density, in this case, water density, ρ_w, according to Equation A.8.

$$\sigma = \frac{\rho_s}{\rho_w}, \tag{A.8}$$

where ρ_w can be obtained by the UNESCO approach (equation A.9) presented at Fischer et al. (1979).

$$\rho_w = 999.842594 + 6.793952 \cdot 10^{-2} \cdot T - 9.09529 \cdot 10^{-3} \cdot T^2 + 1.001685 \cdot 10^{-4} \cdot T^3 - 1.120083 \cdot 10^{-6} \cdot T^4 + 6.536332 \cdot 10^{-9} \cdot T^5 \quad \text{(A.9)}$$

where T is the water temperature in $^{\circ}C$. χ, from equation A.10 is equal to:

$$\chi = \frac{0.29x^4}{0.95 + 1.28x^2 + 0.25x^4} \quad \text{(A.10)}$$

where:

$$x = K \cdot a_p \quad \text{(A.11)}$$

ς is equal to:

$$\varsigma = 0.5 + \frac{9}{4\gamma} \quad \text{(A.12)}$$

γ is equal to:

$$\gamma = \sqrt{\frac{\pi \cdot 1000f}{\nu}} \quad \text{(A.13)}$$

where $\nu = 1.0 \cdot 10^{-6}\ m^2/s$ is the water viscosity. The parameter S, from Equation A.5, is equal to:

$$S = \left[\frac{9}{(4\gamma \cdot a_p)}\right]\left[1 + \frac{4}{(\gamma \cdot a_p)}\right] \quad \text{(A.14)}$$

In the Equation A.4, the first term is related to the attenuation from viscous losses and the second term is related to the scattering losses.

APPENDIX B – LISST-200X Processing Analysis

At this Appendix it will be present the processing steps and analysis of the LISST-200x to obtain the granulomnetric curve.

B.1 In-situ technique and data treatment

The field practice for LISST-200x measurement require a background file for the correct field measurement. In this sence, the background file was measured only once, right before the beginning of the measurement campaign. During the field measurements, the LISSTs were released in the same depth where the water was sampled for laboratory analysis.

The measurements were done by leaving the equipment stand for some minutes (between 2 - 4 minutes) at each depth in order to stabilize the sensors to improve the measurements and create more data at the same location to be used in the final average for sediment estimative and characterization.

During operation, the output from the diffracted laser beam, optical transmission, pressure sensor and water temperature are recorded as raw data and can be downloaded and processed later on for granulometry and total volume concentration.

Together with the LISST instruments it is provided the SOP software that can be used for post-processing analysis. Also, the manufacturer provides specifics Matlab routines that make the inversions and all calculations to obtain the volumetric concentration and therefore the granulometric distribution over the classes of different types of the LISST instrument series.

Since the instrument can be affected by a range of factors intrinsic to the environment and the handling, it is necessary to consider some criteria and filtering to obtain better and reliable results. In this sense it is not uncommon to clear some data from the results if it is considered an outlier or if the measurement was done under suspisious circunstances – eg. too turbidy or too clean water.

B.2 Sensor Corrections

The filtering processing considered the instructions from the manufacturer regarding the Transmission parameter, T. According to Sequoia (2018), if the transmission is $0.100 > T > 0.995$, the data must to discarded. For T values lower than 0.300 and greater than 0.980, the manufacturer indicates wary on these data. So, in this study the criterion

was tighter and all T values: 0.300>T>0.980, were discarded. Figure 58 exemplifies the transmission for one data set from Passauna reservoir.

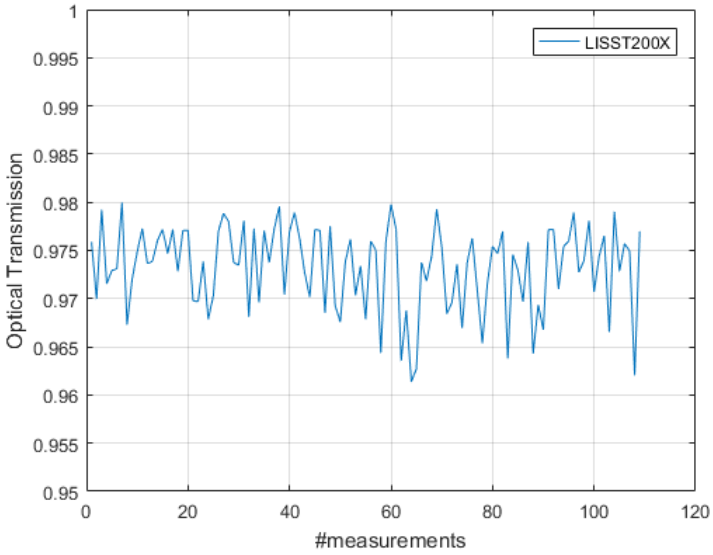

Figure 58 – Optical Transmission.

After filtering all data out of the T range, the quantile method (Q1 – 25% and Q3 – 75%) was applied to the data set, followed by the move mean technique, with a window length of 5, to avoid outliers and abrupt variations in the data to be analyzed (Figure 59).

These corrections are important to avoid possible non-representative particle that could cross the laser path during the measurement. For the post-processing analysis was considered the "random shaped" particles inversion model. The granulometric curve was

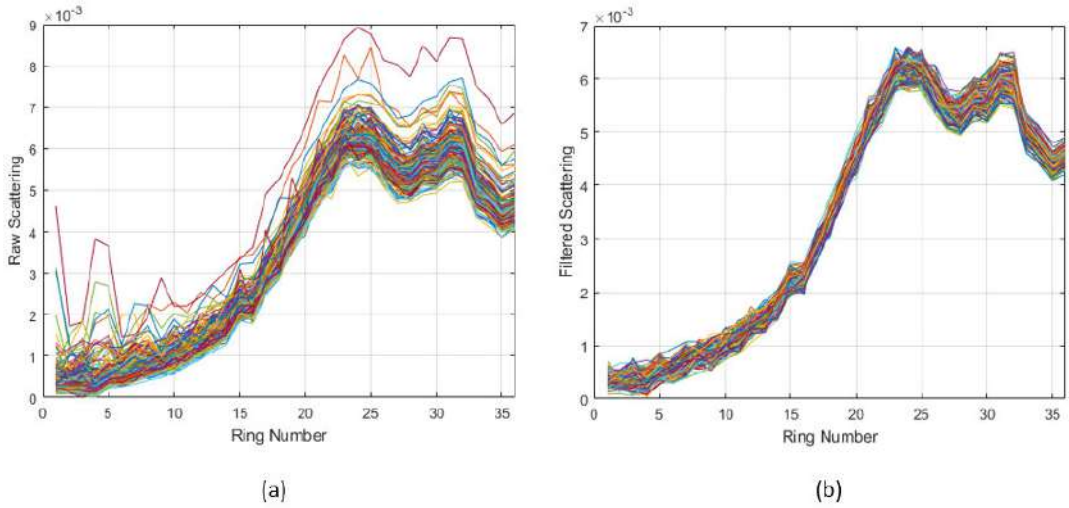

Figure 59 – Scattering Data for LISST200x (a) before and (b) after the filtering application.

computed by linear interpolation of the cumulated volumetric concentration values in each class for both equipment.

APPENDIX C – ADP-M9 Verification of frequency at different operation modes

At this appendix it is shown the relative error between the correlation obtained with the filtration of 3MHz frequency extrated from measurements made with Smart Pulse mode and the correlation obtained with 3MHz measurement (Fixed Frequency mode).

The static ADP measurements were conducted at 6 verticals over the Taquari River cross section in the SPM. During post-processing, only the data recorded by the 3MHz beams in each cross section and vertical were used in the solid determination calculations, avoiding all the 1MHz cells.

In order to test whether removing the 1MHz data had a significant impact on the amount of data available and quality of the solid correlations, one extra measurement was conducted during the last campaign (Jan/2018) using the FFM (3MHz) in addition to the regular measurement made with the SPM. The measurements made with the SPM was filtered to obtain only the 3MHz data.

Table 20 shows the mean signal (SNR_{mean}) for the FFM and SPM and the relative difference between them, which were about 5% on average. The results indicate that SNR_{mean} was higher using the SPM than the FFM in all verticals.

Table 20 – Relative Error between the Smart Pulse and Fixed mode – comparison between 3MHz.

Vertical	Frequency Mode	Mean SNR (dB)	Mean Difference
V1	3 MHz – Fixed Mode	64.53	4%
	3 MHz – Smart Pulse	67.28	
V2	3 MHz – Fixed Mode	59.13	8%
	3 MHz – Smart Pulse	64.10	
V3	3 MHz – Fixed Mode	65.35	3%
	3 MHz – Smart Pulse	67.59	
V4	3 MHz – Fixed Mode	64.68	4%
	3 MHz – Smart Pulse	67.31	
V5	3 MHz – Fixed Mode	63.09	5%
	3 MHz – Smart Pulse	66.37	
V6	3 MHz – Fixed Mode	60.38	5%
	3 MHz – Smart Pulse	63.71	
Average	-	-	5%

These results itself indicated that if the measurements were taken with the FFM (as usually done in all aforementioned studies), on average, the corrected signal strength would be lower than those collected in the SPM. Thus, as will be further explained, test scenarios were created considering the subtraction of 5% over the SNR_{mean}, in order to check its influence on the correlation curve and on the estimated SSC.

It was created two scenarios two evaluate the influence of this 5% difference on the correlation curve:

- Figure 60a is the regression line built with all corrections mentioned: Smart Pulse filtering and total solid attenuation — hereinafter called CBS1
- Figure 60b considered the same approach as in Figure 60a, but with a -5% correction applied to the raw measured mean SNR data due the Smart Pulse filtering — hereinafter called CBS2.

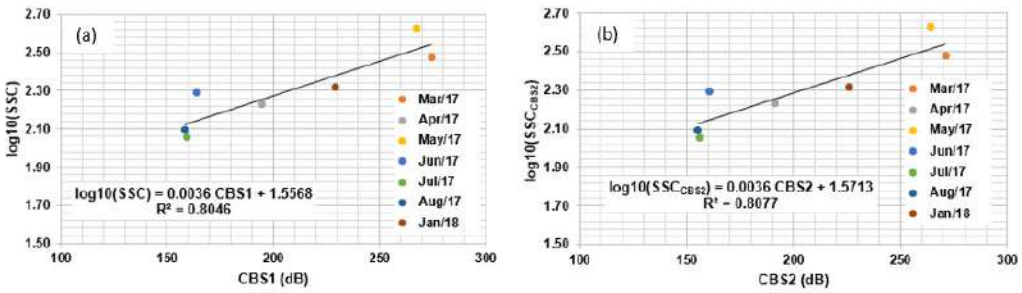

Figure 60 – Mean discharge and mean solid concentration during the field campaigns.

As we can observe from the equations of the regression lines in fig.6, there is no significant difference between CBS1 and CBS2 regressions, meaning that the SmartPulse filtering had little effect on the final results.

Which means that using only the 3MHz from the SPM doesn't produce any significative difference in the correlation curve, therefore in the SS obtained from the ADCP.

APPENDIX D – Mapping Results

At this appendix is shown the mapping of all measured cross-section at Taquari River, Passauna River and Passauna Reservoir.

D.1 Taquari River Mapped cross-setion

Sample integrated collection and Laboratory Analysis by Settling tube Method

- SSC in March/17 = $300.3 mg/L$
- SSC in April/17 = $169.90 mg/L$
- SSC in May/17 = $422.50 mg/L$
- SSC in June/17 = $195.40 mg/L$
- SSC in Jul/17 = $113.60 mg/L$
- SSC in Aug/17 = $124.10 mg/L$
- SSC in Jan/18 = $207.80 mg/L$

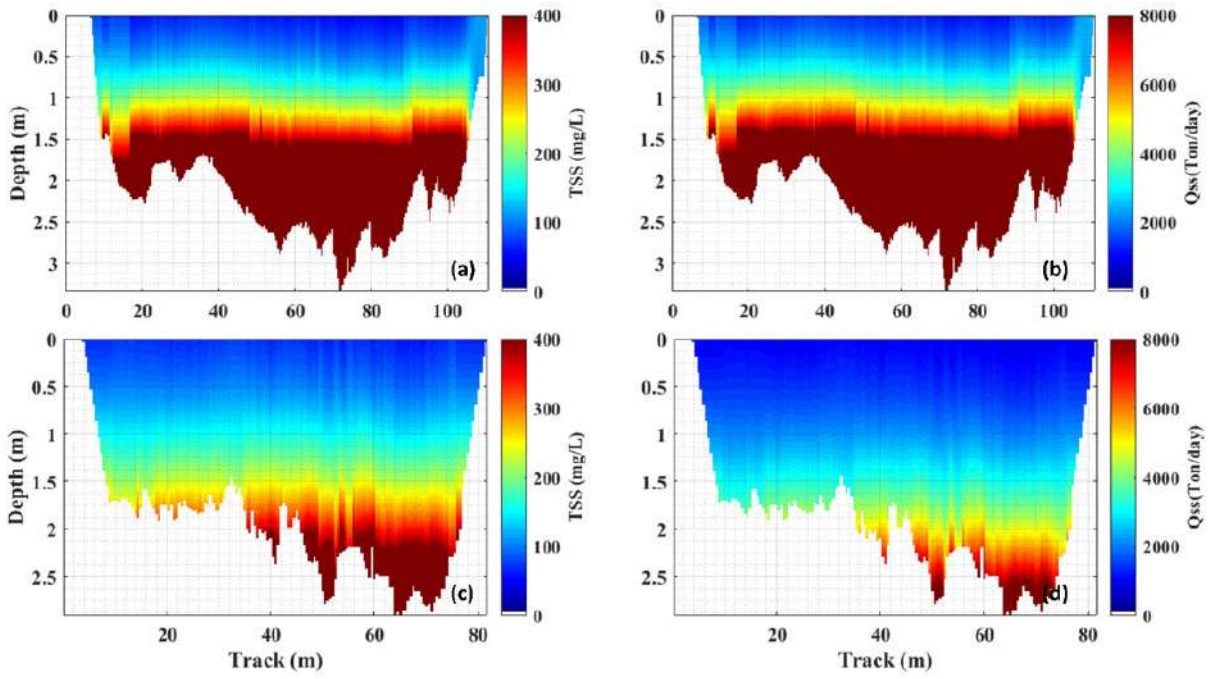

Figure 61 – Mapped cross-section in Mar/17 (a) TSS, (b)Qss and in Apr/17 (c) TSS, (d) Qss.

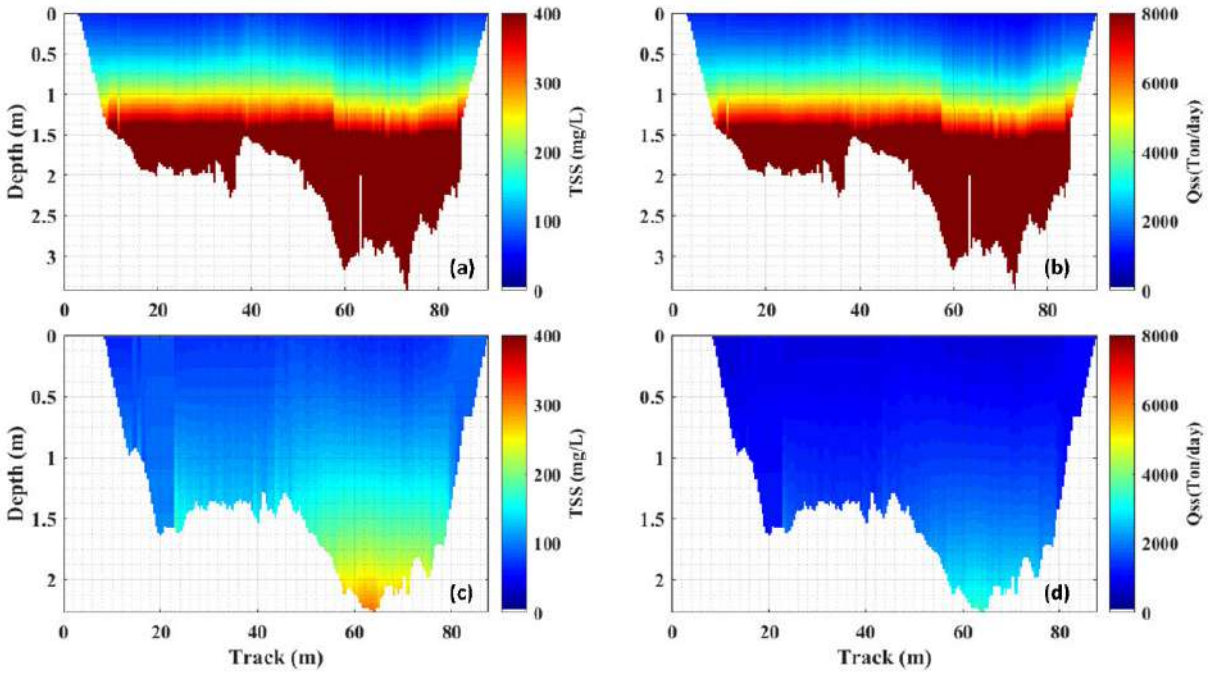

Figure 62 – Mapped cross-section in May/17 (a) TSS, (b)Qss and in June/17 (c) TSS, (d) Qss.

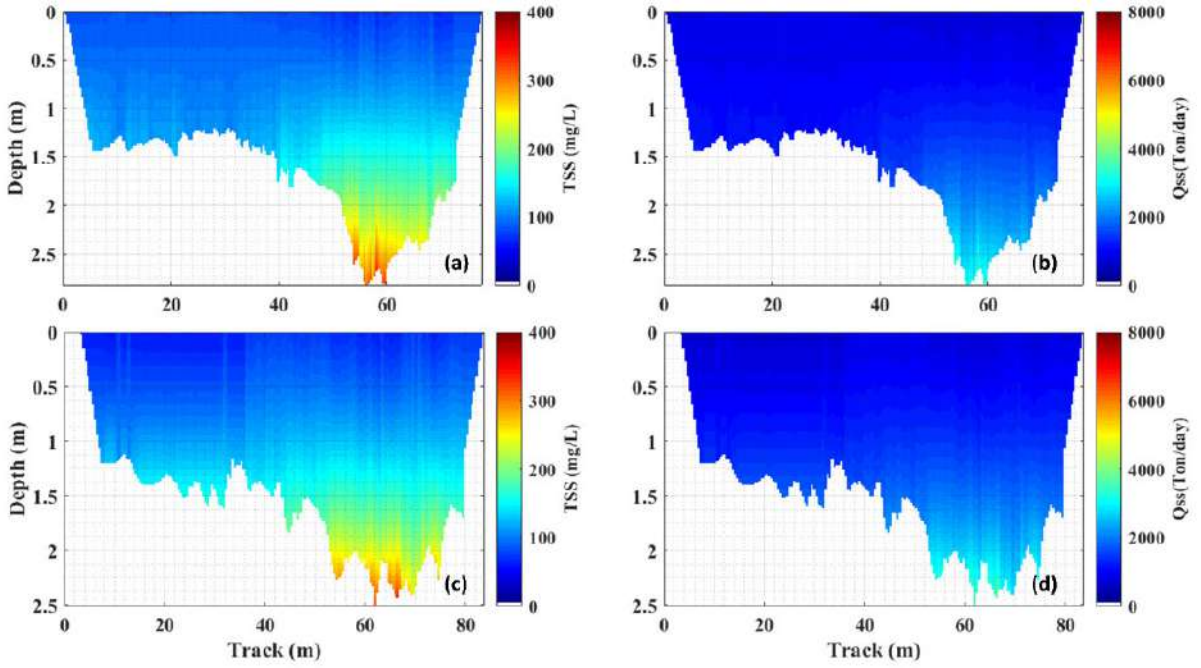

Figure 63 – Mapped cross-section in July/17 (a) TSS, (b)Qss and in August/17 (c) TSS, (d) Qss.

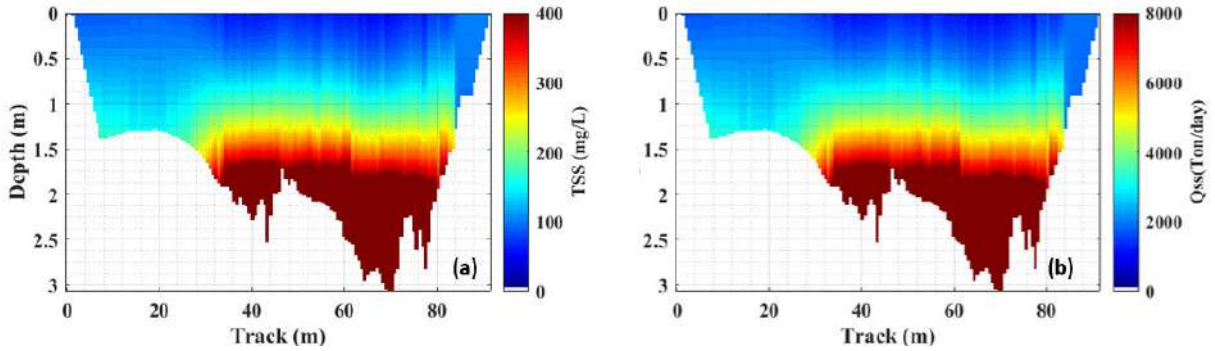

Figure 64 – Mapped cross-section in Jan/18 (a) TSS, (b)Qss.

D.2 Passauna River Mapped cross-setion

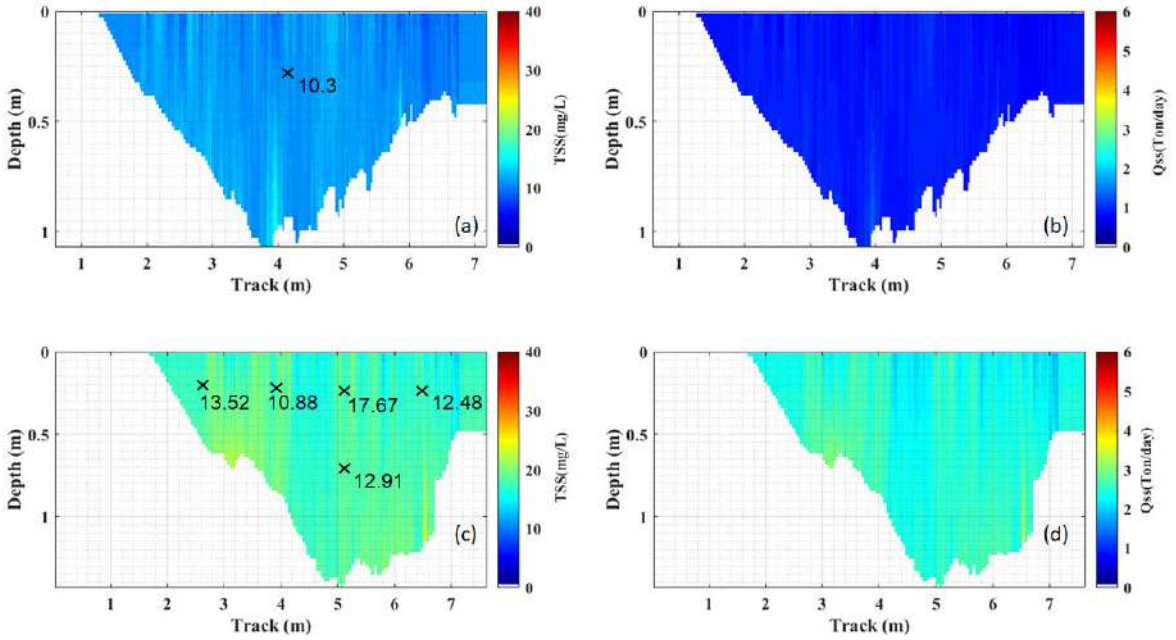

Figure 65 – Mapped cross-section in May/17 (a) TSS, (b)Qss and in Apr/18 (c) TSS, (d) Qss.

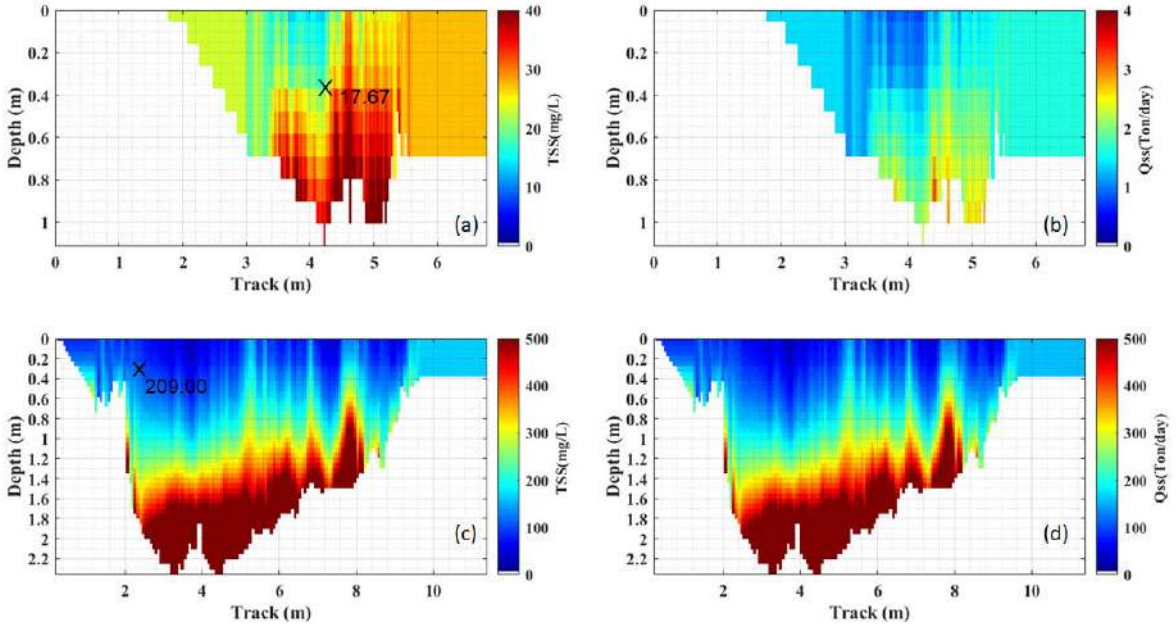

Figure 66 – Mapped cross-section in Aug/18 (a) TSS, (b)Qss and in 18Oct/18 (c) TSS, (d) Qss.

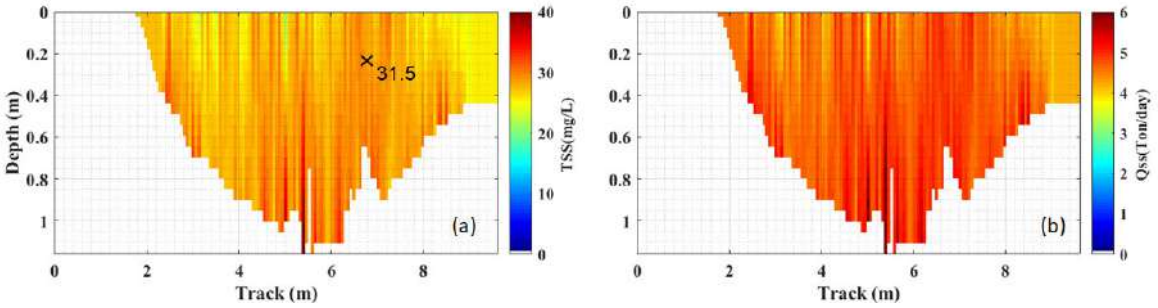

Figure 67 – Mapped cross-section in 20Oct/18 (a) TSS, (b)Qss.

D.3 Ferraria Bridge Mapped cross-setion

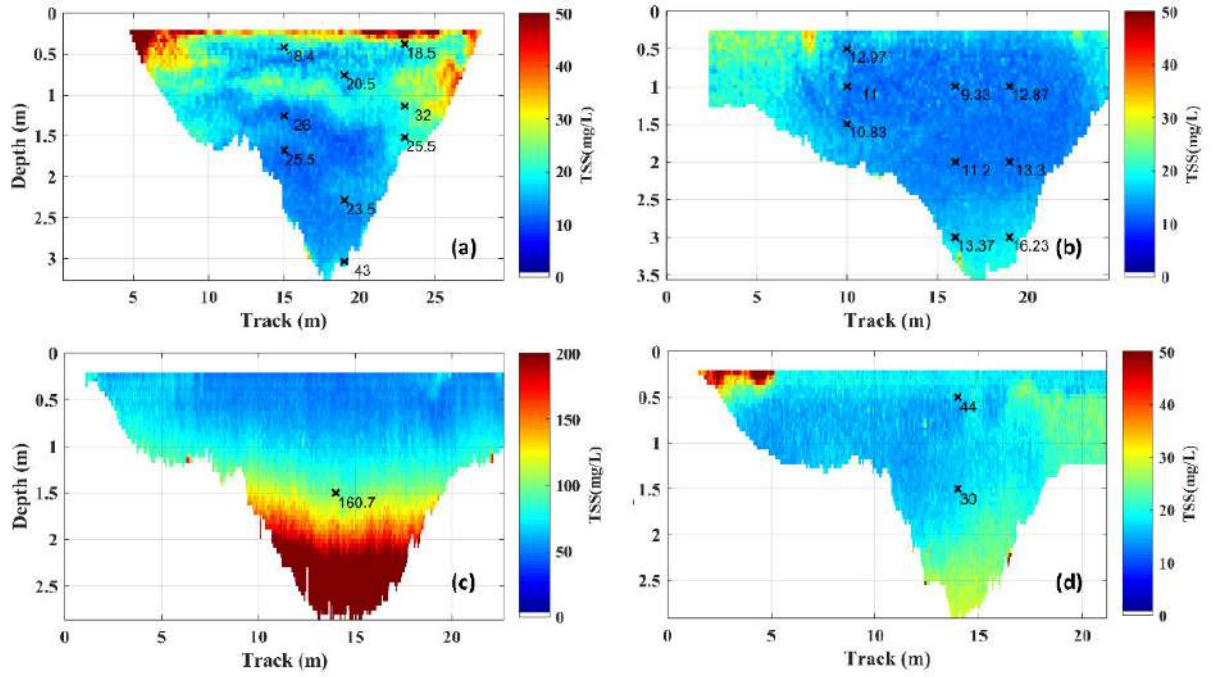

Figure 68 – Mapped cross-section in (a) Aug/17, (b) Feb/18, (c) 18Oct/18 and (d) 20Oct/18.

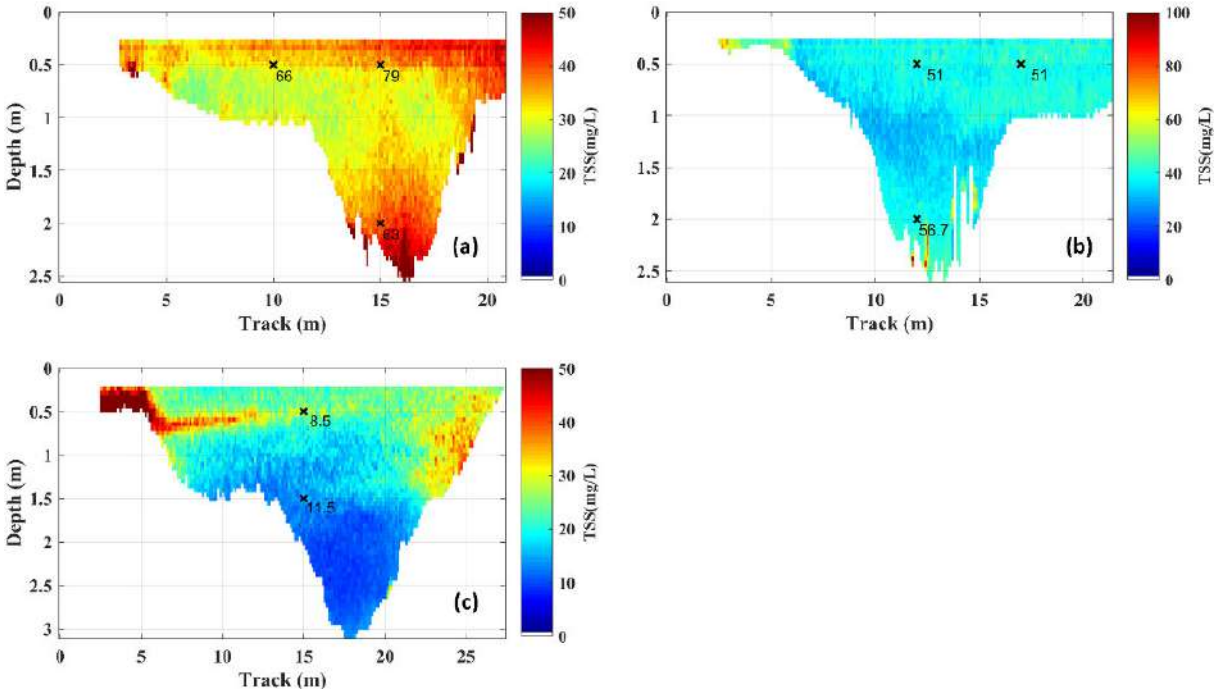

Figure 69 – Mapped cross-section in (a) 04Feb/19, (b) 05Feb/19 and (c) Apr/19.